Mitochondrial Physiology During Doxorubicin-induced Selective Cardiotoxicity

Universidade de Coimbra

Gonçalo C. Pereira, BSc

School of Sciences and Technology

University of Coimbra

Dissertation submitted in partial fulfilment of
the requirements for candidature for degree of

PhD in Biosciences
Specialization in Toxicology

Coimbra, July 2012

goncalocpereira@ci.uc.pt

This dissertation contains information obtained from authentic and highly regarded sources. Reprinted material is quoted with permission, and sources are indicated. A wide variety of references are listed. Reasonable efforts have been made to publish reliable data and information, but the author cannot assume responsibility for the validity of all materials or for the consequences of their use.

This dissertation was written in LaTeX of TeXLive distribution using TexShop as the LaTeX editor.The document style applied is the Oxford style (*ociamthesis.cls* v2.2 written by K.A. Gillow). The bibliography style follows the guideline of PNAS with few modifications. A number of additional packages were applied for graphical displaying and personal stylization. Due to the nature of LaTeX licensing the author undertakes to make available the layout of the thesis after formal request.

Cover Illustration Credit: Élia Sofia eliaramalho@gmail.com
Graphical Printing: Dual Print www.dualprint.net
Published in Portugal on July 2012.

Dedico impreterivelmente esta tese aos meus pais e irmã, pelo apoio nas decisões por mim tomadas ao longo destes anos e pelos sacrifícios suportados durante a minha educação. A vós devo tudo o que sou.

Dedico também esta tese à Inês, pelas horas não partilhadas. Agradeço o teu apoio incondicional e extraordinária compreensão.

“*Breathe, breathe in the air*
Don't be afraid to care
Leave but don't leave me
Look around, choose your own ground”

“Breath” in *Dark Side of the Moon*
by Pink Floyd, 1973

Statement of Originality

This thesis includes material from four original papers that have been previously published in *peer* reviewed journals and are listed below:

> Pereira GC *et al.* **Mitochondrionopathy phenotype in doxorubicin-treated Wistar rats depends on treatment protocol and is cardiac-specific.** *PLoS One*, 2012, 7(6)
>
> Pereira GC *et al.* **Drug-induced cardiac mitochondrial toxicity and protection: from doxorubicin to carvedilol.** *Curr Pharm Des*, 2011, *17*, 2113-2129.
>
> Pereira SP *et al.* **Can drug safety be predicted and animal experiments reduced by using isolated mitochondrial fractions?** *ATLA*, 2009, *37*, 355-365.
>
> Pereira GC and Oliveira PJ. **Pharmacological strategies to counteract doxorubicin-induced cardiotoxicity: the role of mitochondria.** *Journ Pharm Exp Ther*, 2008, *1*, 39-53.

I certify that I have obtained a written permission from the copyright owners to include the above published materials in my thesis. I certify that the above material describe work completed during my registration as graduate student at the University of Coimbra.

I certify that the intellectual content of this thesis is the product of my own work, i.e. key ideas, primary contributions, experimental designs, data analysis and interpretation, were performed by the author. Nevertheless, all assistance received in preparing this thesis and sources have been acknowledged.

I declare that, to the best of my knowledge, my thesis does not infringe upon anyone's copyright nor violate any proprietary rights and that any ideas, techniques, quotations, or any other material from the work of other people included in my thesis, published or otherwise, are fully acknowledged in accordance with the standard referencing practices.

I declare that this is a true copy of my thesis, including any final revisions, as approved by my thesis committee and the Graduate Studies office, and that this thesis has not been submitted for a higher degree to any other University or Institution.

Gonçalo C. Pereira, BSc
July 2012

This work was conducted in the Center for Neurosciences and Cell Biology, Department of Life Sciences, University of Coimbra, Coimbra, Portugal, under the supervision of Paulo J. Oliveira, PhD and António J. Moreno, PhD; and, in the Department of Biochemistry and Molecular Biology, University of Minnesota Medical School, Duluth, MN, USA under the guidance of Kendall B. Wallace, PhD.

The work presented in this dissertation was supported by a PhD fellowship from the Portuguese Foundation for Science and Technology (FCT) addressed to the author (SFRH/BD/36938/2007) and, two research grants from FCT addressed to Paulo J. Oliveira (PTDC/SAU-OSM/6408/2006; PTDC/SAU-OSM/104731/2008).

Abstract

Mitochondria have long been recognized to be involved in several cellular processes beyond their role in energy production. The importance of this organelle for cardiac tissue homeostasis has been largely investigated. It is known that mitochondrial impairment can lead to cell death and consequent organ failure. Several compounds have been described in the literature as having direct effects on cardiac mitochondria providing a mechanistic explanation for their toxicological or pharmacological effects. One classical example of drug-induced cardiac mitochondrial toxicity is doxorubicin (DOX).

Four decades after its discovery, DOX is still one of the most prominent anticancer drug available in clinical practice for the treatment of several human and non-human tumors. However, treatment with DOX is associated with a cumulative and irreversible cardiomyopathy which usually culminates in congestive heart failure. Due to difficulty in detecting the initials signs of DOX-induced cardiotoxicity in conjunction with the lack of efficient counteractive strategies, this topic is under constant investigation. Although the full mechanism behind DOX toxicity remains unclear, available literature points out mitochondrial dysfunction as the main mechanism for drug cardiotoxicity. Most effects are ascribed to redox-cycling of the drug on mitochondrial Complex I which generates increased oxidative stress in the process. Induction of the mitochondrial permeability transition and inhibition of mitochondrial respiration have also been implicated as major determinants in the pathogenesis of DOX cardiotoxicity.

Nevertheless, despite a reasonable amount of work performed, there are still some unanswered issues. One of the main question involves the much larger toxicity of DOX on the cardiac mitochondrial network. The present dissertation proposes to analyze new mechanisms by which DOX is toxic for the cardiac tissue, specially focusing on the role of mitochondria in the pathogenesis of DOX toxicity. One of the aims of this work is to explore

the concept of metabolic threshold applied to the differential toxicity of DOX in mitochondrial bioenergetic processes of different organs. At the same time, calcium loading capacity, a sensitive and accurate marker of mitochondrial performance will also be evaluated in three tissues, including the heart, using Complex I- and Complex II-linked substrates, a comparison that was never performed before. The work was performed using Wistar-Han rats as experimental model.

The collected data support the idea that DOX toxicity is indeed cardioselective but it also depends on the treatment protocol. Impaired mitochondrial bioenergetics was present in several tissues but appeared more pronounced in the heart. However, it was not followed by alterations in mRNA or protein content despite the maximal activity of some respiratory complexes being altered. The explanation may reside in the concept of mitochondrial thresholds as the threshold value for respiratory Complex IV was greatly decreased in heart but without changes for the other analyzed tissues.

Mitochondrial calcium-loading capacity was also decreased in a cardiac-specific manner but no difference between the different respiratory substrates used was detected. Moreover, no changes in the content of classical modulators of the mitochondrial permeability transition pore was perceived despite higher level of oxidative stress was present in the cardiac tissue. Finally, no alterations in blood cardiac-damage biomarkers, echocardiographic profile, histology and cellular ultrastructure was noticeable, even in the presence of mitochondrial alterations.

In conclusion, the present work confirms the cardio-selective nature of DOX toxicity and presents evidence of an early alteration of mitochondrial function in the heart which occurs in the absence of functional alterations. Furthermore, the impaired mitochondria could be responsible for insufficiency of cardiac tissue to adapt to new situations of higher energy demand.

Keywords: doxorubicin, toxicity, mitochondria, heart, liver and kidney

Resumo

Desde muito cedo a mitocôndria foi relacionada com diversos processos celulares para além do seu papel na produção de energia. A importância deste organelo na homeostasia do tecido cardíaco tem sido vastamente investigada e alterações na sua fisiologia podem induzir morte celular e consequente insuficiência do orgão. Diferentes compostos têm sido descritos na literatura como possuindo capacidade de actuar directamente na mitocôndira cardíaca o que poderá explicar os seus efeitos toxicológicos e/ou farmacológicos. Um exemplo clásico de toxicidade cardíaca mitocondrial induzida por fármacos é a doxorrubicina (DOX).

Quatro decadas após a sua descoberta, a DOX permanece como um dos mais proeminentes agentes anticancerígenos disponíveis para o tratamento de diversos tumores em humanos e não humanos. Porém, o tratamento com DOX está associado a uma cardiomiopatia cumulativa e irreversível que culmina em insuficiência cardíaca. Devido à dificuldade na detecção do aparecimento da cardiotoxicidade induzida pela DOX, juntamente com a falta de estratégias eficientes para neutralizá-la, este é um assunto que permanece em contínua investigação. Apesar de o mecanismo por trás da toxicidade causada pela DOX ser ainda incerto, a literatura disponível aponta a disfunção mitocondrial como a principal resposável pela cardiotoxicidade do fármaco. A maioria dos efeitos é atribuída ao ciclo redox do fármaco no Complexo I mitocondrial que leva à produção de elevados níveis de stresse oxidativo. A indução da permeabilidade transitória mitocondrial e a inibição da respiração mitocondrial têm também sido implicadas como factores determinantes na patogénese da cardiotoxicidade da DOX.

Todavia, apesar da considerável quantidade de trabalho realizado, existem ainda algumas questões por responder, uma das quais relaciona-se com a maior toxicidade da DOX na rede mitocondrial cardíaca. Esta dissertação propõe analizar novos mecanismos pelos quais a DOX é tóxica

para o tecido cardíaco, com especial interesse no papel da mitocôndria na patogénese da toxicidade da DOX. Um dos principais objectivos deste trabalho é explorar o conceito de limiares metabólicos e aplicá-lo à toxicidade diferencial da DOX nos processos bioenergéticos de diferentes orgãos. Ao mesmo tempo a capacidade de acumular cálcio, um marcador sensível e preciso do desempenho mitocondrial, será avaliada em vários tecidos, incluindo o coração, utilizando substratos ao nível do Complexo I e Complexo II, uma comparação nunca antes realizada. Para a realização deste trabalho foram utilizados ratos Wistar-Han como modelo.

Os resultados obtidos suportam a ideia de que a toxicidade da DOX é de facto cardio-selectiva sendo, porém, dependente do protocolo de tratamento. A função mitocondrial apresentou-se afectada em diferentes tecidos, mas preferencialmente no coração. Contudo, as alterações não foram acompanhadas por variações nos níveis de mRNA e conteúdo proteíco apesar de a actividade máxima de alguns complexos respiratórios ser diferente comparativamente ao controlo. A explicação poderá ser encontrada no conceito dos limiares mitocôndriais pois o valor do limiar para o Complexo IV estava fortemente diminuído no coração sem alterações nos outros tecidos analizados.

A capacidade de acumular cálcio encontrou-se também diminuída no coração não tendo sido detectada nenhuma diferença entre os diferentes substratos respiratórios utilizados. Além do mais, não foi detectada qualquer alteração no conteúdo dos moduladores clássicos do poro de permeabilidade transitória mitocondrial apesar do elevado stresse oxidativo no tecido cardíaco. Por último, não foram observadas alterações nos marcadores de dano cardíaco no soro, perfil ecocardiográfico, histologia e a ultra-estructura celular.

Em conclusão, o presente trabalho confirma a natureza cardio-selectiva da toxicidade da DOX e apresenta evidências de alterações precoces na função mitocondrial cardíaca que ocorrem na ausência de alterações funcionais do orgão. Ademais, a observada alteração na função mitocondrial poderá ser

responsável pela incapacidade do tecido cardíaco se adaptar a novas situações de maior demanda energética.

Palavras-chave: doxorrubicina, toxicidade, mitocôndria, coração, fígado e rim

Por decisão pessoal do autor, este resumo não segue a ortografia do Acordo do Segundo Protocolo Modificativo do Acordo Ortográfico da Língua Portuguesa, aprovado pela Resolução da Assembleia da República n.o 35/2008 e ratificado pelo Decreto do Presidente da República n.o 52/2008, ambos de 29 de Julho de 2008.

Acknowledgements

In time to finish this part of my scientific journey I wish to express my gratitude to those who have supported, criticized and encouraged me, allowing the realization of the present thesis.

I am thankful to the Portuguese Foundation for Science and Technology for the scholarship and research grants that supported the national research in our laboratory as well as my abroad education. Although the relationship between fellows and FCT falls short I recognize the importance of this governmental entity in the realization of the work.

I have previously praised the virtue of my relationship with Doctor Oliveira along my training thesis. In this dissertation I take the opportunity to reiterate the gratitude and thank his support throughout these years. I am deeply thankful for always believing in my capabilities and for pushing me to the limits. If someone is responsible for everything that I have achieved besides me it is him.

I would like to thank Professor Wallace for the opportunity to work in his lab under is guidance. It was a pleasure and a time to mature my scientific personality as Professor Wallace had always a question regarding my work helping me focus and making me a more capable professional. Moreover, the critical thinking I will share in this dissertation was in great part developed during our professional partnership. I also praise his capabilities of "thinking outside of the box". In addition, I am also grateful for Professor Wallace's family support during my stay in Duluth.

I recognize Doctor Sancha as a cornerstone in obtaining this thesis. Her presence is a laboratory asset for us and I thank all her availability and help in the realization of the most impossible tasks. I thank the "resources" provided whenever laboratory obstacles came across.

To Professor Moreno, I thank the discussions, shared knowledge and clarified questions in the topic of bioenergetics. I am also grateful to him for showing that there is life beyond science.

I am grateful to Jim for the long and endless scientific discussions and for always be willing to listen to my opinion regardless of how right it was. I thank all the help and transmitted knowledge during my stay in Duluth.

In addition to their role in my personal life, I thank Ludgero and Inês for their support and criticism along this work. Their laboratorial help was indispensable for the conclusion of this work. I would like to thank Ludgero for his help in the manipulation of some pictures and in the interpretation of some obtained data.

I thank Susana and Sandro for their friendship throughout these years but, above all, I am grateful for the irreverent and inquisitive Susana's personality that made me consider the way to look and interpret my data and experiments. To Sandro, for his asked questions that helped me broad my knowledge and his innate character to not miss out on something without justification.

I am thankful to the staff of the Department of Earth Sciences, namely D. Paula, who contributed with her dedication and efficient technical support.

I acknowledge the help of all of those who provided scientific material of quality (papers) for the writing of this thesis. I am also thankful to Rute not only for her availability in the discussion of new findings on the topic of bioenergetics but also for her musical advices which made the writing of this thesis more pleasant.

Finally, I would like to thank all those friends who have me accompanied me over the years and which made this chore easier to face. Although they not need to be named as they easily know their importance, one stands out for his support and friendship, Miguel I am grateful for your companionship. To the remaining, I thank all the partnership and support at the time of writing this thesis as well as the bohemian distractions which made it possible for me to envisage the laboratories difficulties (among others) with another courage. To all of you the recognition is guaranteed.

Contents

List of Figures

List of Tables

List of Abbreviations & Constants

Abbreviations

ADP	adenine diphosphate
ALT	alanine aminotransferase
ANOVA	analysis of variances
ANT	adenine nucleotide translocase
APS	ammonium persulfate
AST	aspartate aminotransferase
ATP	adenine triphosphate
BCA	bicinchoninic acid assay
BCN	binuclear center
BHT	butylated hydroxytoluene
BKA	bongkrekic acid
BSA	bovine serum albumine
BUN	blood urea nitrogen
$[Ca^{2+}]_c$	cytosolic calcium concentration
$[Ca^{2+}]_e$	extra-mitochondrial calcium concentration
$[Ca^{2+}]_m$	mitochondrial matrix calcium-free concentration
CATR	carboxyatractyloside
CHOL	cholesterol
CK	creatine kinase
mtCK	mitochondrial isoform of creatine kinase
CoA	coenzyme A
CoQ	ubiquinone
$CoQH_2$	ubiquinol (full-reduced form of ubiquinone)
Cr	creatine
CsA	cyclosporin A
CyP-D	cyclophilin D
DCPIP	2,6-dichlorophenolindophenol
DMSO	dimethyl sulfoxide
DNA	deoxyribonucleic acid
cDNA	circular deoxyribonucleic acid
mtDNA	mitochondrial deoxyribonucleic acid
DOX	doxorubicin
DQH_2	decylubiquinol
DTT	dithiothreitol
ECF	enhanced chemifluorescence
EDTA	ethylenediamine tetraacetic acid
EGTA	ethylene glycol tetraacetic acid

EM	electron microscopy
ER	endoplasmic reticulum
FAD	flavin adenine dinucleotide
FeS	iron-sulfer clusters
FET	forward electron transference
FMN	flavin mono nucleotide
GPx	glutathione peroxidase
Gred	glutathione reductase
GSH	glutathione oxidized form
GSSG	glutathione reduced form
HE	hematoxilin and eosin
H_2O_2	hydrogen peroxide
IC_{50}	half maximal inhibitory concentration
IMM	inner mitochondrial membrane
IP_3	inositol triphosphate
ISP	iron sulfur protein
LDH	lactate dehydrogenase
MCA	metabolic control analysis
mCU	mitochondrial calcium uniporter
mitoKATP	mitochondrial potassium ATP-sensitive channels
mNCX	mitochondrial sodium-calcium exchanger
mPTP	mitochondrial permeability transition pore
MRC	mitochondrial respiratory chain
NAC	*N*-acetylcysteine
NAD^+	nicotinamide adenine dinucleotide oxidized form
NADH	nicotinamide adenine nucleotide reduced form
$NADP^+$	nicotinamide adenine dinucleotide phosphate oxidized form
NMR	nuclear magnetic resonance
NO	nitric oxide
eNOS	endhothelial nitric oxide synthase
iNOS	inducible nitric oxide synthase
nNOS	neuronal nitric oxide synthase
OMM	outer mitochondrial membrane
OSCP	oligomycin-sensitivity conferring protein
OXPHOS	oxidative phosphorylation
PCR	polymerase chain reaction
PCr	phosphocreatine
qPCR	quantitative real-time polymerase chain reaction
PiC	phosphate carrier
Prx	peroxiredoxins
PVC	polyvinyl chloride
PVDF	polyvinylidene difluoride
RaM	rapid calcium uptake mode
RCR	respiratory control ratio
RET	reverse electron transference
mRNA	messenger ribonucleic acid
rRNA	ribosomal ribonucleic acid
siRNA	small interfering ribonucleic acid
tRNA	transfer ribonucleic acid
ROI	region of interest

ROS	reactive oxygen species
RT-PCR	reverse transcriptase-polymerase chain reaction
RuR	ruthenium red
SDS	sodium dodecyl sulfate
SERCA	sarco/endoplasmic reticulum Ca^{2+}-ATPase
SNP	singlenucleotide polymorphism
SOD	superoxide dismutase
Mn-SOD	mitochondrial-specific manganese-superoxide dismutase
TBARS	thiobarbituric acid reactive substances
TBS-T	Tris-buffer saline plus Tween-20
TCA	tricarboxilic acid cycle
TEMED	tetramethylethylenediamine
TIM	translocase of the inner membrane
TNF-α	tumor necrosis factor-alpha
TnI	troponin I
TOM	translocase of outer membrane
TP	total proteins
TPP	tetraphenylphosphonium
TRIG	triglycerides
Trx	thioredoxin
TrxR	tioredoxin reductase
UCP	uncoupling protein
VDAC	voltage-dependent anion channel

Cell Lines

H9c2	original clonal cell line derived from embryonic BD1X rat heart tissue by B. Kimes and B. Brandt which exhibits many of the properties of skeletal muscle. Myoblastic cells in this line will fuse to form multinucleated myotubes and respond to acetylcholine stimulation. Fusion occurs faster if the serum concentration in the medium is reduced to 1%.
HepG2	is a perpetual cell line which was derived from the liver tissue of a 15 year old Caucasian American male with a well differentiated hepatocellular carcinoma. HepG2 cells are a suitable *in vitro* model system for the study of polarized human hepatocytes.
HL-1	is a derived cardiac muscle cell line from the AT-1 mouse atrial cardiomyocyte tumor lineage. HL-1 is the first cell line established that can maintain the differentiated cardiomyocyte-phenotype, morphological, biochemical, and electrophysiological properties and contractile activity *in vitro*.

Mathematical Symbols

Δp	proton motive force	(mV)
ΔpH	pH -difference between mitochondrial matrix and cytosol	(pH units)
$\Delta\psi$	mitochondrial transmembrane electric potential	(mV)
$\tilde{\mu}_X$	electrochemical potential of species X	(kJ mol^{-1})
E_X	electrode potential or electromotive force of species X	(V)
G°	standard Gibbs free energy of formation	(kJ mol^{-1})
G	Gibbs free energy	(kJ mol^{-1})

T	thermodynamic temperature	(K)

Mathematical Constants

F	Faraday constant	$(96\,485.3365(21)\,\mathrm{C\,mol^{-1}})$
R	ideal gas constant	$(8.314\,462\,1(75)\,\mathrm{J\,K^{-1}\,mol^{-1}})$

Part I

General Introduction

Chapter 1

Mitochondria

> *“A human being is a whole world to a mitochondrion, just the way our planet is to us. But we’re much more dependent on our mitochondria than the earth is on us. The earth could get along perfectly well without people, but if anything happened to our mitochondria, we’d die.”*[1]

Mitochondria are usually considered the power plants of the cells, supplying most of the energy needed. This initial section will briefly describe the physiology and

[1] *A Wind in the Door* is a young adult science fantasy novel by Madeleine L’Engle [1]. It is a companion book to *A Wrinkle in Time*, and part of the Time Quartet.

function of mitochondria in the context of cardiomyocyte homeostasis, serving as framework to justify the need to preserve cardiac mitochondrial performance during drug-induced toxicity.

1.1 Mitochondrial morphology

Mitochondria are one of the endomembrane systems found in cells, being surrounded by two lipid bilayer membranes. The outer mitochondrial membrane (OMM) contains traces of cholesterol and is highly permeable to most molecules due in part to the presence of a non-selective channel designated as voltage-dependent anion channel (VDAC) [2, 3]. Similarly, mitochondrial-targeted proteins are imported by specific translocases of outer membrane (TOMs) after a signal/sequence recognition by the transporter protein [4]. The rapid solute equilibration through the OMM results in an

Figure 1.1 ***(following page)*:** Mitochondria are dynamic organelles which can undergo fission and fusion, remodeling cristae and altering the mitochondrial network as well (**Panel A**). These events are regulated by specific proteins, eg. mitofusin (**1**). Although mitochondria are effective machines converting O_2 to water, 1% of the O_2 used in respiration is converted to superoxide anion by electrons leaking from the mitochondrial respiratory chain during specific conditions (**Panel B**, bottom). The superoxide radical can damage lipid membranes and proteins or can be dismutated by type II superoxide dismutase (SOD, **2**) to H_2O_2, which is capable to diffuse to remote areas of the cytoplasm. As a detoxification mechanism, mitochondria convert H_2O_2 to water by catalase (**3**) or glutathione peroxidase (**4**). The latter oxidizes glutathione (GSH) which is the recycled by glutathione reductase (**5**) through oxidation of NADPH. **Panel C** describes the most known function of mitochondria, OXPHOS. Pyruvate is the bridge between glycolysis and TCA cycle which produce substrates for the MRC. The electron flux from complex I to complex IV creates a proton motive force which can be used to phosphorylate ADP by the ATP-synthase, (**6**) or can be dissipated by uncoupling proteins (UCPs, **7**). Mitochondria can also participate in calcium homeostasis (**Panel D**). After uptake by mitochondrial calcium uniporter (**8**) matrix calcium accumulation can have two distinct effects: lower physiological levels can stimulate dehydrogenases in the Krebs cycle, while higher levels can be harmful and induce the opening of the mitochondrial permeability transition pore (MPTP). The consequence of this last event will be outer membrane rupture and consequent release of cytochrome c (**9**) to the cytoplasm resulting in cell death. However, cytochrome c can also be released without the loss of inner membrane integrity, through the formation of Bax (**10**) oligomers in the outer membrane. Cyclophilin D (**11**); ANT - adenine nucleotide translocase (**12**); VDAC - voltage-dependent anion channel (**13**).

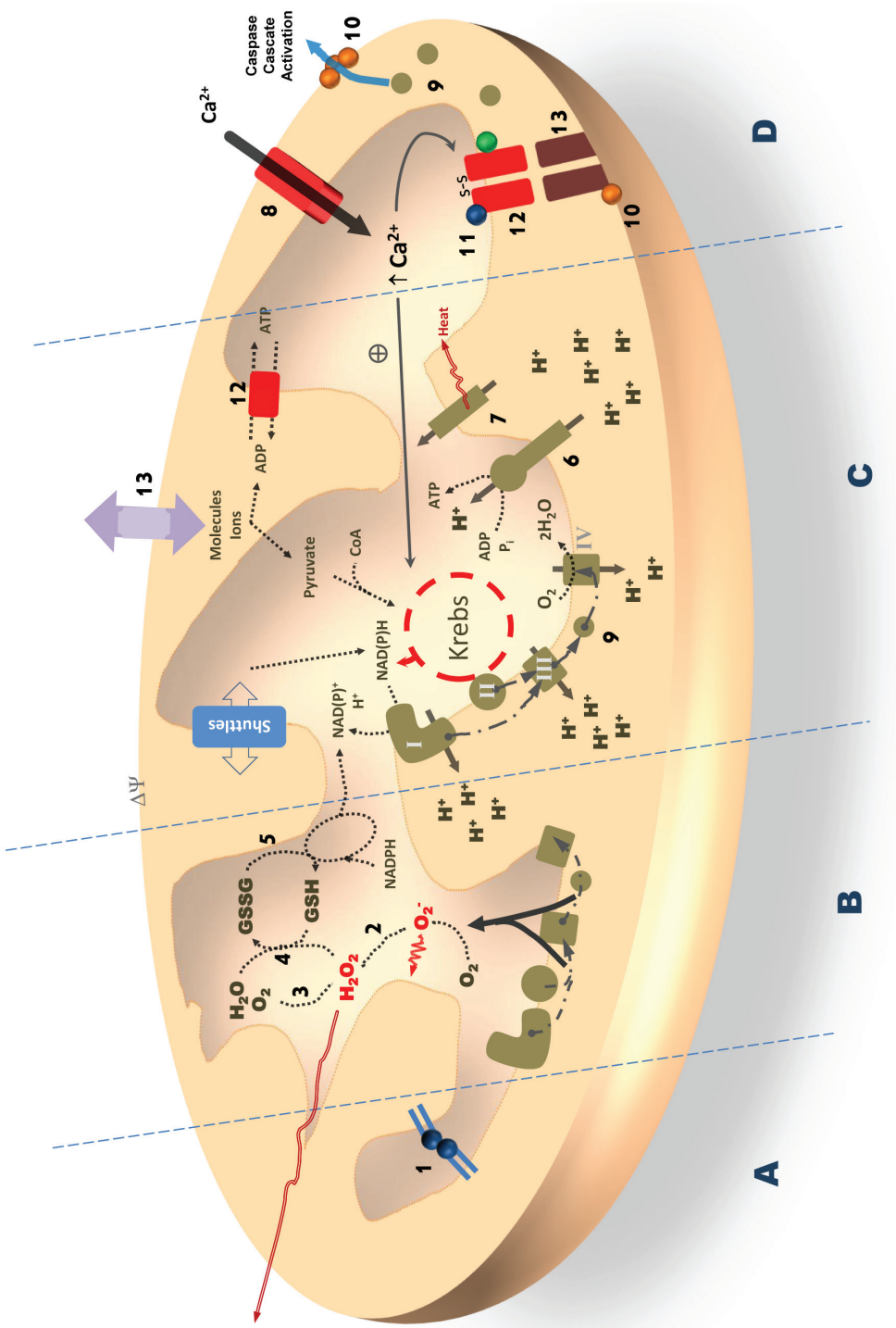
A
B
C
D
Caspase Cascate Activation
Ca2+
↑ Ca2+
S-S
Heat
ATP
ADP
Molecules Ions
Pyruvate
CoA
Krebs
NAD(P)H
NAD(P)+ H+
Shuttles
ΔΨ
NADPH
GSH
GSSG
H2O
O2
H2O2
O2-
2H2O
Pi
I
II
III
IV

inter-membrane space[2] content very similar to cytoplasm. It is also within this space that the proton gradient (sec. 1.2, pag. 8) is accumulated and some important proteins for oxidative phosphorylation (OXPHOS), e.g. cytochrome c, or mitochondrial-dependent proteins responses, e.g. proteins involved in apoptosis pathway, can be found [5].

Contrarily to the OMM, the inner mitochondrial membrane (IMM) is rich in cardiolipin and highly impermeable as it only contains specific transporters (proton pumps or substrate-specific shuttles) [2, 3]. This feature plays a crucial role in the normal mitochondrial physiology allowing selective ion and metabolite transport as well as the formation of ion gradients and ideal thermodynamic conditions for certain biochemical reactions [5]. Moreover, inner mitochondrial membrane allows the creation of a complete different compartment apart from the cytosol, the mitochondrial matrix.

In the matrix, enzymes of the tricarboxilic acid cycle (TCA) with the exception of succinate-dehydrogenase, which is bond to the inner mitochondrial membrane, can be found. Interestingly, NAD^+ and $NADP^+$ mitochondrial pools are separated from the ones found in the cytosol while ADP and ATP communicate with cytoplasm through the adenine nucleotide translocase (ANT) [5]. The idea that the mitochondrial matrix has a high character of complexity is supported by the fact that not only different proteins involved in several mitochondrial processes can be found there but also due to its high protein concentration ($\sim 500\,\mathrm{mg\,ml^{-1}}$) where a considerable strutural organization within this gel-like solution might occur [5].

1.1.1 Cardiac mitochondria

The amount and degree of internal mitochondrial structure varies from tissue to tissue, depending on their metabolic states [6]. Even within the same tissue, mitochondrial heterogeneity can occur. One example occurs in the cardiomyocyte, where two distinct mitochondrial populations can be spacial identified having distinct roles in cardiomyocyte physiology. One population closer to the T-tubules and sarcoplasmic reticulum provides energy in the form of ATP, which is required for calcium influx to the sarcoplasmic reticulum through the sarco/endoplasmic reticulum Ca^{2+}-ATPase (SERCA) pump or, alternatively, to extracellular compartment through the plasma membrane Ca^{2+}-ATPase [7].

[2] space between the inner and outer membrane.

A second mitochondrial sub-population is closely associated with contractile filaments providing energy to the *stroke force*[3]. Although these sub-groups might be slight different in morphology, namely size, shape, number of cristae, volume and length they both share the common characteristics of mitochondria from other tissues.

In conclusion, the energy demand by cardiomyocytes can be attributed to two different mitochondrial sources depending of its final use. One energy source is destined to release myosin from actin allowing not only for relaxation but also for continuous contraction, while the second energy source is essential for calcium homeostasis, a critical step in relaxation and contraction cycle. As a normal heart beats constantly for 1 to 1.7 times per second, it is not difficult to imagine the energy demand of cardiomyocytes [7].

Mitochondrial dynamics and quality control

In adult cardiomyocytes, both mitochondrial populations are largely associated with cytoskeleton and, therefore, the dynamic properties of the organelle are limited [8]. However, the high energy demand character of the heart requires a high bioenergetic state which can only be achieved if refined quality control is verified. In this case, damaged or non-functional mitochondria are removed by autophagy and new mitochondria are formed by biogenesis.

Both situations depend on fission/fusion events but the spatial constrains and crystal-like pattern of cardiac mitochondria, which are found packed between the myofibrils, has generated discussion about the possibility of such events to occur [6, 8]. Supporting the notion of mitochondrial fusion and fission in the myocardium is the fact that cardiomyocytes have all the necessary machinery for the two events to occur and, in certain pathological situations, very small mitochondria (e.g., dilated cardiomyopathy, cardiac rhadbomyoma and ventricular-associated congenital heart diseases) or abnormally large and defective mitochondria (e.g., senescent/aged cardiomyocytes) can be found [6, 8].

Studies done not only in cardiac-like cell lines (e.g., HL-1 and H9c2) but also in neonatal cardiomyocytes have demonstrated a high degree of motility and morphological changes [8, 9]. However, although this type of cell lines shares some characteristics

[3]sliding of myofilaments (actin and myosin) upon calcium binding to troponin C causes an allosteric change in tropomyosin allowing myosin to bind to actin generating the stroke force upon ADP release [7]

of differentiated cardiac cells, they lack the well organized and dense packing that is typical of adult cardiomyocytes. Likewise, studies where mRNA or protein levels are quantified in whole heart content should be interpreted cautiously since the organ consists in several types of cells besides cardiomyocytes [6].

The ultimate answer would be live imaging of adult cardiomyocytes but this carries some technical difficulties: myocytes are difficult to transfect and the spatial resolution of confocal microscopy may not be optimal [6, 8]. Nevertheless, an interesting work compared the dynamics of mitochondria between cell lines and adult cardiomyocytes showing, that under normal conditions, although fusion and fission do not occur, mitochondrial movements were observed which were attributed to transitions between orthodox and condensed form and not to formation of a continuous network [9].

1.2 Mitochondrial energy production by oxidative phosphorylation

The introduction of the supravital dye Janus Green B to stain mitochondria in 1900 by Michaelis [10, 11] was the first element to suggest a connection between these organelles and redox events in cells since mitochondria were capable of reducing the dye. From then until the late 50s [11], numerous biochemical and structural works were conducted that ultimately led to advances in mitochondrial bioenergetics. Several works attempted to elucidate the overall process of ATP generation due to substrate oxidation coupled to ADP phosphorylation, also known as OXPHOS.

Three main conjectures that emerged in the middle of the 20th century and which are the cornerstones of mitochondrial bioenergetics can be considered:

i) **Chemical Hypothesis**
Proposed by Slater in 1953 [12], this was the first interpretation of OXPHOS mechanism and shared its basis with the idea of substrate-level phosphorylation present in glycolysis and TCA [13]. In other words, it postulates the existence of a common chemical intermediate between oxidation reactions and ATP synthesis which conserves the energy of those same reactions. However, high-energy intermediates in OXPHOS were never detected. Moreover, this hypothesis does not explain the need of an intact inner mitochondrial membrane for OXPHOS to occur.

ii) **Conformational Hypothesis**
First proposed by Boyer in 1965 [14], this hypothesis differed from the previous by postulating that the high-energy intermediate was not necessarily a chemical entity but a highly energetic state that would result from a protein conformational change, thus conserving the energy of redox reactions. Although some physical alterations at the membrane level are observed during electron shuttle, it was never demonstrated that those conformational alterations are forward to the ATP-synthase. Nevertheless, nowadays a different interpretation of this theory is used nowadays to explain the mechanism by which ATP-synthase alters the affinity of its active site for ATP or the proton pumping mechanism of each respiratory complex. Both topics will be covered further on.

iii) **Chemiosmotic Hypothesis**
Proposed by Mitchell in 1961 [15], the chemiosmotic theory was a radical alternative to the chemical hypothesis. In this case, the electron transfer through the mitochondrial respiratory chain (MRC) and ATP phosphorylation are not associated through a common chemical intermediate but the redox energy is rather conserved in a physical state under the form of an electrochemical gradient of protons across the inner membrane.

1.2.1 Chemiosmotic theory

Mitchell theorized that free energy released by electrons transfer from the respiratory substrates to molecular oxygen (O_2) by means of the MRC is used to pump proton from mitochondrial matrix [16]. Thus, vectorial transport of protons together with electron shuttle establish a charge and concentration displacement across the inner membrane sufficient to force a secondary pump (ATP-synthase) to synthesize ATP.

Thermodynamics

From a thermodynamic point of view, the above postulated theory can be translated into the following [5, 16]: if an ion X^{m+} is to be transported down across a membrane potential in the presence of a concentration gradient, the free energy change is given

by the general electrochemical equation:

$$\Delta G = \Delta\tilde{\mu}_{X^{m+}} = -mF\Delta\psi + 2.3RT\, log_{10}\frac{[\mathrm{X^{m+}}]_\mathrm{B}}{[\mathrm{X^{m+}}]_\mathrm{A}} \tag{1.1}$$

If the ion to be transported is a proton, the previous equation can be simplified as the pH is a logarithmic function of $[\mathrm{H}^+]$.

$$\Delta\tilde{\mu}_{X^{m+}} = -F\Delta\psi + 2.3RT\,\Delta pH \tag{1.2}$$

Conventionally, to mitochondriologists, this expression is defined in units of voltage negative inside:

$$-\Delta\tilde{\mu}_{X^{m+}}/F = \Delta p = \Delta\psi - 2.3RT/F\,\Delta pH \tag{1.3a}$$

$$\Delta p = \Delta\psi - 59\,\Delta pH \qquad \text{at } 25\,^\circ\mathrm{C} \tag{1.3b}$$

where Δp is the proton motive force defined by Mitchell. The proton gradient, or proton motive force, is therefore composed of two main components in which the electric factor is the main contributor in mitochondria [16].

Similarly, the reduction potential of an electron transfer between a redox couple can be expressed as the difference between the specific donor and acceptor redox potentials and since the redox potential and pH of a solution are directly related, the free energy change is given by:

$$\Delta G = -nF(E_{h(A)} - E_{h(B)}) = -nF\Delta E_h \tag{1.4}$$

However, if the donor and acceptor are at distinct sides of a membrane sustaining an electrical potential that facilitates the transfer, the free energy necessary to accomplish the process is considerably lower. In that case, equation 1.4 must be rewritten:

$$\Delta G = -nF(\Delta E_h + \Delta\psi) \tag{1.5}$$

In conclusion, if n electrons to be transferred between a set of redox acceptors and donors, generate an efflux of n' protons across the membrane against a Δp then the equilibrium is reached when:

$$n'\Delta p = n\Delta E_h \quad \text{if redox pair is on the same side of membrane} \tag{1.6a}$$

$$= n(\Delta E_h + \Delta\psi) \quad \text{if redox pair is across the membrane} \tag{1.6b}$$

Equation 1.6b is the key conception stated by Mitchell, where MRC is looped across the membrane more than once, and that the stoichiometry of proton translocation depends upon the point at which the substrate feeds reducing equivalents into the chain [16].

Ultimately, Δp is primarily used for the purpose of ADP phosphorylation. The free energy change or phosphorylation potential is given by:

$$\Delta G_p = \Delta G^\circ + 2.3RT\, log_{10} \frac{[\mathrm{ATP}]}{[\mathrm{ADP}] + [\mathrm{Pi}]} \tag{1.7}$$

which is in turn dependent on the proton electrochemical gradient:

$$\Delta G_p = n'(-\Delta\tilde{\mu}_{H^+}) \tag{1.8a}$$

$$= n' F \Delta p \tag{1.8b}$$

$$= n' F(\Delta\psi - 59\,\Delta pH) \quad \text{at } 25\,^\circ\mathrm{C} \tag{1.8c}$$

where n' is the number of protons translocated by the ATP-synthase, i.e. the H^+/ATP ratio. However, it is not clearly evident how the electrical and chemical components may exert equivalent forces from a thermodynamical point of view. Therefore, Mitchell introduced a new concept - *the proton well* [16].

The proton well was defined as a proton-conducting cleft passing down into the membrane dielectric (half-channel) in the F_o subunit of ATP-synthase. In the presence of ΔpH, protons flow freely and the pH effective at the bottom of the well is in equilibrium with the aqueous phase. However, if the membrane sustains an electric gradient, it will tend to pull protons to its interior which leads to a decrease in the local pH and abolishment of local membrane potential. In other words, the proton well converts the electrical component to a pH gradient along F_o.

In the light of the chemiosmotic theory, Nicholls has advocated that an ATP-synthesizing organelle as mitochondria can also be compared to an electric circuit mostly because Mitchell's proton circuit resembles the intrinsic properties of an electric circuit (Fig. 1.2 for details) [5, 17].

In fact, mainstream definition of mitochondria as simple 'cell batteries' might not be so inappropriate as recent work using isolated mitochondrial fractions immobilized in synthetic polymer carbon-coated electrode in the presence of biological substrates were capable of producing useful electrical current with a significant stability and *shelf life* (60 days) [18].

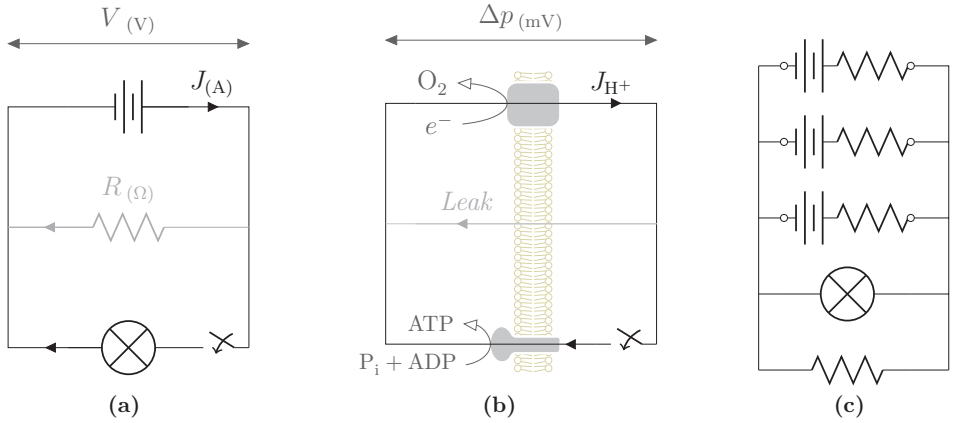

Figure 1.2: Analogy between an electric **(a)** and the proton circuit **(b)**, where a battery and light bulb are compared to the MRC/ATP-synthase apparatus. The switches represent the possibility of circuits to be either in an open or close state, which in the proton circuit is equivalent for example to ATP-synthase inhibition or ATP turnover, respectively. If the circuit is closed, current (proton) flux can be measured and the conductance and voltage can be derived, complying with traditional electrical circuits laws, e.g. Ohm's law ($I = V/R$) . The gray color depicts how the electrical potential may be consumed/dissipated, which in biological terms represents proton leak, ion uptake and metabolites transport. In **(c)** a more truthful representation of the proton circuit is presented with the three respiratory complexes working in serie to feed protons into the circuit. Also, the resistances associated with each complex reflect the fact that $\Delta\psi$ decreases as current drawn increases. Adapted from [5].

Exchange diffusion systems

Finally, mitochondria must also provide mechanisms for ion/cation uptake as stated in the third main postulate of the chemiosmotic theory [16]. Mitchell speculated at the time that diffusion of ions down the membrane potential would lead to their accumulation in an osmotically disruptive fashion unless counterpoised by specific exchange of protons. Moreover, the uptake of certain charged metabolites must be directly or indirectly facilitated by specific exchange of protons. In other words, the Δp is normally consumed to maintain mitochondrial ion and volume homeostasis but it can also be used to drive influx or efflux transport. Hence, metabolite transport across energy-transducing membranes as mitochondria can occur at the expense of [5]:

ΔpH Electroneutral proton symport or hydroxyl antiport, e.g. glutama-

te^-/OH^-;

$\Delta\psi$ Electrical uniport of cations, e.g. Ca^{2+} uniport, or electrical exchange of two metabolites, e.g. ATP^{4-}/ADP^{3-};

Δp Proton symport along with a neutral specie, e.g. *D*-lactate/H^+[19].

1.2.2 Mitochondrial Respiratory Chain

Initially, Mitchell proposed a MRC organized into three loops each comprising two anisotropic circuits: the electron transport and the proton transport [15, 16]. Later, due to practical inconsistencies, Mitchell changed the initial model to accommodate the second and third loop in one integrated system designated by *Q cycle*. Finally, the idea that respiratory complexes may act as single units, i.e. *conformational proton pumps*, resulted mostly from the unequivocal demonstration that Complex IV is able to pump protons when the initial conjecture did not propose any component capable of proton translocation in that area of the MRC [20, 21].

All the respiratory complexes are intrinsically different from each other and therefore the redox potential of each one can be used to sort them in a virtual chain. However, their lipophilicity actually allows for high mobility in IMM and consequently behaving more like a dynamic rather than a static chain. Moreover, Gnaiger has challenged the term *chain* since the term suggests a linear sequence where in fact there is a non-linear convergent arrangement of respiratory complexes at the Q-pool followed by a *linear* route through complex III to complex IV [22]. Usually electrons entering MRC are originated from reduced equivalents derived from TCA or other metabolic pathways and indirectly represent oxidation of different cell fuels. The transference of electrons among several multi-subunit proteins (Complexes I-IV) is driven by the decrease in their redox potential, until reaching oxygen as the final acceptor.

Origin

MRC account up to 50 different polypeptides mostly belonging to NADH:ubiquinone oxidoreductase [23]. The majority of those subunits are encoded by the nuclear genome, translated in cytoplasm and then imported to the inter-membrane space or the inner mitochondrial membrane through a complex machinery system designated

by TIM/TOM complex [4]. This is only feasible since pre-proteins have a mitochondrial signal sequence at N-terminal allowing for recognition by a receptor protein in TOM complex [4]. In fact, this particularity is exploited by bioengineer systems to specifically deliver non-mitochondrial proteins to this compartment [24]. Likewise, other molecules can be targeted to the organelle through different approaches: nucleic acids [25] or antioxidant/chemicals [26].

The remaining 13 polypeptides toghether with 22 transfer RNA (tRNA) and two ribosomal RNA (rRNA) are encoded by the mitochondrial genome, a double stranded circular DNA about 16 kbp devoid of exons, which is usually found in 2-10 copies per mitochondrion body [27]. A complete *in vitro* copy of the mitochondrial DNA (mtDNA) was synthesized in 2010 by Venter's group [28]. Bennett lab, on the other hand, proved that artificial mtDNA can be delivered to mitochondrial compartment [29] making the idea of mitochondrial gene therapy attainable. The high number of mtDNA copies allows the introduction of two new concepts extremely valuable in the

Figure 1.3 ***(following page)*:** Schematic representation of mitochondrial respiratory complexes structure. Protein structure is shown in the cartoon form and the correspondent light colors represent enzyme solvent accessible (1.4 Å radius) surface area. Possible domains included in membrane are also shown. Small structures in red represent prosthetic groups. **I** - structure of *Thermus thermophilus* NADH dehydrogenase at 4.50 Å resolution (PDB#3M9S). The subunit nomenclature shown is the eukaryotic equivalent [5]. The putative CoQ binding site and the point of inhibition by rotenone is shown in the picture. **II** - structure of *Gallus gallus* succinate dehydrogenase at 2.1 Å resolution (PDB#1YQ3). The red structure in CoQ binding site is ubiquinone-1. **III** - structure of *Paracoccus denitrificans* cytochrome bc_1 at 2.7 Å resolution (PDB#2YIU). As explained in the text, this respiratory complex only works as a dimer. Outlined in ligh gray and in cartoon is a monomer of the dimer. Note the prosthetic groups of the other monomer in dark grey. Q_o and Q_i represents the CoQ binding sites close to heme b_L and b_H groups, respectively. Also shown is the blockade of the enzyme inhibitors, antimycin and myxothiazol. **IV** - structure of *Bos taurus* cytochrome c oxidase at 1.95 Å resolution (PDB#2Y69). Although the enzyme works as monomer it is usually found as a homo-dimer. The circle represents a magnification of the active site after a 45° counter-clockwise rotation of the large picture. Numbers represent the distance between atoms in Å. 'HPEVY' ring represent a conserved ring on the active site and is named after its amino acid constituents. In the large scheme, the putative routes for proton translocation are also shown. **V** - structure of ATP synthase with F_1 portion from *Bos taurus* at 3.20 Å resolution (PDB#2WSS) and F_o portion from *Escherichia coli* (PDB#1C17). At the top of the large scheme a representation of the F_o portion after a 90° clockwise rotation is shown. Similarly, at the bottom, the F_1 portion after a 90° anti-clockwise rotation is shown. There, the Walker's nomenclature for the subunits is shown.

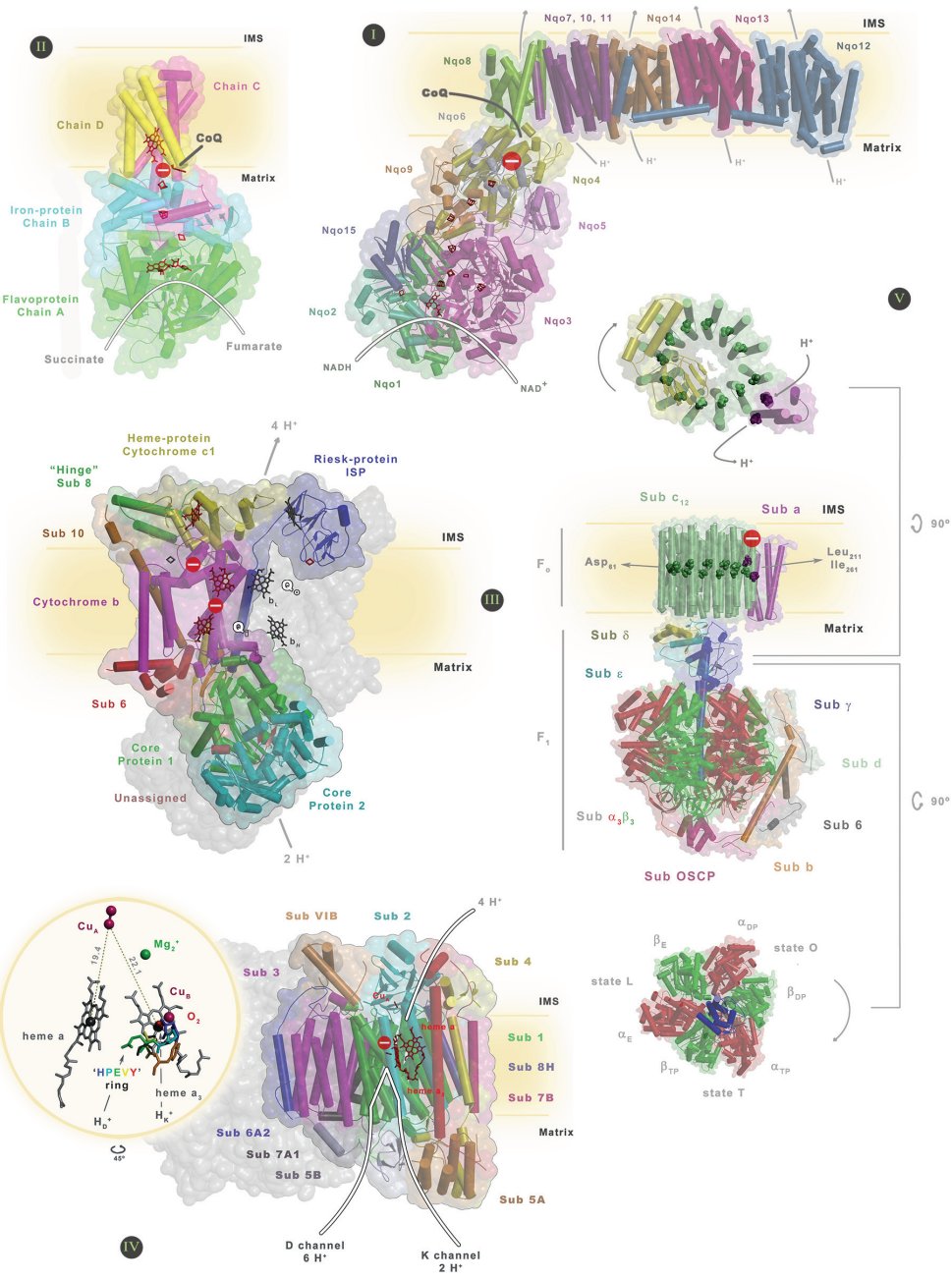
II
IMS
Chain C
Chain D
CoQ
Matrix
Iron-protein
Chain B
Flavoprotein
Chain A
Succinate
Fumarate
I
Nqo7, 10, 11
Nqo14
Nqo13
IMS
Nqo12
Nqo8
CoQ
Nqo6
Matrix
Nqo9
Nqo4
Nqo15
Nqo5
Nqo2
Nqo3
NADH
Nqo1
NAD+
V
H+
H+
III
4 H+
Heme-protein
Cytochrome c1
"Hinge"
Sub 8
Riesk-protein
ISP
Sub 10
IMS
Cytochrome b
Matrix
Sub 6
Core
Protein 1
Unassigned
Core
Protein 2
2 H+
Sub c12
Sub a
IMS
Asp81
Leu211
Ile261
Matrix
Sub δ
Sub ε
Sub γ
Sub d
Sub 6
Sub b
Sub OSCP
Fo
F1
90°
90°
IV
CuA
Mg2+
19.4
22.1
CuB
O2
heme a
'HPEVY'
ring
heme a3
HD+
HK+
45°
Sub VIB
Sub 2
4 H+
Sub 3
Sub 4
CuA
IMS
heme a
Sub 1
heme a3
Sub 8H
Sub 7B
Matrix
Sub 6A2
Sub 7A1
Sub 5B
Sub 5A
D channel
6 H+
K channel
2 H+
αDP
βE
state O
state L
βDP
αE
βTP
αTP
state T

context of hereditary disorders: homoplasmy and heteroplasmy. For example, in some mitochondrial diseases, all mtDNA copies can contain the mutation or alternatively just a few copies can present it. The degree of mutant phenotype will vary depending on the extent of mutation through the mtDNA populations [30, 31]. The situation may be even worse to analyze in the latter since the mutated copies can be restricted to the mitochondrion, i.e., all copies in the organelle are mutated or can be *diluted* among the wild-type.

NADH:ubiquinone oxidoreductase

NADH:ubiquinone oxidoreductase (EC: 1.6.5.3, NADH dehydrogenase, Complex I), is accepted as the first entry point of electron into MRC. The multimeric protein is by far the most complex respiratory complex as it is composed by about 43 subunits, seven of which are mitochondrial encoded [5]. The large complex has a three-dimensional structure similar to an L with the hydrophilic small arm facing the matrix while the large hydrophobic portion extends through the inner membrane [5]. Therefore, it is not difficult to imagine how arduous it is to properly isolate the protein complex for structural analysis. Likewise, an improper isolation of mitochondrial fractions can cause damage or partial inactivation of the complex, which can explain the difficulty in obtaining reliable results in some bioenergetics assays [32].

The complex contains a flavin mononucleotide (FMN) prosthetic group and eight iron-sulfer clusters (FeS) all thermodynamic arranged to allow electron flux through the complex [23]. In fact, from the 43 peptides that constitute the respiratory complex only 14 are indeed associated in electron flux [33]. Moreover, all seven mitochondrial-encoded subunits are essential in that pathway. It is believed that the hydrophobic portion contains all the FeS clusters and FMN since no redox active groups are found in the subunits of the hydrophobic fraction [5]. The remaining subunits are either structural, modulators of activity or essential in complex assembly [33].

Mechanistically, complex I catalyses the transfer of two electrons from NADH to ubiquinone (CoQ) with concomitantly proton translocation across the membrane. Initially, NADH binds to protein and transfers its two electrons simultaneously to FMN. The electrons are then transferred to the second prosthetic group, FeS clusters, and ultimately to CoQ. The electron flow causes the translocation of four protons from the matrix to the inter-membrane space per two electrons transferred but the

mechanism of such event remains to be elucidated [5, 23].

$$NADH + H^+ + CoQ + 4H^+_{in} \rightarrow NAD^+ + CoQH_2 + 4H^+_{out} \quad (1.9)$$

Exprimental mitochondrial Complex I-sustained respiration

In isolated mitochondrial fractions, Complex I-sustained electron transfer through the MRC is achieved with glutamate/malate or pyruvate/malate substrates since NADH by itself is impermeant through the inner mitochondrial membrane. Similarly, glutamate, malate and pyruvate are anions which cannot permeate the inner membrane. However, all have specific carriers which allow their distribution across the membrane in ΔpH -dependent fashion since most carriers operate non-electrogenic by anion exchange or proton co-transport [22].

Both substrates are needed since malate alone cannot support respiration due to inability of oxaloacetate to permeate the inner membrane and also because it cannot be further metabolized in absence of a source of acetyl-CoA [22]. Conversely, glutamate as sole substrate can support respiration although at relatively low rates. Glutamate is transported either by the glutamate-aspartate shuttle or by the electroneutral glutamate/HO^- exchanger and oxidized to 2-oxoglutarate via glutamate dehydrogenase in the matrix with concomitant ammonia equilibrium across the membrane. If malate is used in conjunction with glutamate it allows inhibition of succinate dehydrogenase by equilibrium with fumarate and oxaloacetate (Fig. 1.4) [22]. Accumulated succinate is lost from the mitochondria through dicarboxylate carrier.

Succinate:ubiquinone oxidoreductase

Succinate:ubiquinone oxidoreductase (EC: 1.3.5.1, succinate dehydrogenase, Complex II) can be a second point of entry of electrons into MRC although sometimes is not considered as an integral part of the sequence. This is due in part to the fact that the enzyme provides reducing equivalents to CoQ without respiratory energy conservation. In other words, the potential energy of substrate electron transfer is close to 0 mV which is thermodynamically incompatible with proton translocation [5].

The IMM-bound enzyme contains four subunits which are all nuclear-encoded. Its main role is the conversion of succinate to fumarate in the TCA; however, its membrane-bound character allows direct electron transfer to the CoQ pool via its prosthetic

groups [23]. The subunit of Complex II furthest from the membrane has a covalently bound flavin adenine dinucleotide (FAD) at the active site while the second peripheral subunit has three FeS clusters. The remaining subunits are embedded in the lipid bilayer one of which contains an heme group [23].

Upon succinate oxidation, electrons flow from FAD through the different FeS clusters where are finally transferred to CoQ. The heme cofactor might be acting as an electron sink in the process of CoQ reduction although more research is needed to confirm the hypothesis [34]. Identical controversy is around the origin of protons for CoQ reduction.

$$\text{Succinate} + \text{CoQ} + 2\text{H}^+ \rightarrow \text{Fumarate} + \text{CoQH}_2 \tag{1.10}$$

Exprimental mitochondrial Complex II-sustained respiration

Contrary to complex I-sustained respiration, succinate permeates the inner membrane due to presence of dicarboxylate carriers and is metabolized normally by succinate dehydrogenase. However, as in the presence of malate alone, oxalacetate accumulates in the matrix and furthermore it is also a potent inhibitor of succinate dehydrogenase [22]. To counteract this limitation, succinate is incubated with rotenone, a specific inhibitor of complex I. in this procedure, malate accumulates in the matrix instead of oxaloacetate but since malate permeates the inner membrane, succinate plus rotenone can sustain mitochondrial respiration exclusively via Complex II.

Ubiquinol:cytochrome-c oxidoreductase

Ubiquinol:cytochrome-c oxidoreductase (EC: 1.10.2.2, cytochrome bc_1 complex, Complex III) can be assigned as the mid-point in MRC where electrons flowing from Complex I/II via CoQ are passed to the last respiratory complex for oxygen reduction via cytochrome c. The multimeric protein is composed by 11 subunits but only one is mitochondrial-encoded (cytochrome *b*) [5]. The complex has also four prosthetic groups distributed in three subunits which are responsible for the electron flow: two *b*-type hemes (b_L and b_H) in cytochrome *b* subunit; one *c*-type heme (c_1) in cytochrome *c* subunit; and, one FeS cluster (2Fe/2S) in Rieske iron sulfur protein (ISP) subunit [5].

Surprisingly, Complex III only functions as a dimer, which means that the two monomers do not function independently. The globular domain of ISP interacts with

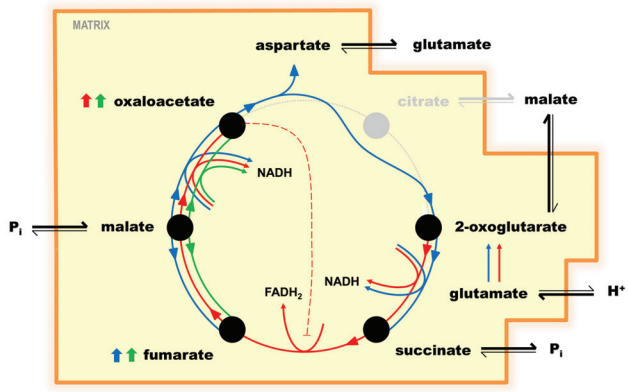

Figure 1.4: Scheme of OXPHOS sustained respiration through different substrates. In **green**, respiration sustained solely with malate; **red**, with glutamate and, **blue**, with glutamate plus malate. Inner mitochondrial membrane is represent in **orange**. Further details in text.

the quinol oxidation site of cytochrome b in the opposite monomer with a three-dimensional arrangement of the two monomers occurring, which allows the formation of two distinct cavities containing the CoQ binding sites [23, 35].

For sake of comprehension, the following lines describe the pathway of electron flow in a Complex III monomer [5, 23]; however, it should be taken into account that in reality, this process occurs as a cross-reaction between the two monomers in the dimer [35]. Non-reduced FeS cluster in IPS globular domain holds great positive charge, weakening its affinity for a spatial position close to the haem c_1 of cytochrome c subunit, causing a conformational alteration towards the CoQ-binding site near membrane outer-leaflet (Q_o) and close to b_L. Now that the full site is formed, a diffusible $CoQH_2$ can bind by interacting with residues in both subunits and one electron channeling from $CoQH_2$ to ISP is allowed. The reduction of FeS cluster attenuates its affinity for Q_o and ISP undergoes a conformational change again, leaving Q_o towards cytochrome c_1 where electron is ultimately passed to the cytochrome c via c_1 haem.

Simultaneously, a free radical semi-CoQ is formed as two protons are released to the inter-membrane space. Then a second electron is transferred from semi-CoQ to b_L and b_H. The position of both haem groups[4] means that electron retains its original energy since the fall to a more positive redox potential is compensated by the disadvantageous migration of a negative charge towards the membrane negative-side [5]. Remarkably, another CoQ binds to a different CoQ-biding site which is located in the membrane inner-leaflet (Q_i) in the vicinity of b_H, allowing electron acceptance and

[4] b_L is closer to the outer-leaflet experiencing the effect of a predominantly positively-charged environment while b_H is close to the matrix-face and therefore experiencing the opposite effect

consequent formation of semi-CoQ. The thermodynamically unfavorable transference became possible because semi-CoQ is strongly bound to the enzyme.

The cycle, initially proposed by Mitchell and termed Q-cycle [16], becomes complete when a new $CoQH_2$ enters the Q_o site and another *bifurcated* electron transference occurs. One of the electrons completes the reduction of tightly-bound semi-CoQ at Q_i and two protons are withdrawn from the matrix to complete the reaction.

$$2CoQH_2 + 2(Fe^{3+}{-}cytc) + CoQ + 2H^+_{in} \rightarrow 2CoQ + 2(Fe^{2+}{-}cytc) + CoQH_2 + 4H^+_{out} \quad (1.11)$$

However, since CoQ/CoQ_2 are indistinguishable when entering and leaving both CoQ-binding sites, equation 1.11 can simplified to:

$$CoQH_2 + 2(Fe^{3+}{-}cytc) \rightarrow CoQ + 2(Fe^{2+}{-}cytc) + 2H^+_{out} \quad (1.12)$$

Cytochrome-c:oxygen oxidoreductase

Cytochrome-c:oxygen oxidoreductase (EC: 1.9.3.1, cytochrome-c oxidase, Complex IV) is the last enzyme in the MRC and is responsible for the reduction of O_2 to water. The redox reaction generates a displacement of charges, i.e. Δp, not only because it consumes protons and electrons from opposite sides of the inner membrane[5] but also because the enzyme pumps four additional protons from matrix to inter-membrane space per reduced oxygen [5].

The multimeric protein is composed by 13 subunits being three of them mitochondrial encoded and responsible for the catalytic site (subunit I, II and III). However, subunit III does not contain cofactors and therefore does not participate in electron tunneling but it may nevertheless provide a channel for oxygen diffusion to the active site [23]. Subunit II includes a bimetallic copper centre (Cu_A) in its globular domain which remains outside the membrane providing a docking site for cytochrome c. Subunit I comprise two A-type haem, a and a_3, being the first one located closer to Cu_A [23]. Although both haem sites are indistinguishable, the latter has one of its coordination positions vacant which allows O_2 to bind. An additional copper (Cu_B) atom is found adjacent to haem a_3 and therefore this site is occasionally designated as binuclear center (BCN). Still, reduction in BCN is only feasible since one histidine of Cu_B is covalently linked to a nearby tyrosine residue, as discovered through crystallographic studies [5].

[5] electrons are delivered to Complex IV via cytochrome c in the inter-membrane space while protons are obtained from the matrix side

Subunit I also accommodates two proton channels resulting from the pathway provided by hydrophilic amino acids [23]. One is named *K* after a conserved lysine residue and leads protons from the matrix to BCN. Another one is named *D* after a conserved aspartate and conducts protons also from the matrix to a conserved glutamic acid residue close to the histidine and tyrosine of BCN. However, there is still a lot of debate in the field regarding which of the channels provide protons for oxygen reduction; if one, both or none are involved in proton pumping to the inter-membrane space; also, it remains to be elucidated the release route upstream from the BCN [23]. Nevertheless, a possible mechanism can be found elsewhere [36].

An extensive description regarding the mechanism of function of Complex IV was reviewed before [36], here we will briefly described a sequence of events. Electrons are delivered to Complex IV via reduced cytochrome c, being then transferred first to Cu_A followed by fast electron tunneling through haem *a* and then a_3 and Cu_B due to their close proximity. A total of four electrons and four protons are required for the reduction of one molecule of oxygen to two of water. The first two electrons are used for the complete reduction of BCN since both metals are assumed to coordinate with hydroxides. This actually involves two individual steps were an electron plus proton reduce a BCN metallic ion each, with simultaneous release of two water molecules.

Fully reduced and empty BCN binds O_2 to form a oxyferrous species which is however very unstable and rapidly decays to an extraordinary intermediate. The striking fact is that although only two electrons are provided by cytochrome c, four electrons are passed simultaneously to oxygen, breaking its double bond and forming two oxide products, one hydroxyl group bound to Cu_B and a high oxidation ferryl (Fe^{4+}=O) species at haem a_3. All transfered electrons have origin in BCN: one from cuprous Cu_B, two from ferrous a_3 and a forth from the covalently linked tyrosine-histidine ligand of Cu_B. The resulting tyrosine radical is uncharged as it donates a proton to the oxygen atom that results in hydroxide bound to Cu_B.

To finalize the cycle, two additional steps that lead to regeneration of oxidized state of BCN exist. Each step requires an haem *a* electron and one matricial proton which firstly reduce and protonate the tyrosine and secondly reduce ferryl to ferric hydroxide species (Fe^{3+}−OH). Despite the controversy around the proton pumping mechanism across the matrix, it is accepted that this involves three key steps which are sufficiently exergonic to drive proton pumping: reduction of the tyrosin, reduction of ferryl species, and complete reduction of BCN.

$$4(Fe^{2+}{-}cytc) + O_2 + 8H^+_{in} \rightarrow 4(Fe^{3+}{-}cytc) + 2H_2O + 4H^+_{out} \tag{1.13}$$

F_OF_1-ATPase

F_OF_1-ATPase, (EC:3.6.3.14, ATP phosphohydrolase (H^+-transporting), ATP-synthase, Complex V) is not commonly considered an integral constituent of MRC as it does not participate in charge displacement, i.e., generation of Δp, but rather uses it for phosphorylation of ATP. Therefore, the enzyme acts as a link between energy-generating and energy-transducing processes. Moreover, in some particular situations, the enzyme can also function in reverse due to its ATPase activity, hydrolyzing ATP to form an electrochemical potential [5].

The enzyme has a knob-like structure with a round part protruding into the matrix while a hydrophobic domains allows for its attachment to the membrane [37]. Upon treatment with specific chemical compounds, the multimeric complex can be dissociated in two major subunits accordingly to their solubility [5]: one is *Fraction 1* (F_1), the water-soluble part of Complex VI which after isolation from the membrane portion holds ATPase activity and which is termed F_1-ATPase. The other, is embedded in the membrane and generates rotary torque force upon proton translocation from the inter-membrane space to the matrix. Due to its sensitivity to oligomycin, this subunit was named F_O. ATP-synthase is homologous between several sources however, the one from mitochondria holds more complexity, which means more subunits. The following nomenclature refers to mitochondria whereas some subunits share the same name as in bacteria, although others have a different name or not even exist in the bacterial counterpart. Also distinct is the stoichiometry of a few subunits [5].

F_1 is constituted by distinct types of subunits: $\alpha_3\beta_3\gamma\delta\epsilon$-OSCP (subscripts refer to stoichiometry) [38]. The three α- and β-subunits are alternately arranged and form the hexameric stator ring around the γ-subunit which acts as rotor shaft. About $\frac{5}{2}$ of γ-subunit protrude from the $\alpha_3\beta_3$ core as a stalk-like structure and adopts a foot-like conformation togheter with $\delta\epsilon$. This allow the rotor shaft to interact and connect the rotor parts of F_1 and F_O [37]. Instead, the OSCP-subunit, which is positioned in the dimple of $\alpha_3\beta_3$ core and interacts with F_O subunit b, forms a second, peripheral, stalk-like structure connecting the stator parts of both subunits. The interaction of b-with OSCP-subunit is thought to act as a stator to counter the tendency of the $\alpha_3\beta_3$ core to follow the rotation of the central stalk [37].

The F_O subunit is composed by three main polypeptides: abc_{10}, where the first two (a and b) are mitochondrial-encoded and, although more subunits can exist, their function still remains obscure and is thought not to directly participate in energy-transducing [38]. The central channel of F_O is formed by ten c-subunits organized in a symmetric ring traversing the inner membrane and which is asymmetrically connected to a- and b-subunit. The rotation of c-ring is thought to be driven by proton channeling through two half channels facing opposite sides of the membrane in a-subunit [38]. Proton enter the half channel exposed to the inter-membrane space and is then transferred to the carboxy residue of c-subunit. This protonation neutralizes the negative charge of the residue, allowing clockwise rotation of the c-subunit away from a [38]. Simultaneously, the neighboring c-subunit at the anti-clockwise side interacts with the other half channel which has a hydrophilic environment to promote deprotonation of the carboxyl residue to the matrix [5]. Due to the stoichometry of 10 c-subunits, ten protons must return to the matrix per complete 360° rotation.

The rotation of the c-ring is transmitted to the asymmetric rotor shaft, γ-subunit, which rotates counter-clockwise against the $\alpha_3\beta_3$ core [39, 40]. Experimental studies have proposed a 'binding-change mechanism' for F_1 where alternating transitions between three chemical states work cooperatively during ATP synthesis [40]. One of the postulates is that at any given time, each catalytic site residing at three α-β boundaries but primarily in the β-subunit is able to assume one of three different conformations, varying in their affinity between substrates (ADP and P_i) and product (ATP). Conformation O (for 'open') is characterized by low affinity to ATP; conformation L loosely binds ADP and P_i; and conformation T tightly binds ADP and P_i. This feature is remarkable since tight bond of adenine nucleotides to the enzyme remarkably decreases the amount of free-energy necessary to promote formation of ATP. Therefore, Complex V displaces the mass-action ratio for ADP phosphorylation by 7 to 10 orders of magnitude from equilibrium allowing ATP formation and, rotary force torque generated by the Δp is transduced in conformational changes used to release formed-bound ATP from the enzyme [5].

Cleverly-designed experiments using F_1 and its ATPase activity concluded that for each complete revolution three ATP molecules are released 120°-wise steps [39]. Recent reports have provided more insights of F_1-ATPase reaction scheme ([41] and references therein). It is revealed that rotation shows two sub-steps or dwelling time at 80° and 40° corresponding to specific events during hydrolysis. Thus, the present reaction scheme of rotation of a single catalytic site is as follows: ATP binding at 0°,

hydrolysis at 200°, ADP release at 240° and P_i release at 320°.

$$10H^+_{out} + 3ADP + 3P_i \rightarrow 10H^+_{in} + 3ATP \tag{1.14}$$

Mitochondrial respiratory supercomplexes

Until the beginning of *XXI* century, the electron transference between respiratory complexes of MRC was believed to occur through random collisions, i.e. intermediary identities, such as CoQ or cytochrome c, would move freely within the IMM and eventually *collide* and transfer electrons from one complex to another [42], an idea initially proposed by Hackenbroock and called "fluid-state model".

However, a new model was introduced that challenged this view, where the interaction between respiratory complexes occurs within high organized supramolecular structures (supercomplexes), the so called "solid-state model" [43]. The existence of supercomplexes is supported by several experimental evidences (enumerated and referenced elsewhere, [42]), ranging from blue-native electrophoresis in-gel activity to electron micrographs.

The main advantage of the existence of supercomplexes is the enhancement of electron transfer through reduction of the diffusion distance of mobile electron carriers between respiratory complexes. Additionally, it was also documented that super complex formation is crucial for assembly and stability of OXPHOS complexes monomers [42, 44].

Excepting Complex II, all other OXPHOS complexes can form supercomplexes structures [42, 44]. The stoichiometry and presence of individual complexes within the supramolecular structure will vary between species, tissue and physiological condition [42, 44]. Complex I can be found associated with dimeric Complex III (Complex III_2) while Complex III_2 itself can associate with up to four individual Complex IV. Additionally, an interaction between Complex I, III_2 and IV can also be found and is sometimes called *respirasome* due to its ability to sustain respiration in the presence of CoQ and cytochrome c [42, 44]. Further organization level of OXPHOS complexes was recently shown [42], as apparently supercomplexes I+III_2+IV can exist in a string or row-like organization comprised by several I_2+III_2+IV_2 subunits. In this context, the cardiolipin phospholipid seems to play an important role during assembly and stability of supercomplexes since, at least on yeast lacking cardiolipin, alterations at the supercomplexes level are correlated with decreased OXPHOS efficiency [44].

In contrast, Complex V does not require cardiolipin for its oligomerization [44]. Although Complex V can function as a monomer it is usually seen as a dimer or even as a long oligomer. In the dimeric form, Complex V F_o portions face each other in an angle ranging from 35-90 ° which causes IMM to curve [42]. This fact supports the role of oligomeric Complex V in crisate morphology.

Pedersen and co-workers have provided evidences of a "metabolon" between Complex V, PiC and ANT in a 1:1:1 stoichiometry which the authors designated by *ATP synthasome* [45]. Pic and ANT are thought to be non-centrally located within the base piece of Complex V and ultimately support an efficient and coordinated mechanism for the terminal steps of OXPHOS.

1.3 Calcium homeostasis and the mitochondrial permeability transition

Despite some initial controversy, in the 60's it became established that mitochondria accumulate and handle calcium (Ca^{2+}, [46] for an insightful review how mitochondria stumble upon Ca^{2+}). Thus, extensive research has been done to know the mechanisms of calcium uptake and release. However, although some pathways are general accepted their molecular players remain to be elucidated. This is the case of the mitochondrial permeability transition pore (mPTP) which suffered a structural reformulation in the last years and, the mitochondrial calcium uniporter (mCU) whose molecular identity was proposed last year by Rizzuto lab [47].

1.3.1 Mitochondrial Ca^{2+} accumulation in cellular context: *a unified model*

Although the Ca^{2+} concentration usually observed in cytoplasm did not seem compatible with the affinity of mCU, it was later found that mitochondria can be located juxtaposing with the endoplasmic reticulum (ER) inositol triphosphate (IP_3) receptors or plasma membrane channels [48, 49]. In fact, intramitochondrial Ca^{2+} spikes close resemble those of cytosolic spikes and the idea of *Ca^{2+} micro-domains* emerged [50]. This theory postulates that although mitochondrial Ca^{2+} affinity is low and the bulk cytosolic calcium slightly rises during excitation, the spatial organization of the mitochondrial network in close proximity to intracellular Ca^{2+} stores allows the mCU

to sense Ca^{2+} concentrations much higher than those in cytosolic bulk [51].

Mitochondria controls Ca^{2+} by three distinct and cooperative means, all tightly coupled to its energetic shape: Ca^{2+} uptake from the extra-mitochondrial compartment ($\Delta\psi$-dependent), Ca^{2+} buffering in mitochondrial matrix (ΔpH-dependent) and Ca^{2+} efflux to adjacent areas (Δp-dependent). It is therefore no surprise that mitochondria play an important role in cellular Ca^{2+} signals by shaping those same signals [50, 52].

As extra-mitochondrial $[Ca^{2+}]$ ($[Ca^{2+}]_e$) increases so does matrix free $[Ca^{2+}]$ ($[Ca^{2+}]_m$) eventually reaching a steady-state equilibrium through the action of the mitochondrial sodium-calcium exchanger (mNCX). At this time, one can say that $[Ca^{2+}]_m$ varies linearly with $[Ca^{2+}]_e$. However, once $[Ca^{2+}]_e$ rises above this *set-point*, usually $\sim$500 nM, the Ca^{2+}-dependent mCU activation comes into action and mitochondrial Ca^{2+} accumulation truly occurs. Still, the Ca^{2+} influx is not synonymous of $[Ca^{2+}]_m$ increase since at this point phosphate-dependent Ca^{2+} buffering counterbalances $[Ca^{2+}]_m$ increase.

If Ca^{2+} is accumulated in mitochondria in the absence of weak acids it will abolish $\Delta\psi$ and decrease Δp, stimulating OXPHOS and thus increasing ΔpH. This will likely be a limiting factor since ΔpH is of limited increase. However, cells contain phosphate and furthermore mitochondria contain a phosphate symporter. In this case, phosphate is electroneutral co-transported along with protons dissipating ΔpH and reestablishing $\Delta\psi$. However, the most striking feature is the role of phosphate which complexes in a alkalization-dependent fashion with free Ca^{2+} resulting in the formation of low solubility complexes and thus buffering and maintaining $[Ca^{2+}]_m$ constant thorough the accumulation process [53].

The importance of mitochondrial Ca^{2+} accumulation is primarily the regulation of metabolism. There are several matrix enzymes that have allosteric Ca^{2+}-dependent activation sites including isocitrate dehydrogenase, α-ketoglutarate dehydrogenase or pyruvate dehydrogenase [54, 55]. The upregulation of these three rate-limiting enzymes results in a net reduction of reducing equivalents, namely NADH and $FADH_2$ [55], and a boost in OXPHOS. Moreover, Ca^{2+} also activates ANT and Complex V [54, 55]. Similarly, a faster calcium uptake mode (RaM, Section 1.3.2) may allow a burst of $[Ca^{2+}]_m$ prior to equilibrium, which is high enough to activate metabolism and minimize the energy cost associated to $[Ca^{2+}]_m$ efflux between $[Ca^{2+}]_e$ pulses [56]. Bringing together all the data, the idea that Ca^{2+} accumulation represents a mechanisms to couple ATP supply with demand is very attractive but still lacks some

experimental support [53, 55, 56].

Mitochondrial Ca^{2+} handling also plays an important role in shaping the spatio-temporal $[Ca^{2+}]_c$ spikes. Nevertheless, the way that such mechanism is depicted in the cellular context will vary depending on the type of cell [53]. For instance, mitochondria in oocytes enhance the propagation and coordination of $[Ca^{2+}]_c$ waves while in astrocytes, mitochondria act as a sink thus limiting the rate and extent of the waves. Alternatively, polarized cells such as pancreatic acinar cells, contain a longitudinal mitochondrial band that isolates the secretory pole restricting therefore the spreading of $[Ca^{2+}]_c$ signals from the apical pole. All previous examples are referenced and delightful exposed elsewhere [53]. Nonetheless, in a normal basis the close apposition of ER and mitochondria allows the latter to: prevent Ca^{2+}-dependent inactivation of IP_3 receptors by removing Ca^{2+} from micro-domains; and, to keep $[Ca^{2+}]_c$ low near the channels thus facilitating calcium influx [49].

Ultimately, when Ca^{2+} uptake exceeds that of *set-point* the buffering mitochondrial capacity is consumed and massive free mitochondrial Ca^{2+} accumulation takes place. In such circumstances, usually associated with supra-physiological conditions, mitochondria became prone to a devastating state denominated by mitochondrial permeability transition (sec. 1.3.4).

1.3.2 Mitochondrial Ca^{2+} uptake pathway

Cytosolic Ca^{2+} has to cross both OMM and IMM to accumulate in the matrix. IMM is highly impermeable thus providing the effective barrier to ion accumulation. However, the role of OMM in regulating the entry of Ca^{2+} in mitochondria where Ca^{2+} was thought to move *freely* between cytosol and inter-membrane space through VDAC has been recently questioned [53, 57].

Regulation of Ca^{2+} influx through the outer membrane by VDAC

VDAC is a highly conserved large α-helix/β-barrels mitochondrial outer transmembrane protein with at least three isoforms in higher eukaryotes [58, 59]. VDAC1 is by far the most abundant in almost all cells and, as all other isoforms, can exist in different oligomerization states [59]. The channel, mainly known for its role in metabolite/ions channeling, is voltage dependent and shows ion selectivity. At low voltages

(10mV), a open-state with weak selectivity for anions over cations is observed while at high potentials (<40 either negative or positive) the channel eventually closes. Still, it can present several sub-states with different selectivities and permeabilities, mostly for small cations [58, 59].

The idea that VDAC controls the process of Ca^{2+} entry in mitochondria originates from several experimental evidences. For example, VDAC modulates its function during several cellular events, e.g. apoptosis or ATP turnover [60], so it is reasonable to believe that Ca^{2+} cross-talk between cytosol and mitochondrial matrix will likely be affected. Another interesting point of view was the fact that over-expression of VDAC was shown to facilitate Ca^{2+} signal propagation into mitochondria [53, 60], raising the possibility of VDAC as an effective drug target.

Moreover, VDAC possesses Ca^{2+} -binding sites, i.e. it might function as a Ca^{2+} -activated Ca^{2+} channel [53, 57]. Additionally, the inhibitory effect of ruthenium red (RuR) on Ca^{2+} accumulation through the inner membrane might not be directly on the mCU but also due to interaction and inhibition of VDAC permeability to Ca^{2+} [57]. Nevertheless, we cannot rule out the possibility of other proteins other than VDAC to modulate the Ca^{2+} uptake pathway at the outer membrane level since VDAC knockdown did not altered the sensitivity of mitochondria to Ca^{2+}, as suggested previously [53].

Mitochondrial calcium uniporter

The primary uptake route of Ca^{2+} through the inner membrane is electrophoretically driven by a uniport system, the mCU. While $\Delta\psi$ is usually referred as the drive-force of Ca^{2+} uptake one should bear in mind that the *effective* energy is in fact the electrochemical potential of Ca^{2+} : $-\Delta\tilde{\mu}_{Ca^{2+}}/F = 2\Delta\psi + 2.3RT\, log_{10}\frac{[Ca^{2+}]_{\text{matrix}}}{[Ca^{2+}]_{\text{cytosol}}}$.

The channel has an electrogenic nature with second-order kinetics (separate Ca^{2+} activation and transport sites) and high selectivity for Ca^{2+} with $K_d < 2\,\text{nM}$ as determined by patch-clamp studies and can be *specifically* inhibited by RuR, a inhibitor of different Ca^{2+} channels [53, 54, 56]. Although found at very low amounts the mCU has very high V_{max} corresponding to a flux of $\sim$ 20000 Ca^{2+} s^{-1} equivalent to those measured for fast gated pores [61]. Besides RuR, magnesium (Mg^{2+}) also antagonizes mCU by a putative Mg^{2+} binding site at the cytosolic side of the channel while several nucleotides have different strength to promote channel inhibition:

ATP>CTP=UTP>GTP [49].

Various protein kinases were in turn able to modulate Ca^{2+} uptake through mCU [49]. However, as pointed out [48], mCU is located in the IMM thus sheltered from the catalytic activity of those kinases. Nevertheless, it could mean an indirected process mediated through modulation of VDAC-Ca^{2+} permeability as suggested in the previous section.

In the past years, the scientific community have suggested some glycoproteins with Ca^{2+} binding and channelling properties as the identity of the channel. Uncoupling proteins (UCP)-2 and -3 were also suggested after observing that they conceive part of RuR-sensitivity and their overexpression increased mitochondrial Ca^{2+} accumulation [53, 54]. However, in one way or another these proposals do not fulfill the role of mCU [61].

Using *in silico* techniques of comparative proteomics and integrative genomics in the MitoCarta[6] database, two groups have suggested three candidates for mCU identity [47, 63, 64]. One *mitochondrial calcium uptake 1* (MICU1) or CABARA1 might serve as regulator while the CCDC109A, or *MCU* as called by the authors, might act as a core component of the channel [63, 64]. Both proteins were found to be inserted in IMM and show RuR sensitivity. However, *MCU* over expression was not able to increase mitochondrial Ca^{2+} accumulation. Authors suggested that other chaperones might be limiting channel activity *in vivo*.

However, that might also suggest that other proteins might be involved in the process. In fact, Rizzuto and colleagues found a different protein using the same approach with properties able to fulfill mCU requirements [47]. The following years will be necessary to tie up loose ends including the question whether is the channel composed by one protein only or is rather a hetero-oligomer. Also, what are the protein-mediated processes regulating/modulating Ca^{2+} flux through mCU?

Rapid uptake mode

A different Ca^{2+} uptake pathway was described in liver and heart and to a less extent in brain mitochondria [52, 65]. The properties of this pathway are distinct from those of uniporter, being named mitochondrial rapid mode calcium uptake (RaM). The

[6] "MitoCarta is an inventory of 1098 mouse genes encoding proteins with strong support of mitochondrial localization." [62] Source: www.broadinstitute.org/pubs/MitoCarta/

uptake is hundred of times faster compared to the uniporter and facilitates therefore rapid Ca^{2+} influx upon cytoplasmic Ca^{2+} pulses which might provide a faster way to quick activate Ca^{2+}-dependent mitochondrial mechanisms.

The pathway also shows different inactivation sensitivities by Ca^{2+} [65]. For example, the pathway saturates quickly in the heart since about one minute is required to reset RaM while in liver the delay drops to a fraction of second upon cytosolic calcium decrease below 100 nM [53, 54]. RaM is inhibited by RuR and activated by spermine and driven by $\Delta\psi$ as the mCU, suggesting a possible high activity mode of the uniporter [49] still, everything is under constant debate.

1.3.3 Mitocondrial Ca^{2+} efflux pathway

Theoretically, if we take into account the Nerst equation and a $\Delta\psi$ of $-180\,\mathrm{mV}$, a thermodynamic equilibrium between cytosolic $[Ca^{2+}]$ ($[Ca^{2+}]_c$) of $\sim 100\,\mathrm{nM}$ would require mitochondria to accumulate $\sim 100\,\mathrm{mM}$ Ca^{2+} in the matrix. However, $[Ca^{2+}]_m$ never reaches such values in larger part due to the two distinct mechanism that lower the *effective* $[Ca^{2+}]_m$: ion buffering and efflux.

Sodium-dependent Ca^{2+} efflux

In excitable cells such as the heart, brain and skeletal muscle as well as in parotid gland, adrenal cortex, brown fat, and many other tissues, the predominant Ca^{2+} efflux pathway is mNCX [54, 56]. The channel show similarities with its counterpart in the plasma membrane but it can be considered a new isoform, mitochondrial specific, of the NCX family [66]. Initially, it was believed that mNCX was electroneutral but nowadays it is suggested that it extrudes Ca^{2+} in a stoichiometry of 1:3 ion of Na^+, an eletrogenic activity which is inhibited by CGP37157, tetraphenylphosphonium (TPP), trifluroperazine, diltiazem, verapamil, clonazepam, and amiloride [48, 56, 66].

The problem with the 3:1 operation is the evidence that it requires $\Delta\psi$ to function and predicts mitochondrial depolarization during calcium efflux. However, the sodium-proton antiporter (Na^+/H^+) can counterbalance the process by building up a Na^+ gradient [53]. From the point of view of kinetics, mNCX shows first-order kinetics for Ca^{2+} and second-order kinetics for Na^+ with V_{max} slight different between tissues but much lower than mCU [56].

Sodium-independent Ca^{2+} efflux

In liver, kidney, lung, and smooth muscle, the dominant Ca^{2+} efflux pathway is the Ca^{2+}/H^+ antiporter [54, 56]. The molecular entity of the channel was uncertain until Clapham *et al.* shed some light into this topic [67]. The work reported a IMM protein, Letm1, capable of Ca^{2+} uptake into mitochondria when over-expressed and which fulfilled the criteria of Ca^{2+}/H^+. However, this challenging idea may be cumbersome because Letm1 was previously ascribed to K^+/H^+ antiporter and its proposed stoichiometry of 1:1 is not with agreement with the initial electroneutral character, as stated in the review by Santo-Domingo and Drago [49, 66]. From the point of view of kinetics, Ca^{2+}/H^+ shows second-order kinetics for Ca^{2+} with V_{max} lower than mCU, being inhibited by TPP, cyanide, and low levels of uncouplers [56].

1.3.4 Mitochondrial permeability transition pore

The mitochondrial permeability transition is characterized by a sudden increase in the permeability of the IMM. This phenomenon is ubiquitously present in all cells and it is accepted that it originates due to the opening of non-selective pores which allows the free passage of any molecule smaller than 1.5 kDa [68]. The mPTP is found in IMM, specially, in contact sites with the OMM [69]. From patch-clamp studies it was found that mPTP is a voltage- and Ca^{2+}-dependent, cyclosporin A (CsA)-sensitive and high conductance mega-channel with ∼2.3 nm diameter [70]. Mitochondrial dysfunction induced by mPTP is a consequence of mitochondrial calcium overload [71]. In fact, *in vitro* studies show that Ca^{2+} is the trigger for mPTP opening although that can still occur without significant Ca^{2+} accumulation since other variables sensitize and lower mPTP Ca^{2+} threshold close to that of resting $[Ca^{2+}]_m$ [72].

mPTP opening is particularly facilitated when Ca^{2+} accumulation is accompanied by oxidative stress [73], mitochondrial depolarization, elevated phosphate concentrations and adenine nucleotide depletion [68]. In opposition, inhibition of the mPTP can be achieved with CsA, Mg^{2+}, ADP and antioxidants [74, 75]. Briefly, sensitizing and/or desensitizing agents should act in one (or several) of the following crucial points of mPTP [70, 72]:

a) *alter CyP-D binding to mPTP membrane component*;
   e.g., ⊕: oxidative stress, increased matrix volume; ⊖: CsA and analogues
b) *regulate nucleotide binding to ANT*;

e.g., ⊕: oxidative stress, thiol reagents, ANT *c* conformation, adenine nucleotide depletion, high phosphate, low $\Delta\psi$; ⊖: ANT *m* conformation, high $\Delta\psi$

c) *alter Ca^{2+} binding to mPTP trigger site.*
e.g., ⊕: high *p*H ; ⊖: low *p*H , Mg^{2+} and other divalent cations

Additionally, several cellular proteins, including several kinases are able to modulate mPTP opening either via the matrix or cytosolic side [76]. When the permeability barrier is disrupted, low molecular weight solutes, including ions and cofactors, move freely through the membrane promoting deleterious effects on mitochondria. One is the disruption of metabolic and ion gradients, from the $\Delta\psi$ to $[Ca^{2+}]_m$ but also the energetic imbalance of ATP/ADP ratio between the matrix and cytosol [68]. Consequently, mitochondria suffer a sharp drop in Δp and ATP hydrolyses occur due to reversal of the ATP-synthase in an attempt to reestablish $\Delta\psi$ [70].

Since mPTP size-exclusion is ∼1.5 kDa, proteins are not usually transferred between the matrix and cytosol. Additionally, protein concentration in cytosol is several times greater than in mitochondrial matrix resulting in a colloidal osmotic pressure that leads to mitochondrial swelling [68]. If the mPTP remain open indefinitely, as usually occurs during pathological events, mitochondrial structural alterations will cause the expansion of IMM and consequent mechanical disruption of OMM, which has a smaller area. Other consequences for the mitochondrion during the mPTP, include membrane depolarization and OXPHOS uncoupling, inhibition of respiration due to loss of co-factors and/or cytochrome c and increase in oxidative stress via direct transfer of electrons to O_2 following loss of redox potential.

A number of compounds and deleterious conditions increase the sensitivity to cardiac mPTP opening *in vitro* as well as *in vivo* and that peculiarity is often used to explain their deleterious effects in the organ. Examples include the anti-cancer doxorubicin ([77–79] and next chapter) and ischemia-reperfusion [73, 80]. Several strategies to prevent such actions are usually applied in the form of antioxidants, calcium chelators or specific inhibitors of the mPTP [81].

Classical model of mPTP

Since mPTP spans mitochondrial membranes initial thoughts were that proteins from both IMM and OMM should comprise in pore structure. Moreover, failure to ob-

serve mPTP in mitoplasts[7] strengthened the idea that OMM was indeed crucial [82]. Thereby it was initially proposed that a multi-protein supercomplex between VDAC–ANT–CyP-D was formed during specific cellular events [76].

There were several evidences supporting this theory. VDAC was among several other proteins shown to co-purify in a complex with ANT and was therefore circumstantially involved in the structure of the pore. When VDAC–ANT complexes were reassembled into liposomes mPTP-like activity was observed [70]. The involvement of ANT was even more evident. mPTP is modulated by [ATP] or [ADP] content and moreover, regulation of the pore can also be achieved by incubation with ANT-specific inhibitors, carboxyatractyloside (CATR) or bongkrekic acid (BKA), either enhancing or decreasing the probability o pore opening [83]. Oxidative stress and chemical agents that stimulate cross-links promote the dimerization of ANT monomers which is intimately related to mPTP formation [70]. Finally, it was found by using an antibody raised agains rat liver ANT that CyP-D immunoprecipitates with the in a CsA-dependent fashion [84]. The knowledge at the time of discover regarding mPTP inhibition by CsA was not sufficient to indicate such mechanism [85]. However, later CyP-D was identified as the target of CsA and has been since then an hallmark in mPTP machinery [86].

The model proposed at that time was that CyP-D binds to ANT and then, when triggered by Ca^{2+} , leads the ANT to undergo a conformational change to induce pore formation [82, 83]. Alternatively, Lemasters suggested a different perspective [87] where oxidatively damaged or misfolded proteins aggregate in mitochondrial membranes exposing their hydrophilic residues thus forming mPTP. Chaperone proteins were then capable to inhibit the process through binding to mPTP proteins with Ca^{2+} causing CyP-D to disturb protein–chaperone complexes and opening of the pore.

"The three make one Pore"... do they?

Molecular genetics were able to shed more light in the role of each individual component of mPTP by generation of double knock-out mice. The creation of $ANT^{-/-}$ was the first step to acknowledge that molecular structure of mPTP was far from being established. Around seven years ago, Wallace *et al.* observed that $ANT^{-/-}$ mice still show mPTP CsA-sensitive activity although increased $[Ca^{2+}]_m$ was necessary to activate mPTP, although no longer regulated by ANT ligands [88]. The work provided

[7] mitochondria fractions lacking the outer membrane

strong evidences that ANT was not essential for pore formation, i.e. was not the channel identity element, but could rather play a role in its regulation.

One year later, Baines and three other independent groups showed that CyP-D$^{-/-}$ mice are highly resistance to Ca^{2+}-induced mPTP opening behaving similarly with its wild-type counterparts treated with CsA [86, 89–91]. Moreover, these mice do not exhibit CsA-sensitive mPTP opening. These observations are consistent with the idea that mPTP pore opening presuppose a conformational change in a membrane protein that is triggered by Ca^{2+} and facilitated by CyP-D, although it can still occur in mitochondria lacking functional CyP-D. Basically, from the mPTP point of view, CyP-D is the unique target of CsA and an important regulator but is not a component of the channel. Additionally, it was also proved that CyP-D is not crucial in the apoptotic pathway and mPTP role in cell death is mainly through necrotic rather than apoptotic pathways [92].

The previous lines still suggest CyP-D interaction with a membrane protein but its identity was yet to be known. However, the group who initially identified the possible ANT–CyP-D interaction [84] reported recently that the antibody used was not specific to ANT but rather to the phosphate carrier (PiC) [83, 93]. Moreover, the interaction is increased in conditions that enhance pore formation and decreased by mPTP desensitizers [93]. This strongly suggest that PiC rather than ANT is the major protein interacting with CyP-D in forming mPTP. Additionally work using CATR-treated mitochondria passed through a phenylarsine oxide[8] identified an interaction between ANT and PiC which could be prevented by mPTP inhibitors [93]. Therefore the authors remodeled the mPTP in which PiC has the lead role instead of ANT but where the interaction of ANT *c* conformation with PiC favors the pore formation [70]. The conformational changes of both proteins are triggered by Ca^{2+} and facilitated by CyP-D activity but can still occur in the absence of the chaperone at high [Ca^{2+}].

At the same time, Bernardi *et al.* demonstrated that CyP-D ablation unmasks an inhibitory site for phosphate which is the actual mPTP desensitizer [94]. In their view [95], when CyP-D is present and bound to mPTP the site for phosphate is not available and the pore favors its open state. However, if CyP-D is removed either genetically or pharmacologically by addition of CsA the phosphate site becomes exposed and phosphate binding enhances the closed state. Additionally, if phosphate

[8] used in experiments within the context of mPTP as a vicinal thiol group cross-linker

concentration is high enough it can still favor the closed state in the presence of CyP-D. Nevertheless, a serious discussion is in place regarding the role of phosphate and its carrier on mPTP formation and regulation [76, 93–96]. The last report with respect to siRNA for PiC in HeLa cells (∼70% decrease) showed no differences in mPTP sensitivity between silenced and control cells [96].

If the doubts were not ample enough, recent reports throw more players in the mPTP regulation. The electroneutral ATP-Mg^{2+}/Pi antiporter desensitizes mPTP by Ca^{2+} buffering [97] and CyP-D was found to interact with ATP-synthase in phosphate-dependent fashion and competed for CsA rising suspicions about the role of Complex V in mPTP [95, 98].

1.4 Mitochondrial role in oxidative stress

MRC is most likely the major redox system in the cell and is therefore acceptable to assign it as one important source of reactive oxygen species (ROS), as several redox carriers can potentially leak single electrons to molecular oxygen. As expected, initial work by Chance [99] showed that isolated mitochondria can produce ROS; since then literature has erroneously reported that 1% of O_2 consumed by mitochondria is converted in ROS. However, as the original authors warned, the *in vitro* conditions that isolated mitochondria were subject to, such as O_2 pressure, NADH/NAD^+ or Δp are far from those to be experienced inside the cell [100]. In fact, if variables are molded to achieve a *quasi*-physiological state, mitochondria ROS production is lowered to a negligible ∼0.1 to 0.01% of the total O_2 consumed [101, 102]. This question was recently reviewed with a bold title: '*There is no evidence that mitochondria are the main source of ROS [...]*' [102]. In fact, besides MRC there are several others redox systems throughout the cell reported as capable of forming significant amounts of ROS ([102], and references therein):

a) *Endoplasmic reticulum*;
   e.g., cytochrome P450 and *b5* and diamine oxidase;
b) *Peroxisomes*;
   e.g., fatty acid oxidation enzymes, D-amino acid oxidase, L-2-hydroxyacid oxidase and urate oxidase;
c) *Cytosol*
   e.g., NO synthase, lipoxygenases and prostaglandin H synthase;

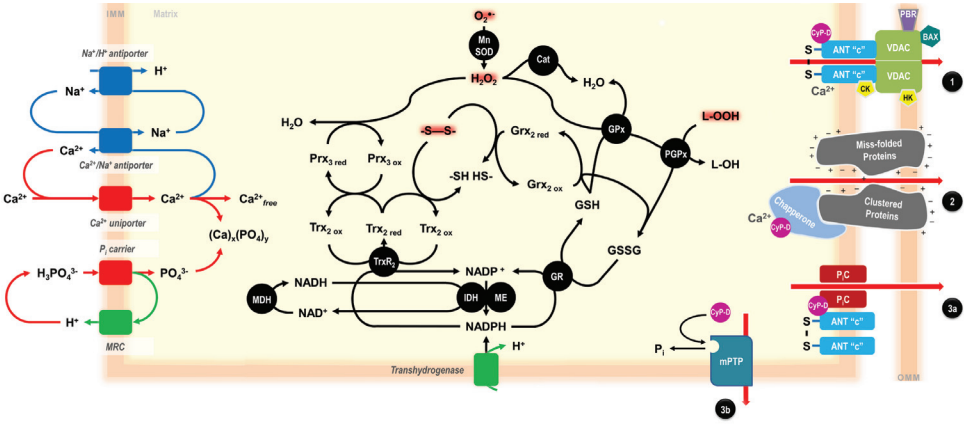

Figure 1.5: Mitochondrial calcium homeostasis and redox status maintenance. On the **left**, calcium influx (**red**) and eflux (**blue**) pathways; **center**, antioxidant machinery; and, **right**, proposed mPTP structures: **1** - classical model [83], **2** - Lemaster's model [87], **3a** - Halestrap most recent model [70] and **3b** - Bernardi most recent model [95]. See text for further details. Abbreviations: *-SS-* - disulfide bonds; *-SH HS-* - sulfhydryl groups; *L-OOH* - lipid hydroperoxide; *L-OH* - lipid hydroxide; *GSH* - glutathione; *GSSG* - oxidized glutathione; *Mn-SOD* - manganese superoxide dismutase; *Cat* - catalase; Prx_3 - peroxiredoxin 3; Grx_2 - glutaredoxin 2; *GPx* - glutathione peroxidase; *PGPx* - phospholipid hydroperoxide glutathione peroxidase; Trx_2 - thioredoxin 2; $TrxR_2$ - thioredoxin reductase 2; *GR* - glutathione reductase; *MDH* - malate dehydrogenase; *IDH* - isocitric dehydrogenase; *ME* - malic enzyme; *PBR* - peripheral benzodiazepine receptor; *CK* - creatine kinase; *HK* - hexokinase; P_iC - phosphate carrier.

d) *Plasma membrane*

e.g., NADPH oxidase, lypoxygenase;

e) *Extracellular matrix*

e.g., xanthine oxidase.

Hence, one of the few works that have carried a systematic study relating production of hydrogen peroxide (H_2O_2) and specific cellular structures showed that microsomes, peroxisomes, mitochondria and cytosol contribute 45%, 35%, 15% and 5%, respectively to total ROS production in rat liver [102, 103]. Certainly, the distribution will differ between cell type, species, physiological and pathophysiological conditions, and probably the type of ROS.

It is worth to introduce two new concepts: compartmentalization and antioxidant systems. These are important to define how a cellular structure definitely has a net production of ROS that can be detected by other parts of the cell. The compartmen-

talization not only defines the ability of the ROS molecule to cross membranes and diffuse throughout the cell or be restricted in its site of formation instead, but also how the antioxidant machinery works independently between organelles. These will be discussed in detail in the following sections. Regarding our last example, great part of H_2O_2 is readily eliminated by catalase within peroxisomes thus net ROS production in peroxisomes will be substantially decreased [102].

Intracellular ROS are inexorable and their role in physiological signaling has received great attention in recent years [104]. Nevertheless, the cell and particularly mitochondria seems to have evolved to have a tight control of the process. Still, if the orchestra is spatio-temporally out of tune, either by a stimulation of basal ROS production or by failure of antioxidant defenses to neutralize radicalar species, the resulting imbalance will increase ROS levels to a harmful state termed oxidative stress. An interesting alternate definition, "a disruption of electron transfer reactions leading to an oxi-antioxidant imbalance and oxidative damage", can be found elsewhere [105] .

1.4.1 Eeny, meeny, miny, moe... The ROS inventory

Paramagnetic molecular oxygen is a fat-soluble molecule which has two unpaired electrons in anti-bonding orbitals with parallel spins allowing one-electron reduction [100, 106]. Thus, ROS are partially reduced derivatives of O_2 initiated by primary *semi*-reduction of O_2 to superoxide anion ($O_2^{\bullet-}$). Although this reaction is not thermodynamically favored due to its low standard reduction potential of $-160\,\text{mV}$ at pH 7 [100], the actual reduction potential is quite high ($E_h = 68\,\text{mV}$) even at low [O_2] and high [$O_2^{\bullet-}$] [100, 106]. The reaction is further favored by immediate dismutation of $O_2^{\bullet-}$ to H_2O_2 which kepts [$O_2^{\bullet-}$] low.

The process can occur spontaneously in a second-order kinetics through co-ordinated loss of an electron pair to oxygen resulting in the production of H_2O_2. However, this reaction is relatively slow ($k = 10^6\,\text{M}^{-1}\,\text{s}^{-1}$) compared with its enzymatic counterpart catalyzed by superoxide dismutase (SOD, $k = 2\times10^9\,\text{M}^{-1}\,\text{s}^{-1}$) [100]. $O_2^{\bullet-}$ has a low pK_a (4.7) and at physiological pH its membrane-soluble protonated form, hydroperoxyl radical ($HO_2^{\bullet}$) exist only at non-significant levels [107]. In the presence of high [H_2O_2] and [$O_2^{\bullet-}$] the former may react with free metal irons, particularly ferrous iron (Fe^{2+}) released from FeS-containing proteins, via the Fenton reaction yielding ferric iron (Fe^{3+}), hydroxide anion and the highly reactive hydroxyl radical ($HO^{\bullet}$).

The reactivity of each radical and thus its biological risk is closely related to their half-life ($t_{1/2}$). $HO^{\bullet}$ is by far the most unstable and high reactive form of ROS ($t_{1/2}$ =10^{-9} s) followed by $O_2^{\bullet-}$ (10^{-6} s) and H_2O_2 (10^{-5} s) [106]. Additionally, biological risk is also proportional to their radius of action dictated by the free aqueous diffusion distance with $O_2^{\bullet-}$ and H_2O_2 present in the upper limit with 0.16 to 0.46 µm, respectively [106]. Nevertheless, the real values in mitochondrial matrix will be considerable lower due to its high viscosity and high activity of the antioxidant machinery. In conclusion, $O_2^{\bullet-}$ can be considered as a *local* signaling ROS while H_2O_2 acts as global signaling one.

1.4.2 Mitochondrial sources of ROS

Although several redox pairs in mitochondria have enough reduction potential to promote one-electron reduction of O_2, only a small part actually perform it [100]. The insulation by bulky protein groups confers to some extent protection to these redox couples by keeping O_2 at a safe distance. Therefore, sites in MRC where one-electron reduction occurs, e.g. FeS centers, or where stable one-electron reduced stable intermediates are formed, e.g. flavins prosthetic groups or quinones, are hotspots in terms of ROS production.

Murphy suggested an interesting equation to address the determinant factors in $O_2^{\bullet-}$ production mediated by proteins [100]: $d[O_2^{\bullet-}]/dt = k[O_2]P_R[E]$. From his point of view, rate is directly proportional to $[O_2]$ perceived in mitochondria and the total amount of enzyme. However, the most important factor is probably the reduced form of enzyme capable of reacting with O_2 (P_R) which is intimately related with its E_m. Therefore, events affecting E_m such as inhibition, damage, mutation or post-translational protein modification are capable of affecting P_R as well [100]. Lastly, reaction will directly depend on the second-order rate constant (k) which is believed to occur in accordance to Marcus theory [100, 108]. The theory explains the rate at which an electron can move or jump between redox pairs by an outer-sphere mechanism. The same line of thought is applied for electron tunneling in MRC where carriers must be at maximum distance of 14 Å for successful transference [109].

Although several mitochondrial enzymes are able to produce ROS (cytochrome b_5, monamine oxidase, α-glycerophosphate dehydrogenase, α-ketoglutarate and electron-transfering flavoprotein:ubiquinone oxireductase) [110] the next two sections will give particular focus on the two respiratory complexes that have been described to generate

sufficient amounts of ROS.

Complex I

This respiratory complex is believed to produce ROS at three distinct reduced sites including FMN, FeS clusters and CoQ binding site [54, 102], although continuing discussion regarding the true locus of production being FeS or FMN proceeds [107, 111]. Besides, Complex I has two different pathways for ROS production, namely forward electron transference (FET) and reverse electron transference (RET).

The latter is usually observed in isolated mitochondria in the presence of succinate-sustained respiration. The resulting high Δp and reduced Q-pool drive electrons thermodynamically upward into Complex I with concomitantly reduction of NAD^+. This event is without question were the majority of ROS production is observed and is easily inhibited by rotenone and uncouplers while being further increased by antimycin A [101, 110]. However, its biological significance is small since Complex II is not the primary entry of electrons in MRC in cells and the Δp is considerably lower due to constant ATP demand and production [100, 101, 111].

FET is usually observed in the presence of NAD^+-linked substrates but ROS produced trough this route are considerably negligible [110]. However, in the presence of inhibitors, ROS production increases although not as much as in RET [111]. In this case, $NADH/NAD^+$ ratio is pivotal in determining the proportion of reduced FMN (P_R) since electrons entering the complex with diminished capacity to exit through their normal route and high reduced flavin results in an increased probability of de-route to O_2 [100]. Moreover, Δp dependence is not as demanding as in RET since ROS are produced in the presence of rotenone [107, 110]. Nevertheless, Complex I is more sensitive to ΔpH component of Δp since nigericin[9] abolishes $O_2^{\bullet-}$ production [100, 107].

Complex III

ROS production at Complex III is nearly at the same magnitude as in FET, although considerably lower than in RET [111]. The mechanism described in section 1.2.2 (pag. 18) is fairly rapid so no significant accumulation of semi-CoQ is appreciated.

[9] H^+/K^+ antiporter which converts ΔpH into $\Delta\psi$

However, in the presence of antimycin A[10] electrons are still channeled to cytochrome b_H but the half-time of semi-CoQ at Q_O site is increased, therefore maximizing the chance of electron slip to O_2 and a robust production of ROS [100, 111]. An even clearer proof of the molecular identity responsible for ROS production can be achieved in the presence of myxothiazol[11] since no ROS is observed in this situation [100, 107, 111].

Complex III also shows dependance on Δp, primarily its $\Delta\psi$ component, since electron tunneling through *b*-type hames is strongly dependent on $\Delta\psi$ (sec. 1.2.2, pag. 18), i.e. electron transfer is hampered at high $\Delta\psi$ increasing the semiCoQ occurrence [5]. In conclusion, although Complex III can be induced to produce ROS by specific antimycin A inhibition, the normal physiological status of cells does not fulfill such requirements and one can state that Complex III-induced ROS production is quite small under normal conditions [100].

1.4.3 Mitochondrial antioxidant machinery

An interesting experimental design with either intact or permeabilized isolated mitochondria in the presence of the extra-mitochondrial ROS-sensitive probe Amplex Red allows two simple interpretations [110]: first, mitochondria do not accumulate ROS, since they are promptly annihilated upon emergence; second, detoxifying events occur within the mitochondria and are Δp-dependent. Certainly, mitochondrial antioxidant capacity is finite and once spent, ROS levels will increase progressively.

Mitochondria can actively regulate ROS production/levels directly or indirectly. The prior relates to the high reliance of ROS in Δp leading to development of the 'mild uncoupling' theory [112], which states that a small decrease of $\Delta\psi$ of about 10% is sufficient to decrease ROS formation by the MRC. Therefore the protective mechanism of UCPs or mitochondrial potassium ATP-sensitive channels (mitoK_{ATP}) is thought to be due to increased permeability to cations [54]. In the same line of thought, Ca^{2+} would decrease $\Delta\psi$ and therefore lower ROS production. However, this cation is peculiar as it will also activate TCA enzymes increasing therefore NADH levels and give rise to a more reduced MRC, which will concomitantly increase ROS levels. This dichotomy can probably explain the different results reported in the literature [54].

[10] inhibits electron transference from cytochrome b_H to CoQ at Q_i site
[11] inhibits binding of CoQ to the Q^O site

Indirectly, mitochondria can reduce ROS by enzymatic or non-enzymatic approaches. Non-enzymatic strategies include membrane soluble α-tocopherol (vitamin E), ascorbic acid (vitamin C), retinol (vitamin A), flavonoids and lipoid acid [106, 110]. α-tocopherol is very important in stopping lipid peroxidation progression due to its high octanol/water partition coefficient [106]. Moreover, its antioxidant capacity is infinite since the parental molecule can be regenerated as long as a functional MRC and/or glutathione (GSH) are present [110].

GSH is another non-enzymatic molecule constituted by three peptides (L-γ-glutamyl-L-cysteinylglycine) with its thiol group of cysteine being responsible for its activity, reduction of disulfide bounds, through donation of its proton. In the cell, mitochondrial and cytosolic GSH pools are distinct. In fact, GSH is synthesized in cytosol and only $\sim$10% of the total amount is transported into mitochondria although the small volume of the organelle allows [GSH] to be much higher in the matrix [106, 110]. Additionally, GSH acts as cofactor for glutathione peroxidase (GPx).

Worth to mention is the fact that upon extracellular/plasma membrane insults, cytoplasmic GSH pool is consumed while the mitochondrial one remains intact [113]. Although this represent an independent compartmentalization of both pools it was also demonstrated that even in global stressful events, mitochondrial GSH pool is the last one to be oxidized [114].

Mitochondrial antioxidant enzymes includes: mitochondrial-specific manganese-SOD (MnSOD), catalase, cytochrome c, glutathione reductase (Gred), Gpx, peroxi- and thioredoxins. MnSOD is found exclusively in mitochondrial matrix and its only known function is to dismutate very rapidly (k $\sim$2.3$\times$10^9 M^{-1} s^{-1}) $O_2^{\bullet-}$ to H_2O_2 in a firs-order kinetics in respect to the prior [100]. MnSOD activity is higher in liver and kidney when compared to heart [110]. Catalase can further break down two H_2O_2 molecules to H_2O and O_2 although Gpex and peroxiredoxins (Prx) can also perform that function [110]. Catalase is mainly expressed in peroxisomes and is found in high levels in liver followed by kidneys and heart [106, 110].

Alternatively, H_2O_2 can be eliminated by Gpx through conversion of H_2O_2 to H_2O mediated by GSH with its consequent oxidization (GSSG). Gpx is found throughout the cell and its levels are high in liver, kidney and heart [110]. Since GSSG cannot be transported into cytosol it must me reduced in the matrix, a task carried out by Gred which requires NADPH as cofactor [110]. NADPH has two possible routes of formation either by a Δp-dependent transhydrogenases or by a NADP-linked isocitrate

dehydrogenase [5].

Finally, oxidized Prx can be reduced by direct reaction with thioredoxin (Trx) which in turns can be recycled by the action of Trx reductase (TrxR) in a NADPH-dependent fashion [106]. In addition, Trx can directly reduce protein disulfides. Prx is highly expressed in heart [110].

1.4.4 Involvement in cell death

ROS generation by Complex I and III [73] is increased under pathological conditions such as ischemia and reperfusion [115]. Increased mitochondrial oxidative stress results in mitochondrial proteins damage and lipid peroxidation [73] which consequently promotes loss of mitochondrial functional integrity [115].

Another consequence of increased mitochondrial oxidative stress is damage of the genetic apparatus of the organelle. In fact, accumulation of oxidized mtDNA has been reported in several human pathologies and lead ultimately to a decrease in mtDNA copy number and progressive loss of proteins involved in energy production [116]. Myocardial remodeling can also constitute a maladaptive consequence of increased ROS generation through activation of specific proteins including metalloproteinases [117, 118].

If mitochondrial ROS generation is too extensive and overload the antioxidant network, one consequence would be the removal of damaged mitochondria by autophagy [119], or a more drastic solution, the triggering of cell death [120]. If the imbalance in oxidative stress is present concomitantly with alterations in cytosolic and mitochondrial calcium, the MPT may occur, with the rupture of OMM leading to the release of several apoptotic initiators usually enclosed in the inter-membrane space [121], e.g., cytochrome c, the apoptosis-inducing factor (AIF) and the second mitochondria-derived activator of caspase/direct inhibitor of apoptosis (IAP)-binding protein with low isoelectric point (SMAC/DIABLO) protein.

Various links between mitochondrial oxidative stress and protein-mediated pro-apoptotic OMM permeabilization have already been described [122, 123]. Furthermore, oxidative stress can lead to the oxidation of cardiolipin residues, which decreases the affinity of this phospholipid for cytochrome c, contributing for its release to the cytosol after OMM permeabilization due to a pro-apoptotic stimuli [124, 125].

1.5 Mitochondria as tool for toxicological research

Isolated mitochondrial fractions from different tissues, more frequently from liver, proved to be good *in vitro* systems to predict drug toxicity before more complex and expensive *in vivo* experiments [126]. Isolated mitochondrial fractions are used to obtain toxicological parameters such as IC_{50}, the half maximal inhibitory concentration of a substance, in order to establish a ranking of compound toxicity, however, one obvious disadvantage is the lack of complexity of the biological system.

Nevertheless, isolated mitochondrial fractions can be used as a good indicator to predict drug safety, being in fact in use by several major pharmaceutical companies [121, 127]. Moreover, mitochondria along with other living systems, such as bacteria, frog embryos, fertilized chicken eggs, and cultured animal cells have contributed to the reduction in the number of animals that are subjected to testing. Actually, a great deal of progress has been made over the last few years in the development of high-throughput and cost-effective *in vitro* tests to fulfill testing requirements, and also to reduce the number of animals used in toxicity testing, particularly in the area of acute toxicity.

But why is mitochondrial toxicity screening that important? For example, after extensive research mitochondria began to be linked with several pathologies such as Huntington's and Parkinson's disease [128], diabetes [129] and several cardiovascular disorders, including atherosclerosis, cardiac failure and ischemic heart disease [130] which demonstrates that mitochondrial function is critical for tissue homeostasis.

Organs such as cardiac and skeletal muscles and the brain are metabolically more active, implying a higher dependence of mitochondrial-produced energy [131], with a consequent increase in tissue damage resulting from drug-induced mitochondrial failure. Additionally, mitochondrial *in vitro* tests can provide important preliminary screens for chemical toxicity, by identifying chemicals which have the lowest probability of toxicity, so that animals are exposed only to the least toxic chemicals.

The opportunity to undertake specific dose-response studies on mitochondria, represents a step towards the reduction of animal use in drug discovery and development, and thus should be suggested as a first step into the generation of safe pharmaceuticals. In a proposed flow-chart for assessing compound toxicity, *in vitro* study of mitochondrial toxicity would be the first step [132] after selection of a group of compounds to be tested. It is possible to change the type of studies to be performed,

according to what it is known from previous data on compounds of the same family.

Besides eliminating compounds with higher toxicity, data obtained from initial mitochondrial studies would also allow the prediction of idiosyncratic reactions of compounds with low mitochondrial toxicity in patients with diagnosed mitochondrial diseases or in individuals that are known to be exposed to stress conditions that affect mitochondrial function in different tissues (e.g. tobacco or drug consumption, exposure to environmental toxins, aging, or a chronic treatment with clinical-used drugs presenting mitochondrial liabilities). In conclusion, isolated mitochondrial fractions can be an excellent toxicological sensor to predict drug safety.

The fact that several drugs present mitochondrial liabilities [121, 133–135] justifies studying mitochondria as a nexus of damage and protection in the context of human health. One particular example of drug-mediated organ dysfunction based on mitochondrial liability involves the anti-cancer agent doxorubicin.

Chapter 2

Doxorubicin

Doxorubicin[1] {*(7S,9S)*-7-[*(2R,4S,5S,6S)*-4-amino-5-hydroxy-6-methyloxan-2-yl]oxy-6,-9,11,-trihydroxy-9-(2-hydroxyacetyl)-4-metoxy-8,10-dihydro-*7H*-tertacene-5,12-dione, $C_{27}H_{29}NO_{11}$, DOX, Fig. 2.1}, was discovered in the late 1960s by the pharmaceutical company "Farmitalia Research Laboratories" and was initially named Adriamycin, due to the site of discovery (the Adriatic Sea). DOX is an antibiotic belonging to the anthracycline family and was isolated from a variant culture of the *Streptomyces peucetius* (*Streptomyces peucetius caesius*) by aerobic fermentation after mutagenic treatment [136, 137]. The new molecule was chemically characterized and found to possess an anthraquinone moiety connected to a glycoside group [137, 138]. The spe-

[1] also known or commercially available as Adriamycin, Adriablastin, 14-Hydroxydaunomycin, Doxil, Rubex, Myocet or Resmycin. Source: http://pubchem.ncbi.nlm.nih.gov/

cific chemical structure is responsible not only for the antineoplastic activity but also for its toxicity, which will be discussed further on in this chapter.

Initial studies have shown that DOX is able to stop the progression of tumors in rats [139] and its use in clinical trials achieved great success [140, 141]. However, it was later described that patients undergoing DOX treatment developed signs of cardiac toxicity and cardiomyopathy [141, 142], hence a cardio-selective toxicity was soon considered one effect of DOX chemotherapy. Nevertheless, the clinical use of DOX continued and still nowadays is probably one of the most potent anticancer agents in clinical practice [143].

2.1 Clinical use and side effects

DOX is commonly used to treat several types of human and non-human tumors, from leukemia and lymphomas to soft-tissue sarcomas and solid tumors, including: breast carcinoma, osteosarcoma, Kaposi's sarcoma, Hodgkin's and non-Hodgkin's lymphomas [140, 141]. Patients subjected to DOX-chemotherapy usually exhibit symptoms such as nausea, vomiting, alopecia, myelosuppression, stomatitis and gastrointestinal disturbances [144, 145], which are all clinically manageable side effects. Nevertheless, cardiotoxicity is a completely different story, being probably the most hazardous side-effect associated with DOX treatment, sometimes reaching 50% mortality for the highest cumulative dosages.

Acute toxicity accounts for 11% of all cases [146] with symptoms such as myopericardits, sinus tachycardia, reversible arrhythmias, prolonged QT interval and flattening of the T wave [146], occurring during or right after the last administered dose, and disappearing right after discontinuation of the treatment. Alternatively, chronic DOX-induced cardiotoxicity can be observed within one month or even years later after the treatment ceases [142].

Although the incidence of this type of delayed toxicity is much lower (around 1.7%), it is rather dose-dependent, i.e., the probability of developing cardiomyopathy increases with the total cumulative dose [147]. Total dosages between 500-550mg/m^2 have a 5% probability of inducing cardiac heart failure [147] and, therefore, this threshold was established as the maximum dosage of DOX tolerable in chemotherapy. Naturally, the downside of such approach is a decrease in the performance of the drug as an anti-cancer agent.

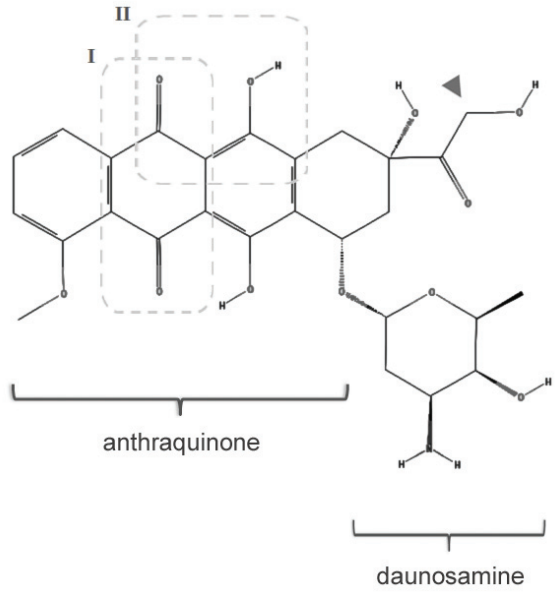

Figure 2.1: Chemical structure of DOX. Picture shows the drug planar anthraquinone tetracyclic ring attached to the deoxy amino sugar daunosamine. DOX results from a 14-hydroxylation of daunorubicin, here represented by the triangle. In ***I***, the molecular part of DOX responsible for the redox cycle is shown, whereas in ***II***, the portion of the molecule that allows the formation of DOX-iron complexes (see Fig. 2.2 on page 52 for further details) is highlighted. Structure was withdrawn from the public website PubChem.

In addition to the cumulative dose, other risk factors can lower the toxicity threshold, including co-treatment with other drugs, mediastinal radiation therapy, age, gender, as well as a previous history of cardiovascular problems, hypertension and liver disease [144, 146]. Still, not all patients show signs of cardiomyopathy even when high doses of DOX are applied suggesting intrinsic differences between subjects, at the genetic background. Another important issue is the peak plasma concentration of drug delivered to the heart during treatment. It was hypothesized that DOX toxicity is primarily related to the peak dose concentration while the antitumor efficacy is more related to total drug exposure [148].

The idea of genetic polymorphisms in DOX-induced toxicity has been previously suggested [149] with other clinical situations using this type of approach used to deliver a more selective therapeutically dosage to patients [150]. Although so far there are no experiments performed regarding polymorphisms associated with DOX cardiac toxicity, isolated experiments with knock-out or genetically engineered animals give new understandings about the topic of polymorphism or SNPs and its relationship with drug-induced toxicity. In a relatively recent report [151], these aspects were reviewed and genes related to drug efflux transporters, antioxidant and detoxification enzymes as well as some enzymes capable of reducing DOX were pointed as possible targets for this type of analysis. Nevertheless, the authors mention that further work

is needed to better address this important question.

2.2 Monitoring doxorubicin cardiotoxicity

Presently, there is no effective approach that fully prevents or even treats DOX-associated toxicity and, therefore, the best strategy is the early detection of cardiomyopathy end-points. However, the idea may not be so straightforward because clinical manifestation of DOX-induced toxicity share symptoms with other cardio and non-cardiovascular illnesses and the current methods used to follow heart function lacks sensitivity or specificity [144].

Currently, from all the techniques available [144, 149] only two of them constitute the best methodology to follow-up the progression of cardiomyopathy during and/or after DOX treatment: serial echocardiography and endomyocardial biopsy. Although the latter is the most sensitive and specific method it is also the more invasive and less available for the clinician. Echocardiography has its advantages over other methods because is widely available, noninvasive and highly reliable being the study of ejection fraction to detect signs of early cardiomyopathy one of the main advantages of the technique [144, 146], the sensitivity of which can be increased when associated with some particular protocols (e.g., exercise) or Doppler imaging [152, 153].

Measurement of cardiac enzymes or humoral factors, such as troponin I and T and B-type natriuretic peptide, can be an additional strategy to detect early signs of DOX-induced cardiotoxicity, however these markers represent general cardiac tissue damage and are not specific of DOX-induced damage [154]. Nevertheless, the combined use of specific cardiac damage markers together with imaging techniques can increase the sensitivity of the detection and demonstrate that marker levels are directly proportional to cardiomyopathy score.

Unfortunately, there is no effective treatment available for patients with established cardiomyopathy even though the mortality rate is incredibly high once the prognosis is revealed [147]. The reason for that situation is probably related to the fact that standard therapy for cardiac heart failure fails to relieve the symptoms of DOX-treated patients [149, 155].

The only solution is cardiac transplantation but besides its radical character, it has also specific disadvantages in addition to the drawbacks of general cardiac transplan-

tation [155]:

1) the immunosuppressive condition after transplantation may increase the risk of cancer recurrence;
2) patients qualified as able to receive a new heart must provide evidences that are cancer-free for at least a period of 5 years.

However, because the incidence of cancer-related death is so high in patients receiving DOX therapy, the majority of them die before the time frame is complete. Still, the use of ventricular-assist devices may be a temporary alternative for this group of patients until the requirements for cardiac transplantation are met [155].

2.3 Mechanism for doxorubicin antineoplastic activity

Despite the existing controversy, it is being more widely accepted that DOX-induced cardiotoxicity is completely independent from its anticancer activity. The idea gets further support if one agrees that cardiomyocytes, as terminal differentiated cells, should not be as sensitive to the primary antineoplastic activity, which is related with cell cycle blockage. Nevertheless, the inhibition of transcription of certain proteins can contribute to the cardiomyopathy, although a causal relationship between both still needs to be addressed.

The planar structure of DOX anthraquinone moiety allows the intercalation of the drug into the DNA double strand, which will not only unwind nucleic acids, as it will also cause a stereochemical disorder and consequent block transcription and replication processes [156]. Meanwhile, topoisomerase II is also inhibited and downstream effects are triggered due to the formation of DNA double-strand breaks.

All these effects result in cell cycle arrest that culminates in the activation of the apoptosis machinery leading to the death of cancer cells and tumor growth arrest. Obviously, one could not ignore the hypothesis that DNA interference may also occur in cardiomyocytes. However, other DNA intercalating compounds such as cisplatin or actinomycin D do not cause cardiotoxicity [157] and therefore the mechanism described is not likely responsible for degeneration of cardiac function.

2.4 DOX-induced cardiotoxicity: *The role of mitochondria*

The cardiac tissue has a high energy demand and consequently any interference in the energy production machinery will clearly affect the whole physiology and heart contraction. Cardiomyocytes depend approximately 90% on ATP production by the mitochondrial OXPHOS, thus mitochondria appear as one attractive target for DOX toxicity. In fact, it is widely recognized that DOX-induced cardiotoxicity has a strong mitochondrial component [158, 159]. Mitochondria from DOX-treated animals show traces of the drug [160], which could be due to its affinity for particular biomolecules within the organelle.

As with nuclear DNA, DOX also forms adducts with mtDNA [148], while complexes between DOX and cardiolipin have also been described [161]. Once accumulated in the mitochondrion, DOX can initiate its direct and deleterious effects which include stimulation of ROS production, induction of mPTP and inhibition of OXPHOS.

2.4.1 Oxidative stress

Reactive oxygen species

As pointed out earlier, the chemical structure of DOX, namely the anthraquinone group, also accounts for the toxic response of the drug. The quinone at the central ring (Fig. 2.1 box I, p. 47) is prone to reduction with a redox potential of approximately $-320\,\mathrm{mV}$, similar to reduced NADH [158]. Therefore, DOX can divert electrons from Complex I as well as from several other cellular dehydrogenases, namely NADH transdehydrogenase, xanthine oxidase and cytochrome P450, being converted into a semiquinone radical along the process (Fig. 2.2) [158]. Afterwards, in the presence of O_2, DOX univalent reduced form, can donate its unpaired electron resulting in the formation of $O_2^{\bullet-}$, regenerating the parent drug in the process [162].

The fact that *in vitro* studies with Complex I-specific inhibitor rotenone exacerbated ROS formation suggests that the site of DOX activation in the enzyme is upstream to the binding site of the inhibitor [163]. Since theoretically no net consumption of DOX occurs, the redox-cycle can take place endlessly.

In addition to the possible action of iron as a catalyst for production of $HO^{\bullet}$ through

Fenton reaction with DOX semiquinone participating by recycling Fe^{2+}, the metal ion may also establish complexes with DOX (Fig. 2.2), stimulating the production of H_2O_2 [148, 164]. However, significant levels of free iron are unlikely to be observed in cells during physiological conditions [148, 165] and therefore, it is possible that DOX may induce first a dysregulation of iron homeostasis.

Aconitase is known to be very sensitive to variations in oxidative stress and it is possible that when damaged, iron from aconitase FeS clusters can be displaced thus increasing free iron in mitochondria. The most important aspect is the fact that this enzyme has a double role, since in its iron-free form, it can act as an iron-regulating protein, facilitating iron uptake over iron sequestration hence increasing the pool of free iron available to react with DOX [148, 164].

Reactive nitrogen species

In the context of reactive radical species, nitric oxide (NO) plays a particular important role in the cardiovascular system, being responsible for the increase in contraction, myocardial relaxation and diastolic function, Frank-Starling response, heart rate, β-adrenergic response, myocardial energetics and substrate metabolism [167, 168]. For this basal action to occur, cardiomyocytes and endothelial cells constitutively express two different isoforms, neuronal NO synthase (nNOS) and endothelial NO synthase (eNOS). Yet, a third isoform with higher output, the inducible NO synthase (iNOS), whose abundance increases upon several stimuli, was proposed to be linked to different cardiac pathologies [169].

During DOX administration, transcription of eNOS in endothelial cells and iNOS in cardiomyocytes was shown to be increased, resulting in unbalanced amounts of NO and consequent deleterious effects [142, 168]. Moreover, DOX can be directly metabolized by all NOS isoforms similarly to the mentioned reductases, uncoupling NO production and increasing $O_2^{\bullet-}$ [142, 168]. In fact, the turnover of DOX cycle for iNOS is $\sim$10 fold higher than for nNOS and eNOS, which alone have a K_m about $\sim$100 fold lower than NADH-dehydrogenase [142, 168]. During the deregulated production of NO and $O_2^{\bullet-}$ both molecules can react decreasing their cellular amount. Although this may seem like a protective mechanism, in fact it leads to the production of peroxynitrite ($ONOO^-$), a much more reactive molecule when compared to NO which is relatively inert [168].

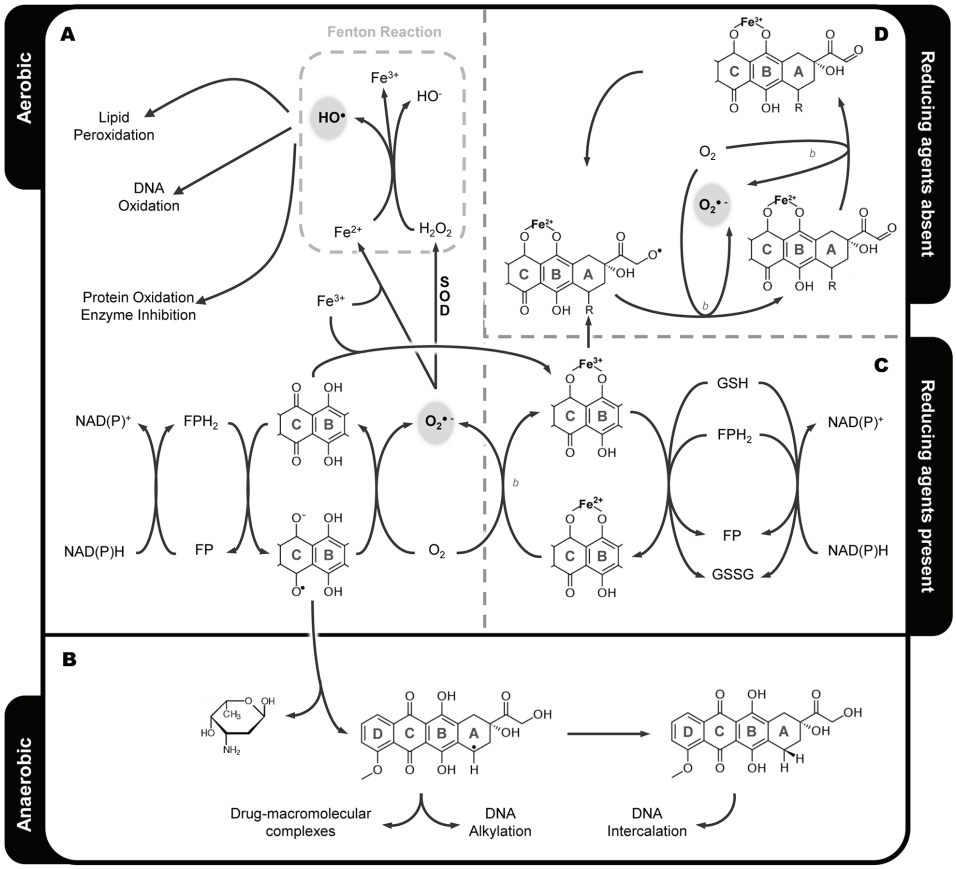

Figure 2.2: Different mechanisms proposed for DOX activation and stimulation of ROS production. DOX can suffer univalent reduction by several cellular NAD(P)H-dependent flavoproteins originating a semiquinone free radical intermediate. Under aerobic conditions (**A**), molecular oxygen is not limiting and DOX semiquinone undergoes a futile cycle. However, under anaerobic conditions (**B**), the semiquinone undergoes aglycosilation and further reduction giving rise to the deoxy-aglycone of DOX. Alternatively, DOX can form complexes with cellular free-iron (**C** and **D**). DOX-Fe^{3+} complexes can be enzymatically reduced by different flavoproteins or by low-molecular-weight compounds such as glutathione (**C**). In the absence of reducing agents, the ferric ion component of the drug-metal complex can be reduced at the expense of intramolecular oxidation of DOX (**D**). In the presence of oxygen, oxidation of DOX can continue until the fully oxidized end product of DOX (9-COOH-DOX) is reached, releasing ROS in the process. Both in **A** and **C**, futile cycles will lead to pyrimidine nucleotides and antioxidant defenses depletion. The reactions indicated as a can also be catalyzed by H_2O_2 with concomitant production of $HO^{\cdot}$. Adapted from [164, 166]. Partial molecular structure of DOX is presented in some schemes for ease of comprehension. Abbreviations: *SOD*, superoxide dismutase; *FP*, flavoprotein; *FPH_2*, reduced flavoprotein; *GSH*, reduced glutathione; *GSSG*, oxidized glutathione.

The importance of NO in cardiac toxicity induced by DOX was confirmed when *in vivo* studies performed by inhibiting iNOS, or by using $ONOO^-$ scavengers, delayed or prevented DOX-induced cardiomyopathy [168, 170]. Nevertheless, some contradictory information is reported in the literature regarding the impact of NO production inhibition during DOX treatment [167, 171]. One view suggested that the protection afforded by NO was mediated by $O_2^{\bullet -}$ since both radical species can react together, which synergizes with SOD in the removal of $O_2^{\bullet -}$ [167]. In fact, overexpression of Mn-SOD in NO-null mice prevented the deleterious effects of DOX [167]. A second study demonstrated that iNOS overexpression or delivered as a bolus increases the toxicity of DOX on human breast cancer cells in culture but not on H9c2 cardiomyoblasts, suggesting that NO can act to prevent DOX toxicity in cardiac cells but can act to improve the clinical efficacy of DOX as an anti-tumor agent in cancer cells [171].

Cellular targets of radical species

Biomolecule oxidation can directly affect mitochondrial function, or alternatively lead to secondary responses. For instance, oxidation of mtDNA can result in a defective respiratory chain, which will not only be unable to respond to high energy demands but will also increase electron leak to O_2, increasing ROS production [172]. ROS can directly inhibit the respiratory complexes of OXPHOS, e.g., Complex IV [173], but alternatively the oxidation of certain residues or functional groups, e.g., thiol groups which are very vulnerable to oxidation, can induce conformational changes inhibiting protein function. Several mitochondrial proteins show oxidation of this particular group after DOX treatment which forms disulfide bonds upon oxidation [172, 174]. One of such proteins is the ANT and the consequence of its oxidation will be explained in the following section.

2.4.2 Ca^{2+} homeostasis

Mitochondrial permeability transition

Some authors suggest that oxidation of ANT vicinal cysteines allows the formation of dimers which are crucial for the formation and opening of mPTP [175]. In fact, mitochondria treated *in vitro* with DOX show increased susceptibility to mPTP [78, 79] when treated with inhibitors and modulators of mPTP, e.g., ATP, dithiothreitol

(DTT), butylated hydroxytoluene (BHT) and CsA, this phenomenon was prevented. The same authors showed that secondary metabolites, such as DOX aglycones, are even more powerful in the induction of mPTP [79]. The *in vitro* mPTP-inducing effects may actually be due to increased oxidative stress, oxidation of pyridine nucleotides, depletion of adenine nucleotides and decrease in $\Delta\psi$, while increased sensitivity to mPTP observed in cardiac mitochondria from DOX-treated animals [77] is probably due to the synergistic action of such effects with Ca^{2+} homeostasis dysregulation.

In fact, DOX has been described to interfere with the flux of Ca^{2+} from the sarcoplasmic reticulum by increasing the opening state probability of Ca^{2+} release channels [176]. Additionally, DOX also interferes with the Na^+/Ca^{2+} and Na^+/K^+ pumps which can contribute for enhanced $[Ca^{2+}]_c$s and, therefore contributing to augment $[Ca^{2+}]_m$ [176]. Similarly to *in vitro* experiments, cardiac mitochondria from DOX-treated animals have a lower capacity to accumulate and retain Ca^{2+} [77, 158, 174, 177–179]. The effect is more pronounced if the cumulative dose of DOX is increased and persists for long periods after the end of the treatment [77]. Therefore, the loss of mitochondrial Ca^{2+} loading capacity can be a sensitive marker for DOX-induced cardiotoxicity [174] which is strongly supported by the fact that RuR not only decreased the production of ROS but also increased cell viability [180].

The co-administration of CsA *in vivo* was capable to prevent DOX-induced cardiomyopathy demonstrating the importance of Ca^{2+} homeostasis and induction of mPTP in the toxicity mechanism of the drug. Nonetheless, caution should be taken when inferring the results, since FK-506 also inhibited DOX cardiotoxicity and this compound is not a mPTP inhibitor, being in fact an immunosuppressant similarly as CsA [179]. An improved knowledge on this issue could be accomplished if some of the new specific mPTP inhibitors were used instead [181, 182].

Another intriguing aspect is the *ex vivo* use of CsA on cardiac mitochondria from DOX-treated animals resulted in restoration of respiration to control values, which suggests that mPTP or CyP-D are involved in DOX-induced inhibition of mitochondrial respiration [174]. The authors suggest that binding of CsA to CyP-D may cause a disassembling of pre-formed pores allowing crucial components such as the ANT to become available again to participate in OXPHOS.

Agreeing with the possible role of the ANT on DOX-induced toxicity, a decrease in functional ANT was detected after DOX treatment, suggesting a genetic or biochem-

ical interference of DOX with this protein which results in a reduction of bioenergetic capacity and decrease mitochondrial Ca^{2+} loading capacity [177]. Nevertheless, an evident direct interaction between drug-enzyme is still to be described in the literature for almost all OXPHOS enzymes, as pointed before [161], and the described inhibitory effects are due to increased oxidative stress or to the displacement of lipid-enzyme environment, as is in the case of DOX-induced inhibition of Complex IV [161].

2.4.3 Oxidative phosphorylation

Mitochondrial respiration

A decrease in state 3 respiration also seems to be another mitochondrial marker of DOX-induced cardiomyopathy, as it was already been described in several models of chronic exposure to the drug [174, 183–185]. The same effect was observed *in vitro* together with a slight stimulation of state 4 [186], usually attributed to the diversion of electrons from the respiratory chain to DOX during its redox cycle with concomitant increase of oxidation. However, it is the *ex vivo* effect of DTT on mitochondrial respiration from DOX-treated rats that allows to draw major conclusions since it reverses respiratory state 3 inhibition, supporting the idea that DOX oxidation of thiol groups causes several of the mitochondrial alterations observed [174].

Nevertheless, as already pointed out [158], one must have some moderation in mind when analysis and conclusions are inferred from two distinct models of toxicity. *In vitro* effects are mainly due to the direct interaction of the drug with mitochondria and its membranes and may result from direct production of ROS by drug redox cycling. The changes in bioenergetics observed after the *in vivo* treatment may reflect alterations that are persistent, even after the drug is washed out from the system (*memory effect*). This may also result, among other possibilities, from genetic alterations.

Moreover, the large variability in the percentage inhibition of isolated respiratory complexes activity and/or intact mitochondria respiration, as reported in different *in vivo* studies, can be explained by different DOX whole body distribution, binding specificity, and metabolism. Alternatively, the differences may indicate that mitochondrial oxygen consumption is not a sensitive method to evaluate mitochondrial dysfunction, as has already been pointed out [187]. It was proposed instead that altered mitochondrial Ca^{2+}-loading capacity as a more sensitive and quantifiable indicator of mitochondrial dysfunction upon DOX treatment [158, 174, 187–189].

Enzymatic damage

Exposure to DOX has been described to inhibit several OXPHOS enzymes, including Complex I, ISP, Complex II, Complex IV, creatine kinase (CK), carnitine palmitoyl tranferase, fatty acid oxidation-related enzymes as well as the translocation of phosphate and pyruvate to the mitochondrial matrix ([158] and references therein).

A proteomic profile of sub-chronic anthracycline-induced cardiotoxicity was recently performed [190]. In order to perform the experiments, authors used the well established rabbit model [191] and chose the parent compound of DOX, daunorubicin, to induce cardiac toxicity. Although interpretations should to be taken cautiously, since the degree of toxicity between the two compounds is slightly different [192], we can infer that the most drastic changes found in the study can be shared between both drugs.

The authors showed that most of the observed alterations were in proteins related with the cytoskeleton, OXPHOS and antioxidant detoxifying system [191], all of are considered typical markers of DOX-toxicity. One limitation of the work is related with the end-stage of the experiment and, therefore, one cannot discern cause from consequence. Nevertheless, daunorubicin caused a large specific increase of desmin in cardiomyocytes which was suggested to act as rescue event for the loss of myofibril stability and for reposition of energy production and consumption sites since proteins related to energy production and channeling (see below) were decreased.Interestingly, desmin abundance was directly proportional to the extension of DOX-induced cardiac dysfunction and increased levels of this protein were detected even in animals without congestive heart failure and thus might be used as another early marker of DOX-toxicity progression.

An additional aspect is the dichotomy between cytoplasmic and mitochondrial abundance of SOD, which is increased in the former and decreased in the latter after DOX treatment, suggesting the possible compartmentalization of oxidative stress, as suggested by the authors. Supporting this study, another previous work investigated the variation of transcripts in the heart over time after a single treatment with DOX [193]. Contrarily to the increased expression and activity of Complex IV observed in some works, the expression of at least some of its subunits as well as its activity appear diminished in other reports [173], which makes this respiratory complex another possible target during DOX toxicity.

Metabolic remodeling

Interestingly, analysis of different metabolic pathways (including OXPHOS) through the use of microarrays and quantitative PCR showed that despite the variety of enzymes affected, the most affected biochemical networks are fatty acids mitochondrial β-oxidation and glycolysis [159]. This result suggests alterations on substrate utilization, an event that is usually associated with myocardial remodeling and the development of cardiac pathologies.

In fact decrease in cardiac fatty acid utilization was already reported in DOX-treated animals, occurring before any functional change [194]. More recently, ^{13}C-isotope analysis of isolated perfused hearts from DOX-treated rats showed a metabolic shift from fatty acid oxidation towards glycolysis [195]. In this particular study, the use of the cardioprotector dexrazoxane proved to be capable of reversing the observed shift, shedding some light once again in the role of the imbalance of oxidative stress. Nevertheless, it remains to be elucidated if it is the impairment of the mitochondrial function that results in the metabolic remodeling. If indeed is this the case, the inability of the cardiac tissue to sustain energy production by glycolysis may be due to the fact that DOX treatment results in alterations of glucose intracellular transport and initial metabolism [196].

Following proteomic studies, treatment with anthracyclines induces a decrease in the fatty acid binding protein responsible for the import of such molecule fuels into cardiomyocytes [190]. Such decrease, in addition to the increased abundance of the rate limiting enzyme pyruvate dehydrogenase [190] might explain the metabolic shift observed during DOX-treatment. In addition, the same study attempts to link heart failure to metabolic remodeling since it was also found that anthracyclines decrease the triosephosphate isomerase enzyme important in the glucose metabolism and which was previous found to be sensitive to oxidative stress and associated with cardiomyocytes and mitochondrial degeneration [190].

Energetic substrate channeling

Another problematic issue identified in cardiomyocytes after exposure to DOX is the interference with the channeling of ATP and phosphocreatine (PCr) from mitochondria to the cytosol, i.e., the energy shuttle between production and consumption sites. The easily diffusible creatine (Cr) and its phosphorylated form PCr act like global or

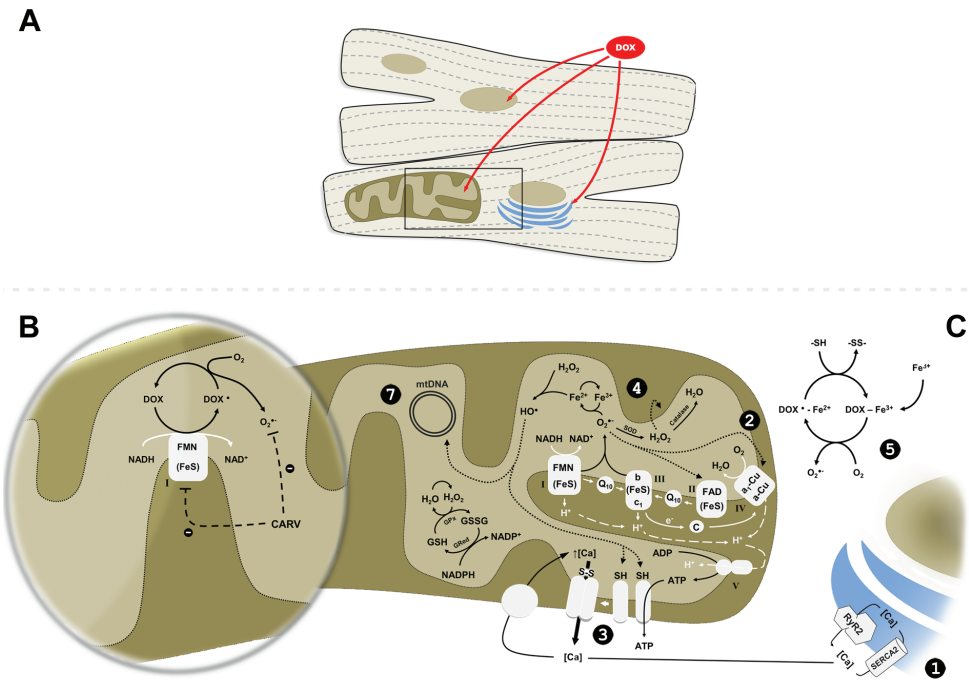

Figure 2.3: Mitochondrial function and oxidative stress in cardiomyocytes and modulation by DOX and carvedilol. DOX targets distinct cardiomyocyte compartments (Panel **A**) and induces an imbalance between ROS production and antioxidant defenses, through the induction of a redox cycle on Complex I (**B**). In the presence of DOX, Ca^{2+} uptake by mitochondria is decreased and cellular Ca^{2+} homeostasis is disturbed, involving also disturbance of endoplasmic reticulum cardiac-type ryanodine receptors (**1**). Augmented ROS generation by DOX redox cycle have multiple negative effects on mitochondria including inhibition of the respiratory chain (**2**), induction of the mPTP pore, through oxidation of critical residues (**3**) and lipid peroxidation (**4**). DOX can interact with the cellular iron cycle, sequestrating Fe^{3+} for the assembling of DOX trimeric complex (**5**). DOX can also interfere with nuclear and mitochondrial genomes (**8**). Panel **B** - Carvedilol is shown as inhibitor of mitochondrial oxidative stress and inhibitor of the mitochondrial NADH-ubiquinone-oxireductase, which is responsible for DOX-semiquinone formation and consequent ROS formation. Full white arrows represent electron flux; dashed white arrows represent proton flux; full black arrows represent typical cellular metabolism; dashed black lines represent inhibition and dotted black arrows represent oxidative damage. Panel **C** is a magnification of the box represented in A. Abbreviations: *c* - cytochrome c; *Ca* - Ca^{2+} ; *CARV* - carvedilol; *DOX*$^{\cdot}$ - DOX semiquinone; *GPx* - glutathione peroxidase; *Gred* - glutathione reductase; *GSH* - reduced glutathione; *GSSG* - oxidized glutathione; *SERCA* - sarco/endoplasmic reticulum Ca^{2+} ATPase; *Q10* - ubiquinone; RyR - ryanodine receptor; SH - reduced thiolic groups; SS - oxidized thiolic groups; *SOD* - superoxide dismutase.

local buffers of ATP/ADP ratios, and are extremely important in heart physiology [197].

The term "*channeling*" is generally used when the CK is associated with ATP-providing or -consuming transporters, pumps or enzymes. In the heart, different CK isoenzymes can be found free in the cytosol or bound to sarcoplasmic or mitochondrial membranes. The mitochondrial isoform (mtCK) has high affinity for cardiolipin forming complexes with it and establishing a strict environment around the ANT, allowing not only the regeneration of intramitochondrial ADP but also the generation of the diffusible energy molecule PCr from ATP and Cr [197].

As it was mentioned before, DOX competes for cardiolipin binding sites and therefore, mtCK is a very likely target. In fact, *in vitro* assays showed that the drug was not only able to displace the complexes between the enzyme and phospholipids, but it was also capable to cause a direct oxidation of mtCK, namely in its cysteine residues [196]. *In vivo*, DOX also decreases the activity of mtCK and induces a shift of the expression of the isoenzymes towards an embryonic profile, an event that was already observed in several other cardiac pathologies [198]. All these effects are likely to be responsible for the decrease in the cellular PCr pool as assessed by NMR [199].

2.4.4 Apoptosis

All adverse effects above stated can drive the cardiomyocyte to undergo signaling resulting into cell death; being post-mitotic cells, cardiomyocytes cannot be regenerated leading to cardiac failure. There are several apoptotic markers present in individuals after DOX treatment which are covered elsewhere [200]. Several studies indicate that the transcription factor p53 is also involved in DOX cardiotoxicity. Targeted disruption of p53, either in knockout mice [201] or by using pifthrin-α, a specific p53 inhibitor on cardiomyoblasts in culture [202, 203] prevents DOX cardiotoxicity.

Mitochondrial dysfunction has been attributed to induction of BAX expression and mitochondrial translocation following initial nuclear DOX accumulation and DNA damage in cardiomyoblasts [202, 203]. Furthermore, DOX induces mitochondrial p53 translocation [202] but it is however unclear whether this translocation is involved in the apoptotic process or rather is part of a defense mechanism aimed at eliminating defective organelles [204]. DOX-induced cell death also results in depletion of cardiac stem cell pool which is critical for cardioprotection and repair [205].

2.4.5 Quality control: autophagy

Lastly, the importance of autophagy in mitochondrial quality control in the heart should also been taken into account due to the intensive work accomplished in this area in the last decades [119, 206–212]. Autophagy is the process by which the cell seeks to recycle damaged macromolecules or non-functional organelles and therefore promote cell survival. This is particular important in the cardiac tissue due to its high energy and terminal differentiated state.

Nevertheless, autophagy is a two-edged sword because when disproportionate, it can lead to cell death [206], being in fact augmented under certain pathological conditions; however, the precise event responsible for that dichotomy remains to be elucidated. Autophagy might be triggered by starvation, i.e. energy depletion, ROS, accumulation of misfolded/oxidized proteins, mitochondrial depolarization and mPTP induction [208–211], all of which are present after DOX treatment. Therefore, it is reasonable to consider that DOX treatment would activate the autophagic pathway in a protective manner to remove damaged mitochondria but interestingly the few works performed so far show the opposite [213, 214].

Although at this time is difficult to discriminate if autophagy is directly activated by DOX or it is induced as a consequence of mitochondrial dysfunction, it arises as another putative pathway for cardiomyocyte death, (in)dependent of apoptosis or necrosis. Kobayashi and co-workers stressed out the role of the heart-specific transcription factor GATA4 in the progression of DOX-toxicity and found that its abundance is inversely proportional to the autophagic flux, which is modulated by the expression of Bcl-2 related genes [213]. However, further investigations should be carried out to prove that the direct or indirect inhibition of the autophagic pathway is actually protective during DOX treatment.

2.5 Why is heart more affected?

Despite all the knowledge acquired over the years, one important doubt remains about DOX toxicity - why is the heart the most affected organ? Obviously, several authors have tried to explain the observed organ selectivity, however, most ideas still remain as simple hypothesis with little practical support.

2.5.1 Previous theories

Different drug accumulation in tissues was previously proposed [215]. Apparently, during its systemic circulation, DOX accumulates slowly in the tissues being the liver the organ showing the highest accumulation, perhaps because biliary secretion constitutes the major route of DOX elimination [216]. However, after several DOX administrations, the concentration in the cardiac tissue can increase up to 6-fold without changes in the rate of accumulation in other tissues [215]. It could be a specific cellular accumulation or differences in drug efflux as it was pointed earlier in this section.

Another possible explanation is that the cardiac tissue apparently shows decreased levels of antioxidant defenses when compared with other organs, e.g. the liver [217]. This would make the heart less capable of dealing with the increased oxidative stress induced by DOX. One author also suggested the existence of a cardio-selective external NADH dehydrogenase, alternative to OXPHOS Complex I and similar to those found in plants [163]. The presence of this enzyme in the outer leaflet of the inner mitochondrial membrane would exacerbate the DOX redox cycle. Also, the fact that myocardial tissue possesses a higher mitochondrial content [218] due to higher dependence on mitochondrial ATP could also contribute to enhanced DOX activation.

Finally, one could point to the fact that different tissues possess different energy demands and therefore different dependence on mitochondrial bioenergetics. In addition, some tissues can present higher reserves of certain important proteins for mitochondrial function, being consequently less sensitive to damage or decline in expression of those same proteins or respiratory complex [219]. This idea is usually presented to explain the severity of certain mitochondrial hereditary disorders in specific tissues but it might also be applied to DOX toxicity.

2.5.2 Doxorubicin toxicity in other organs

Hepatotoxicity

During DOX treatment, liver tissue accumulates high amounts of DOX and its metabolites, since it is one of the principal organs responsible for detoxification in the organism and drug clearance. Certainly is not a surprise that about 40% of patients present signs of liver failure after treatment [145]. Besides inducing changes in the

expression of antioxidant enzymes and decreases the energy charge of hepatocytes, DOX also increases the basal production of ROS since one can find several other NADPH-oxireductases in the tissue [145].

As it was observed in the heart, mtDNA from hepatic mitochondria is oxidized after DOX treatment although in a reduced manner when compared to cardiac mitochondria [220]. Other effects on mitochondrial function include a slight decrease in the respiratory control ratio (RCR) and decrease Ca^{2+} loading capacity which contributes to the observed mitochondrial vacuolization and swelling pattern in histology [145, 185].

Nephrotoxicity

Nephrotoxicity sometimes accompanies the treatment and its cause is probably related to apoptosis of glomerular podocytes [145]. If the extent of injury is mild to high, renal filtration process is likely to be affected and proteinuria can be observed. One of the mechanisms proposed for renal toxicity is the formation of iron-DOX complexes, i.e., increased ROS production which will cause mtDNA damage and the production of a defective respiratory chain [145].

Brain toxicity

DOX also affects the brain although it must be stressed that DOX itself cannot cross the blood-brain barrier [145]. Therefore, DOX-induced effects in the brain are probably indirect and mediated through cytokines, mainly tumor necrosis factor-alpha (TNF-α). The role of the cytokine on brain injury gains further ground when treatment is accompanied by an anti-TNF-α, decreasing the high levels of the circulating cytokine usually observed in patients and preventing brain damage [145].

In the brain, DOX indirectly induces an increase in oxidative stress seen as increased levels of malondialdehyde, thiobarbituric acid reactive substances (TBARS) and protein carbonyl groups [145]. Once more, the mechanism underlying DOX-induced toxicity appears to be related to the stimulation of ROS production. Mitochondria fractions isolated from this tissue also present increased sensitivity to mPTP, a phenomenon clearly modulated by the redox balance of the organelle, supporting the previous idea [221].

Lung toxicity

Sub-chronic treatment with DOX was found to retain unchanged the levels of apoptotic and mitochondrial membrane permeabilization proteins in the lung but it did exhibit markers of lipid peroxidation, however if it is a direct effect of the drug or rather an indirect effect as observed in the brain tissue remains to be elucidated [222].

2.6 Prevention of doxorubicin cardiotoxicity

As the cure for DOX-induced cardiac heart failure is not presently available, prevention remains the best therapeutic. The idea is not only to counteract DOX-induced toxicity but to increase the therapeutic efficacy of the drug either by allowing the use of higher dosage ($>500\,\mathrm{mg\,m^{-2}}$) or to decrease the toxic response without interfering with the antineoplastic activity. However, the benefits from all preventive approaches currently available are limited. Nevertheless, a preventive approach can be achieved either by pharmacologically or non-pharmacologically means.

2.6.1 Non-pharmacological strategies

Schedule administration

One obvious approach is achieved by limiting the cumulative dose of DOX to less than $450\,\mathrm{mg\,m^{-2}}$ or by decreasing the drug peak plasma results in a reduction of the toxicity. A precise schedule for drug administration and/or choosing a continuous bolus infusion over a single infusion has proven to attain less damage to the heart and therefore decrease the probability of heart failure since both strategies can decrease drug concentration in the plasma [148, 176].

In these particular reports, weekly administrations of DOX decreased the incidence of heart failure compared to the standard schedule in which DOX is administered every three weeks [148]. Similarly, administering DOX by continuous infusion over a 48 h period rather than the standard 15 min bolus infusion was capable of reducing the drug peak plasma and also the damage in cardiac tissue as accessed by biopsy [148, 223]. However, this procedure was later discarded when it was determined that continuous infusion might also reduce antitumor efficacy probably due to a decrease

in the initial concentration at tumor level [224].

Analogues

Alternatively, new anthracyclines analogs that have the same or better therapeutically effect but lack the toxic activity has been proposed. The rationale behind this idea goes back to late 1960s, since DOX is derived from its parent compound, daunorubicin, by the substitution of a hydrogen atom by a hydroxyl group, increasing the therapeutic efficacy (Fig. 2.1, p. 47) [137]. Due to the tetracyclic ring and amino-sugar moiety, several modifications can be made.

However, from the almost 2000 analogues investigated in the last 4 decades, only a few have reached clinical approval [148, 176]. Epirubicin has been one of the most extensively investigated DOX analogues and is now widely used as an alternative to DOX [148, 225]. Epirubicin shows the same spectrum of antitumoral efficacy although with different pharmacokinetics and metabolism. The toxicity effects are the same in quality but quantitatively less when compared to DOX, which enabled an increase in cumulative doses to almost double of those of DOX (900 to 1000 $\mathrm{mg\,m^{-2}}$).

New formulations

Use of liposome-encapsulated or tumor-targeted delivery of DOX is probably one of the most investigated strategies in the past decade [226]. The fact that vasculature around tumors is more permeable, i. e., higher fenestration, allows for higher accumulation of liposomes at the tumor site, therefore decreasing systemic drug concentration and improving the targeting of the treatment. Lipossomal formulations of DOX have proven improved efficacy over free DOX and are currently used in the clinic [148, 149, 176].

The improvement can be explained by several factors including prolonged half-life, prevention of metabolic conversion of DOX to inactive forms or even to aglycones and secondary alcohol metabolites, preferential distribution and prolonged release of the drug within the tumor mass and, finally, limited accumulation in healthy tissues [148]. Currently, two different preparations of DOX-liposomal formulations with superior action and fewer side effects when compared with free DOX have been assessed in experimental models and clinical trials.

The first one is a polyethyleneglycol-coated (pegylated) liposomal DOX that has more favorable pharmacokinetics than free DOX and is also capable of overcoming the blood-brain barrier [148, 225]. The other preparation involves uncoated citrate-containing liposomal DOX formulation, where citrate is included to increase DOX encapsulation. The results showed less pronounced pharmacokinetics indexes than pegylated liposomal DOX [227].

2.6.2 Co-administration of protective agents

If no plausible replacement is obtained for DOX, one sounding strategy is to spare the non-target organ by co-administrating DOX with compounds capable of prevent side effects, e.g. by preventing DOX-induced cardiomyopathy. Along the years, strategies used included antioxidants, iron chelators, lipid-lowering drugs and β-blockers.

Antioxidants

Several naturally occurring or synthetic antioxidants have been co-administered with DOX [228, 229]. Cellular levels of GSH can be increased by thiol-containing agents such as *N*-acetylcysteine(NAC), a molecule with high bioavailability which upon hydrolysis releases cysteine, a precursor of GSH biosynthesis [230, 231]. Similarly, cystamine or its reduced form cysteamine, as well as metallothionein, are able to increase cellular GSH content [232, 233]. The use of these compounds both *in vitro* and *in vivo* has decreased DOX toxicity [232]. Unfortunately, the use of NAC had no success in clinical trials even when high doses were administered to patients [234].

The use of antioxidant nutrients have been shown to prevent some damage on cardiac tissue caused by DOX treatment [235]. Vitamins (E, C and A), CoQ, and flavonoids/polyphenols normally found in the diet increased the cellular contents of GSH and SOD and also decreased malonyldialdehyde and lipid peroxidation demonstrating the capacity to prevent DOX toxicity. In the case of vitamin E, this antioxidant agent decreased oxidative stress induced by DOX without preventing the mitochondrial dysfunction associated with the treatment [188]. In one particular work, a diet enriched in vitamin E did not afford protection against DOX-induced State 3 and State 4 respiration inhibition and decreased Ca^{2+} loading capacity. However, protein carbonyl content, a marker of oxidized proteins, was decreased in the DOX-treated group fed with a Vitamin E enriched diet.

In conclusion whereas some *in vitro* studies demonstrated positive effects caused by direct antioxidant activity or indirectly, by stimulating the production of natural antioxidant defenses, *in vivo* results were disappointing. The lack of positive outcome might be due to the poor bioavailability of the protective compounds after oral administration or to a limited availability in the critical sites where DOX exerts its toxic effects, one example being mitochondria.

Targeting of antioxidants

Ideally, the best strategy to counteract the increase in DOX-induced oxidative stress would be the ability to overexpress celular detoxification system enzymes in cardiomyocytes. In fact, transgenic mice overexpressing catalase or glutathione peroxidase, or even SOD, were demonstrated to decrease cardiac damage after DOX treatment [232]. Overexpression of the radical scavenger metallothionein in the hearts of transgenic mice also prevented DOX-induced cardiotoxicity [232, 236] supporting the concept that detoxification by overexpressing antioxidant proteins might be a plausible strategy to circumvent DOX toxicity. However, this expression may not always be restricted to the heart, thus making it necessary to first design a specific cardiac overexpression system.

Alternativelly, while no specific cardiac overexpression system is available, one could specifically target common antioxidants to mitochondrial compartment and its membranes in an attempt to circuvent the limitations apointed above. Currently, two similar approaches are proposed to achieve such objective: linking antioxidants to the lipophilic cationic ion TPP, e.g., coenzyme Q_{10} forming the molecule MitoQ [26] or plastoquinone in the case of Skulachev ions [237]. Due to the positively charge nature of these compounds and higher negative-inside $\Delta\psi$ of mitochondria, the compounds can accumulate up to 200-fold in the matrix. Besides, the natural character of such molecules enables the recycling of the molecule by OXPHOS after scavenging the radical species and, theoretically, the process can continue indefinitely (Fig. 2.4).

Theoretically, any molecule can be linked to TPP moiety to satisfy different targeting strategies. Several antioxidants targeted to mitochondria have been developed, including MitoSOD ($O_2^{\bullet-}$), MitoPeroxidase (H_2O_2), MitoTEMPOL ($HO^{\bullet}$), MitoE_2 and MitoQ_{10} (lipid peroxidation) [26] but only MitoQ was used in the context of DOX toxicity [173]. The report states that the cationic molecule was capable to prevent alterations on the echocardiographic profile and the extension of fibrosis in cardiac

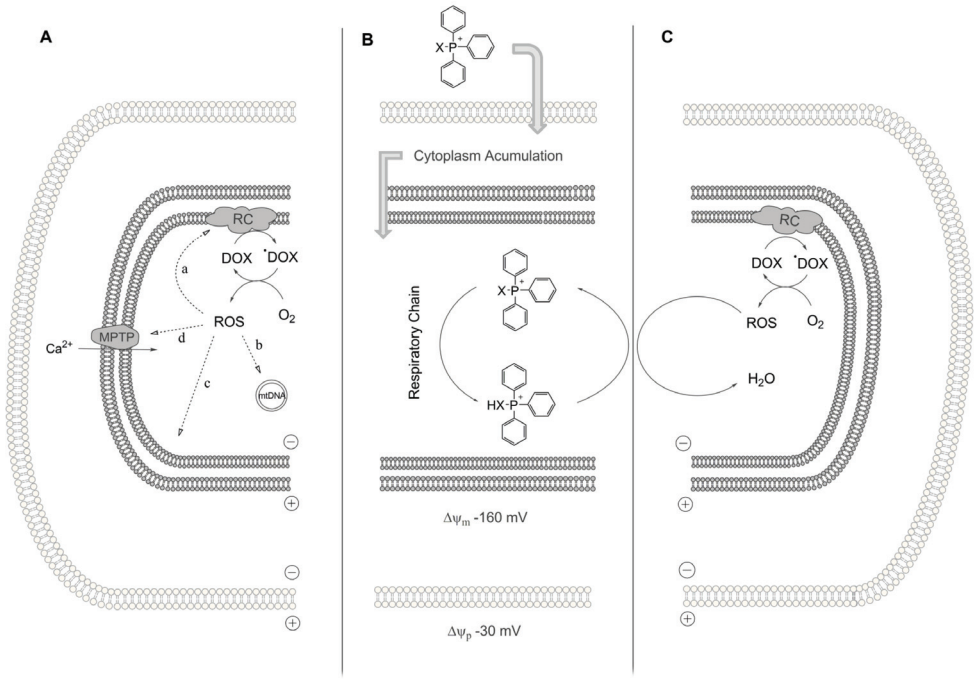

Figure 2.4: Doxorubicin toxicity and a possible strategy to counteract it. For the sake of simplicity, a single cell, surrounded by a light colored bilayer, contains only one mitochondrial body, surrounded by a dark lipid bilayer. **A**) Summary of DOX targets and effects. DOX redox cycling at Complex I results in the generation of oxidative stress, which contributes to the oxidation and decline in function of critical mitochondrial proteins (**a**), DNA (**b**), membrane lipids (**c**) and to the formation and opening of the mPTP pore (**d**). **B**) Cellular accumulation of a bioactive molecule (X) linked to TPP which is a lipophilic cation and can, therefore, accumulate 5-fold in the cytoplasm due membrane potential. Moreover, the high negative mitochondrial membrane potential allows for a 200-fold accumulation inside the organelle. If the linked molecule behaves as an antioxidant, it is possible to have it regenerated by the mitochondrial respiratory chain. Adapted from Murphy [26]. **C**) Hypothetical strategy to overcome DOX-increased ROS production. If a TPP-antioxidant construct is actively accumulated in mitochondria, it would be possible in theory to counteract DOX-induced oxidative stress, by scavenging free radicals resulting from DOX redox cycle. Abbreviations: *RC*, respiratory chain; *MPTP*, mPTP pore.

tissue. Moreover, MitoQ restored the expression of Complex IV subunits and therefore the activity of the enzyme [173], although no further end-points of mitochondrial dysfunction were investigated.

Iron chelators

Many agents able to remove iron from a complex with DOX have been investigated as possible cardioprotectors. Dexrazoxane[2], which belongs to the bisdioxopiperazine family, is currently the bestf therapeutic approach of choice, reaching significant efficacy in counteracting DOX-associated toxicity [148]. In fact, dexrazoxane is the only approved drug used in co-administration with DOX with the ultimate aim of preventing DOX-induced cardiac damage. The molecule is an analogue of EDTA and was initially designed as an antitumor agent [225]. Its mechanism of action involves its ability to chelate free iron and to displace iron from DOX-iron complexes. Once accumulated into cardiomycocytes, dexrazoxane is hydrolyzed to form an open-ring which has strong chelating characteristics [148, 225].

However, some caution should be taken when using this compound since it can also deplete iron from intracellular stores and interfere with iron transport [238]. Moreover, it possesses myelosuppressive action which can aggravate the same suppressive action of DOX [239]. Thus, despite the cardioprotective capacity of dexrazoxane, its clinical use is not free of risks and other iron-chelating agents should be developed and tested.

β-Blockers

Another approach to decrease DOX toxicity would be to decrease the rate of cardiac contraction. The rationale behind this strategy is that by decreasing the energy demand of a myocardium with impaired mitochondrial capacity, one can maintain heart function with a limited mitochondrial supply. β-blockers are commonly used to decrease hypertension and can be used to control cardiomyopathies although some caution should be taken when interpreting results or long treatment periods [240].

Carvedilol[3] is a β-adrenergic receptor antagonist, which has demonstrated efficacy in preventing DOX-induced cardiac toxicity [187]. It has been described that the protective effects of carvedilol against DOX-induced cardiotoxicity go beyond the hemodynamic effects and directly involve protection of mitochondrial function. An early study by Fazio and co-workers [241] was the first to demonstrate that carvedilol was able to induce complete recovery in a patient undergoing DOX treatment and used to

[2]also known or commercially available as Cardioxane, Zinecard, Eucardion, ICRF-187, ADR 529 or Raxozane (S)-isomer. Source: http://pubchem.ncbi.nlm.nih.gov/

[3]also known or commercially available as coreg, dilatrend, eucardic, kredex, querto, artist or coropress. Source: http://pubchem.ncbi.nlm.nih.gov/

show signs of congestive heart failure. Following this work, an animal model of DOX-induced cardiac toxicity showed a remarkable protective effect of carvedilol, attributed to its antioxidant and lipid-lowering properties [242]. Nevertheless, it remained to be known whether the protective effect of carvedilol on DOX-induced cardiac toxicity originated from the prevention of cardiac mitochondrial degeneration.

Co-administration of carvedilol decreased the extent of cellular vacuolization in cardiac myocytes and prevented the inhibitory effect of DOX on mitochondrial respiration in both heart and liver [185]. Interestingly, co-treatment with carvedilol protected cardiac mitochondria from DOX-induced decrease in Ca^{2+} loading capacity but did not protect liver mitochondria. One additional logical concern would be that carvedilol, besides preventing DOX mitochondrionopathy, also decrease the anti-neoplastic activity of DOX. Nevertheless, it was observed that carvedilol reduces P-glycoprotein activity increasing therefore the sensitivity to DOX cytotoxicity in cell cultures of two human breast cell sub-lines [185].

Further *in vivo* studies with DOX-treated rats have confirmed that carvedilol is able to prevent cardiac mitochondrionopathy through an antioxidant mechanism [243]. Rats submitted to long-term treatment with DOX present several mitochondrial alterations, including decreased Ca^{2+} loading capacity [187]. Although carvedilol and atenolol[4] were able to preserve ATP levels in the tissue, only carvedilol was capable to preserve mitochondrial function by preventing the loss of mitochondrial Ca^{2+} loading capacity and by inhibiting the appearance of protein carbonyl groups. The protective effect of carvedilol was not shared by atenolol, once more demonstrating the importance of carvedilol antioxidant activity [187]. Another common consequence of DOX-induced increase in oxidative stress is lipid peroxidation and once more, carvedilol was able to avoid such harmful occurrence in DOX-co-treated animals as assessed by TBARS levels [242].

Mitochondrial ATP-sensitive K^+ channels activators

Although some caution should be taken, ischemic events and DOX-induced cardiomyopathy are fairly similar. For example, in both processes increased ROS production and Ca^{2+} accumulation are observed, resulting (in some cases) in the stimulation of mPTP. Previous studies have suggested that mitoKATP play a role in the mechanism of ischemic preconditioning mediated cardioprotection [244] even though an argument

[4] β-blocker without antioxidant properties

regarding the actual existence of mitoKATP exists [245].

No doubt exist regarding K^+ cycling through the IMM; influx occurs as a result of diffusive leak and efflux through the electroneutral K^+/H^+ antiporter, with cation main role being regulation of mitochondrial volume, respiration, and $\Delta\psi$ [245]. However, the protein-mediated influx pathway for K^+ suggested in the 90's [246] has no specific non-physiological agonist or agonist which contributes to the established disagreement together with the molecular identity of the channel, which remains yet to be elucidated [245]. Nevertheless, putting the issue aside mitoKATP activity is probably associated with cellular energy charge as channel opening probability increases proportional to ATP decrease [247]. Also, opening of mitoKATP appears beneficial as the low rate of K^+ transport is yet sufficient to lower $\Delta\psi$ so decreased levels of ROS or Ca^{2+} uptake are observed [246].

Despite this controversy, if mitoKATP really exist, is thus acceptable to think that mitoKATP opening may attenuate DOX-induced toxicity and, in fact, this approach was already explored showing promising preliminary results [248, 249]. However, most mitoKATP agonists and antagonists also present other effects on mitochondrial and cellular function, even at micromolar concentrations [244]. One of the strategies used combined sildenafil and a selective inhibitor of cGMP specific phosphodiesterase-5, which protected against oxidative stress injury through opening mitoKATP in a chronic model of DOX cardiotoxicity [248]. In this model, sildenafil was capable of attenuating cardiomyocyte apoptosis, of maintaining mitochondrial membrane potential, and preventing left ventricular dysfunction and ST prolongation. All protective effects were abolished in the presence of mitoKATP inhibitors. As also referred by the authors, sildenafil has proved to be a safe drug for different pathologies, including erectile dysfunction and pulmonary hypotension, which makes it acceptable to counteract DOX-induced cardiotoxicity. Although its effects on DOX neoplastic activity were not evaluated, sildenafil would allow the use of increased doses of DOX improving its treatment efficacy.

2.6.3 Exercise

Finally, it has been demonstrated that exercise prevents DOX-induced cardiac damage [250–252] and specifically protect cardiac mitochondria [253, 254] from the deleterious effects of that anti-neoplastic agent. Aerobic exercise was shown to increase both systolic and diastolic heart function while decreasing the extent of cardiac remodeling

thus increasing resistance of cardiac tissue to fatigue [253]. The complete mechanism by which exercise achieves protection against DOX-induced cardiotoxicity is yet to be complete; however, its action is probably associated with increased expression of antioxidant enzymes and OXPHOS complexes activity but not heat-shock proteins [178, 251, 254]. Additionally, exercise was effective in preventing β-myosin heavy chain increase, i.e. the shift from α (normal) to β (pathological) form [252].

However, despite the beneficial nature of exercise practice in DOX context or chemotherapy in general, extrapolation to a clinical situation should be made with caution. For example, what is the chance that a future chemotherapy patient has practiced intense exercise in the couple weeks before the beginning of the treatment? Moreover, even though exercise may be protective during treatment, patients may show decreased exercise capacity and most works in the literature are based on the treadmill training which is considered to be of high intensity. Nevertheless, more recent reports also present the voluntary wheel training as capable of preventing DOX cardiotoxicity with a less intensive protocol. In this situation, although DOX treatment decreased the running activity and distance of treated animals the cardioprotective response was not dissimilar from the treadmill training group [252].

Chapter 3

Hypotesis and Aim of the Present Dissertation

As described in Chapter 2, DOX cardiotoxicity greatly limits its utility in clinical practice. However, although several reports point the selectivity of the drug for the cardiac tissue, scarce information regarding this selectivity actually exists. Therefore, work capable of discerning such effects are of great clinical value, as more compelling counteractive strategies can be develop.

Nonetheless, from the author's point of view, which is explored in Chapter 5, there is actually a lack of studies involving other tissues besides the heart that could be taken as negative controls in the interpretation of results, in an attempt to better address the selectivity of the drug.

Hence, one of the main objectives of the present thesis is to provide a comparison of DOX toxicity across three distinct and vital organs, including the heart. The hypothesis of the present work is that DOX treatment will show tissue-specific effects with cardiac tissue being the one with most injuries, in terms of extension and persistence. It is the author's ambition to present new non-reported mechanisms of DOX-induced cardio-selective toxicity.

A detailed characterization of the *in vivo* model used is present in Chapter 5. Furthermore, the information here presented allows indirect comparison with a previously well established rodent model of sub-chronic exposure to DOX. Likewise, it also consider the hypothesis that alterations of mitochondrial bioenergetics occur predominantly in the heart, as possible early and sensitive markers of DOX-induced toxicity.

In Chapter 6, the role of sensitivity to MPTP will be further investigated. Despite being already demonstrated that cardiac mitochondria, as opposed to liver mitochondria, from DOX-treated rats suffer from enhanced permeability transition, the experiments were always performed with succinate as substrate. Apparently, cardiac mitochondrial Complex I is selectively targeted by DOX which raises the possibility that the difference between cardiac mitochondria from DOX-treated rats and their control counterparts may be exacerbated when Complex I substrates are used instead. Besides, little or nothing is known about differential MPTP induction with both substrates in the three organs.

Moreover, although ANT was previously reported to be decreased in content in the cardiac tissue no information exists regarding other modulators of the MPTP. The work presented in Chapter 6 will evaluate the expression and levels of such proteins and comprehend if the effect is once more tissue-specific. Additionally, one will assess the *in vitro* production of H_2O_2 through the MRC to better interpret the role of oxidative stress in MPTP opening.

Finally, Chapter 7 will attempt to contextualize the idea of metabolic thresholds in DOX cardio-selective toxicity. As it was briefly introduced in Section 2.5.1, Mazat's group [30, 219] showed that, despite constant and common mitochondrial DNA mutations or deletions, some organs do not show any affected mitochondrial function until a certain threshold is reached. The authors explained the result with the concept of metabolic threshold, that is, the amount of inhibition of an OXPHOS complex necessary to observe visible changes in the final activity. The value of this threshold for a given OXPHOS complex can vary according to the tissue.

Thus, the author intend to use the metabolic threshold theory to demonstrate that heart mitochondria are mostly affected by DOX because the enzyme reserves in this tissue are lower when compared with other tissues. In other words, inhibition of an enzyme activity causes a much early response in the entire metabolic flux in the heart when compared with the other tissues.

As has been repeatedly suggested throughout the text, the study of mechanisms of DOX-induced cardiac-selective toxicity are of extreme importance in order to design new strategies to minimize cardiomyopathies associated with acute and chronic treatments without compromising the therapeutic action of the drug.

Part II

Experimental Results

Chapter 4

Material and Methods

4.1 Reagents

All reagents used were of the highest grade of purity commercially available (analytical or better). Aqueous solutions were prepared in ultrapure (type I) water (Milli-Q Biocel A10 with pre-treatment via Elix 5, Millipore, Billerica, MA, USA). For non-aqueous solutions, ethanol (99.5 %, Sigma-Aldrich Quimica SA, Sintra, Portugal) or

DMSO (Sigma-Aldrich) were used as solvents.

4.1.1 Doxorubicin solution for injection

DOX hydrochloride, 98 % chemical purity was obtained from Sigma-Aldrich and prepared in a sterile saline solution, NaCl 0.9 % (*p*H 3.0, HCl) and stored at 4 °C, for no longer than 5 d upon rehydration. Vials were used from the same batch for each treatment protocol.

4.1.2 Decylubiquinol

Decylubiquinol (DQH_2) was prepared by reduction of decylubiquinone as previously reported [255], with minor adaptations. Lyophilized decylubiquinone (Sigma-Aldrich) was diluted in pure ethanol to 10 mg ml^{-1} and *p*H acidified to 2.0 with small amounts of 1 M HCl to stabilize quinol form after reduction. The reduction *per se* was initiated by the addition of a few granules of sodium borohydride ($NaBH_4$) which turned the yellow color solution into a colorless one. The excess of $NaBH_4$ was removed upon addition of 1 volume of H_2O.

Decylubiquinol was recovered by two successive extractions in 3 volumes of 2:1 mixture of diethylether-cyclohexane subjected to vigorously shaking. Upon collection of both upper phases, 2 volumes of 2 M NaCl were added and the solution was vigorously shaken. The upper phase was collected and evaporated to dryness under a stream of N_2 gas. Finally, the residue was resuspended in 1 volume of ethanol acidified to *p*H 2.0 with small amounts of 1 M HCl to stabilize and prevent the oxidation of DQH_2.

Since one cannot assume all DQH_2 was reduced, an estimation of the concentration of DQH_2 was performed by spectrophotometry in a Jasco V-560 spectrophotometer (Jasco Inc., Easton, MD, USA) as the amount oxidized by 5 M NaOH [255]. Autozero was performed at 320 nm with ethanol in two quartz cuvettes and then 10 µl of decylubiquinone were added to the front cuvette and scanned from 320 to 220 nm at 100 nm min^{-1} and 2 nm band width. Absorbance at 275 nm was noted and 10 µl of 5 M NaOH were added to both cuvettes and the scan repeated. The change in absorbance at 275 nm was noted and DQH_2 concentration was calculated as follow, with ε_{275} =12.25 mM^{-1} cm^{-1} [255]:

$$[DQH_2] = \frac{A_{DQ}^{275} - A_{DQH2}^{275}}{\varepsilon_{275}} \times \text{dilution factor} \quad (4.1)$$

DQH_2 was stored at −80 °C for no more than 15 d which showed no significant oxidation of the molecule.

4.1.3 Reduced cytochrome c

Reduced cytochrome c was prepared through reduction of cytochrome c by DTT, as described in the datasheet for cytochrome c oxidase assay kit from Sigma (CYTOCOX1, Sigma-Aldrich). Lyophilized cytochrome c (bovine heart, Sigma-Aldrich) was resuspended in phosphate buffer (see sec. 4.16.1) to 10 mg ml^{-1} with gently mixed for complete solubilization and an aliquot (oxidized cytochrome) was saved. The reduction *per se* was initiated by addition of fresh-prepared DTT (100 mM) to a final 500 µM concentration. Reaction was complete after 15-30 min where the solution turned from dark orange-red to pale purple-red and a second aliquot (reduced cytochrome) was saved.

A spectral scanning of both aliquots from 350 to 750 nm was run in a Nanodrop (NanoDrop 2000, ThermoScientific, Wilmington, DE, USA). If the reduction was effective, two peaks for reduced cytochrome c instead of only one for oxidized cytochrome c at 530 nm can be observed. The most important peak is the one at 550 nm where the ratio of $A_{\text{cyt-cred}}^{550}/A_{\text{cyt-cred}}^{600}$ should be greater than ten. Reduced cytochrome c concentration was calculated through Beer-Lambert equation using ϵ_{550} =19.1 mM^{-1} cm^{-1} [256] and l =0.1 cm. Reduced cytochrome c was store in aliquots at −80 °C.

4.2 Animal Care

Animal handling was conducted in accordance with the European Convention for the Protection of Vertebrate Animals used for Experimental and Other Scientific Purposes (CETS no.123) and Portuguese rules (DL 129/92). Animal handlers were credited by FELASA category C for animal experimentation (accreditation no. 020/08) .

Male Wistar rats, Crl:WI(Han), were purchased from Charles River (France) with 14 weeks of age (acute treatment) or 6 weeks of age (sub-chronic treatment) and acclimated for 10-14 days prior to the initiation of experiments and maintained in local

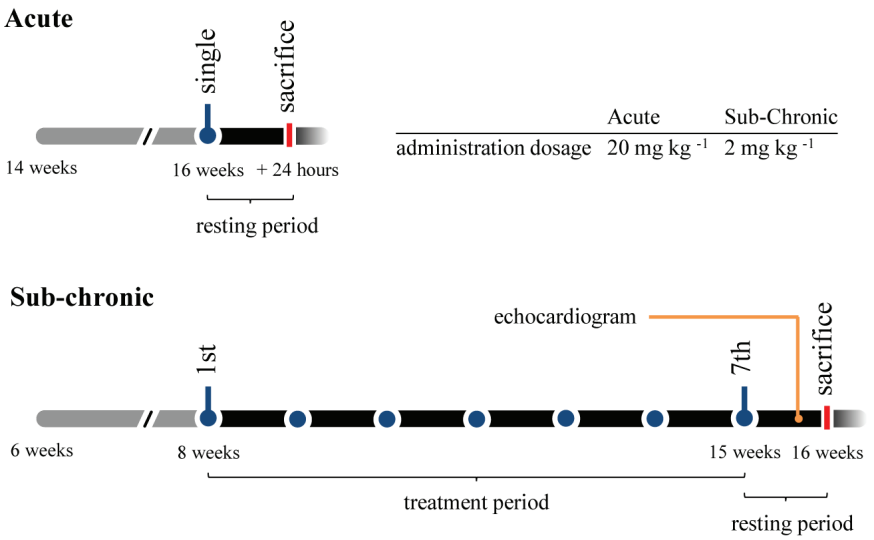

Figure 4.1: Timeline of the experimental design of DOX treatment. In the acute model, animals were divided in two groups and received either a single dose of DOX or equivalent volume of vehicle solution (NaCl 0.9 %) via intraperitoneal injection and were sacrificed 24 hours later. In the sub-chronic model, animals were divided in two groups and received seven weekly doses of DOX or equivalent volume of vehicle solution via subcutaneous injection and were allowed to rest for one week before sacrifice. In this model, the total dosage of DOX was 14 mg kg^{-1} of body weight. Some animals of the sub-chronic model were submitted to an echocardiogram five day after the last injection (7th). Blue dots represent single administrations.

animal house facilities (CNC – School of Medicine, University of Coimbra, Coimbra, Portugal).

Animals were group-housed in type III-H cages (Tecniplast, Italy) with irradiated corn cob grit bedding (Scobis Due, Mucedola, Italy) and environmental enrichment, maintained in controlled environmental requirements (22 °C, 45-65 % humidity, 15-20 air changes/hour, 12 hours artificial light/dark cycle, noise level <55 dB) and free access to standard rodent food (4RF21 GLP certificate, Mucedola, Italy) and acidified water (at *p*H 2.6 with HCl) *ad libitum*.

4.3 Experimental Design

For the acute study, experimental manipulation was initiated with 16 weeks old rats (N=34) randomly grouped in pairs and administered either with DOX (20 mg kg^{-1}

of body weight, n=17) or with an equivalent volume of vehicle solution (NaCl 0.9 %, n=17) into the *peritoneum* cavity (intraperitoneal injection) exactly 24 hours before sacrifice (Fig. 4.1), as previously described [184].

For the sub-chronic study, the experimental protocol was performed with 8 weeks old rats (N=40) randomly grouped in pairs and weekly injected with a subcutaneous injection in the scruff or flank of either DOX ($2\,mg\,kg^{-1}$ of body weight, n=20) or equivalent volume of vehicle solution (NaCl 0.9 %, n=20) during seven weeks, and allowed to rest one week after the last injection (Fig. 4.1), as previously described [187].

All animals were injected during the light phase of the cycle, observed daily and weighed at the beginning and at the end of the experimental treatment period, being also weekly weighed at the time of injection. Animals were euthanized in pairs daily after the end of protocol treatment by cervical dislocation followed by decapitation, to confirm death, and exsanguination, in order to collect blood.

Rats were sacrificed between 9:00 and 10:00 AM to eliminate possible effects due to diurnal variation and were not fasted before sacrifice. Organs were immediately extracted from the body and quickly washed in appropriate buffer before being weighed.

4.4 Echocardiogram

Transthoracic echocardiograms were performed under the same specifications as previously described [257]. Five days after the last injection (Fig. 4.1), sub-chronically-treated animals, free of anesthesia, were examined lying in the left lateral decubitus position and using a commercial available echocardiograph system (VIVID i, G.E. Helthcare, Buckinghamshire, UK), equipped with an 11.5 MHz transducer.

A two-dimension short-axis view of left ventricle was obtained at the level of the papilary muscles and M-mode tracings were recorded through the inter-ventricular septum and posterior wall. Inter-ventricular septum and posterior wall thickness (end diastolic) and left ventricle internal dimensions (systolic and diastolic) were measured from at least three consecutive cardiac cycles on the M-mode tracings. All the exams were performed by the same observer in the same day.

Every parameter was measured accordingly to the American Society for Echocardio-

graphy guidelines[1] and results were directly obtained from the equipment software by a cardiologist blinded for treatment groups. Left ventricular mass (LV mass) was calculated using a standard cube formula which assumes a spherical left ventricular geometry [257] according to the following equation:

$$LV\,mass = 1.04 \times [(LVDd + LVPW + IVS)^3 - LVDd^3] \tag{4.2}$$

where results are expressed in mg and 1.04 represents the specific gravity of muscle.

4.5 Histological Analysis

Organs were immersion-fixed in Bouin's solution for 24 hours and then washed with 70 % alcohol until the solution became clear and stored in 70 % alcohol until the histological analysis was performed. At that time, after several incubations with increasing alcohol percentages (70 %, 90 %, and 100 %) and xylol, tissues were processed in the normal paraffin procedure and sectioned (3 µm thick). The sections were then deparaffinized with xylol and incubated with solutions with decreasing alcohol content (100 % and 95 %).

All the slides were stained with hematoxilin and eosin (HE) by using standard procedures. The samples were covered with coverslips in Eukitt mounting medium and then visualized in a Nikon Eclipse 80I microscope (Nikon Instruments Europe B.V., Amstelveen, The Netherlands) coupled with a camera and computer. Analyses were conducted in a blind fashion without performing a histological score by a certified professional.

4.6 Electron Microscopy

After extraction and washing, a small slice (2-5 mm) of the harvested organs was cut with the help of a scalpel and fixed in 3 % glutaraldehyde in phosphate buffer (100 mM NaH_2PO_4, *p*H 7.3). Samples were left in the fixative solution until processed. Then, postfixed in 1 % osmium tetroxide in same buffer and dehydrated in solution containing increasing alcohol percentages (70 %, 90 %, and 100 %) before being embedded in Spurr's resin. A detailed scheme of the procedure is depicted in Fig. 4.2.

[1] available at www.asecho.org/guidelines/

Ultrathin sections were obtained with an LKB ultra-microtome Ultrotome III (GE Healthcare, Little Chalfont, Buckinghamshire, UK), stained with methanolic uranyl acetate followed by lead citrate, and examined with a JEOL Jem-100SX electron microscope (JEOL, Tokyo, Japan) operated at 80 kV. The operator was blinded to treatment groups and took 5 to 10 micrographs in random fields for global cell and mitochondrial profiles characterization.

4.7 Blood Analyses

Blood was collected after decapitation to sterile tubes without additives. After blood clot formation, serum was separated by centrifugation at 1600 ×g , 10 min at 4 °C (Sigma 3-16K, 1333 rotor). Supernatant was then transferred to microtubes and centrifuged at 16 000 ×g , 20 min at 4 °C(Eppendorf 5415 R, FL062 rotor). Serum samples were maintained for a short time at 4 °C for analysis by an external certified laboratory (Clinical Analysis Laboratory, School of Pharmacy, University of Coimbra, Portugal), or stored frozen at −80 °C (less than 24 months) for troponin I (TnI) analysis using the singleplex Rat Cardiovascular Panel (RCVD1-89K, Millipore, Arium, Portugal). All analysis were performed by external trained personal blinded for treatment groups.

4.8 Isolation of Mitochondrial Fractions

Mitochondria were isolated by the standard procedure usually used in our laboratory based on previous established methods [258, 259] (Fig. 4.3). Organs were excised from the animal and after connective tissue and fat were removed, tissue was finely minced in an ice-cold homogenization buffer (250 mM sucrose, 10 mM HEPES *p*H 7.4 (KOH), 1 mM EGTA, supplemented with 0.1 % defatted BSA) and washed several times with this buffer to remove blood excess.

The minced blood-free tissue was then homogenized with a tightly fitted glass/Teflon power-driven Potter-Elvejhem homogenizer. For the isolation of cardiac mitochondrial fractions, the homogenization medium was supplemented with 0.5 µg ml^{-1} of protease (Subtilisin A, Type VIII from *Bacillus licheniformis*, Sigma-Aldrich). Exposure to protease was limited to 2-3 min in order to minimize loss of mitochondrial membrane

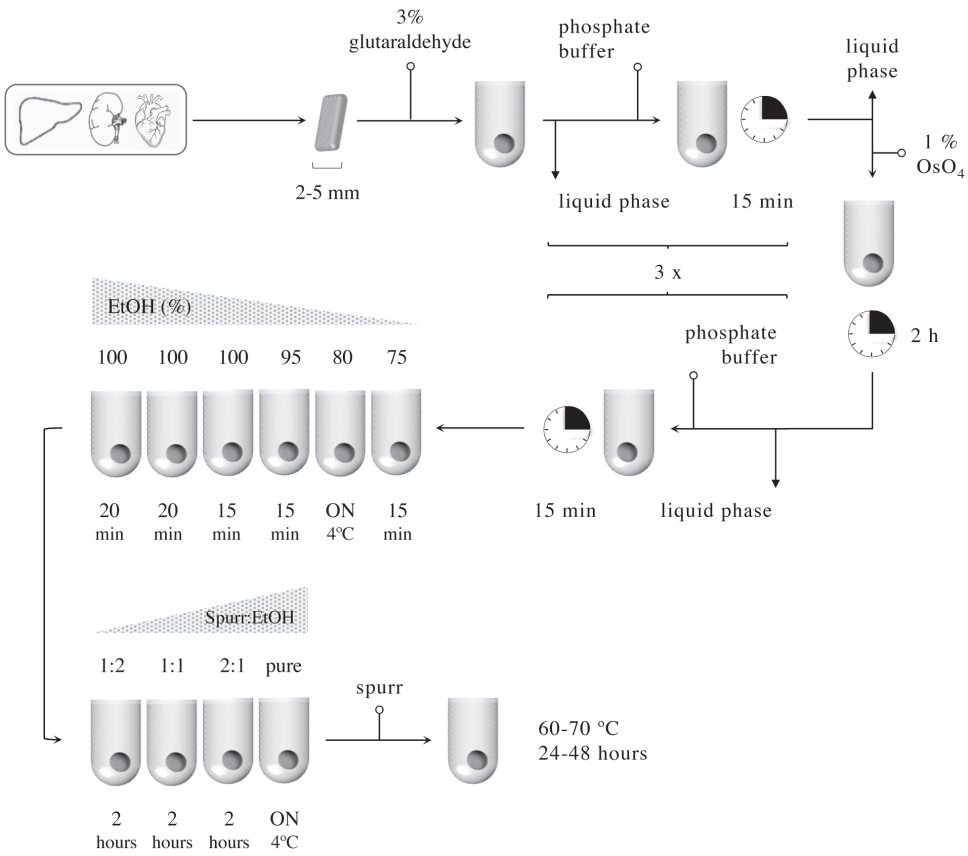

Figure 4.2: Flowchart for the preparation of tissue samples for electron microscopy. Small pieces of each tissue were fixed in 3 % glutaraldehyde, overnight at 4 °C and then postfixed in 1 % osmium tetroxide and dehydrated in increasing alcohol percentage before being embedded in resin. *ON* - overnight.

integrity.

The homogenate was then submitted to a differential centrifugation in order to obtain mitochondrial fractions. In the case of heart, it was necessary first to remove the protease from the solution. Therefore, the homogenate was centrifuged at 14 400 ×g for 10 min at 4 °C (Sorvall RC-6 Plus or Sorvall Evolution RC, SS-34 rotor, Thermo Fisher Scientific Inc., Rockford, IL, USA). The supernatant fluid was decanted and the pellet, essentially devoid of protease, was gently homogenized to its original volume in homogenization buffer with a loose-fitting glass/Teflon hand-held Potter-Elvejhem homogenizer.

At this point, the homogenate of all organs were subjected to the same centrifugations steps. Initially, homogenates were centrifuged at 800 ×g for 10 min at 4 °C and the resulting supernatant centrifuged at 10 000 ×g for 10 min at 4 °C. The pellet was ressuspended in washing buffer containing 250 mM sucrose, 10 mM HEPES *p*H 7.2 (KOH) using a paintbrush and repelleted once (heart) or twice (liver and kidney) at 10 000 ×g for 10 min at 4 °C before obtaining a final mitochondrial suspension (cardiac mitochondria was resuspended in a 500 µl of washing medium, liver in 2 ml and kidney in 1 ml).

The mitochondrial protein after isolation was quantified by the biuret method (see section 4.10.1, pag. 87) using BSA as a standard and mitochondrial preparation was kept on ice during experiments, which were carried out after a 20 minutes recovery and within 5-6 h post-isolation.

4.9 Material harvesting

Tissues were preserved in RNA*later* solution (Ambion, Austin, TX, USA). Before immersion, large tissue samples were cut into small pieces and then placed in 5-10 volumes of RNA*later* solution for incubation at 4 °C overnight. In the following day, samples were withdrawn from solution and stored at −80 °C until extraction.

4.9.1 Total tissue protein

In the day of extraction, 70 to 150 mg of RNA*later*-conserved frozen tissue was thawed and grounded in a glass pestle hand-held homogenizer in a 20 % (*w*/*v*) RIPA buffer (150 mM NaCl, 50 mM Tris *p*H 8.0 (HCl), 0.5 % sodium deoxycholate (DOC), 1 % IGEPAL (CA-630) and 0.1 % sodium dodecyl sulfate (SDS)), supplemented with 5 µl/100 mg (tissue) of protease inhibitors cocktail (P8340, Sigma-Aldrich Inc) followed by further homogenization in a 1 ml syringe with a 27 gauge needle (10 passages).

The suspension was kept on ice for 15-20 min and then centrifuged at 14 000 ×g for 5 min at 4 °C to remove cellular debris. Pellet was discarded and protein concentration in the supernatant was determined by BCA assay (see section 4.10.2) using BSA as standard.

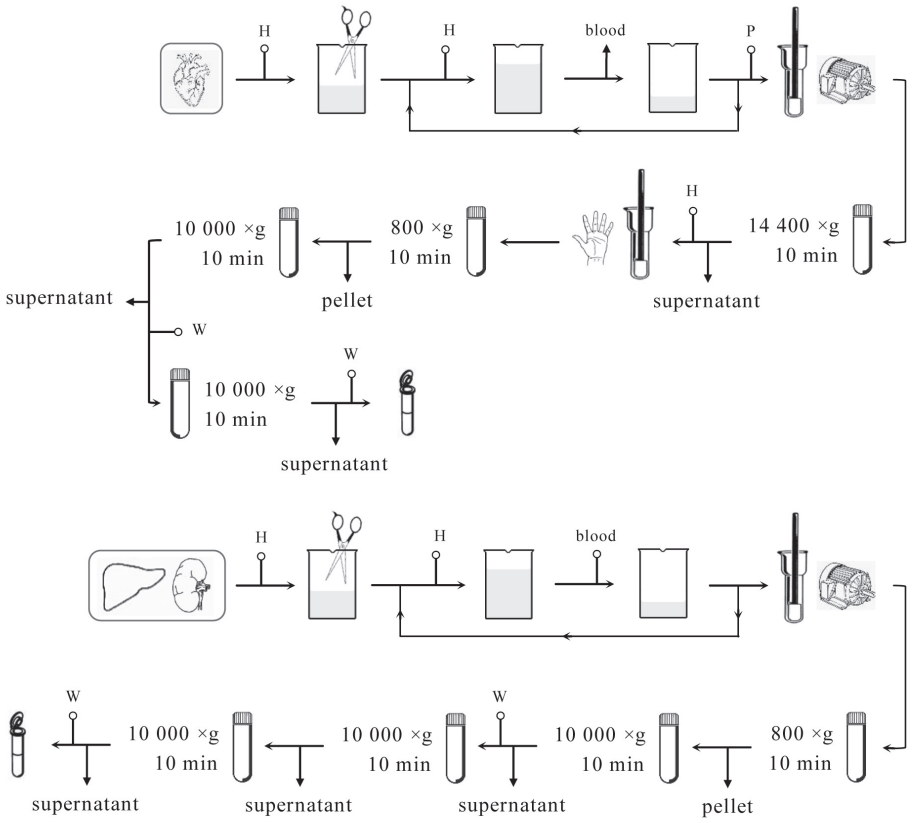

Figure 4.3: Flowchart for isolation of mitochondrial fractions. The difference in the homogenization procedure between the two groups resides in the addition of protease to the heart homogenate. All the material was kept on ice during the isolation procedure. Motor and hand icon represent motor-driven and handheld homogenization, respectively. *H* - homogenization buffer; *P* - protease; *W* - washing buffer.

4.9.2 Total tissue mRNA

Total RNA was isolated using the RNeasy Mini Kit (Qiagen Inc., Valencia, CA, USA). In the day of extraction, 20 mg of each RNA*later*-conserved frozen tissue was thawed and grounded in a glass pestle hand-held homogenizer in 600 µl RLT buffer supplemented with 1 % of β-mercaptoethanol followed by further homogenization in a 1 ml tuberculin syringe with a 27 gauge needle (10 passages). Due to the fibrous character of the cardiac tissue, samples were additionally subjected to protease digestion with proteinase K (Quiagen Inc.), 6 mAU at 55 °C for 10 min following centrifugation

at 10 000 ×g for 3 min. For the remaining tissues, homogenates were centrifuged at 10 000 ×g for 3 min at room temperature and the pellet discarded.

Different volumes and percentage of ethanol were added to the supernatant depending on the tissue being processed and accordingly to the manufacturer's suggestion: 1/2 volume of 100 % ethanol for heart and 1 volume of 50 % or 70 % ethanol for liver and kidney, respectively.

The resulting solution was transfered to a RNeasy spin column placed in a 2 ml microtube and centrifuge at ≥ 8000 ×g for 15 s. After discarding the flow-through, column was washed with RW1 buffer at ≥ 8000 ×g for 15 s followed by a on-column DNase digestion performed by adding 80 µl DNase I incubation mix (RNase-Free DNase Set, Quiage Inc.) directly to the column and incubating for 30 min at room temperature.

The column was then washed once with RW1 buffer (≥ 8000 ×g for 15 s) and twice with RPE (first, ≥ 8000 ×g for 15 s; second, ≥ 8000 ×g for 2 min). An additional centrifugation was made at 10 000 ×g for 1 min to eliminate any possible carryover of RPE buffer or residual flow-through.

RNA was eluted from the columns with 30 µl RNase-free water to a new microtube and then quantified using a NanoDrop spectrophotometer (Thermo Fisher Scientific Inc., Rockford, IL, USA) to measure the absorbance at 260 nm (A_{260}). RNA quality and purity was assessed by observing a spectral scan with a single prominent A_{260} peak and an A_{260}/A_{280} ratio with a minimum value of 2.

4.10 Protein Quantification

4.10.1 Biuret Assay

The biuret assay was used to quantify the protein amount in mitochondrial suspension after isolation. The procedure follows the conventional colorimetric method by Gornall [260].

The method is based on the spectrophotometric determination of the color developed by the reaction of an alkaline solution of copper reagent (Cu^{2+}) with the polypeptide chain more specifically through the coordination of the metal ion with four neighor peptide bonds and concomitantly reduction of Cu^{2+} to Cu^{1+} (Eq. 4.3).

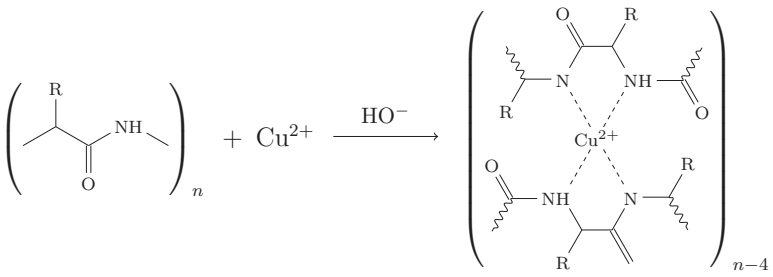

(4.3)

The reaction is initiated by adding 2 ml of biuret reagent to 20 µl sample containing up to 2 mg of protein and 10 % DOC. After 15-20 min incubation at room temperature, the color was read at 540 nm in a Spectronic 21 spectrometer (Bausch & Lomb, Rochester, NY, USA) . The standard curve ranging from 0.5 to 2.0 mg ml^{-1} was made using a solution of BSA (type V, Sigma-Aldrich).

4.10.2 Bicinchoninic Acid Assay

The buret method is not compatible with samples in RIPA buffer due to the high levels of detergents present (see section 4.9.1); therefore the bicinchoninic acid assay (BCA) assay was used as an alternative. The procedure follows the initial method by Smith [261] and uses the comercial Pierce BCA assay kit (Thermo Fisher Scientific, Rockford, IL, USA).

The BCA method is based on the reduction of Cu^{2+} to Cu^{1+} by protein in an alkaline medium as in the biuret method (Eq. 4.3 or 4.4a). However, there is a second step that involves the detection of the cuprous cation (Cu^{1+}) by BCA more specifically the chelation of two molecules of BCA with one cuprous ion (Eq. 4.4b).

$$\text{Protein} + Cu^{2+} \xrightarrow{HO^-} Cu^{1+} \tag{4.4a}$$

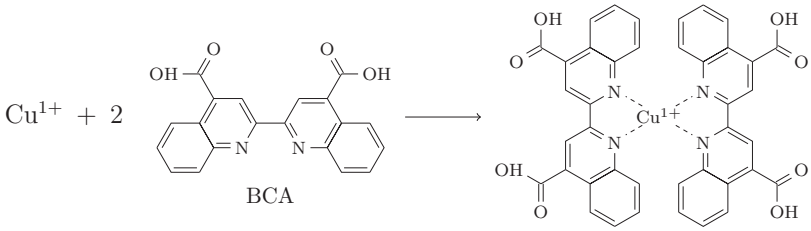

(4.4b)

The reaction is initiated by adding 200 µl of working reagent to 25 µl sample diluted 1:100 in water, in a standard polystyrene flat bottom 96-well microplate. After 30 min

incubation at 37 °C, the color was read at 562 nm in a SpectraMax Plus 384 microplate reader (Molecular Devices, Inc., Sunnyvale, CA, USA). The standard curve ranging from 25 to 2000 µg ml^{-1} was made using a solution of BSA (type V, Sigma-Aldrich). Standards and unknown samples were run at least in duplicates.

4.11 Oxygen Consumption

Oxygen consumption from a suspension of isolated mitochondrial fraction was monitored polarographically with a Clark-type oxygen electrode (YSI 5331, Yellow Springs Instruments, Yellow Springs, OH, USA) [262]. The electrode consists in a platinum (Pt) electrode which is maintained at 0.7 V negatively polarized against a silver (Ag/AgCl) reference electrode protected from the incubation by a thin Teflon oxygen-permeable membrane (YSI 5775, Yellow Springs Instruments).

O_2 is electrolytically reduced to H_2O at the cathode (Pt electrode) which allows the current to flow proportionally to the oxygen concentration in the medium (Eq. 4.5), creating therefore a potential difference which is delivered to an oxygen electrode control system (YSI 5300) connected to a BD1112 or BD12 Dual Channel compact flatbed chart recorder (Kipp & Zonen, Delf, Netherlands).

Overall reaction in Clark-type oxygen electrode:

$$4\,Ag + 4\,e^- + O_2 + 2\,H_2O + 4\,Cl^- \longrightarrow 4\,AgCl + 4\,OH^- + 4\,e^- \tag{4.5a}$$

Half reactions in each electrode:

$$\text{Anode (Ag) oxidation reaction:} \quad 2\,Ag + 2\,Cl^- \longrightarrow 2\,AgCl + 2\,e^- \tag{4.5b}$$

$$\text{Cathode (Pt) reduction reaction:} \quad 2\,e^- + \tfrac{1}{2}\,O_2 + H_2O \longrightarrow 2\,OH^- \tag{4.5c}$$

Since the electrode slowly consumes O_2 the suspension was under continuously stirring to prevent the formation of a depletion layer at the membrane. Magnetic stirring (Heidolph MR300, Heidolph Instruments, Schwabach, Germany) together with a thermostatic water-jacketed handmade chamber connected to a immersion thermostat pump Falc FA90 (Falc Instruments s.r.l., Treviglio, BG, Italy) were used to maintain a controlled temperature at 30 °C during the assay. The electrode was calibrated as described by Rickwood and co-workers [263] using air-saturated water at 30 °C.

The concentration of water-dissolved O_2 was calculated using the following equation[2] which originates from the well known Henry's[3] and Dalton's[4] laws:

$$[O_2] = \frac{P_{atm} - P_w(T)}{P_N} \times \frac{\%\,\text{air-saturation}}{100} \times f_{O_2} \times \alpha(T) \times \frac{1}{V_M} \times 10{\times}10^6 \qquad (4.6)$$

where $[O_2]$ is given in µM, P_{atm} and P_N are the actual atmospheric and standard pressures, $P_w(T)$ vapor pressure of water at temperature T, f_{O_2} is the molar fraction of O_2 in air, $\alpha(T)$ is the Bunsen absorption coefficient at temperature T given in $\text{cm}^3_{O_2}\,\text{cm}^{-1}$ and, V_M is the molar volume of ideal gases ($22.414\,\text{l}\,\text{mol}^{-1}$). Using tabulated values[2] for 30 °C and standard pressure with 100 % air-saturation, eq. 4.6 returns a $[O_2]$ concentration of 236 µM, which was used in the following calculations.

For most experiments, oxygen consumption and $\Delta\psi$ was determined simultaneously (see 4.12). Standard respiration medium consisted in 130 mM sucrose, 10 µM EGTA, 50 mM KCl, 5 mM H_2PO_4, 5 mM HEPES *p*H 7.3 (KOH) and supplemented with 2.5 mM $MgCl_2$ for liver and kidney. Mitochondria were suspended at a protein concentration of $0.5\,\text{mg}\,\text{ml}^{-1}$ (heart) or $1.0\,\text{mg}\,\text{ml}^{-1}$ (liver and kidney) in the respiration medium. Energization was achieved with 5 mM glutamate/malate or 5 mM succinate in the presence of 1 µM rotenone and the phosphorylative cycle through the addition of 225 to 250 nmol ADP. The oxidation rates are expressed in nanoatoms of oxygen consumed per minute per milligram of protein ($\text{natms}_O\,\text{min}^{-1}\,\text{mg}^{-1}_{\text{protein}}$).

Oxidation rates, as well as other parameters associated with phosphorylation, such as the ADP/O ratio and the RCR were determined according to classical techniques [262, 264]. The addition of known amounts of ADP results in an increase of substrates oxidation rates which ceases as soon as ADP is phosphorylated to ATP. The RCR represents the ratio between state 3 respiration, attained during maximal ATP synthesis, and respiration in absence of ATP synthesis which immediately follows the previously referred state (state 4). Moreover RCR is an indication of the control efficiency exercised by phosphorylation on oxidation [262, 264].

[2] a complete description and derivation of the equation is available in the appendix of datasheet for "oxy4-micro", a four channel fiber-optic oxygen meter, from PreSens (Regensburg, Germany). Source: www.presens.de/fileadmin/user_upload/downloads/manuals/OXY-4_micro_UM3.pdf

[3] "at a constant temperature, the amount of a given gas that dissolves in a given type and volume of liquid is directly proportional to the partial pressure of that gas in equilibrium with that liquid": $C_i = K_i.P_i$

[4] "the total pressure exerted by the mixture of non-reactive gases is equal to the sum of the partial pressures of individual gases": $P_i = P_{total}.f_i$

It is also possible to measure the efficiency of OXPHOS through direct determination of the ADP/O ratio, which is independent of the oxidation rates and characteristic of the substrate used. ADP/O is expressed as the ratio between the amount of ADP added (in nanomoles) and the oxygen consumed during state 3 respiration (in nanoatoms) [262, 264].

4.11.1 Titration curves for mitochondrial proteins

The titrations curves of the various steps involved in OXPHOS were determined using specific inhibitors of each of those steps: rotenone (10 to 300 nM) for Complex I, antimycin A (15 to 250 nM) for Complex III, KCN (10 to 140 µM) for Complex IV and CATR (25 to 2500 nM) for ANT. The methodology used in this section was exactly as described in the previous section, with the exception of a closed-chamber and the amount of ADP which was set to 2 mM to mantain a stable steady state of respiration. It was also attempted to match previously published works [219, 265, 266] whenever possible.

After measurement of the starting oxygen consumption rate, small amounts of the inhibitor were sequentially introduced into the chamber at appropriate intervals. The intervals of addition were chosen to allow adequate time for constant slope measurments and to construct detailed inhibition curves.

4.12 Mitochondrial Transembrane Electrical Potential

Generation of $\Delta\psi$ and its variations were indirectly monitored with an electrode sensitive to the TPP cation (TPP^+) [267]. This molecule is highly liposoluble and moreover has a π-orbital system which allows the shield charge of the central phosphorus ion enhancing therefore the lipid solubility. For this reason TPP^+ is able to accumulate electrophoretically inside mitochondria upon energization [5].

The TPP^+ electrode was handmade in our laboratory according to previous publications [267, 268] by glueing a polyvinyl chloride (PVC) membrane containing tetraphenylborate as ion exchanger to a PVC tube (inner diameter 0.2 mm) with tetrahydrofuran. The electrode was then filled with 10 mM TPP^+ as reference solution together with a silver wire coated with AgCl.

The complete setup consisted in the TPP^+ electrode coupled to a Ag/AgCl/KCl reference electrode (MI402, Microelectrodes Inc., Bedford, NH, USA) both connected to an adequate potentiometer (Jenway 3305 *p*H meter, Jenway Essex, Staffordshire, UK) which delivered the signal to a BD12E Dual Channel compact flatbed chart recorder (Kipp & Zonen, Delf, Netherlands) via a manufactured potential compensatory box [269]. The diameter of both electrodes is small enough to allow their introduction into the oxygen electrode chamber thereby simultaneously measuring rates of oxygen consumption and membrane potential. Experimental conditions were the same as in oxygen consumption assay (see 4.11) and a final concentration of 3 µM TPP^+ was used.

The TPP^+ electrode like all diffusion electrodes has a Nernstian response:

$$E = 2.303\,\frac{RT}{zF} \times \log_{10}\frac{[\mathrm{TPP}^+]_\mathrm{o}}{[\mathrm{TPP}^+]_\mathrm{i}}$$

where E, R, T, z and F have their usual thermodynamic significance and $[\mathrm{TPP}^+]_\mathrm{o}$ and $[\mathrm{TPP}^+]_\mathrm{i}$ are the cation concentration in medium and inside the electrode respectively. At a constant temperature, R, T, n, F and $[\mathrm{TPP}^+]_\mathrm{i}$ became a single constant and therefore the electrode voltage varies linearly with the logarithm of TPP^+ concentration in the medium with a slope of 60 mV per decade concentration:

$$E = 60\,\mathrm{mV} \times \log_{10}[\mathrm{TPP}^+]_\mathrm{o} + K \tag{4.7}$$

where K is a correction for any interferring substance in the medium.

$\Delta\psi$ was estimated according to Kamo [267] without correction for the "passive" binding contribution of TPP^+ to the mitochondrial membranes as experiments intended to show relative changes in potential rather than absolute values. As a consequence, we can anticipate some overestimation for the $\Delta\psi$ values. The used equation was:

$$\Delta\Psi = 2.303\,\frac{RT}{zF} \times \log_{10}\left(\frac{v}{V}\right) \;-\; 2.303\,\frac{RT}{zF} \times \log_{10}(10^{\,F\Delta E/2.303\,RT} - 1) \tag{4.8a}$$

$$= 60\,\log_{10}\left(\frac{v}{V}\right) \;-\; 60\,\log_{10}(10^{\,\Delta E/60} - 1) \quad \text{at } 30\,^\circ\mathrm{C} \tag{4.8b}$$

where v is the mitochondrial matrix volume, V is the volume of incubation medium and ΔE is the deflection of the electrode potential from the baseline. A matrix volume of 1.1 µl $\mathrm{mg}^{-1}_{\mathrm{protein}}$ was assumed [270].

The parameters analyzed were maximum transmembrane electrical potential (corre-

sponding to state 2), ADP-induced depolarization (corresponding to depolarization elicit by the addition of ADP) and lag phase (interval of time correspondent to ADP phosphorylation).

4.13 Mitochondrial Calcium Movements

Extramitochondrial free Ca^{2+} was assayed by monitoring the variations in fluorescence of the Calcium Green 5-N hexapotassium salt dye (CG5N, C-3737, Invitrogen, Spain) as previously described [271]. The dye has particular biochemical characteristics that makes it suitable for this procedure:

1) low affinity for Ca^{2+} (high K_d) making it useful for measuring high concentrations of this ion and advantageous for rapid kinetics;
2) exhibit an increase in fluorescence emission upon Ca^{2+} binding with no significant shift in wavelength;
3) is relatively insensitive to Mg^{2+} which improves its selectivity;
4) contrarily to esterified mitochondrial permeable probes, CG5N is not dependent on $\Delta\psi$ and does not require enzymatic cleavage by esterases;
5) is a long-wavelength indicator and consequently its emission is in regions of the spectrum where cellular autofluorescence and scattering backgrounds are minor;
6) the energy of the excitation light is low, reducing the potential for photodamage.

The fluorescence was continuously recorded at 506 nm excitation wavelength and 531 nm emission wavelength with 5 nm slits in a PerkinElmer LS-55 spectrofluorometer (PerkinElmer Inc., Waltham, MA, USA) equipped with a magnetic stirrer and a water-jacketed cuvette holder connected to a LKB 2219 Multitemp II refrigerated circulator (LKB Instruments, Mt Waverley, VIC, Australia) set to 30 °C. The assays were performed in 2 ml of swelling medium (200 mM sucrose, 10 mM Tris *p*H 7.3 (HCl), 10 µM EGTA and 5 mM KH_2PO_4 or 1 mM KH_2PO_4 for liver and kidney mitochondria) supplemented with 812 nM CG5N and a final protein concentration of 0.25 mg ml^{-1} (heart) or 0.75 mg ml^{-1} (liver and kidney). After mitochondrial energization with 2.5 mM glutamate/malate or 2.5 mM succinate in the presence of 1 µM rotenone a baseline of 60 sec was performed before the addition of a single pulse of calcium of 65 to 100 nmol, 50 to 100 nmol and 40 to 65 nmol for heart, liver and kidney mitochon-

dria of the acute protocol or, 6.5 to 10 nmol, 5 to 10 nmol and 4 to 6.5 nmol for heart, liver and kidney mitochondria of the sub-chronic protocol.

4.14 Mitochondrial Swelling

Mitochondrial osmotic volume changes were assessed by turbimetry since mitochondrial suspensions are turbid and scatter light due to the difference on refractive index between the matrix content and the medium [5]. Therefore, a semiquantitative analysis can be performed by monitoring the decrease in light scattering, i.e., an increase in transmitted light in a spectophotometer during the swelling process and concomitant decrease in absorbance. So, at the beginning of the assay:

$$n_{matrix} > n_{medium} \Rightarrow I_{begin} < I_0 \tag{4.9a}$$

but whenever a process induces changes in the matrix refractive index, such as when solutes move into the matrix causing a compensatory water flux resulting from the internal osmotic pressure:

$$n_{matrix} \approx n_{medium} \Rightarrow I_{end} \approx I_0 \tag{4.9b}$$

and a consequent decrease in absorbance is observed:

$$\begin{aligned} \Delta A &= A_{end} - A_{begin} \\ &= \log_{10} T_{begin} - \log_{10} T_{end} \\ &= \log_{10}(I_{begin}/I_0) - \log_{10}(I_{end}/I_0) \\ &= \log_{10} I_{begin} - \log_{10} I_{end} \end{aligned} \tag{4.9c}$$

$$\Delta A < 0, \quad I_{begin} < I_0 \approx I_{end} \tag{4.9d}$$

Where n is the refractive index, I_0 is the intensity of incident light, I_{begin} and I_{end} are the intensities of transmitted light at the beginning and end of the assay, respectively, A is the absorbance and T the transmittance.

The optical density was monitored at 540 nm with a Jasco V-560 spectrophotometer (Jasco Inc., Easton, MD, USA) equipped with a magnetic stirrer (STR-458, Jasco Inc.) and a water-jacketed cuvette holder connected to a NESLAB RTE-101 Bath Circulator (Thermo Scientific, Newington, NH, USA) set to 30 °C. The assays were performed in 2 ml of swelling medium (200 mM sucrose, 10 mM Tris *p*H 7.3 (HCl),

10 µM EGTA and 5 mM KH_2PO_4 or 1 mM KH_2PO_4 for liver and kidney mitochondria) with protein concentration of 0.5 mg ml^{-1} (heart) or 1.0 mg ml^{-1} (liver and kidney). After mitochondrial energization with 2.5 mM glutamate/malate or 2.5 mM succinate in the presence of 1 µM rotenone a baseline of 60 sec was performed before the addition of a single pulse of calcium of 50 to 100 nmol for all mitochondrial preparations of the acute protocol or 20 to 50 nmol, 10 to 50 nmol and 10 to 50 nmol for heart, liver and kidney mitochondria of the sub-chronic protocol, regardless of the respiratory substrate used.

4.15 Hydrogen Peroxide Production

H_2O_2 generation was measured fluorimetrically using a modification of the methodology previously described by Barja and reviewed in [272]. A detailed description of the approach with its advantages and drawbacks in comparison to other detecting systems can also be found elsewhere [272]. Basically, the method uses the non-fluorescent probe 2-(4-hydroxy-3-methoxy-phenyl)acetic acid, also known as homovalinic acid, which reacts with H_2O_2 in the presence of horsereadish peroxidase to form a dimer, 2,*2'*-dihydroxy-3,*3'*-dimethoxydiphenyl-5,*5'*-diacetic acid, strongly fluorescent at 312 nm excitation and 420 nm emission:

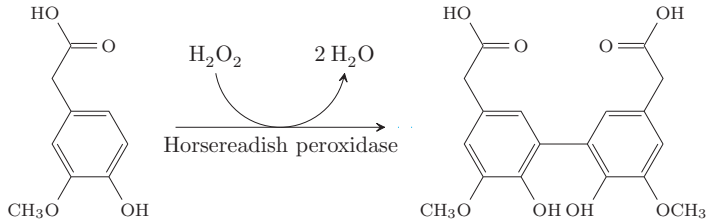

Homovanillic acid Fluorescent dimer (4.10)

Reactions (500 µl) were conducted in standard glass test tubes (15 mm×100 mm) under constant magnetic stirring (Vari-Mag, Telemodel 20 P, Osaka, Japan) and incubated in a plastic water bath with an immersion thermostat Heidolph T51 (Heidolph Instruments, Schwabach, Germany) at 30 °C secured to it. Small volumes of reactants were combined in the following order to pre-added incubation medium (145 mM KCl, 30 mM Hepes *p*H 7.4 (KOH), 5 mM KH_2PO_4, 3 mM $MgCl_2$, 100 µM EGTA, 0.1 % fatty-acid-free albumin) to reach the presented concentrations: 0.125 $\mu g_{protein}$ mitochondria, 6 U/ml horsereadish peroxidase and 100 µM homovanillic acid.

Reactions started upon addition of mitochondrial substrates/inhibitors and stopped 30 min later through the addition of 250 µl ice-cold stop solution (2 M glycine *p*H 12 (NaOH), 25 mM EDTA) which increases the sensitivity and makes the final fluorescence essentially *p*H-independent. Mitochondrial suspensions were then centrifuged at 850 ×g for 5 min (Eppendorf 5415R, FA-45-24-11 rotor, Hamburg, Germany) and 200 µl supernatant were loaded into standard 96-well flat bottom black polystyrene microplate. End-point fluorescence was read in a Gemini EM Fluorescence Microplate Reader (Molecular Devices) at 312 nm excitation wavelength and 420 nm emission wavelength.

The H_2O_2 production was determined in mitochondria energized with 5 mM glutamate/malate or 5 mM succinate. At these concentrations, H_2O_2 production is not substrate-dependent. In some experiments specific inhibitors for Complex I (1 µM rotenone) or for Complex III (0.5 µg antimycin A) were used in combination with respiratory substrates to block electron transport and maximally stimulate H_2O_2 production.

Arbitary fluorescence units were converted to $nmol_{H_2O_2}$ by extrapolation through a standard curve built from addition of known amounts of H_2O_2 in the presence of horseradish peroxidase and homovanillic acid. Since µM H_2O_2 solutions are unstable fresh solutions were prepared daily from stable mM H_2O_2 solutions. Values were then normalized to protein amount and expressed as nmol (H_2O_2)/ 15 min/mg (protein).

4.16 Enzymatic Activities

4.16.1 OXPHOS enzymes

All assays follow microplate adaptations of previous well establish standard methods in the evaluation of respiratory enzyme activities [256, 273–277]. Some reports in the literature [278–281] already attempted this approach. If not stated in contrary, all assays here to be described virtually follow all aspects optimized in a recent report [273].

As previously described [256], mitochondrial membranes are easily disrupted by freeze-thaw cycles in hypotonic medium while maintaining high enzymatic activity. Thus, frozen isolated mitochondrial fraction in 'washing medium' (see pag. 83) were thawed

and diluted in hypotonic phosphate buffer (25 mM KH_2PO_4 *p*H 7.2 (KOH) and 5 mM $MgCl_2$) to final 5 mg ml^{-1} concentration. Samples were kept on ice during 30 min and then were subjected to three cycles of freeze-thaw in liquid nitrogen and water bath at 30 °C.

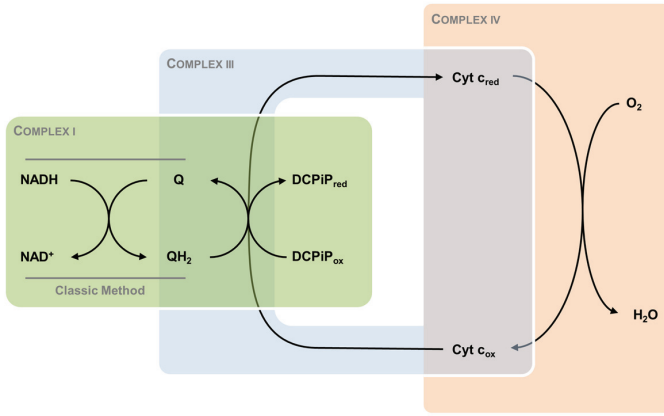

Figure 4.4: Schematic of the experimental procedure for evaluation of the enzymatic activity of OXPHOS respiratory complexes. Overlapping colors reflect reactants/products common between reactions of different enzymatic assays. In Complex I, gray lines delineate the reaction corresponding to the classical method which has been adjusted to a more recent methodology. Abrreviations: *Q* - quinone (coenzyme Q_1 or decylubiquinone, for complex I and III, respectively); QH_2 - quinol; *DCPIP* - 2,6-dichlorophenolindophenol; Cyt c - cytochrome c.

Complex I

Classical methods for *in vitro* quantification of Complex I activity rely on measurement of NADH absorbance/fluorescence. However, UV-transparent microplates are still quite expensive and NADH extinction coefficient is rather low, therefore a new approach was used instead as previously reported [280, 281]. Instead of using exogenous ubiquinone as final electron acceptor of NADH oxidation, the assessment relies on the final reduction of the blue 2,6-dichlorophenolindophenol (DCPIP) to a colorless compound (Fig. 4.4, in green). This strategy has the further advantage of preventing ubiquinol accumulation which was reported to inhibit Complex I activity [282].

For this purpose, 190 µl of reaction medium (25 mM KH_2PO_4 *p*H 7.5 (KOH), 5 mM $MgCl_2$, 300 µM KCN, 4 µM antimycin A, 3 mg ml^{-1} BSA, 60 µM coenzyme Q_1, 160 µM DCPIP and 5 µg ml$^{-1}_{\text{protein}}$ for heart and kidney or 10 µg ml$^{-1}_{\text{protein}}$ for liver) were added to

a standard polystyrene flat bottom 96-well microplate. Coenzyme Q_1 was chosen since Complex I linearity increase in inverse proportion of the size of the hydrocarbon chain of ubiquinone [273, 283]. An half-logarithmic dilution of rotenone was prepared fresh in ethanol and 5 µl were added to the plate. Since the accumulation of rotenone on its binding site was reported not to be instantaneous [284], a $\sim$5 min pre-incubation at 30 °C was performed. During that period, reduction of DCPIP in control or with any inhibitor concentration was negligible.

Enzymatic activity was followed by decrease in absorbance of DCPIP upon addition of 100 µM fresh-prepared NADH in a VICTOR *X*3 plate reader (Perkin Elmer) by repeating 30 read cycles (81.2 s cycle^{-1}) each comprising of an orbital 3 s shaking followed by a 2 s delay before absorbance reading at 600 nm with a 590/7 nm filter during 0.2 s and operating at 30 °C. Enzyme activity was calculated through the mean of the slopes, of duplicates, obtained during the linear phase (10, 20 and 15 cycles for heart, liver and kidney, respectively). Complex I-specific activity was calculated by subtracting the basal activity in presence of the highest concentration of rotenone. An extinction coefficient of ε_{600} =19.1 mM^{-1} cm^{-1} [256] and normalization to protein amount were applied to express the activity as nmol$_{\text{DCPIP}}$ min^{-1} mg$^{-1}_{\text{protein}}$.

Complex III

Complex III activity was measured by following the reduction of cytochrome c at 550 nm in the presence of DQH_2 (sec. 4.1.2, pag. 78; Fig. 4.4, in blue). For this purpose, 190 µl of reaction medium (25 mM KH_2PO_4 *p*H 7.5 (KOH), 500 µM KCN, 4 µM rotenone, 0.025 % Tween-20, 75 µM cytochrome c and 1.25 µg ml$^{-1}_{\text{protein}}$, 12.5 µg ml$^{-1}_{\text{protein}}$ or 5 µg ml$^{-1}_{\text{protein}}$ for heart, liver and kidney, respectively) were added to a standard polystyrene flat bottom 96-well microplate. The nonionic detergent Tween-20 was chosen over the common used *n*-dodecyl-*β*-*D*-maltoside since recent reports showed increased specific activity and linearity [273, 277]. Contrarily to Complex I, Complex III activity is directly proportional to the size of the hydrocarbon chain of ubiquinone [256] therefore, a balance between chain size and aqueous solubility picked DQH_2. A $\frac{37}{100}$-logarithmic dilution of antimycin A was prepared fresh in ethanol and 5 µl were added to the plate.

Enzymatic activity was followed by increase in absorbance of reduced cytochrome c upon addition of 100 µM fresh-diluted DQH_2 in a VICTOR *X*3 plate reader (Perkin Elmer) by repeating 25 cycles (33.9 s cycle^{-1} of absorbance reading at 550 nm with a

544/15 nm filter during 0.2 s and operating at 30 °C. Enzyme activity was calculated through the mean of the slopes, of duplicates, obtained during the linear phase (5 cycles for all tissue samples). Complex III-specific activity was calculated by subtracting the basal activity in presence of the highest concentration of antimycin A. An extinction coefficient of ε_{550} =19.1 $\mathrm{mM^{-1}\,cm^{-1}}$ [256] and normalization to protein amount were applied to express the activity as $\mathrm{nmol_{cyt-c\,red}\,min^{-1}\,mg^{-1}_{protein}}$.

Complex IV

Complex IV activity was measured by following the oxidation of reduced cytochrome c (see sec. 4.1.3, pag. 79) at 550 nm (Fig. 4.4, in red). For this purpose, 190 µl of reaction medium (50 mM KH_2PO_4 *p*H 7.0 (KOH), 4 µM antimycin A, 0.05 % *n*-dodecyl-*β*-*D*-maltoside and 0.3125 $\mathrm{\mu g_{protein}\,ml^{-1}}$, 1.25 $\mathrm{\mu g_{protein}\,ml^{-1}}$ or 0.625 $\mathrm{\mu g\,ml^{-1}_{protein}}$ for heart, liver and kidney, respectively) were added to a standard polystyrene flat bottom 96-well microplate. Contrarily to Complex III, *n*-dodecyl-*β*-*D*-maltoside was the chosen detergent since it increased the specific activity of Complex IV [256, 273]. A $\frac{7}{20}$-logarithmic dilution of KCN was prepared fresh in H_2O and 5 µl were added to the plate.

Enzymatic activity was followed by decrease in absorbance of reduced cytochrome c at 550 nm upon addition of 57 µM of the fresh-diluted molecule in a VICTOR *X*3 plate reader (Perkin Elmer) by repeating 20 cycles (33.9 $\mathrm{s\,cycle^{-1}}$) of absorbance reading at 550 nm with a 544/15 nm filter during 0.2 s and operating at 30 °C. Enzyme activity was calculated through the mean of the slopes, of duplicates, obtained during the linear phase (5 cycles for all tissue samples). Complex IV-specific activity was calculated by subtracting the basal activity in presence of the highest concentration of KCN. An extinction coefficient of ε_{550} =19.1 $\mathrm{mM^{-1}\,cm^{-1}}$ [256] and normalization to protein amount were applied to express the activity as $\mathrm{nmol_{cyt-c\,red}\,min^{-1}\,mg^{-1}_{protein}}$.

4.16.2 Aconitase Activity

Aconitase (aconitate hydratase, EC:4.2.1.3) is an iron-sulfur protein that catalyzes the reversible inter-conversion of citrate and isocitrate, via a *cis*-aconitate intermediate (Eq. 4.11), in both the TCA and glyoxylate cycles. Besides specific inhibitors, ROS and RNS such as $ONOO^-$, H_2O_2 and $O_2^{\bullet-}$ are also known to inactivate the enzyme by changing the [4Fe-4S] to a [3Fe-4S] cluster. The present method measures the activity

of aconitase in a sample by following the conversion of isocitrate to *cis*-aconitate as an increase in absorbance at UV 240 nm [285].

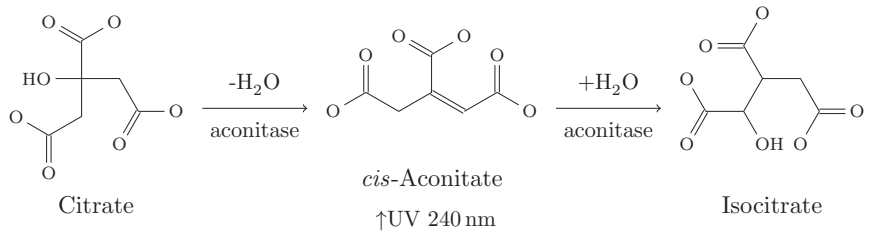

(4.11)

For this purpose, mitochondrial protein (200 µg) was diluted in 0.6 ml buffer containing 50 mM Tris *p*H 7.4 (HCl) and 0.6 mM $MnCl_2$ and then sonicated for 10-20 s, followed by centrifugation at 16 000 ×g for 5 min. Reactions were made in triplicated and initiated by the addition of 20 mM isocitrate to 200 µl (supernatant)/ 800 µl (buffer) after a 60 s baseline in a 1 ml quartz cuvette placed in a Jasco V-560 spectrophotometer (Jasco Inc., Easton, MD, USA) equipped with a magnetic stirrer (STR-458, Jasco Inc.) and a water-jacketed cuvette holder connected to a NESLAB RTE-101 Bath Circulator (Thermo Scientific, Newington, NH, USA) set to 30 °C.

Enzyme activity was calculated through the mean of the slopes, of the three replicates, obtained in the record before reaching a plateau using the manufacturer's device software. A extinction coefficient of ε_{240} =3.6 $mM^{-1}\,cm^{-1}$ [285] and normalization to protein amount were applied to express the activity as $nmol_{cis-aconitate}\,min^{-1}\,mg^{-1}_{protein}$.

4.17 Protein Analysis

4.17.1 One-Dimensional Sodium Dodecyl Sulfate-Polyacrylamide Gel Electrophoresis

Electrophoresis was used to separate tissue protein content based on molecular size through a discontinous vertical polyacrylamide gel electrophoresis under denaturing conditions, i.e., in the presence of SDS, since proteins migrate from negative to possitive electrode in response to an electrical field through pores in the gel matrix, as previously established by Laemmli [286, 287].

Polyacrylamide gels were formed after vinyl addition polymerization of monomeric acrylamide into polymeric polyacrylamide chains and cross-linking of the chains by

N,N'-methylenebisacrylamide through a reaction initiated by ammonium persulfate (APS) and catalyzed by TEMED.

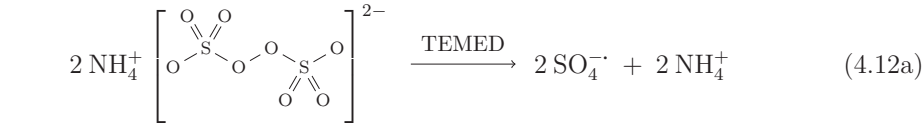

(4.12a)

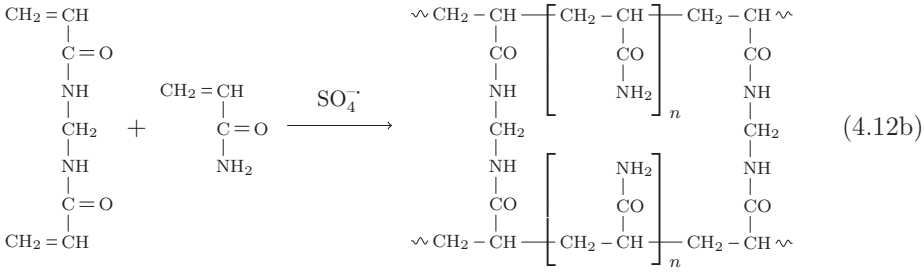

(4.12b)

Gels were casted as a separating gel topped by a stacking gel and secured in an electrophoresis apparatus. Separating gel consisted in 12 % acrylamide/bis, 375 mM Tris *p*H 8.8 (HCl), 0.1 % SDS, 0.05 % TEMED and 0.05 % APS while stacking gel consisted in 4 % acrylamide/bis, 126 mM Tris *p*H 6.8 (HCl), 0.1 % SDS, 0.1 % TEMED and 0.05 % APS. The chloride and glycine ions have different electrical mobilities in the stacking gel due to the buffer low *p*H resulting in a zone of lower conductivity between chlorine/glycine ions and the migrating protein. The higher voltage gradient in this zone allows the proteins to move faster and to stack. After leaving the stacking gel, the protein enters the separating gel which has smaller pore size, a higher salt concentration, and higher *p*H compared to the stacking gel. Therefore the glycine ions become deprotonated migrating past the proteins.

Extracted proteins (see 4.9.1) were diluted in Laemmli buffer (62.5 mM Tris *p*H 6.8 (HCl), 50 % glycerol, 2 % SDS, 0.005 % bromophenol blue, supplemented with 5 % β-mercaptoethano) and boiled at 95 °C for 5 min in a AccuBlock D1100 Dry Bath (Labnet, Woodbridge, NJ, USA). Since SDS is an anionic detergent that binds to the vast majority of proteins at a constant ratio it distributes a negative charge to all the proteins masking their inherent charge and giving an equal charge-to-mass ratio. Therefore, mobility becomes a function of molecular weight only.

The complete setup consisted in 10\12-wells polyacrilamide gels fitted in a Mini-PROTEAN 3 Cell (Bio-Rad) filled with running buffer (25 mM Tris, 192 mM glycine, 0.1 % SDS) and connected to a PowerPac Basic Power Supply (Bio-Rad) outputing a constant voltge of 150 V during 70-80 min at room temperature. In each gel, the first

lane was loaded with 5 µl Precision Plus Protein Dual Color Standards (Bio-Rad) for monitoring electrophoresis, transfer efficiency and molecular weight estimation. The other lanes were loaded with 25 or 62.5 $\mu g_{protein}$.

4.17.2 Immunoblotting

Immunoblotting was used to identify specific proteins recognized by polyclonal or monoclonal antibodies after eletrophoretical transference of separated proteins from polyacrilamide gels to membranes [288, 289]. The proteins move from within the gel onto the membrane while maintaining the organization they had within the gel. As a result of this "blotting" process, the proteins are exposed on a thin surface layer for detection.

Polyvinylidene difluoride membrane (PVDF, 0.45 µm, Millipore, Billerica, MA, USA) was choosen due to its high protein binding capacity, non-specific protein binding, target retention and resistance to cracking, repeated stripping and reprobing applications. The hydrophobicity of PVDF makes it impossible to wet the membrane with aqueous solutions therefore it does require a prewetting step in alcohol prior to equilibration in transfer buffer (25 mM Tris, 190 mM glycine and 20 % methanol).

The gel and membrane were place in a plastic support in a standard *sandwich* in which both are in direct contact and surrounded by sheet of filter paper and Scotch-Brite pads. Afterwards, the entire assembly was placed in a Mini Trans-Blot Cell (Bio-Rad) containing transfer buffer. Since proteins are "coated" with SDS and therefore negatively charged, the membrane was positioned towards the anode electrode while gels faces the cathode. To complete the setup, a magnetic stirr bar was added to maintain even buffer temperature and ion distribution and the tank was placed in a container full of ice being thereafter connected to a PowerPac Basic Power Supply (Bio-Rad) outputing a constant voltge of 100 V during 90 min.

Once the transference is complete, membrane is labelled for future identification (Permanent Waterproof Staedtler Lumocolor Glasochrom Pencil Black #108209, Staedtler, Germany) and is incubated with blocking solution, 5 % non-fat dry milk in Tris-buffered saline Tween-20 (TBS-T; 154 mM NaCl, 50 mM Tris *p*H 8.0 (HCl) and 0.1 % Tween-20) for 2 h at room temperature under continuous agitation (Stuart SRT6 tube roller, VWR, Leuven, Belgium), to block non-specific binding. After washing the membrane three times in TBS-T for 5 min each, membranes were incubated with pri-

Table 4.1: List of antibodies used in immunodetection.
Dilutions represent incubation conditions of membranes containing samples of the different tissues.

Accession Number [a]	Personal Code	Dilution	Host Species	Manufacturer Code	Manufacturer
NP_001091	ACTIN [b]	1:10 000	Mouse	mab1501	Millipore
P12235	ANT1 [c]	1:400	Goat	sc-9299	Santa Cruz
P05141	ANT2 [d]	1:100	Goat	sc-70205	Santa Cruz
P25705	ATP5A1	1:1000	Mouse	MS604	MitoSciences
P48047	ATP5O	1:1000	Mouse	ab58684	AbCam
P00395	COXI	1:1000	Mouse	MS604	MitoSciences
P13073	COXIV	1:1000	Rabbit	4844	Cell Signaling
P99999	CYCS	1:500	Mouse	556433	BD Biosciences
P30405	CYP-D	1:10 000	Mouse	MSA04	MitoSciences
O95169	NDUFB8	1:1000	Mouse	MS604	MitoSciences
O75489	NDUFS3	1:1000	Mouse	ab14711	AbCam
P31040	SDHA	1:1000	Mouse	sc-59687	Santa Cruz
P21912	SDHB	1:1000	Mouse	MS604	MitoSciences
Q15388	TOM20	1:1000	Rabbit	sc-11415	Santa Cruz
P47985	UQCRFS1	1:6000	Mouse	ab14746	AbCam
P21796	VDAC [b]	1:1000 [e]	Rabbit	ab34726	AbCam

[a] as provided by manufacturer and available on www.ncbi.nlm.nih.gov/protein
[b] detects all isoforms
[c] used only in cardiac samples
[d] used for hepatic and renal samples
[e] for hepatic samples a 1:500 dilution was used instead
Antibodies were diluted in 1 % non-fat dry milk in TBS-T supplemented with 0.02 % sodium azide to a final volume of 5 ml and stored at 4 °C for no longer than 4 months or used for a maximum of 4-5 times.

mary antiboby directed against the respective protein (listed in Table 4.1) overnight at 4 °C under continuous agitation (Stuart SRT6 tube roller), except actin which was 2 h at room temperature. On the next day, membranes were washed three times in TBS-T for 5 min each and then incubated with the respective alkaline phosphatase-linked secondary antibody (1:10 000), prepared in TBS-T, for 1 h at room temperature under continuous agitation (Stuart SRT6 tube roller). Finally, membranes were washed once again three times in TBS-T for 5 min each before immunodetection.

4.17.3 Immunodetection

Membranes were processed for protein detection using the Enhanced Chemi-Fluorescence system (ECF; GE Healthcare, Buckinghamshire, UK). The alkaline phosphatase linked to the secondary antibody catalyses the conversion of ECF substrate to a highly

fluorescent product which fluoresces strongly at 540-560 nm. Blots were drained and placed with the protein side down on a flat plastic plate of the size of the blot pre-filled with small droplets of ECF substrate ensuring no air bubbles were trapped and incubating for 5 min at room temperature. For membranes with high levels of the target protein, blot was immediately removed from the ECF substrate when protein bands began to become visible.

Chemi-fluorescence data was collected using a UVP Biospectrum 500 Imaging System eqquiped with a BioChemi HR Camera (UVP, Upland, CA, USA) through UV (365 nm) epi-illumination. One or two membranes were imaged at a time and each tissue was independently imaged to not cause sub-exposure of the signal. The holder was set to its highest position and camera set to its maximum aperture to allow input of all the emitted signal. Images were previewed with 4x4 binning with real time exposure compensation. Camera settings were manipulated in preview mode to optimize the exposure and determine the appropriate final exposure settings. Data processing was performed with on-chip integration using the auto-exposure feature which ensures maximum exposure without signal saturation.

Resultant images were displayed and analyzed in the VisionWorks LS software package (UVP). For densitometry, a rectangle with the maximum size similar to the band of greater length present in the blot was considered as the region of interest (ROI). The same ROI was used through all the blot and the Total Density was used for the following calculations. The software defines Total Density as the sum of all pixels intensity corrected for the local mean background. The local mean background reflects the sum of all pixels intensity in a 3 pixels wide border of each ROI divided by the total number of pixels of that border. For each blot, data was first normalized as percentage of the sum of all bands total densities and then normalized to its respective actin immunoreactivity to prove even amounts of protein loading in gels.

Reprobing

When more than one protein was investigated on the same blot, e.g. a protein of interest and a loading control, the membrane was reprobed. Subsequent reprobing of membrane with a variety of antibodies is possible as long as the target proteins can be distinguished from each other by differences in their size. If not, then it is

necessary to preform a stripping protocol[5] first.

Briefly, following manufacturer suggestion in ECF kit, membrane is incubated with methanol (100 %) at room temperature in constant agitation for ∼30 min and then rinse twice in TBS-T 5 min each. Afterwards, membrane is incubated in stripping buffer (200 mM Glycine *p*H 2.5 (HCl), 0.005 % Tween-20, 0.1 % SDS and 100 mM β-mercaptoethanol) under constant agitation (Bambino Hybridization Oven, BOE230-300, Diamed, Mississauga, ON, USA) at 50 °C during 1 h whereas solution is renewed after 30 min. At the end, membranes are washed in large volumes of TBS-T, twice, at room temperature for at least 15 min each and then proceed to standard protocol blocking step and subsequent probing.

4.18 Quantitative PCR

RNA transcripts levels were quantified by real-time reverse transcriptase- (RT) polymerase chain reaction (PCR) involving two separated steps: first the reverse transcription of purified RNA into cDNA followed by PCR amplification of the cDNA. Since the second reaction is followed in real time by monitoring SYBR green fluorescence, the quantity of initial cDNA can be determined during the exponential phase of the PCR.

4.18.1 Reverse Transcriptase Reaction

RT is used *in vitro* for first-strand cDNA synthesis with RNA as the starting template. The conversion from RNA to cDNA is necessary for qPCR as the Taq polymerase is a DNA-dependent enzyme. *In vitro*, only two of the three enzymatic activities of RT are used: RNA-dependent DNA polymerase and a hybrid-dependent exoribonuclease (RNase H). The first transcribes cDNA from an RNA template while the second specifically degrades the RNA in RNA:DNA hybrids but not pure RNA.

cDNA was synthesized from extracted RNA (0.5-1.5 µg; see 4.9.2) using random primers along with the Omniscript Reverse Transcription Kit (Qiagen Inc., Valencia, CA, USA). The random priming technique, established by Feinberg [290], consists in the use of a mixture of oligonucleotides representing all possible nonamer sequences,

[5]term used to describe the removal of primary and secondary antibodies from a western blot membrane

5'-NNN NNN NNN-3' with $4^9 = 262\,144$ permutations. Random nonanucleotide primers bind to mRNA at a variety of complementary sites and lead to short, partial length cDNAs. The major benefits of random priming are the production of shorter cDNA fragments and increasing the probability that *5'* ends of the mRNA would be converted to cDNA.

All the reactions were kept on ice during handling and a single cycle of 60 min at 37 °C was performed in a thermal cycler (Perkin Elmer 2400 Geneamp PCR System). Finished RT reactions were diluted 1:100 for 18S mRNA quantitation and 1:10 for the other targets in RNase-free water and stored at −20 °C.

4.18.2 Real-Time Polymerase Chain Reaction

Quantitative real-time PCR (qPCR) has become the most precise method for analyzing gene expression because it meassures the starting copy number and is therefore able to detect small differences in expression leves [291]. qPCR quantifies the PCR product while the amplification is in progress by the use of a fluorescence detector in conjunction with the thermal cycler resulting in a amplification plot with an exponential, linear, and plateau phase.

The fluorescent reagent used in our protocol was a non-sequence-specific intercalating dye SYBR Green which exhibit a large increase in fluorescence emission when bind to double-stranded DNA. However, it will also bind to primer-dimer artifacts or incorrect amplification products and is therefore necessary to confirm the specificity of the reaction through analysis of the melting curve.

All primers (Table 4.2) used for real-time PCR were designed using the web-based PrimerQuest software and ordered through the same company (Integrated DNA Technologies, Inc., Coralville, IA). Target mRNA sequences or accession numbers were first obtained in GenBank and then inserted in the web-based software. The algorithm was allowed to run in default mode in order to obtain the best pair of primers. However, personal selection was based on the following specifications:

1) primer set should flank an exon to avoid co-amplification of genomic DNA;
2) primer set should anneal towards the *3'* of the target due to possible inefficiency of RT reaction;
3) amplicon should be between 80-200 base pairs;

Table 4.2: List of primer sets used in qPCR.
Melting temperatures (T_m) represent values used in standards preparation and qPCR runs. Amplicon (Amp) represent the length of product amplification.

Accession Number [a]	**Personal Code**	**Sequence** [b]	**Amp** bp	$\boldsymbol{T_m}$ [c] °C
NM_053515	ANT1	*5'* TCTC TGTG CAGG GCAT CATC ATCT *3'*	128	60
		3' TGTC ACAC TCTG GGCA ATCA TCCA *5'*		
NM_057102	ANT2	*5'* GCTT TCAA CATG ACAG ATGC CGCT *3'*	154	60
		3' TATC TGCC GTGA TTTG CTTG CTGG *5'*		
NM_138883	ATP5O	*5'* CACA GTGA CCAC AGCG TTTC CTTT *3'*	153	60
		3' TTCG GACA ATCA TCCC ACCC ATGA *5'*		
AC_000022	ATP6 [d]	*5'* GGGC TTCT TCCC CATA CATT *3'*	135	60
		3' CGGT GAGA AGTG GGCT AAAG *5'*		
AC_000022	ATP8 [d]	*5'* TTCT TCCC AAAC CTTT CCTG *3'*	113	60
		3' GGGG TAAT GAAA GAGG CAAA *5'*		
AC_000022	COX I [d]	*5'* ACAT GAGC AAAA GCCC ACTT *3'*	172	60
		3' CGGC CGTA AGTG AGAT GAAT *5'*		
AC_000022	COX II [d]	*5'* TGAG CCAT CCCT TCAC TAGG *3'*	107	60
		3' TCAG AGCA TTGG CCAT AGAA *5'*		
AC_000022	COX III [d]	*5'* AGCC CATG ACCA CTAA CAGG*3'*	170	60
		3' TGGC CTTG GTAT GTTC CTTC *5'*		
NM_017202	COX IV	*5'* ACGA GAGC TTCG CTGA GATG AACA *3'*	111	60
		3' AGCT CTTC TCCC AGAT CAGC ACAA *5'*		
NM_053586	COX Vb	*5'* GCGA GATG GCTT CAAG GTTA *3'*	180	60
		3' GTCC CCTC TGTG CTGC TATC *5'*		
NM_012839	CYCS	*5'* TGAT CCTT TGTG GTGT TGAC CAGC *3'*	145	60
		3' ACCA TGGA GGTT TGGT CCAG TCTT *5'*		
NM_001004279	CYP-D	*5'* AGCC CTCC AATT CCAA GAAC *3'*	149	60
		3' AGTG CCCT TTTC TCCT GTAC *5'*		
AC_000022	CYT-B [d]	*5'* GCTT CTTC GCAT TCCA CTTC *3'*	137	60
		3' TGGA TGGA ATGG GATT TTGT *5'*		
AC_000022	ND1 [d]	*5'* AAAG AACC CATA CGCC CTCT *3'*	162	60
		3' AAGG CTGG ATGT GGCT AGAA *5'*		
AC_000022	ND2 [d]	*5'* ACCC AAGG AATT CCCC TACA *3'*	176	60
		3' TTTC GTGT TTGG GTCT GGTT *5'*		
AC_000022	ND3 [d]	*5'* TCCG AAAA AGCA AACC CATA *3'*	158	60
		3' TTGG TTGT TTGA ATCG CTCA *5'*		
EU104721	ND4 [d]	*5'* GATG AGGC AACC AAAC AGAA CGCT *3'*	174	60
		3' TGTT GGAT CATG TTGA GGGT AGGG *5'*		
EU104720	ND4L [d]	*5'* CTAC TCTC CTCT GCCT AGAA GGAA *3'*	145	60
		3' GCTA AACC TACT GCTG CTTC GCA *5'*		
AC_000022	ND5 [d]	*5'* ACCC ATGC ATTC TTCA AAGC *3'*	150	60
		3' AAGG GCTA GGCT TCCG ATAA *5'*		
AC_000022	ND6 [d]	*5'* ACCA ACAT CCCA CCCA AATA *3'*	148	60

continues on next page

Table 4.2 – Continued

Accession Number [a]	Personal Code	Sequence [b]	Amp bp	T_m [c] °C
		3' GTCT AGGG TTGG CGTT GAAG *5'*		
XM_001064382	NDUFA9	*5'* CAGG TTGT TAGA GCGC TTCC *3'*	112	60
		3' TCCC ATGA GGTA TGAC AGCA *5'*		
NM_001106489	NDUFS3	*5'* CTGT GTGT GTTT TCCG GCTA *3'*	199	60
		3' CATC ACTC GAGG GTCT GACA *5'*		
NM_001025146	ND3UFS4	*5'* AAGA AGAT GCGG TTGC CTTT GCAG *3'*	96	60
		3' TTGC ACCG TAAG ACTT GGAC TTGG *5'*		
NM_001106322	ND3UFS8	*5'* GTAT CTAC TGTG GTTT CTGC CAGG *3'*	102	60
		3' TGTA CAGC AACT CCTC ATGC GTCT *5'*		
NM_130428	SDHA	*5'* AGTC TATC GCTG AGGC TTGC *3'*	136	60
		3' GCCT TCTT GCTC TCAC CAAC *5'*		
XM_216558	SDHB	*5'* TGTA TGAG TGCA TCCT GTGT GCCT *3'*	109	60
		3' ATCC AGCG ATAA GCCT GCAT GAGA *5'*		
NM_001006970	UQCRC2	*5'* TTGG TGAT TGCT TCTC TGGA *3'*	173	60
		3' TCAA TTCC ACGG GTGA TCTT *5'*		
NM_001008888	UQCRFS1	*5'* TGTA CTGG CCAT GTCGȦAGA *3'*	103	60
		3' TCTA TGGC GCAC AAAC AGAG *5'*		
NM_031353	VDAC1	*5'* GTAT GGGC TGAC GTTT ACTG AG *3'*	172	60
		3' GATA TGCT CCCT CTTG TACC C *5'*		
NM_031354	VDAC2	*5'* AATT TGTA TCCC TCCA CCCT ATG *3'*	156	60
		3' CCAGT GTCT GTAT TAGAT GAGC C *5'*		
NM_031355	VDAC3	*5'* CTGT AACT ACGG GCTC ATCT TC *3'*	189	60
		3' CTGC CCAC ACTA AAAC AATC C *5'*		
V01270	18S	*5'* CGCC GCTA GAGG TGAA ATTC TT *3'*	149	60
		3' CAGT CGGC ATCG TTTA TGGT C *5'*		

[a] available at www.ncbi.nlm.nih.gov/nucleotide/

[b] $5' - 3'$ is the forward primer and $3' - 5'$ the reverse primer

[c] values represent the temperature conditions used in PCR experiments and not the theoretic thermodynamic values

[d] mitochondrial-encoded transcript

4) intra-primer complementary should be kept at minimum to avoid hairpins (checked through UNAFold web-based software from IDT);
5) complementary between primers should be kept at minimum to avoid primer dimer (checked through agarose gels);
6) primers should be specific implying no off-target genes sequences in the target genome (checked through a BLAST search and in agarose gels).

Real-time PCR was carried out using 2 µl of the purified cDNA samples and amplified with FastStart SYBR Green I Kit (Roche Diagnostics, Indianapolis, IN, USA) in 10 µl total reaction volume. Amplification and quantification of generated products

were performed in a LightCycler Instrument (Roche Diagnostics) under the following cycling conditions: pre-incubation at 95 °C for 8 min, followed by 35-40 cycles denaturation at 95 °C for 8 s, annealing at 60 °C[6] for 5 s, extension at 72 °C for x[7] s with single-point fluorescence acquisition.

Real time PCR of control and treated samples for each gene was performed on the same run to control for potential run-to-run variability and used also the same mastermix. The melting peaks of all PCR products were routinely determined by melting-curve analysis (a temperature ramp from 65 to 90 °C with increments of 0.2 °C s^{-1}) in order to ascertain that only the expected products had been generated.

Samples were quantified using a serial dilution of a well characterized DNA standard, which provided a comparative measure to verify the integrity of the reaction. 18S ribosomal RNA was used to normalize gene expression. The range of concentrations tested in the standard curve was across 5 $logs_{10}$ which covered the range in the test unknowns without extrapolating. Serial cDNA dilutions were made using cDNA from HepG2 cell line amplified through a simple PCR reaction using the HotStartTaq Master Mix Kit (Qiagen) under the following cycling conditions: pre-incubation at 95 °C for 15 min, followed by 30 cycles denaturation at 94 °C for 30 s, annealing at 60 °C[2] for 30 s, extension at 72 °C for 45 s and a final extension step at 72 °C for 10 min.

The amplification product was run in a 4 % agarose gel and if a single product was detect the remaining reaction was purified using the QIAquick PCR Purification Kit (Qiagen) and thereafter quantified in NanoDrop (ND-1000, NanoDrop Technologies, Wilmington, DE, USA). A standard stock solution of 5×10^9 copies was prepared using the following equation and stored at −20 °C:

$$number\,of\,copies = \frac{amount \times 6.022\times10^{23}}{length \times 1\times10^9 \times 650} \tag{4.13}$$

where the *amount* is in µg ml^{-1}, 6.022×10^{23} is Avogrado's number in molecules/mol, *length* is the length of the amplicon in base pairs and 650 is the average weight of a base pair in Da.

[6] see table 4.2 for exact primers target temperature used
[7] time was dependent on product size since Taq polymerase has an enzyme activity of 25 bp s^{-1}

4.19 Data processing and statistical analysis

Normality and homocedasticity

All data was assessed for normality using the Kolmogorov-Smirnov test with Dallal-Wilkinson-Lilliefor correction (when using Graph Pad Prism software, see below) or Shapiro-Wilk (when using JMP-SAS software, see below). Similarly, all data was assessed for equality of variances using the F test, in the case of Stundent's t test, or Bartlett's test, for the remaning procedures. Since group sample sizes are equal and the parametric statistical tests applied are robust for moderate deviations from homoscedasticity [292], parametric tests were still applied when homoscedasticity was not observed. However, when data normality was rejected, a squared-root, logarithmic or reciprocal transformation was applied in an attempt to achieve normality. If data still rejected normality, the correspondent non-parametric statistical test was used.

Nevertheless, data is presented to the reader in non-transformed values for ease of comprehension. In the text, data is expressed as percentage of the difference of means plus its standard error or as percentage of the means difference plus its standard error, for data related to isolated mitochondrial fractions. In both situations, the percentage value shown regards the saline group in the same model.

Non-linear regression

To generate global-flux curves the raw data for each preparation (n) , i.e. respiration rates, were first normalized to a common scale between 0 and 100 % relative to the respiration rate in the absence of inhibitor. The curve-fitting model used was the one previously established by Gellerich [293] for non-competitive inhibition and reviewed by Small [294], which assumes the following general equation:

$$J^I / J^0\,(\%) = 100 \times \frac{E_j^I}{E_j^I - C_{E_j}^j \times (E_j^I - E_j^0)} \tag{4.14a}$$

with

$$E_j^I = -1/2 \times (\alpha - \sqrt{\alpha^2 + 4E_j^0.K_d}) \tag{4.14b}$$

and

$$\alpha = [I] + K_d - E_j^0 \tag{4.14c}$$

where J^0 and E_j^0 are the flux and the enzyme concentration in the absence of inhibitor, respectively; E_j^I the total enzyme concentration not bound to inhibitor at a given inhibitor concentration; K_d is the dissociation constant for enzyme-inhibitor complex, J^I is the resulting flux at a given inhibition level and, $C_{E_j}^J$ is the control coefficient of the enzyme with respect to the flux being measured.

To generate dose-response/isolated-step curves, raw data, i.e. enzymatic rates, were first normalized to a common scale between 0 and 100 % where *zero* was defined as the smallest value in each data set and *one hundred* as the value in the absence of enzyme inhibitor. Then, the abscissa values (inhibitor concentration) were *log* transformed in order to apply the curve-fitting model. The preferential model was a *four parameter logistic* using the least squares fit. However, whenever the data presented itself to be asymmetric around the inflection point, discrimination between the previous model and a *five parameter logistic* was established through the extra sum-of-squares followed by a F test, and the latter model was prefered at 5 % level or otherwise discarded.

In the specific case of ANT it is not possible to evaluate its activity alone since it depends crucially in the Δp generated by OXPHOS. Therefore, equation 4.14 was used to simulate the activity of the isolated step by imposing $C_{E_j}^J = 0$ and using K_d and E_j^0 values obtained from the global flux curve-fitting, as previously described [219].

Simulation of threshold curves

Threshold curves originates from the titration curves of global flux and isolated step and represent the state 3 respiration rate (%) as a function of OXPHOS enzyme inhibition (%). Therefore, the theoretical equations of the model used for curve-fitting of the isolated step were solved for $[I]$ and substituted in equation 4.14:

$$[I] = \left(\frac{10^{\log IC_{50} \times \text{Hill Slope}+2}}{\%\text{ of Inhibition}} - 10^{\log IC_{50} \times \text{Hill Slope}} \right)^{1/\text{Hill Slope}} \tag{4.15a}$$

for Complex I, III and IV and where IC_{50} and *Hill Slope* are parameters obtained from the curve-fitting;

$$[I] = \frac{\%\text{ of Inhibition} \,.\, [E_j^0 \,.\, (\%\text{ of Inhibition} - 100) - 100.K_d]}{100 \times (\%\text{ of Inhibition} - 100)} \tag{4.15b}$$

for the specific case of ANT.

The threshold values were determined as described by Rossignol [219] with few adaptations. Using the general definition of a tangent line to a curve[8] and the first derivative of the threshold curve, two tangent lines were calculated at 1% enzyme inhibition and at the inflection point. The threshold value was defined as the abscissa of the intersection point between the two tangents.

Statistical tests

Statistical significance between means was determined using two-tailed Student's t test. In lack of homoscedasticity a Welch's correction was applied and in lack of normality the Mann-Whitney test was used instead. To exclude the random effect associated with daily mitochondrial isolation and electrode variability, a matched pairs Student's t test or its non-parametric correspondent Wilcoxon matched pairs test were performed. Differences were considered significant at 5 % level and p value was categorized accordingly to their interval of confidence.

When three or more groups were to be analyzed, a one-way ANOVA or a within-subjects ANOVA (similar to a paired test) was used instead. Corrections for multiple comparisons were made using the Tukey pos-hoc test, when all possible comparisons were required, or Bonferroni pos-hoc test, when only specific comparisons were to be made. Differences were considered significant at 5 % level and p value was categorized accordingly to their interval of confidence.

In the specific case when seeking to ascertain whether changes between saline and DOX group in the heart are actually different from changes in other tissues, regardless of the inter-tissue baseline, the procedure was as follow. Data was *log* transformed and analyzed through a two-way ANOVA with planned contrasts against the interaction between treatment and tissue so that significant relative changes (fold-change) are dependent on tissue. Random effects were included in the statistical model of the sub-chronic protocol since all the three tissues were collected from the same individual, i.e. each animal is intrinsically different from each other as well is the response of each one to the treatment; therefore, *animal* and *animal* x *tissue* were used as random effects in a restricted maximum likelihood (REML) approach. In both cases, p values were adjusted for multiple comparisons through Sidak pos-hoc test and differences were considered significant at 5 % level and p value was categorized accordingly to their interval of confidence.

[8] $y = f(a) + f'(a)(x - a)$ returns the tangent line at the point $(a,\ f(a))$

Software

Statistical analyses were performed using Graph Pad Prism version 5.0 (GraphPad Software, Inc., San Diego, CA, USA), with the exception of the two-way ANOVA which was performed using JMP-SAS version 9.03 (SAS Campus Drive, Cary, NC, USA). Non-linear regressions and simulations were performed using Graph Pad Prism.

Chapter 5

Mitochondrionopathy Phenotype in Doxorubicin-Treated Wistar Rats Depends on Treatment Protocol and is Cardiac-specific

Previous works in animal models have failed to use a multi-organ approach to demonstrate that DOX-associated toxicity is selective to the cardiac tissue. In this context, the work presented in this chapter aims to investigate *in vivo* DOX cardiac, hepatic and renal toxicity in the same animal model, with a special focus on alterations of mitochondrial bioenergetics. Wistar rats were sub-chronically or acutely treated with DOX and allowed to rest for one week or 24 h after the last injection, respectively. Alterations of mitochondrial bioenergetics showed a treatment-dependent pattern between tissues. No alterations were observed for cardiac mitochondria in the acute model but decreased ADP-stimulated respiration was detected in the sub-chronic treatment. In the acute treatment, ADP-stimulated respiration was increased in liver and decreased in kidney mitochondria. Aconitase activity was decreased in renal mitochondria in the acute and in heart in the sub-chronic model. Interestingly, alterations of cardiac mitochondrial bioenergetics co-existed with an absence of echocardiograph, histolopathological or ultra-structural alterations. Besides, no plasma markers of cardiac injury were found in any of the time studied. The data confirms that alterations of mitochondrial function, which are more evident in the heart, are an early marker of DOX-induced toxicity, existing in the absence of cardiac functional alterations.

5.1 Introduction

As introduced in Chapter 2, DOX acute cardiac toxicity occurs during the early treatment and usually include myopericardits, sinus tachycardia, reversible arrhythmias, prolonged QT interval and flattening of the T wave, being easily manageable and disappearing once the treatment is ceased [196].

Alternatively, a significant number of patients develop chronic cardiotoxicity which can appear right after the end of the treatment or even years later [142]. Unlike acute toxicity, the dose-dependence together with its difficult early detection, converts the chronic toxicity in life-threatening and largely uncontrolled condition.

The mechanisms underlying DOX-selective cardiotoxicity was summarized in Chapter 2 but still there is hardly any consensual conclusion. Nevertheless, it is accepted that the antitumor activity is completely independent from cardiac toxicity, which may involve alterations of mitochondrial function, as was exposed in section 2.4. Hallmarks of mitochondrial dysfunction in cardiac tissue upon DOX-treatment include inhibition of oxidative phosphorylation, decreased calcium-loading capacity and stimulated ROS production [174, 295].

Despite the fact that DOX toxicity has been described as being cardiac selective, none of the theories proposed to date (see sec. 2.5.1, page 61) fully explain the pronounced effects on cardiac tissue in comparison to other vital tissues. Although several animal models have been generated to investigate both sub-chronic [77, 159, 183, 221, 296] or acute [184, 297, 298] DOX toxicity, one limitation of the majority of studies is that only one organ was investigated. Thus, comparing DOX multi-organ effects from different papers becomes non-accurate, confusing and sometimes contradictory since animals species, strain, age and treatment protocols differ from publication to publication.

The objective of the work presented in the current chapter was to measure alterations of mitochondrial bioenergetics in the heart, liver and kidney after two distinct treatment protocols (acute vs. sub-chronic) in Wistar rats, and compare mitochondrial end-points with tissue histological alterations (all three organs) and function (heart).

Our hypothesis is that alterations of mitochondrial bioenergetics occur predominantly in the heart, being an early and sensitive marker of DOX-induced toxicity which may occur even in the absence of histological alterations. A second tandem hypothesis is that cardiac mitochondrial toxicity is detectable only in the sub-chronic treatment.

5.2 Results

5.2.1 Animal and organs mass

In the acute model, control and DOX-treated animals did not show changes in their body mass in the 24 h subsequent to DOX administration (Table 5.1). However, when the animals were individually analyzed, i.e. when the mean of the arithmetic difference between initial and final body mass of every individual was calculated for the first 24 h, the control group showed a body mass variation of -0.35 ± 1.02 g ($n=17$) while variation in DOX-treated group, -15.1 ± 1.7 g ($n=17$) representing about 4 % of total body mass, was significantly lower ($p<0.001$).

Surprisingly, a decrease of 7.6±2.7 % in heart mass was observed 24 h after a single DOX injection but no alteration was observed in other tested tissues (1.6±4.4 % increase in liver and 3.1±3.9 % decrease for kidney, Table 5.1). Therefore, heart mass over body mass ratio showed a significant decrease of 5.8±2.3 % while no changes were found for liver or kidney (3.6±2.6 % increase and 1.4±3.6 % decrease, respectively; Table 5.1).

Weekly treatment of 8 week-old rats with DOX during seven weeks caused a significant reduction in body mass gain of animals, as can be seen by the difference of end-point body mass values between groups (13.8±2.1 %; Table 5.1). While the body mass variation of the control group during the 8 weeks of treatment showed an increase of 49.1±2.9 %, the DOX- treated group increased their body mass only 31.2±3.1 %, which can be easily observed in the body mass gain profile depicted in Fig. 5.1. However, it was interestingly to observe that the alteration in heart mass detected in the acute model was not present in the sub-chronic protocol at the end of the treatment period (Table 5.1).

Since only a non-significant decrease of all tissues (2.4±5.6 %, 3.2±4.0 % and 5.2±3.6 % for heart, liver and kidney, respectively) was observed, the ratio of organ mass to body mass was increased in all analyzed tissues (13.7±6.6 %, 12.4±3.5 % and 10.0±4.1 % for heart, liver and kidney, respectively; Table 5.1). The results reflect a change in body mass rather than alterations in tissue mass.

It should be noticed that although the objective of the experimental protocol was to induce a sub-chronic response and therefore a lower rate of mortality, one animal died during DOX treatment (marked with an arrow, Fig. 5.1). This treated animal received

Table 5.1: Body and organs mass profile of animals subjected to DOX treatment protocols.

Model	Treatment	**Initial body mass** (g)		**Final body mass** (g)		**Heart organ mass** (g)		**HM:BM** (×1000)		**Liver organ mass** (g)		**LM:BM** (×1000)		**Kidney organ mass** (g)		**KM:BM** (×1000)	
		Mean	*SE*	Mean	*SE*	Mean	*SE*	Mean	*SE*	Mean	*SE*	Mean	*SE*	Mean	*SE*	Mean	*SE*
Acute	Saline (n=17)	377.5	7.8	377.2	7.9	0.972	0.020	2.58	0.05	11.6	0.3	30.8	0.1	2.19	0.05	5.84	0.02
	DOX (n=17)	385.1	9.7	370.0	9.6	0.898**	0.018	2.44*	0.04	11.8	0.4	32.9	0.1	2.13	0.07	5.76	0.02
Sub-Chronic	Saline (n=19)	263.0	5.0	391.8	5.9	1.250	0.040	3.20	1.29	12.3	0.4	31.4	0.1	2.50	0.06	6.40	0.02
	DOX (n=19)	255.4	5.3	337.4***	5.8	1.220	0.050	3.64*	1.65	11.9	0.3	35.3**	0.1	2.36	0.06	7.03*	0.02

Data refers to wet organ mass and its ratio to body mass was obtained dividing the organ mass over the respective total animal mass times 1000. The deceased DOX-treated rat and its matched control in the sub-chronic model were excluded from this analysis. Differences between treatment groups means within the same model were evaluated by Student's t test (see 4.19, p. 110). *, $p \geq 0.05$; **, $p \geq 0.01$ ***, $p \geq 0.001$ *vs* saline group of the same treatment protocol.
Abbreviations: *HM:BM* - heart mass to body mass ratio; *LM:BM* - liver mass to body mass ratio; *KM:BM* - kidney mass to body mass ratio; *SE* - standard error.

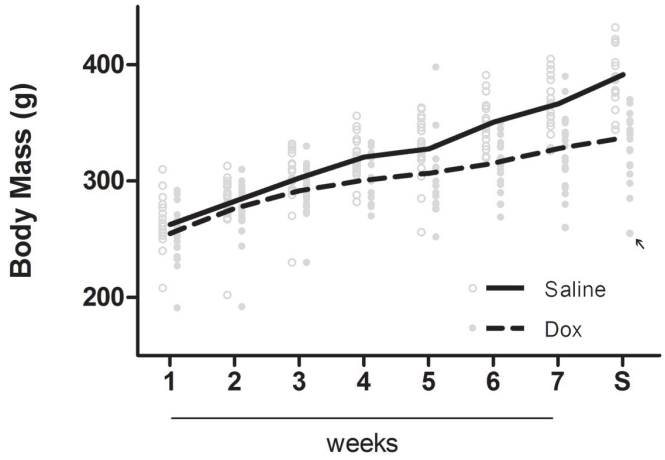

Figure 5.1: DOX decreases body mass gain over time in a sub-chronic toxicity model. After the fourth injection, the body mass of treated animals started to become farther apart from the control and therefore the growth profile is dramatically changed at the end of treatment. Only one DOX-treated animal died during the protocol (denoted by black arrow). Animals in control group are depicted by open circles while DOX-treated animals are in full circles. Lines represent the means of each group at each time point. *S* - sacrifice.

all seven DOX injections and died precisely one week after the last. Nonetheless, the animal did not show any distinct sign of distress or illness when compared with its counterparts. Therefore, the mortality rate associated with the present study is 5% (1 out of 20).

5.2.2 Serum biochemistry

In acute model, despite the fact that lactate dehydrogenase, a general marker for tissue damage, is not altered (21.8±14.0 %; Table 5.2) the non-specific hepatic marker, aspartate aminotransferase (AST), is markedly elevated 91.0±17.2 %. Serum creatine kinase is unchanged (1.7±16.0 %) as well as markers of renal function, namely urea, creatinine, uric acid or blood urea nitrogen (BUN).

The observed high levels of the hepatic-specific marker, alanine aminotransferase (ALT), 141±26 %, together with the lower AST to ALT ratio (15.3±7.5 %) and total protein levels (TP; 9.8±1.7 %) suggest an impaired liver function in DOX-treated animals. Increased cardiac injury, as evaluated by measuring troponin I (TnI) was not significantly increased in the acute model (value increased 15±11 % vs. control).

Table 5.2: Blood plasma profile after DOX treatment.

Model	Treatment	CK (U/l)		TnI[a] (µg l^{-1})		TRIG (mg dl^{-1})		CHOL (mg dl^{-1})		AST (U/l)		ALT (U/l)		AST/ALT –		TP (g dl^{-1})	
		Mean	*SE*	Mean	*SE*	Mean	*SE*	Mean	*SE*	Mean	*SE*	Mean	*SE*	Mean	*SE*	Mean	*SE*
Acute	Saline (n=15)	13 039	1555	916	62	114.5	14.3	38.8	2.0	178.7	15.3	57.1	3.0	3.11	0.18	71.4	0.9
	DOX (n=15)	12 816	1564	1053	84	54.1***	4.2	40.6	1.9	341.0***	26.9	137.8***	14.6	2.64*	0.15	64.4***	0.9
Sub-Chronic	Saline (n=18)	9130	1007	840	57	126.9	8.9	41.0	1.2	183.1	10.6	51.5	2.5	3.63	0.20	71.5	0.6
	DOX (n=18)	6262*	709	933	86	376.3***	49.6	93.1***	9.7	139.6***	5.0	43.9*	1.5	3.20	0.10	62.3***	0.9

LDH (U/l)		CREA (mg dl^{-1})		Urea (mg dl^{-1})		UA (mg dl^{-1})		BUN (mg dl^{-1})	
Mean	*SE*	Mean	*SE*	Mean	*SE*	Mean	*SE*	Mean	*SE*
2507	224	0.59	0.02	35.0	1.8	1.71	0.14	16.3	0.9
3055	271	0.57	0.02	34.5	1.3	1.66	0.09	16.1	0.6
4224	432	0.64	0.01	38.8	0.7	1.63	0.12	18.1	0.3
3561	497	0.58**	0.01	33.7***	0.7	1.39	0.09	15.7***	0.3

[a] For troponin I analysis, only 13 and 16 samples were measured in acute and sub-chronic protocol, respectively due to limitations in the analytical kit used.

Differences between treatment groups means within the same model were evaluated by Student's t test, when assumptions were not achieved a Welch correction or the non-parametric Mann-Whitney test were applied (see 4.19, p. 110). *, $p \geq 0.05$; **, $p \geq 0.01$; ***, $p \geq 0.01$ *vs* saline group of the same treatment protocol.

Abbreviations: *CK* - creatine kinase; *TnI* - troponin I; *TRIG* - triglycerides; *CHOL* - total cholesterol; *AST* - aspartate aminotransferase; *ALT* - alanine aminotransferase; *TP* - total serum proteins; *LDH* - lactate dehydrogenase; *CREA* - creatinine; *UA* - uric acid; *BUN* - blood urea nitrogen; *SE* - standard error.

Regarding circulating-blood lipids, triglycerides were decreased by 53±13 % 24 h after the acute treatment but no alteration was found in total cholesterol, 4.6±7.0 %.

Notwithstanding, chronically-DOX-treated rats were hyperlipidemic with the treated group showing both an increase in triglycerides and cholesterol (196±40 % and 127±24 %, respectively; Table 5.2). TnI levels were also increased by 11±12 %, although not statistically significant. Interestingly, all other parameters analyzed were decreased in comparison to control animals (average of the parameters variation of 17.3 %, ranging from 8.7 % to 31.4 %), with the exception of lactate dehydrogenase (LDH), uric acid and transaminases ratio.

5.2.3 Echocardiography

Animals from sub-chronic DOX treatment were submitted to an echocardiogram 5 d after the 7^{th} injection in order to evaluate shape and function of the heart. No abnormality was found in the four animals analyzed (Table 5.3). Thickness of the walls and left ventricular diameter, ejection fraction and fraction shortening were not different from the control group at this time point (average of the parameters variation of 0.25 %, ranging from 0.16 to 0.40 %).

5.2.4 Histopathology

When analyzing at least three different samples from each tissue and from each treatment protocol, no obvious sign of damage or morphological alterations were found after histological analysis. Fig. 5.2 is representative of the histological characterization of each tissue. Hearts from treated animals in both models did not present signs of fibrosis or any hallmarks of later stages of DOX toxicity. However, in the representative pictures of cardiac slices, minor cytoplasmic vacuolization in the acute model (Fig. 5.2 , Panel B) and also minor increase in cellular volume in the sub-chronic model (Fig. 5.2 , Panel D) can be observed.

Livers were morphologically normal; however, minor centrilobular dilation was observed, while hepatocytes showed citoplasmic heterogeneity due to vacuolization. Nevertheless, the vacuolization was more prominent in slices from the sub-chronic model (Fig. 5.2 , Panel F and H). When renal slices were observed with HE stain, no differences were found between control and treated group regardless of the treatment

Table 5.3: Echocardiogram parameters in the sub-chronic protocol

Model	Treatment	IVS (mm)		LPWT (mm)		LVDd (mm)		LVDs (mm)		LVEF (%)		FS (mm)		LV mass (mg)		AT s/d (bpm)	
		Mean	*SE*	Mean	*SE*	Mean	*SE*	Mean	*SE*	Mean	*SE*	Mean	*SE*	Mean	*SE*	Mean	*SE*
Sub-Chronic	Saline (n=4)	1.49	0.05	1.54	0.05	5.02	0.21	2.44	0.13	87.3	0.8	51.2	1.1	416	45	521	15
	DOX (n=4)	1.50	0.03	1.55	0.02	5.00	0.22	2.45	0.16	87.0	1.2	51.2	1.3	412	23	538	16

Differences between treatment groups were evaluated by non-parametric Mann-Whitney test due to their lack of normality (see 4.19, p. 110).
Abbreviations: *IVS* - interventricular septum; *LPWT* - left posterior wall thickness; *LVDd* - left ventricular diastolic dimension; *LVDs* - left ventricular systolic dimension; *LVEF* - left ventricular ejection fraction; *FS* - fraction shortening; *AT s/d* - arterial tension systole/diastole.

protocol used (Fig. 5.2 , Panel J and L).

In terms of tissue ultrastructure, electron micrographs of cardiac slices from acutely treated animals (Fig. 5.3, Panel B and D) showed a cellular structure not dissimilar to control (Fig. 5.3, Panel A and C). The myofibrillar disorganization, cytoplasm vacuolization and swollen mitochondria usually observed after DOX treatment in other rodent models [187, 188] were not present in our acute model (Fig. 5.3, Panel A-D). In fact, myofibrillar Z-bands were well defined and with narrow A-bands (Fig. 5.3, Panel C and D).

Likewise, kidney electron micrographs were similar to control counterparts (Fig. 5.3, Panel H-K). However, hepatic slices presented more heterogeneous cytoplasm with high numbers of vacuoles and lipid-like droplets (Fig. 5.3, Panel E). Moreover, liver mitochondria from DOX acute treated animals appear to be preferentially in the condensed conformation (Fig. 5.3, Panel G) rather than the orthodox one observed in control micrographs (Fig. 5.3, Panel D and F).

Regarding the sub-chronic model (Fig. 5.3, Panel L-X), cardiac samples from treated animals also showed normal sarcomeres with well-defined Z-bands and organized myofibrils (Fig. 5.3, Panel A-D). Nevertheless, cytoplasm appeared to present more vacuolization (Fig. 5.3, Panel M) although mitochondrial morphology was not dissimilar from control micrographs (Fig. 5.3, Panel L and N).

In the liver, the striking evidence is the abundance of small vacuoles in the cytoplasm of hepatocytes from sub-chronically treated animals (Fig. 5.3, Panel S) and, although mitochondria appear to be greater in volume in some panels the overall observation is that they are not different in morphology when compared with the control (Fig. 5.3, Panel P and R). Mitochondria from renal slices appear in an intermediate conformation between orthodox and condensed forms (Fig. 5.3, Panel X).

5.2.5 Mitochondrial bioenergetics

Mitochondrial bioenergetics was evaluated in the three tissues. State 3 respiration mimics an increase in workload which is observed *in vitro* after ADP-induced simulation. State 4 respiration is observed after all ADP is phosphorylated, representing a steady-state of the respiratory chain, controlled by the passive and unspecific diffusion of protons through the inner mitochondrial membrane. Similarly, the phosphorylation lag phase represents the time needed for the phosphorylative system to convert

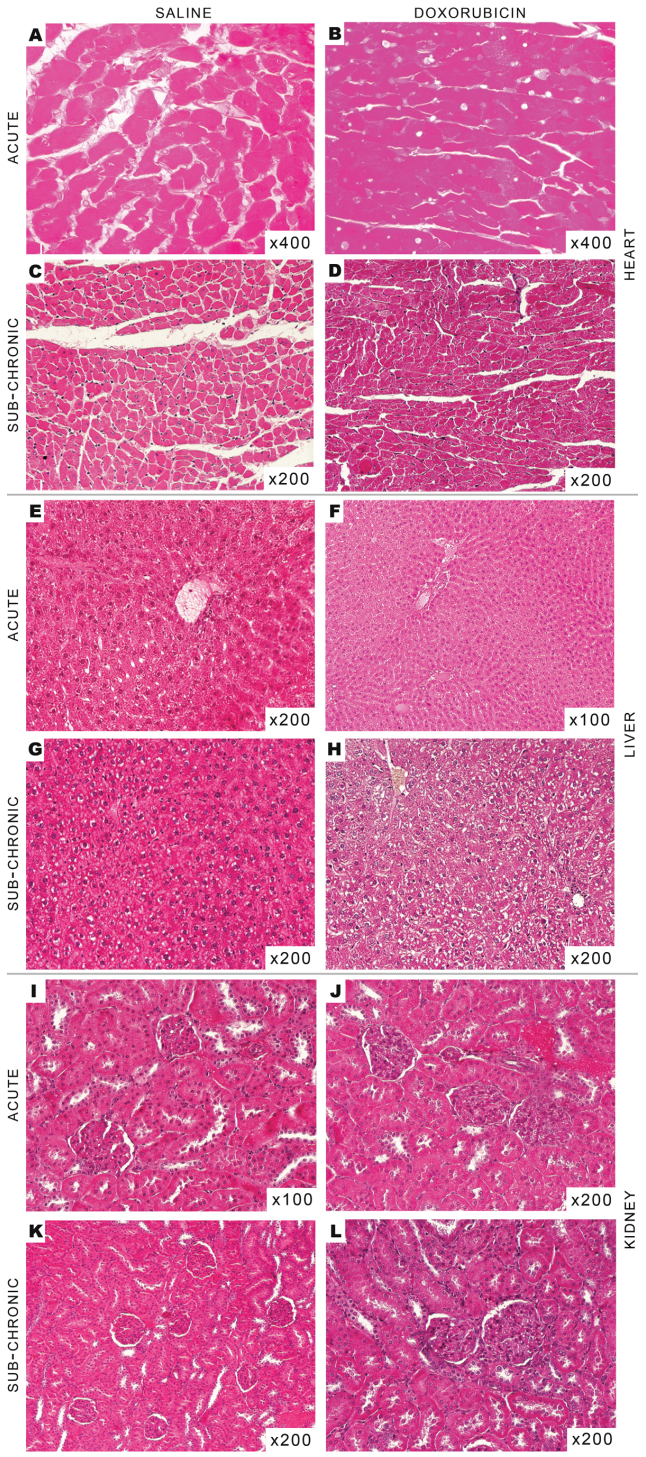

Figure 5.2: Histological analysis of organs collected from rats treated with DOX. No notorious differences or hallmarks of DOX toxicity were found in the different tissues in both protocols. Panels represent HE photographs of random chosen tissues: hearts present minor cytoplasmatic vacuolization (Panel **B**) and cytoplasmatic dilatation (Panel **D**); liver usually show minor cytoplasmatic vacuolization (Panel **F** and **H**); no changes in kidneys (Panel **J** and **L**). Organs were fixed in Bouin's solution, processed through standard histological procedures and stained with HE (for more information, see sec. 4.5, p. 82).

all added ADP to ATP, i.e time to repolarize after ADP depolarization.

In the acute model, complex I-sustained mitochondrial state 3 respiration was increased in hepatic, decreased in renal and not altered in cardiac mitochondrial fractions (14.7±5.5 %, 5.3±2.0 % and 4.4±5.3 %, respectively; Fig. 5.4). However, despite equal variation patterns observed for lag phase, ranging from 13 to 17 % between tissues, there was no statistically difference between groups (Table 5.4).

The previous detected differences for complex I- sustained mitochondrial state 3 respiration were absent when substrates for complex II were used (4.1±6.0 %, 5.9±7.9 % and 6.7±6.7% for heart, liver and kidney, respectively). State 4 respiration, RCR and ADP/O remained unchanged in all fractions regardless of the respiration substrate used (Fig. 5.4 and 5.5). The same was observed for all other parameters related to mitochondrial membrane potential (Table 5.4).

In the sub-chronic model, cardiac mitochondria from treated animals presented decreased state 3 respiration for both respiratory complexes (15.8±4.9 % and 12.8±3.6 % for complex I and II, respectively; Fig. 5.4) and lower state 4 respiration, although only statistically significant when substrates for complex II were used (12.0±6.6 % and 19.8±4.2% for complex I and complex II, respectively). Likewise and in a complementary manner, lag phase was increased for both complex I- and complex II-sustained respiration (10.7±6.0 % and 13.1±5.5 %, respectively; Table 5.4) and $\Delta\psi$ was only slight, yet significantly, decreased when substrates for complex II were used (1.1±0.5 % and 2.2±0.6 % for complex I and II, respectively).

Hepatic and renal mitochondrial fractions behaved similarly, with both having decreased $\Delta\psi$ with complex I substrates (1.9±0.5 % and 1.6±0.4 %, respectively; Table 5.4) and demonstrated slower state 3 respiration (6.6±3.8 %) in hepatic fractions

Figure 5.3 ***(following page)*****:** Cellular ultra-structure remains intact after acute or sub-chronic DOX treatment. No notorious differences or hallmarks of DOX toxicity were found in the different tissues in both protocols. Panels represent electron microphotographs of random chosen tissues: hearts present well- defined Z-bands and organized myofibrils (Panel **C**, **D** and **L**-**O**) and minor cytoplasmatic dilatation (Panel **M** and **O**); livers show cytoplasmatic vacuolization (Panel **E**, **G** and **S**) and lipid-like droplets structures (Panel **Q**) and some mitochondria appear in the condensed conformation (Panel **G**); renal mitochondria appear in an intermediated conformation between orthodox and condensed form (Panel **X**). Organs were fixed in 4% gluteraldehyde and post-fixed in osmium (for more information, see sec. 4.6, p. 82).

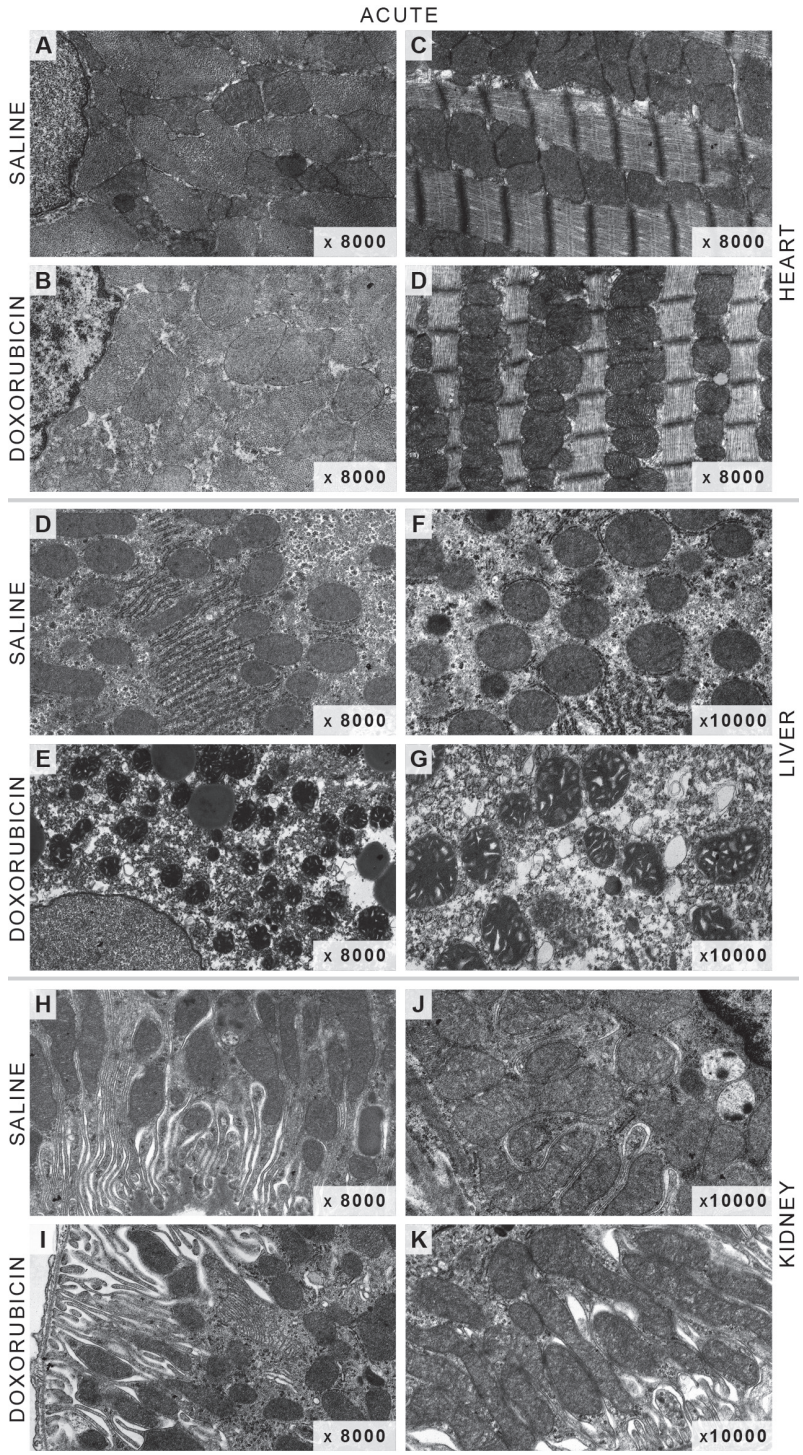
ACUTE
A
C
SALINE
x 8000
x 8000
B
D
DOXORUBICIN
x 8000
x 8000
HEART
D
F
SALINE
x 8000
x10000
E
G
DOXORUBICIN
x 8000
x10000
LIVER
H
J
SALINE
x 8000
x10000
I
K
DOXORUBICIN
x 8000
x10000
KIDNEY

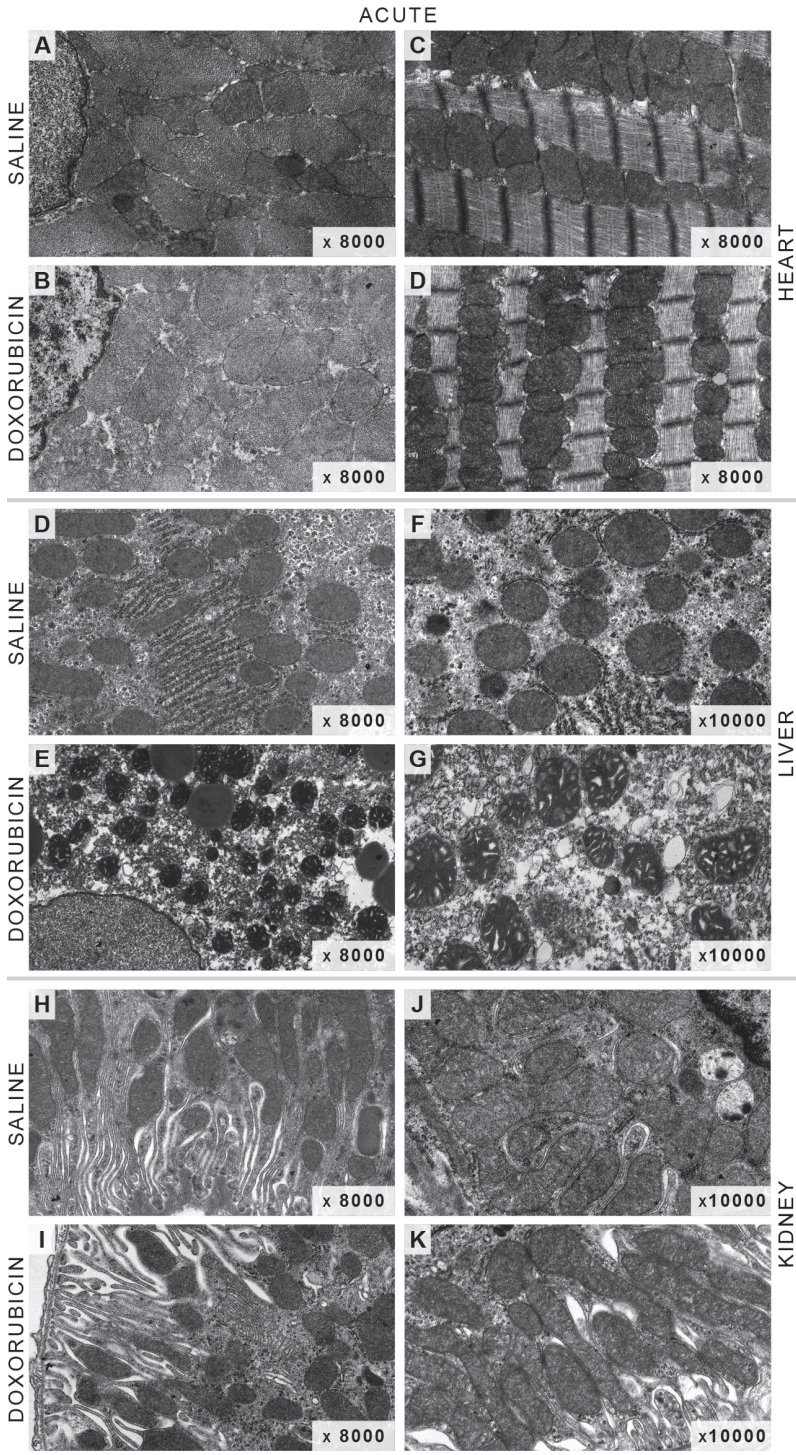
ACUTE
A
C
SALINE
x 8000
x 8000
B
D
DOXORUBICIN
HEART
x 8000
x 8000
D
F
SALINE
x 8000
x10000
E
G
DOXORUBICIN
LIVER
x 8000
x10000
H
J
SALINE
x 8000
x10000
I
K
DOXORUBICIN
KIDNEY
x 8000
x10000

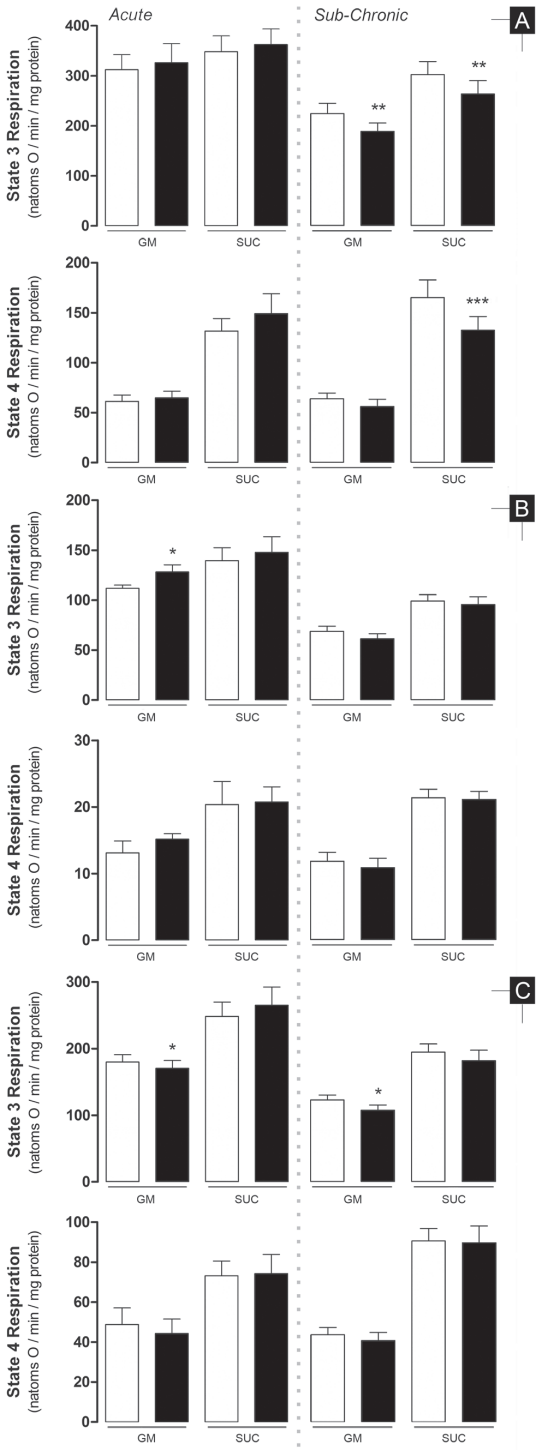

Figure 5.4: Treatment with DOX markedly affects mitochondrial respiration during ADP phosphorylation, which is clearly observed in heart mitochondria during sub-chronic treatment but absent when animals were acutely treated. A reverse pattern is observed in the other two organs tested. Data represents mitochondrial oxygen consumption rates collected with a Clark electrode (for details, see 4.11, p. 89) where 225-250 nmol ADP was added to induce state 3. State 4 is generally described as the rate of oxygen consumption after complete phosphorylation of added ADP. **A** - heart; **B** - liver; **C** - kidney. Bars represent means of treatment groups (saline in **white** bars; DOX in **black** bars) with SE. Differences between treatment groups means within the same model were evaluated by matched pairs Student's t test to exclude the variability related to mitochondrial isolation and electrode calibration but when assumptions were rejected the non-parametric Wilcoxon matched pairs test was applied (see 4.19, p. 110). *, $p \leq 0.05$; **, $p \leq 0.01$; ***, $p \leq 0.001$ *vs* saline group of the same model. $n = 10$, 9 and 10 (acute model - heart, liver and kidney, respectively) or n =12, 11 and 12 (sub-chronic model - heart, liver and kidney, respectively). *GM* - glutamate/malate; *SUC* - succinate.

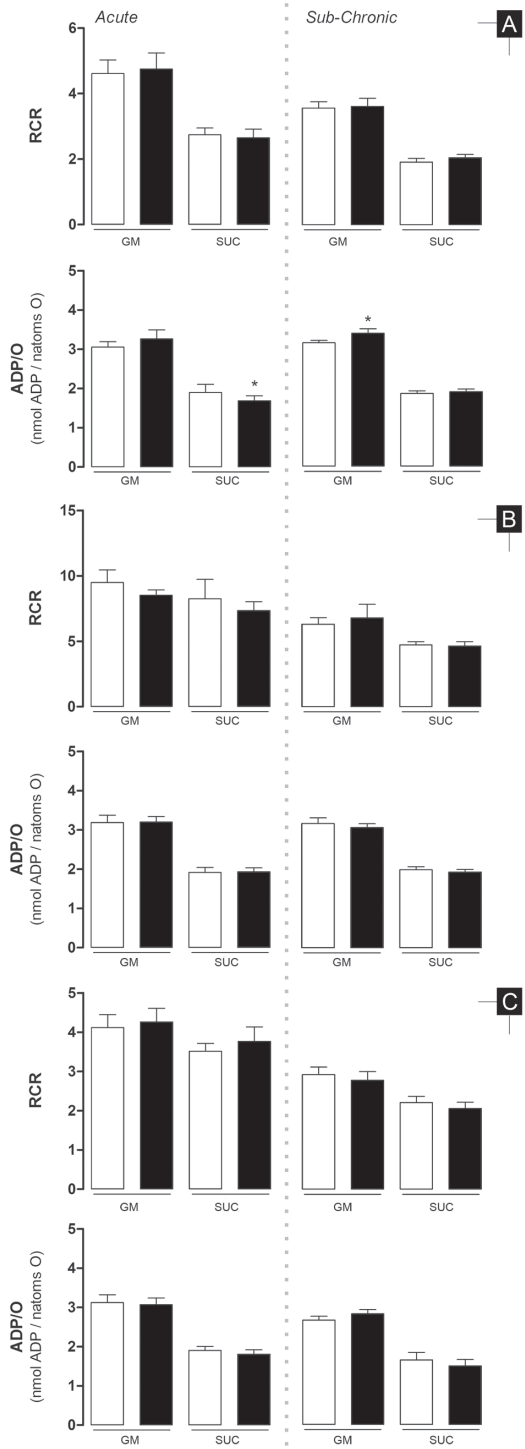

Figure 5.5: Respiratory Control Ratio (RCR) and ADP phosphorylation per consumed oxygen ratio (ADP/O). **A** - heart; **B** - liver; **C** - kidney. Bars represent means of treatment groups (saline in **white** bars; DOX in **black** bars) with SE. Differences between treatment groups means within the same model were evaluated by matched pairs Student's t test to exclude the variability related to mitochondrial isolation and electrode calibration but when assumptions were rejected the non-parametric Wilcoxon matched pairs test was applied (see 4.19, p. 110). *, $p \leq 0.05$ *vs* saline group of the same model. $n =$ 10, 9 and 10 (acute model - heart, liver and kidney, respectively) or n =12, 11 and 12 (sub-chronic model - heart, liver and kidney, respectively). *GM* - glutamate/malate; *SUC* - succinate.

Table 5.4: Effects of DOX on mitochondrial transmembrane electric potential.

		$\Delta\psi$ (− mV)						**ADP Depolarization** (mV)						**Phosphorylative Lag Phase** (s)					
Substr.	**Treat.**	Heart		Liver		Kidney		Heart		Liver		Kidney		Heart		Liver		Kidney	
		Mean	*SE*	Mean	*SE*	Mean	*SE*	Mean	*SE*	Mean	*SE*	Mean	*SE*	Mean	*SE*	Mean	*SE*	Mean	*SE*
Acute		$n = 10$		$n = 9$		$n = 10$		$n = 10$		$n = 9$		$n = 10$		$n = 10$		$n = 9$		$n = 10$	
Glutam.	Saline	222.2	3.9	226.3	5.7	219.2	2.6	33.7	2.5	27.7	2.6	27.3	1.4	30.6	5.5	51.5	6.6	22.8	1.8
Malate	DOX	224.3	5.4	226.4	4.4	217.8	2.9	38.1	3.2	27.7	2.9	29.0	1.0	25.5	3.2	43.3	4.9	25.8	2.8
Succ.	Saline	223.7	2.9	231.8	5.0	222.9	2.7	42.2	1.4	33.3	1.8	31.7	0.8	41.6	6.8	68.0	8.4	27.4	2.8
	DOX	227.7	2.2	227.3	2.0	223.1	2.9	44.8	1.4	32.6	1.4	32.2	1.3	48.6	10.4	64.0	10.5	27.3	2.9
Chronic		$n = 10$		$n = 9$		$n = 10$		$n = 10$		$n = 9$		$n = 10$		$n = 10$		$n = 9$		$n = 10$	
Glutam.	Saline	210.4	2.6	211.3	1.7	208.4	2.0	24.3	1.3	21.2	1.8	18.1	1.5	29.1	2.5	55.8	6.1	34.9	3.7
Malate	DOX	208.1	3.1	207.4**	2.1	205.0**	1.7	24.2	0.9	22.4	1.4	18.9	1.9	32.2*	1.7	70.9*	11.5	38.9	3.5
Succ.	Saline	214.9	2.6	217	1.6	211.1	3.4	27.0	1.6	26.2	1.7	19.7	2.0	38.4	3.1	64.4	6.2	38.2	3.6
	DOX	210.2**	3.0	216.5	2.4	209.2	4.1	27.0	1.7	26.5	1.9	19.2	2.2	43.5*	3.7	76.1	8.1	46.4	6.3

Data was collected with a TPP^+-sensitive electrode (for details see 4.12, p. 91) where 225-250 nmol ADP was added to induce depolarization (phosphorylative cycle). Differences between treatment groups means within the same model were evaluated by matched pairs Student's t test to exclude the variability related to mitochondrial isolation and electrode calibration but when assumptions were rejected the non-parametric Wilcoxon matched pairs test was applied (see 4.19, p. 110). *, $p \geq 0.05$ and **, $p \geq 0.01$ *vs* saline group of the same treatment protocol.
Abbreviations: *Substr.* - substrate; *Treat.* - treatment; *Glutama.* - glutamate; *Succ.* - succinate; *SE* - standard error.

Table 5.5: Effects of DOX on mitochondrial aconitase activity.

Model	Treatment	Heart		Liver		Kidney	
		Mean	*SE*	Mean	*SE*	Mean	*SE*
				%			
Acute	Saline ($n = 6$)	100.0	13.1	100.0	12.5	100.0	12.7
	DOX ($n = 6$)	100.3	12.8	85.0	18.9	72.2**	9.0
Sub-chronic	Saline ($n = 5$)	100.0	10.4	100.0	14.7	100.0	11.7
	DOX ($n = 5$)	78.5*	14.5	112.9	25.9	105.4	12.4

Differences between treatment groups means within the same model were evaluated by matched pairs Student's t test to exclude the variability related to mitochondrial isolation (see 4.19, p. 110). *, $p \geq 0.05$ and **, $p \geq 0.01$ *vs* saline group of the same treatment protocol.
Abbreviations: *SE* - standard error.

and 12.6±4.2 % in kidney with complex I substrates. Along with this decreased state 3 respiration, liver mitochondria also presented a higher phosphorylative lag phase (27.1±11.6%). RCR and ADP/O values were the same between control and treated group in liver and renal mitochondrial (Fig 5.5).

5.2.6 Aconitase activity

Aconitase activity was measured in all mitochondrial fractions as a marker of oxidative stress since its activity is severely affected by excessive ROS generation [285]. Alterations in aconitase activity were tissue-specific and treatment-dependent. The only tissue that showed a decreased enzyme activity in the acute model was the kidney (27.8±6.7 %) while the activity remained unaltered in the heart and liver (0.3±11.8 % and 15.0±12.3 %, respectively; Table 5.5).

Cardiac mitochondrial aconitase in the chronic model was decrease by 21.5±7.7 % in the DOX-treated group while the two other organs were unaltered (12.9±15.6 % and 5.4±9.0% for liver and kidney, respectively)

5.3 Discussion

Despite DOX effective anti-cancer properties, the treatment is also followed by a dose- dependent and irreversible cardiomyopathy, decreasing therefore the therapeutic window of the drug. Although DOX side effects have been subject of exhaustive

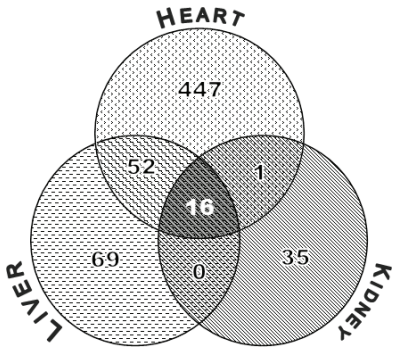

Figure 5.6: PubMed results distribution of doxorubicin and mitochondrial reports accordingly to tissue category. For further details on how search was performed please see Appendix A, p. 201

study, the full mechanism that explain DOX-induced cardiotoxicity is not yet fully understood, despite being acknowledge that DOX-toxicity has a strong mitochondrial component [174, 295]. Nevertheless, despite the several different experimental protocols and models described in the literature [162, 177, 184, 220, 221, 296–303] it is still largely undetermined the selectivity of the toxic effect for the heart.

To the author opinion, the large variety of studies investigating DOX toxicity makes comparisons between different works difficult, sometimes leading to misleading interpretations. By searching PubMed (see Appendix A, p. 201; assessment date February 27th) for reports on the keywords "mitochondria" and "doxorubicin" and narrowing the search to works performed in animals and in the three main tissues (heart, liver and kidney), 534 reports can be found. From then, 52 describe work performed in liver and heart, only 1 in kidney and heart and, 16 in all three tissues harvested in the same experimental protocol (Fig. 5.6). The latter, except two relatively recent works, mainly includes reports from the 80s which did not compare mitochondrial dysfunction with pathophysiological state, genetics, metabolomics or proteomics, which we believe are crucial to better understand DOX-tissue toxicity. In an attempt to increase the knowledge regarding DOX-induced selective cardiotoxicity, it is here presented a multi-organ study in a rodent model for DOX-induced toxicity. Wistar rats were treated acutely or sub- chronically with sub-clinical dosages of DOX and mitochondrial function alterations were analyzed with other tissue damage proteins.

The author's objective was not to induce substantial changes or damage to the different organs but to mimic biochemical and functional alterations that are usually seen in DOX-treated patients before the onset of serious cardiac complications. Therefore, the dosages here employed were closer as possible to a clinical situation. Using an equation already described [298]:

$$BSA = k \times \frac{w^{\frac{2}{3}}}{10^4} \tag{5.1}$$

where k is a shape constant for a given species in $m^2\,g^{-1}$ chosen to 9.5 and w is the weight of the animal in g ([298] and references therein), the actual total dosages were $400\,mg\,m^{-2}$ and $332\,mg\,m^{-2}$ for acute and sub-chronic models, respectively. Therefore, both models are in agreement with the maximum dosage allowed in human chemotherapy which has been described as 500 to $550\,mg\,m^{-2}$ [146]. Notwithstanding, the sub-chronic and acute models were previously used in the literature [184, 187] as accepted models to investigate DOX-mitochondriopathy.

In general, DOX-treatment induced different responses depending on the schedule used. Transaminases and total serum protein levels suggest that the acute treatment targets mainly the liver tissue. Minor cytoplasmic vacuolization observed in histological and electron microscopy of thin slices from hepatic tissue may also suggest metabolic alterations in hepatocytes, which are supported by decreased TRIG levels, despite no alterations in plasma CHOL (Table 5.2). Moreover, the slight increase of state 3 respiration in the presence of compex I-linked substrates (Fig. 5.4), which are the most important in cellular context, and adoption of the condensed mitochondrial conformation as seen by electron microscopy (Fig. 5.3) support the idea of metabolic alteration in hepatocytes after the acute treatment. Nevertheless, it is however unclear at the moment if alterations in lipid metabolism can contribute to worsen the cardiovascular fitness in treated animals.

However, hyperlipidemia was clearly observable in the sub-chronic treatment and liver histology showed slightly more vacuolization that in the acute model (Table 5.2 and Fig. 5.2), suggesting that altered lipid metabolism might be a secondary response to drug treatment. Still, hypocholesterolemic drugs, such as statins, usually used in prevention of cardiovascular problems associated with high levels of circulating lipids showed moderate protection on DOX-induced cardiomyopathy [304].

It was intriguing that chronically-treated animals showed only increase in plasma lipids, while other parameters and markers were consistently decreased even those which are usually increased in chronic exposure to DOX [145, 146] (Table 5.2). Nevertheless, because no substantial alterations in histology and ultrastructure analysis were also detected (Fig. 5.2 and 5.3), we believe that the organism of treated animals reached a new adaptive steady-state following sub-chronic DOX toxicity. Nevertheless organ alterations may probably exist undetected which may lead to a disrupted

response when subjected to metabolic or physiological stress.

Another interesting difference between treatments relates to heart mass which was the only organ in both models to show an alteration in its value. However, it was surprising to observe it merely in the acute model since hypertrophy is usually reported along with DOX-induced cardiotoxicity [143, 148]. Also surprisingly was the 7% decrease in heart mass after 24 h of treatment (Table 5.1). One hypothesis relates to apoptotic and/or necrotic events associated with DOX peak dosage in the plasma [148] and often observed in cardiac cells exposed to DOX [202]. However, one cannot assume this idea as irrefutable and ignore other possible explanation since no visible signs of cellular apoptosis were observed in other assays, namely:

a) histology was normal without signs of fibrosis;
b) biochemical analysis of TnI showed similar levels to control.

Nevertheless, in a previous work, a single injection of $10\,\mathrm{mg\,kg^{-1}}$ DOX caused primarily a decrease in heart mass followed by a restoration to control values [302], which may explain why no alterations were observed in the sub-chronic model. However, sample size in the mentioned study was too small for a good interpretation of results but nevertheless the authors explained the weight recovery to an increase in cytoplasm volume and dilated ventricles as a signal of hypertrophy, which was not observed in our two models.

The loss of cardiac structure and deteriorated function usually observed in long-term treatment with DOX [305, 306] was not present in the present model, supporting the idea of unaltered organ physiology. However, an interesting work conducted on young mice demonstrated that chronic DOX treatment did not result into any sign of cardiomyopathy until animals were subject to a stressful swimming protocol [183]. The dissimilarities between studies, including the one here presented, where no alterations in heart mass in DOX-treated rats were detected and other reports where those alterations were measured [174, 183, 299, 303], may be explained by the different rat strain used or by the fact that the alterations may only be triggered in the presence of a physiological stress. In fact, this idea is in use in the clinical practice where general diagnostic techniques for cardiac function, as an echocardiogram, are performed with increased workload and demands for higher cardiac output increasing therefore the specificity of screening and decreasing the number of false negatives [152, 153].

In fact, the concept of normal organ physiology during resting conditions but altered when submitted to stress led us to investigate mitochondrial function, since we can

artificially stimulate this model system, creating a pseudo-metabolic stress by the addition of ADP. Furthermore, alterations of cardiac mitochondrial function were already described [153]. Once again, a distinct treatment response was observed between the two models. Mitochondrial alterations, assessed by oxygen consumption and transmembrane potential, were noticeable in both treatment protocols but the degree of effect and their targets were distinct.

If one assumes that the extension of statistical significance of the 7 distinct end-points regarding respiration/transmembrane electric potential (Table 5.4, Fig. 5.4 and 5.5) can specify the extension of treatment damage to mitochondria (total of 14 parameters for tissue specificity, 21 for respiratory complex specificity and 42 for model specificity) we may be able to make the following assumptions. Mitochondrial dysfunction is clearly more identified in the sub- chronic model with 11/42 parameters altered in comparison to 2/42 in the acute. Cardiac mitochondria from acute model are the less affected population with 0/14 altered parameters while both hepatic and renal mitochondria have at least one (1/14) altered parameter. Contrarily, heart mitochondria is the most affected population in the sub-chronic model with 6/14 altered parameters comparing to liver (3/14) and kidney (2/14). DOX-treatment also leads to more alterations in complex-I sustained respiration with 2/21 and 8/21 altered parameters in acute and sub-chronic model, respectively, in comparison to complex-II sustained respiration which had 0/21 and 4/21 altered parameters in same models, respectively. It seems therefore plausible to consider that mitochondrial dysfunction, namely at the bioenergetics state, together with harmful effects of DOX on energy substrate channeling, synthesis and availability [196] might be prior and thus responsible for altered cardiac metabolism and structure remodeling.

Oxygen consumption and calcium-loading capacity were previously reported to be good markers for DOX-induced mitochondriopathy [177, 184, 187, 188, 196]. Although some argue about the sensitivity of mitochondrial bioenergetics parameters [187], state 3 respiration was in this study a good indicator for mitochondrial dysfunction since it revealed differences between tissues and treatment protocols. Importantly, changes in this parameter were detected before changes in structure or function of the organs.

DOX is known for its futile redox cycle at mitochondrial complex I level [162]. DOX enhances the production of ROS which are closely related to mitochondrial toxicity and further damage to cell tissue. In the present study, an indirect but specific marker of oxidative stress imbalance, inhibition of the TCA enzyme aconitase, was used. The profile of enzyme inhibition followed the previous idea of tissue-target dependence

on treatment schedule; cardiac aconitase activity was decreased in the sub-chronic model while it was unchanged in the acute (Table 5.5). The results suggest increased cardiac mitochondrial oxidative stress in the sub-chronic model but not in the acute; in this latter case, only kidney mitochondria presented decreased aconitase activity. This was rather surprising since we were expecting effects in both models due to the fact that DOX accumulates rapidly in the tissue and remains at high levels even after the treatment is ended [215, 307].

In fact, DOX-induced increase in oxidative stress is exacerbated in long-term treatments since the primary damage of ROS on mitochondrial DNA can lead to a defective respiratory chain, increasing therefore the productions of ROS. Nevertheless, the author believes that oxidative stress is indeed present in the acute model but perhaps antioxidant enzymes were also up-regulated, as previously described [178], although more work is needed in this regard. Interestingly, most models in literature that subjected animal models to a single injection with higher DOX concentrations found evidences of cardiomyopathy several days later [298, 304, 308, 309]. This observation is not very consistent to the well-known late-onset DOX-induced cardiomyopathy, the author believes that previous studies combined with our data suggest a possible time window where strategies to counteract the drug toxicity can be effectively applied.

To the author knowledge this was the first time that a *7+1* week treatment protocol was used in Wistar rats. Since different rat strains differ in their metabolism and susceptibility to toxic agents [310, 311], data interpretation from the present work is not straightforward comparable to previous data using other rat strains, including Sprague-Dawley [177, 187, 188, 220, 299, 303], which may present different tolerance to DOX. Interestingly, the results from Sprague-Dawley [77, 174, 187] and Wistar rats (the present study) suggest that the former are more susceptible to DOX cardiotoxicity. Although worth of a separate study these differences corroborates the idea of polymorphism-driven susceptibility to chemotherapy [150, 151]. In fact, the same sub-chronic protocol in Sprague-Dawley caused extensive ascites (Oliveira, personal communication), a marker of heart failure, which was absent in the present work.

The data here presented confirms once again the idea of a preferential toxicity targeted to the heart but this time confirmed in a multi-organ test model. Moreover, mitochondrial dysfunction is present before any sign of cardiomyopathy as assessed by echocardiography, or morphological changes. Animals appear to be mostly normal although presenting impaired cardiac mitochondrial function, which may pre-dispose these organelles for failure during stressful events. The results suggest that DOX

cardiotoxicity is better revealed when animals models or humans are placed under stress, as referred in this study [183]. Stressful events can include pregnancy, which has been described to present a higher risk in survivors of childhood leukemia treated with DOX [312].

The data confirms that mitochondrial dysfunction is one major cause of DOX-selective cardiotoxicity and not as a consequence as sometimes is questioned [148].

5.4 Conclusion

In conclusion, the work exposed in the current chapter is the first to provide a three organ analysis of DOX toxicity using two different experimental protocols in Wistar rats. DOX did not cause substantial morphological or echocardiographic alterations in the heart or any other organs analyzed, although cardiac mitochondria showed alterations. Therefore, data confirm that mitochondrial alterations result from DOX treatment, being more severe in the heart and which are very dependent on the treatment protocol. The results confirm that mitochondrial dysfunction is an early marker of DOX toxicity, although it remains to be determined if mitochondrial alterations in organs such as liver and kidney are a direct effect of DOX on mitochondria or instead if they result from secondary effects of DOX on other targets.

Acknowledgements

The present work would not be possible without contribution of the following people, therefore I am thankful to Lina Carvalho (Services of Pathological Anatomy and Medical Oncology, Hospitals of University of Coimbra) for histological analyses; Cristina Brás (Institute of Experimental Pathology, Faculty of Medicine, University of Coimbra) for echocardiograms; Mário Grãos (Biocant, Cantanhede, Coimbra) for the troponin I multiplex assay; Susana Pereira, Cláudia Pereira, Maria Sancha Santos (Center for Neuroscience and Cell Biology), José Lumini, José Magalhães and António Ascensão (Faculty of Health Sciences, University of Fernando Pessoa, Porto) for general collaboration.

Chapter 6

Increased Susceptibility to mPTP After DOX Treatment is Cardiac Specific and Occurs Without Alterations in the Classic Pore Components

Although mPTP-induced mitochondrial dysfunction is an hallmark of DOX cardiotoxicity, the majority of experimental setups usually use Complex II-linked substrates in the presence of rotenone. However, not only DOX suffers a redox cycle on Complex I as this multi-component enzyme has also received great attention in mPTP modulation. Therefore, the present chapter tests the hypothesis that an increased loss in calcium loading capacity is observed when mPTP is evaluated through Complex I energization. Results showed increase sensitivity to mPTP solely for cardiac mitochondria from the sub-chronic protocol although no increased effect was detected when Complex I substrates were used. Likewise, cardiac mitochondria from DOX-treated rats produced less H_2O_2 when respiring with Complex II-linked substrates. Contrarily, cardiac and hepatic mitochondria from acutely treated animals showed increased H_2O_2 levels when the MRC was inhibited, regardless of the substrate used. Intringuingly, increased mPTP sensitivity was not followed by alterations on mRNA or protein content levels of classical participants of mPTP. In conclusion, data confirms that mitochondrial calcium dysfunction is an early marker of DOX toxicity.

6.1 Introduction

Mitochondrial dysfunction often observed during DOX treatment includes an enhanced sensitivity to mPTP opening, as explained previously in more detail in section 2.4.2. As it was already introduced in section 1.3.4, the mPTP is characterized by a sudden increase in (inner) membrane permeability which is often associated with increased $[Ca^{2+}]_m$ accumulation and stimulated ROS production. The end-point of this event is a collapse of ion and metabolite potentials followed by water influx into the matrix, which depending on extent of the event may lead to rupture of the OMM.

The number of reports describing decreased calcium-loading capacity in DOX-treated rats, both in acute and sub-chronic protocols, is vast [77, 174, 177–179]. Nevertheless, and despite some work demonstrating a specific effect on mitochondrial Complex I activity [185], no references are available discussing mitochondrial calcium loading capacity when mitochondria are energized with more physiologic Complex I-linked substrates. Moreover, although it was already demonstrated that cardiac mitochondria, as opposed to liver mitochondria, from DOX-treated rats suffer from enhanced permeability transition [185] little or nothing is known about differential mPTP induction with both substrates in the three organs being evaluated in the present thesis.

Due to this lack of information in the literature, the present chapter aims to investigate the sensitivity to mPTP opening in saline and DOX-treated animals after two different protocols (acute *vs* sub-chronic) in three distinct organs (heart, liver and kidney). One expects to observe increased susceptibility to mPTP in both protocols for cardiac mitochondria while no changes are anticipated in the other tissues to be analyzed, regardless of treatment protocol.

Additionally, the current chapter will also investigate the extent of mPTP when *in vitro* mitochondrial respiration is sustained with Complex I-linked substrates. Due to pro-oxidant effect of DOX on mitochondrial Complex I, we hypothesize to find an even larger decrease of calcium loading capacity when Complex I is the site of entry on the oxidative system, in comparison with what is observed with Complex II-linked substrates. Moreover, the author hypothesizes that this will be a cardio-specific effect.

Also, possible regulators of mPTP opening will be evaluated: ROS, a classic mPTP opener [313] will be measured as H_2O_2 production by the MRC. Additionally, expression and content of certain proteins which have been involved in mPTP will also be measured.

6.2 Results

6.2.1 Mitochondrial hydrogen peroxide production

ROS have long been recognized as one of the strongest physiological sensitizers of the mPTP, in such a way that even without alterations in $[Ca^{2+}]_m$ the threshold for pore opening is lowered to concentrations close to resting condition[70, 82]. It is believed that redox modulation of the phosphate carrier is associated with two distinct ANT cysteine residues or, alternatively, in the phosphate carrier [70, 175]. Previously, DOX treatment induced an increase in mitochondrial oxidized thiol groups [174, 184, 188] which possibly explains the increased sensitivity of these mitochondria to undergo the mPTP.

In Table 6.1, H_2O_2 production profile of three different mitochondrial fractions is presented. No differences were observed between treatment groups in any of the analyzed tissues regarding *basal* values of H_2O_2 production, which were measured in the absence of external-added respiratory substrate and/or inhibitors. Due to the absence of alterations in the basal condition, the following states were analyzed as fold-change relative to basal values for ease of comprehension and allow better inter-tissues comparison.

Inter-tissue comparison

As predicted from the classic bioenergetics, the addition of respiratory substrates to mitochondrial suspension increases the production of H_2O_2. However, while that increase in cardiac mitochondria was about 3 to 8 -fold, the change in liver or kidney mitochondria was only 1 to 3 -fold (Table 6.1). The incubation of Complex I inhibitor rotenone with mitochondria respiring with Complex I linked substrates induced an increase in H_2O_2 levels, although occasionally the effect was not so evident (see lack of statistical significance in 'Rot' condition in Table 6.1). Similarly to the *substrate-only* condition, the H_2O_2 production in the presence of rotenone in heart mitochondria was 3 to 6 times higher in comparison to the hepatic or renal mitochondria.

When mitochondria were incubated with antimycin A instead of rotenone, the effect of stimulated H_2O_2 production was more visible. Moreover, heart mitochondria showed an extensive production relatively to the other two mitochondrial preparations. Nevertheless, as previously mentioned in 'Rot' condition, in certain occasions

Table 6.1: H_2O_2 production profile through the MRC in different tissues.

Model	Treat.	Incubation	Heart				Liver				Kidney			
			GM		SUC		GM		SUC		GM		SUC	
			Mean	SE	Mean	SE	Mean	SE	Mean	SE	Mean	SE	Mean	SE
			nmol (H_2O_2)/mg (protein)/15 min											
Acute	Saline	Basal	1583	288	1583	288	589	155	589	155	1389	372	1389	372
			relative fold-change to basal values											
		Subst	4.28	0.81	3.10	0.51	1.28	0.42	1.24	0.28	1.98	0.54	1.87	0.58
		Rot	9.51^{***}	1.92	3.92	0.65	2.42	0.74	1.61	0.17	2.40	0.60	1.96	0.44
		AA	19.80^{***}	3.90	14.10^{**}	2.70	3.62	1.11	2.70	0.87	3.74	0.76	3.65^{*}	0.71
		Rot + AA	10.90	2.20	17.40	4.20	4.08^{*}	0.64	3.05	0.78	4.40^{*}	0.80	3.88	0.79
			nmol (H_2O_2)/mg (protein)/15 min											
	DOX	Basal	1948	610	1948	610	453	117	453	117	1985	690	1985	690
			relative fold-change to basal values											
		Subst	3.25	0.86	7.28	1.76	1.32	0.30	1.54	0.29	1.08	0.22	1.74	0.43
		Rot	7.21	2.19	4.93	1.08	3.27^{*}	0.67	1.12	0.15	2.02	0.22	1.57	0.36
		AA	18.20^{**}	6.60	14.20^{***}	4.40	5.13	1.26	2.73	0.88	2.96	0.84	2.47	0.72
		Rot + AA	9.00	2.90	14.20	4.00	6.40^{*}	1.46	3.10	0.84	3.39	0.79	2.52	0.59
			nmol (H_2O_2)/mg (protein)/15 min											
Sub-chronic	Saline	Basal	484	54	484	54	559	77	559	77	787	89	787	89
			relative fold-change to basal values											
		Subst	5.53	1.15	8.45	1.18	1.24	0.10	1.85	0.43	2.93	0.22	n.a.	n.a.
		Rot	17.00^{**}	4.66	8.45	0.63	1.96^{*}	0.23	1.39	0.15	3.80	0.26	3.03	0.31
		AA	59.90^{***}	15.30	50.70^{**}	9.00	3.02^{**}	0.41	2.84^{**}	0.37	7.80^{**}	0.59	n.a.	n.a.

continues on next page

Table 6.1 – Continued

Model	Treat.	Incubation	Heart				Liver				Kidney			
			GM		SUC		GM		SUC		GM		SUC	
			Mean	SE	Mean	SE	Mean	SE	Mean	SE	Mean	SE	Mean	SE
		Rot + AA	25.60	5.65	56.80	29.90	3.78***	0.37	3.08	0.46	7.10***	0.75	9.23	1.38
			nmol (H_2O_2)/mg (protein)/15 min											
	DOX	Basal	424	78	424	78	522	103	522	103	923	60	923	60
			relative fold-change to basal values											
		Subst	5.09	0.97	5.41	0.83	1.66	0.14	1.92	0.50	2.69	0.21		
		Rot	13.80	25.30	6.76	0.60	2.44*	0.20	1.51	0.12	3.55	0.36	2.52	0.29
		AA	51.40***	8.67	44.00**	7.80	3.47**	0.33	3.06***	0.28	6.83***	0.84	n.a.	n.a.
		Rot + AA	21.60	2.00	50.40	11.10	4.74***	0.46	3.04	0.36	6.77***	0.71	7.37	1.06

H_2O_2 levels were measured through Barja's method (see sec. 4.15, p. 95) after 15 min reaction. Differences between incubation conditions for each treatment groups and respiratory substrates were evaluated by a within-subjects ANOVA followed by pair-wise comparisons through Bonferroni post-hoc analysis (see sec. 4.19, p. 110):
Subst *vs* Rot; Rot *vs* AA;Rot *vs* Rot+AA, in glutamate/malate-sustained respiration.
Subst *vs* Rot; Rot *vs* AA;AA *vs* Rot+AA, in succinate-sustained respiration.
*, $p \geq 0.05$; **, $p \geq 0.01$ and ***, $p \geq 0.001$.
Abbreviations: *GM* - glutamate/malate; *SUC* - succinate; *Rot* - rotenone; *AA* - antimycin A; *SE* - standard error; *n.a.* - not available.

the increase in H_2O_2 levels in the presence of antimycin A was not so noticeable (see lack of statistical significance in 'AA' condition in Table 6.1).

When both inhibitors, rotenone plus antimycin A, were incubated simultaneously in heart mitochondria with Complex I sustained respiration, H_2O_2 levels were not dissimilar to those when rotenone was incubated alone. However, this behavior was not observed in hepatic and renal mitochondrial preparations. In fact, in these preparations the maximum of H_2O_2 production was only achieved in the presence of both inhibitors, with H_2O_2 levels between 'Rot' and 'Rot+AA' being clearly detected, except in kidney mitochondria from DOX-treated animals (Table 6.1).

Regarding Complex II sustained respiration there was no difference detected between the *substrate-only* condition and that in the presence of rotenone in any mitochondrial preparation, suggesting that RET was not present under this experimental setup (Table 6.1). Contrarily, incubation with Complex III inhibitor antimycin A produced a massive H_2O_2 production in all types of mitochondria. Nevertheless, it is important to note that the maximum levels of production were not dissimilar regardless of the respiratory substrate used and were always higher in cardiac mitochondria. The levels of H_2O_2 production in the presence of rotenone plus antimycin A in mitochondria respiring with Complex II linked substrates were similar to those of antimycin A alone. In fact, a small yet not statistically significant increase between both states was observed (Table 6.1).

It should also be noticed that although the previous mentioned trends were always present, the statistical test applied was not always able to detected those differences and, therefore, some mitochondrial preparations appear to have an H_2O_2 production which is insensitive to classical OXPHOS inhibitors, namely, hepatic mitochondria from both treatment groups in the acute protocol with Complex II linked substrates; and, renal mitochondria from DOX-treated animals in the acute protocol for both respiratory substrates (Table 6.1).

Treatment-dependent effects

A comparison of the previous mentioned states/conditions with respect to DOX treatment can be found in Fig. 6.1. Regarding the acute protocol and Complex I sustained respiration, the H_2O_2 production in all conditions were similar to control values for heart and kidney mitochondria. However, in hepatic mitochondria the H_2O_2 pro-

duction in the presence of rotenone was higher in mitochondria from DOX-treated animals (11±3 %) although no differences were observed in the presence of substrate alone (1±14 %) or in the presence of antimycin A (18±10 %) or antimycin A plus rotenone (1±2 %).

However, when respiration was sustained with Complex II-linked substrates, cardiac mitochondria from DOX-treated animals of the acute protocol showed increased production of H_2O_2 in the presence of the substrate, yet it was not statistically significant (164±72 %, p= 0.06; Fig. 6.1). Still, this alteration was solely in the absence of respiratory inhibitors as other conditions were not dissimilar from controls.

With respect to liver mitochondria, the DOX-treated group showed only increased H_2O_2 levels when ROS generated by MRC was stimulated to its maximum production, i.e. in the presence of antimycin A plus rotenone (31±16 %). Notice the fact that the same mitochondrial population appear to produce less H_2O_2 in the presence of rotenone alone (5±2 %, p= 0.08) with other conditions being close to control values. Still in the acute model and Complex II-sustained respiration, renal mitochondria from DOX-treated animals did not show significant alterations in the levels of H_2O_2 production in the measured conditions.

Regarding the sub-chronic model, mitochondria respiring with Complex I-linked substrates showed H_2O_2 production levels similar to control for all mitochondrial preparations and conditions measured (Fig. 6.1). A similar situation was observed in Complex II sustained respiration where liver and kidney mitochondria H_2O_2 levels were not dissimilar to control group.

However, cardiac mitochondria from DOX sub-chronically treated animals showed a consistent decrease in H_2O_2 production in all measured conditions when respiration was sustained with Complex II-linked substrates (37±10 %, 19±4 %, 11±4 % and 8±3 % p= 0.056, for 'Subst', 'Rot', 'AA' and 'Rot+AA', respectively; Fig. 6.1).

6.2.2 Mitochondrial calcium loading capacity

To assess mitochondrial calcium handling and the sensitivity of each preparation to the mPTP, isolated mitochondrial fractions were incubated in a sucrose-rich medium in the presence of the calcium-sensitive fluorescent probe Ca5GN.

Cardiac mitochondria from acute-treated animals showed no alteration neither in

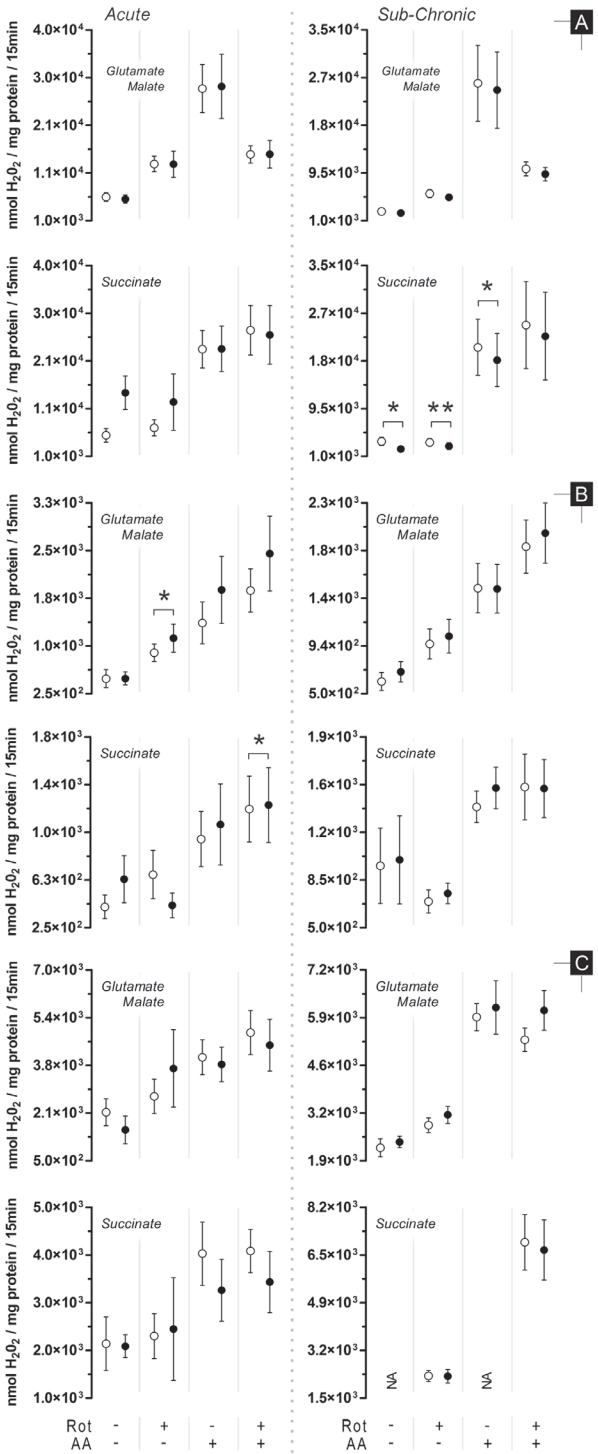

Figure 6.1: Effects of DOX treatment on mitochondrial H_2O_2 production. After 15 min, end-point H_2O_2 levels were measured fluorimetrically through reaction with homovalinic acid (for details, see 4.15, p. 95). **A** - heart; **B** - liver; **C** - kidney. Circles represent means of treatment groups (saline in **white** circles; DOX in **black** circles) with SE (error bars are smaller than symbols when not visible). Differences between treatment groups means within the same model were evaluated by matched pairs Student's t test to exclude the variability related to mitochondrial isolation but when assumptions were rejected the non-parametric Wilcoxon matched pairs test was applied (see 4.19, p. 110). *, $p \geq 0.05$ and **, $p \geq 0.01$ *vs* saline group of the same model. $n = 8$, 7 and 6 (acute model - heart, liver and kidney, respectively) or $n = 6$ (sub-chronic model, all tissues). *Rot* - rotenone; *AA* - antimycin A; *NA* - not available.

retention time or calcium release rate, regardless of the respiratory substrate used. Similarly, both parameters remained unchanged in kidney mitochondria (Fig. 6.2).

However, hepatic mitochondria from acute-treated animals appear less sensitive to mPTP opening as the mitochondrial preparation retained calcium to a greater extent (43±30 % and 36±19 % for glutamate/malate and succinate, respectively) and released it more slowly (49±19 % and 18±27 % for glutamate/malate and succinate, respectively), at least when Complex I-linked substrates were used. Still, significance was not always achieved due to the high variability in response to the treatment (Fig. 6.2). Nevertheless, the trend is observable when mitochondrial respiration was sustained with either of the two respiratory substrates used.

Regarding the sub-chronic protocol (Fig. 6.2), cardiac mitochondria were less capable of accumulating calcium comparing to liver and kidney mitochondria. In fact, when heart mitochondria were incubated with Complex I-linked substrates a decrease of 29±9 % in retention time was observed although the release rate remained constant. If Complex II-linked substrates were used instead, similar reduction in retention time was attained (38±10 %) with concomitant increase in calcium release rate by 18±8 %. For the remaining mitochondrial preparations, both parameters were not altered regardless of the respiratory substrate used (Fig. 6.2).

Confirming that all previous mentioned alterations were related to the mPTP opening is the fact that pre-incubation with CsA, the classic pore inhibitor [314] abolished all the effects (Table 6.2).

Additionally, the same mitochondrial preparations were assessed for calcium-induced mitochondrial swelling in similar conditions to those mentioned above. Corroborating the previous results, cardiac mitochondrial swelling amplitude and swelling rate were not altered after acute treatment with DOX, regardless of the respiratory substrate used (Fig. 6.3). Likewise, in kidney mitochondria, amplitude values and swelling rate were not different from control.

However, liver mitochondria from acutely treated animals appear to had a slower swelling rate (6±12 % and 21±37 % for glutamate/malate and succinate, respectively; Fig. 6.3) despite no apparent change in swelling amplitude (20±30 % and 11±31 % for glutamate/malate and succinate, respectively). As in calcium movements measurements, a high variability in response to the treatment was observed in liver mitochondria.

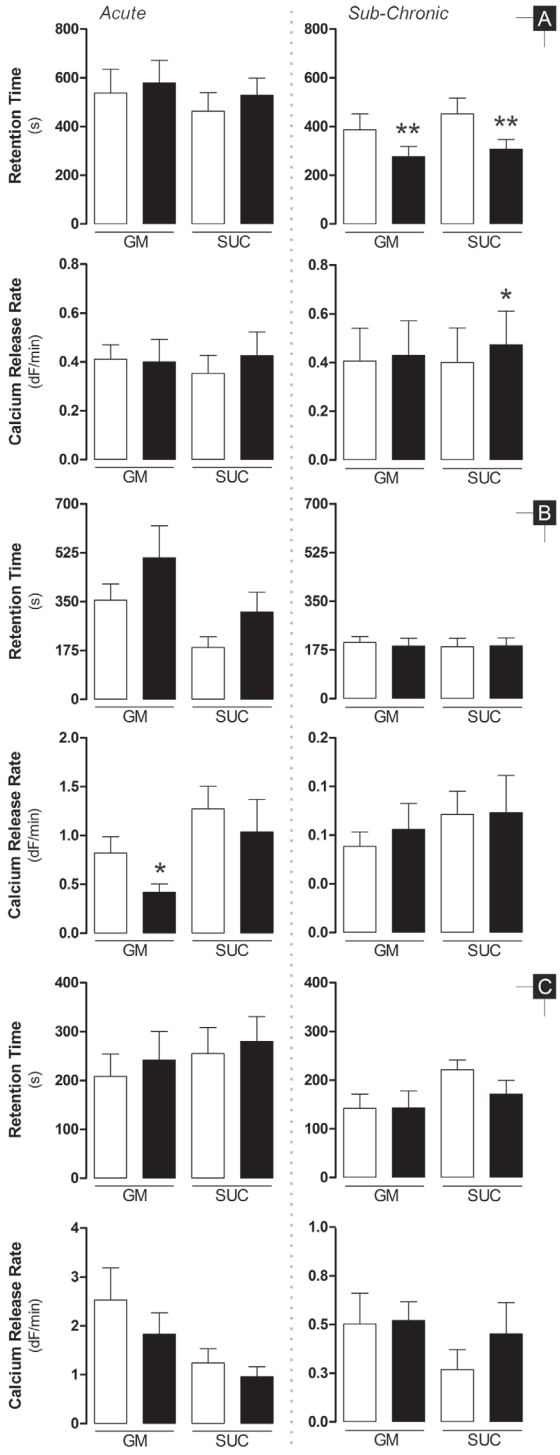

Figure 6.2: Effects of DOX treatment on mitochondrial calcium loading capacity. Ca^{2+} movements were evaluated using the extra-mitochondrial fluorescent probe Ca5GN after addition of a single pulse of Ca^{2+} (for details, see 4.13, p. 93). The retention time is defined by the time interval between the influx and efflux of Ca^{2+} whose fluorescence value equals the peak half-height fluorescence upon addition of calcium (larger values mean less sensitivity to mPTP). **A** - heart; **B** - liver; **C** - kidney. Bars represent means of treatment groups (saline in **white** bars; DOX in **black** bars) with SE. Differences between treatment groups means within the same model were evaluated by matched pairs Student's t test to exclude the variability related to mitochondrial isolation (see 4.19, p. 110). *, $p \leq 0.05$; **, $p \leq 0.01$ *vs* saline group of the same model. n = 10, 9 and 10 (acute model - heart, liver and kidney, respectively) or n =11, 11 and 10 (sub-chronic model - heart, liver and kidney, respectively). *GM* - glutamate/malate; *SUC* - succinate.

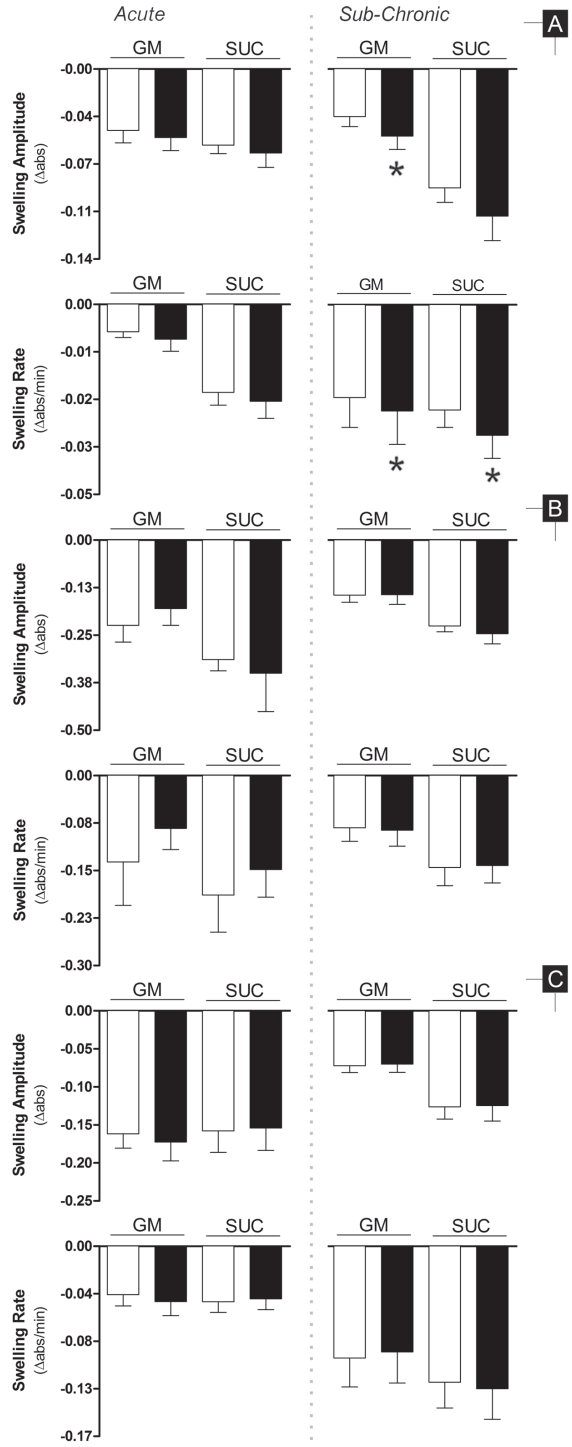

Figure 6.3: Effects of DOX treatment on calcium-induced mitochondrial swelling. Mitochondrial swelling was evaluated by following the decrease in apparent absorbance of the mitochondrial suspension at 540 nm after addition of a single pulse of Ca^{2+} (for details, see 4.14, p. 94). The swelling amplitude presented in the graphs is defined as the difference in absorbance between the point which corresponds to half of the maximum swelling amplitude of the control record and the maximum absorbance upon calcium addition (larger values mean greater sensitivity to mPTP). **A** - heart; **B** - liver; **C** - kidney. Bars represent means of treatment groups (saline in **white** bars; DOX in **black** bars) with SE. Differences between treatment groups means within the same model were evaluated by matched pairs Student's t test to exclude the variability related to mitochondrial isolation but when assumptions were rejected the non-parametric Wilcoxon matched pairs test was applied (see 4.19, p. 110). *, $p \leq 0.05$ *vs* saline group of the same model. $n = 10$, 9 and 10 (acute model - heart, liver and kidney, respectively) or n =10, 11 and 11 (sub-chronic model - heart, liver and kidney, respectively). *GM* - glutamate/malate; *SUC* - succinate.

Table 6.2: Effect of CsA on mitochondrial calcium release rate.

Substrate	Treat.	Heart		Liver		Kidney	
		Diff. Means	Pooled *SE*	Diff. Means	Pooled *SE*	Diff. Means	Pooled *SE*
		% of inhibition					
Acute		$n_{CsA} = 4$		$n_{CsA} = 6$		$n_{CsA} = 5$	
Glutamate	Saline	85.9^{**}	25.0	107.0^{***}	21.0	98.8^{***}	17.0
Malate	DOX	96.4^{**}	24.6	101.0^{***}	22.0	96.0^{**}	24.4
Succinate	Saline	92.2^{*}	37.2	72.6^{***}	11.7	101.4^{**}	23.7
	DOX	97.0^{*}	39.6	100.0^{*}	32.0	98.5^{**}	21.9
Sub-chronic		$n_{CsA} = 5$		$n_{CsA} = 7$		$n_{CsA} = 6$	
Glutamate	Saline	97.4^{*}	50.4	118.0^{***}	17.7	99.7^{*}	35.4
Malate	DOX	89.3^{**}	49.9	119.2^{***}	32.6	97.1^{*}	20.2
Succinate	Saline	104.4^{**}	53.3	104.0^{***}	20.3	110.4^{***}	50.4
	DOX	102.2^{**}	29.6	96.6^{*}	32.8	106.0^{***}	35.0

Tabulated values represent the difference between means of groups in the absence of CsA and groups with CsA, e.g. *saline-glutamate/malate vs saline-glutamate/malate+ CsA*, and are expressed as relative percentage to the group without CsA. *, $p \geq 0.05$; **, $p \geq 0.01$ and ***, $p \geq 0.001$ *vs* group with CsA, as evaluated by an unpaired Student's t test. Alternatively, a Welch correction or the non-parametric Mann-Whitney test were applied when assumptions of t test were not achieved (see 4.19, p. 110).
Abbreviations: *Treat.* - treatment; *Diff. Means* - difference between group means; *Pooled SE* - pooled standard error; n_{CsA} - replicates number in CsA group (for the other group see Fig. 6.2 details).

Regarding the sub-chronic protocol with respect to the calcium-induced mitochondrial swelling, the heart was the tissue where more alterations were found (Fig. 6.3). Swelling amplitude was increase by 41±20 % in glutamate/malate-sustained respiration and by 10±4 % in succinate-sustained respiration although the latter was not significant ($p = 0.057$). The concomitant increase in swelling rate was also observed, 8±3 % for glutamate/malate and 24±10 % for succinate, as respiratory substrates. The remaining mitochondrial preparations, liver and kidney, did not show alterations in any of the two measured parameters regardless of the respiratory substrate used (Fig. 6.3).

Once more, incorporation of CsA in the experimental conditions was able to abolish the previous mentioned alterations, thus demonstrating that effects were related to the mPTP opening (Table 6.3).

Considering that the altered susceptibility of cardiac mitochondria from sub-chronical-

Table 6.3: Effect of CsA on calcium-induced mitochondrial swelling rate.

Substrate	Treat.	Heart		Liver		Kidney	
		Diff. Means	Pooled *SE*	Diff. Means	Pooled *SE*	Diff. Means	Pooled *SE*
		% of inhibition					
Acute		$n_{CsA} = 4$		$n_{CsA} = 6$		$n_{CsA} = 5$	
Glutamate	Saline	80.6^{*}	34.8	108.6^{***}	24.8	87.0^{**}	23.6
Malate	DOX	76.6^{**}	33.7	80.9^{**}	22.2	90.7^{**}	25.3
Succinate	Saline	91.6^{***}	14.4	99.0^{***}	38.3	88.0^{**}	18.9
	DOX	93.8^{**}	28.7	98.1^{*}	29.3	87.3^{**}	20.5
Sub-chronic		$n_{CsA} = 5$		$n_{CsA} = 7$		$n_{CsA} = 6$	
Glutamate	Saline	81.8^{*}	32.2	88.6^{**}	39.3	89.6^{**}	35.7
Malate	DOX	87.9^{**}	45.6	95.5^{**}	51.2	89.7^{*}	40.6
Succinate	Saline	76.8^{**}	17.5	85.9^{**}	22.7	84.0^{**}	26.1
	DOX	75.9^{**}	18.6	95.8^{***}	19.4	81.9^{**}	21.7

Tabulated values represent the difference between means of groups absent of CsA and groups with CsA, e.g. *saline-glutamate/malate vs saline-glutamate/malate+ CsA*, and are expressed as relative percentage to the group without CsA. *, $p \geq 0.05$; **, $p \geq 0.01$ and ***, $p \geq 0.001$ *vs* group with CsA, as evaluated by an unpaired Student's t test. Alternatively, a Welch correction or the non-parametric Mann-Whitney test were applied when assumptions of t test were not achieved (see 4.19, p. 110).
Abbreviations: *Treat.* - treatment; *Diff. Means* - difference between group means; *Pooled SE* - pooled standard error; n_{CsA} - replicates number in CsA group (for the other group see Fig. 6.3 details).

ly treated animals to undergo swelling could be related to pre-swollen mitochondria in the initial preparation, an aliquot was collected and processed for EM analysis. However, Fig. 6.4 clearly shows that heart mitochondria from DOX-treated animals do not differ significantly from the control group. Mitochondrial body size, matrix volume, cristae number and membrane integrity appear similar to control, excluding the idea of pre-swollen or damaged mitochondria.

6.2.3 Expression and content of mPTP related proteins

After extraction of total mRNA from each tissue the transcript levels of some proteins which are considered important in modulation and/or structure of mPTP were analyzed.

First, by analyzing the basal levels of each transcript with respect to tissue one can

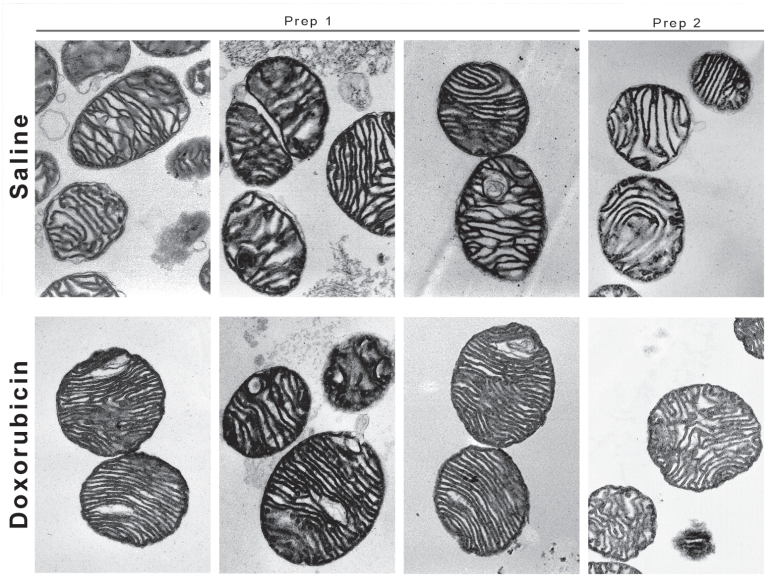

Figure 6.4: Ultrastructure of isolated cardiac mitochondrial fractions from the sub-chronically treated animals. After mitochondrial isolation an aliquot was collected and processed for EM analysis. Each sub-panel represent different thin slices of the same preparation and two independent mitochondrial preparations (**Prep 1** and **Prep 2**) were analyzed. A magnification of 10 000× was used in all panels.

observe that CyP-D levels are of the same order of magnitude in all three whereas ANT is by far more abundant in heart (Fig. 6.5). Moreover, the levels of ANT isoform 1 in cardiac tissue is one order of magnitude higher than its isoform 2 counterpart. However, the opposite occurs in the liver with ANT2 levels being higher than ANT1 while in kidney both isoforms are of the same order of magnitude (Fig. 6.5). Nevertheless, VDAC is found in equal amounts in heart and kidney with both tissues

Figure 6.5 ***(following page)*:** Effects of DOX treatment on transcript levels of proteins related to modulation of mPTP opening. Total mRNA was extracted from each tissue and transcript levels were analyzed through two-step real-time qPCR (see sec. 4.18, p. 105) with the transcript copy number being thereafter normalized to 18S copy number. **A** - heart; **B** - liver; **C** - kidney. Bars represent means of treatment groups (saline in **white** bars; DOX in **black** bars) with SE. Differences between treatment groups means within the same model were evaluated by matched pairs Student's t test but when assumptions were rejected the non-parametric Wilcoxon matched pairs test was applied (see 4.19, p. 110). *, $p \geq 0.05$; **, $p \geq 0.01$ and ***, $p \geq 0.001$ *vs* saline group of the same model. $n = 6$ for acute model (all tissues) or $n = 8$ for sub-chronic mode (all tissues).

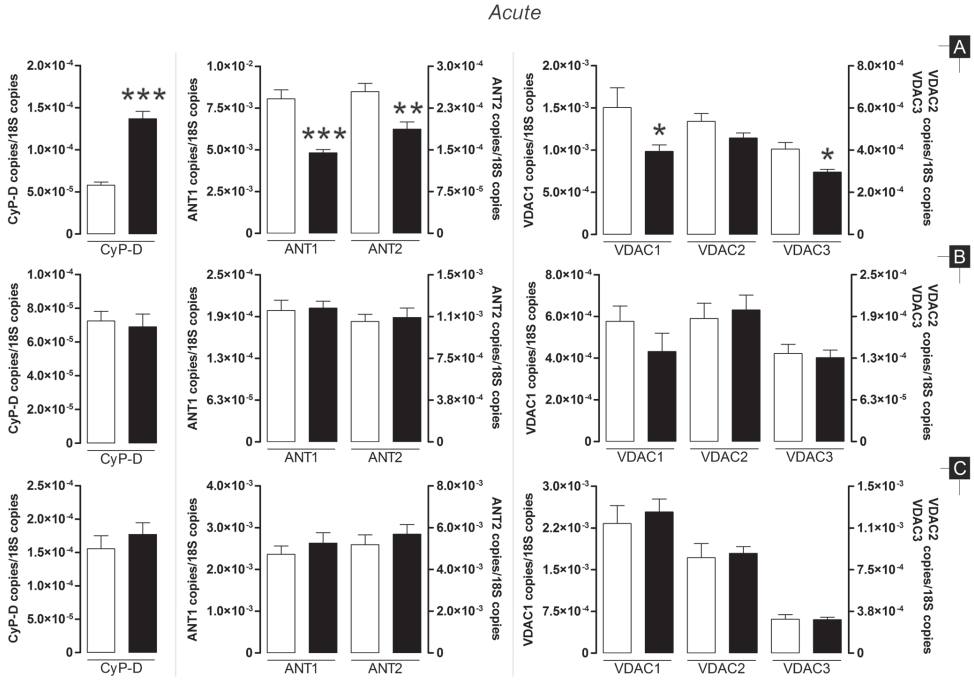
Acute
A
B
C
CyP-D copies/18S copies
ANT1 copies/18S copies
ANT2 copies/18S copies
VDAC1 copies/18S copies
VDAC2 copies/18S copies
VDAC3 copies/18S copies
CyP-D
ANT1
ANT2
VDAC1
VDAC2
VDAC3
***
**
*

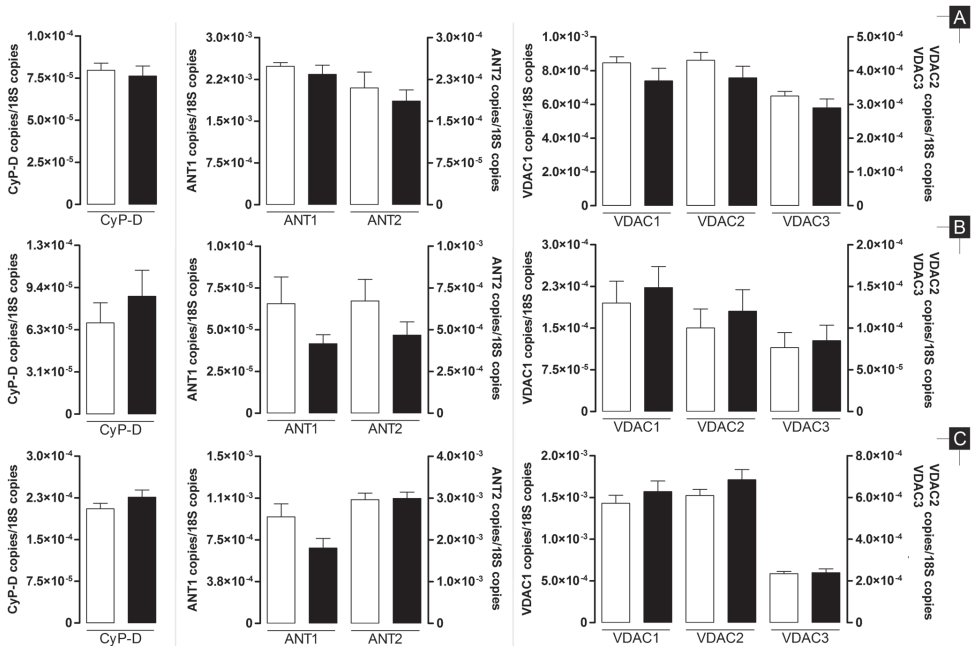
Sub-Chronic
A
B
C
CyP-D copies/18S copies
ANT1 copies/18S copies
ANT2 copies/18S copies
VDAC1 copies/18S copies
VDAC2 copies/18S copies
VDAC3 copies/18S copies
CyP-D
ANT1
ANT2
VDAC1
VDAC2
VDAC3

having at least one order of magnitude higher levels than liver. In terms of VDAC isoforms, VDAC1 is constitutively more expressed in all tissues followed by VDAC2 and VDAC3.

Regarding the effect of DOX treatment, CyP-D levels were dramatically increased (136±15 %) in cardiac mitochondria after acute treatment with DOX (Fig. 6.5). However, liver and kidney did not show alterations in this transcript. Similarly, both ANT isoforms were decreased in heart tissue (40±6 % and 26±6 % for ANT1 and ANT2, respectively) but not altered in liver or kidney. The acute treatment also caused a decrease in all VDAC isoforms but once more only in cardiac tissue (35±12 %, 15±7 % p= 0.08 and 27±10 % for VDAC1, VDAC2 and VDAC3, respectively; Fig. 6.5).

Interestingly, no alteration in mRNA levels of any of transcripts measured were found in any tissue after a sub-chronic treatment with DOX (Fig. 6.5). For example, variation on CyP-D (4±8 %), ANT1 (6±6 %) and VDAC1 (12±9 %) levels were negligible in heart tissue.

The next step was to verify if alterations in transcript levels were also translated into alterations in protein levels (acute) or despite mRNA levels remain unaltered there were still variations in protein content (sub-chronic). However, no alterations in protein levels were observed regardless of the treatment protocol used or analyzed tissue, as summarized in Table 6.4. A short explanatory note regarding the absence of values for the ANT in cardiac tissue of sub-chronic model relates to the fact that it was not possible to obtain a good immunolabeling signal for quantification in these samples despite author's efforts. Nevertheless, a representative image is presented in Fig. 6.6.

6.3 Discussion

DOX was shown to be capable of inducing mPTP opening when added to an isolated cardiac mitochondrial suspension [79] but more important was the demonstration that DOX-treated animals showed increased sensitivity to mPTP which persisted after treatment cessation [77, 303].

The gold standard procedure for evaluation of mPTP on isolated mitochondria is by means of sustaining mitochondrial respiration through Complex II-linked substrates in combination of Complex I inhibitor rotenone. Although there is not an apparent

Table 6.4: Effects of DOX treatment on content level of mPTP-related proteins.

	CyP-D (A.U.)						**VDAC** (A.U.)						**ANT** (A.U.)					
Treatment	Heart		Liver		Kidney		Heart		Liver		Kidney		Heart		Liver		Kidney	
	Mean	*SE*	Mean	*SE*	Mean	*SE*	Mean	*SE*	Mean	*SE*	Mean	*SE*	Mean	*SE*	Mean	*SE*	Mean	*SE*
Acute	$n = 6$		$n = 6$		$n = 6$		$n = 6$		$n = 6$		$n = 6$		$n = 6$		$n = 6$		$n = 6$	
Saline	1.00	0.03	1.00	0.07	1.06	0.04	0.96	0.02	1.00	0.10	0.95	0.11	1.02	0.05	0.97	0.08	1.02	0.05
DOX	1.01	0.02	1.01	0.04	0.95	0.05	1.04	0.05	0.99	0.08	1.04	0.08	0.97	0.08	1.04	0.04	0.99	0.05
Sub-chronic	$n = 8$		$n = 8$		$n = 8$		$n = 8$		$n = 8$		$n = 8$		$n = 8$		$n = 8$		$n = 8$	
Saline	0.94	0.03	0.92	0.10	0.99	0.08	1.05	0.30	0.92	0.14	1.08	0.17	n.a.	n.a.	1.07	0.11	1.05	0.16
DOX	0.98	0.06	1.13	0.15	1.02	0.07	0.95	0.14	1.30	0.32	1.26	0.45	n.a.	n.a.	1.04	0.07	0.98	0.07

Data are presented as arbitrary units and represent densitometry analysis of western blot membranes after image acquisition.; *n.a.* - not available. For details on data processing see sec. 4.17.3, page 103. Differences between treatment group means within the same model were evaluated by matched pairs Student's t test (see 4.19, p. 110).
Abbreviations: *A.U.* - arbitrary units of densitometry; *SE* - standard error.

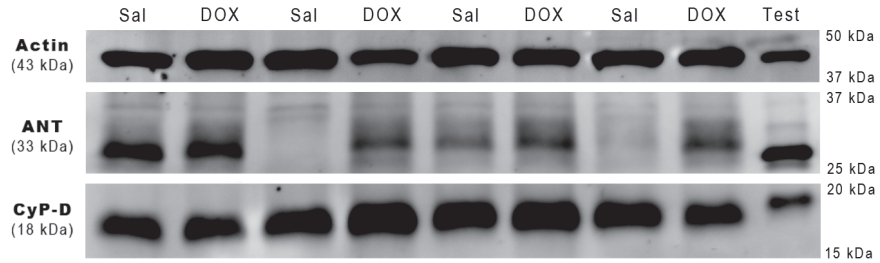

Figure 6.6: Representative image of immunoblot detection on cardiac sub-chronic samples. Reactivity agains actin and CyP-D are presented to show to the reader that not all targets fail to react and provide good signal for densitometry quantification, as in the case of ANT. In such cases, despite different loading quantities, antibody dilution as well as incubation times and running buffer composition tested in an attempt to achieve better results, no positive effect was attained. *'Test'* sample represent a total extract collected from an heart of a normal Wistar rat (same age and gender) distinct from those of the experimental design, but which was processed identically as all other protein samples. The author used this sample to test antibodies and thus consider it as a *positive control*. At the right, molecular weight of the standards are shown. For details in sample preparation and western blot procedure see sec. 4.9.1,pag. 4.9.1 and sec. 4.17 pag. 4.17, respectively. Abbreviations: *Sal* - saline; *DOX* - doxorubicin.

explanation for that, the fact that succinate oxidation in the presence of rotenone maintain constant the pool of matrix pyridine nucleotide may explain such procedure [315]. Additionally, if isolation is not done carefully there might be partial destruction of the multimeric enzyme as well as inhibition of its activity.

Nevertheless, attempts for measuring mPTP with mitochondrial respiration with Complex I-linked substrates were already made [316] and showed that under this condition, mitochondria are less capable of handling Ca^{2+} or in other words a lower amount of Ca^{2+} is needed to trigger mPTP. Moreover, great importance has been given to Complex I and its role in the modulation of mPTP. For instances, ρ^0 cells[1] do not present a typical calcium-induced mPTP response [73] and of the five OXPHOS respiratory complexes, Complex I was apparently the most important to this phenotype. Additionally, Complex I may regulate the opening probability of mPTP by controlling electron flux through the MRC which suggest that CoQ may modulate mPTP negatively [315, 316].

Taking all the above mentioned information into account and knowing that DOX suffers not only a redox cycle at Complex I but it is also capable of inhibiting this

[1] cells lacking mt-DNA and therefore without a functional MRC

respiratory complex, one possibility is that differences between cardiac mitochondria from saline and DOX-treated rats may be exacerbated when Complex I substrates are used as site of entry on the OXPHOS. Supporting this idea is the fact that cell lines containing mutations at Complex I level and enhanced oxidant environment were sensitized against mPTP [73]. To the author's knowledge, there is no report in the literature with respect of DOX effects on mPTP through Complex I modulation.

Regarding the higher sensitivity to mPTP during energization by using Complex I as previously reported [316], the experimental setup here presented was not able to detect any difference in mPTP sensitivity between Complex I- or Complex II-linked substrates (Fig 6.2 and 6.3). Although we used one single and equivalent amount of calcium with both substrates instead of successive small calcium pulses the measured parameters were very similar when using Complex I or II substrates with minor differences in the record traces, for any mitochondrial preparations used. However, Fontaine *et al.* [316] described that although the effect is ubiquitously present in different tissues the experimental conditions, namely the phosphate content and Mg^{2+} concentration, might induce differences between MPT with distinct substrates. In fact, mPTP modulation by electron flux, at least in the liver, was distinct if phosphate concentration differed by almost an order of magnitude being apparently less pronounced when the phosphate concentration was low. In our experimental setup, the phosphate concentrations chosen were the same as those previously used in our laboratory to investigate mPTP opening *in vitro* by different drugs, including DOX, which had always attained acceptable results [172, 174, 177, 187]. Nevertheless, this concentrations are considerably lower than the ones used in the mentioned report [316], in any mitochondrial preparation, which could explain our difficulty in detecting mPTP modulation by electron flux. Additionally, with the recent ongoing discussion regarding the phosphate carrier and/or phosphate-induced mPTP inhibition [76, 93–96] extra caution should be taken regarding the role of phosphate on MPTP induction.

Similarly, the initial hypothesis of enhanced sensitivity to mPTP of DOX treated animals when evaluated through Complex I-linked substrates was not confirmed in any mitochondrial preparations. However, it remains to be clarified whether the absence of effect is due to the fact that the initial postulate [316] was not confirmed in this experimental setup. Nevertheless, a cardiac-specific protocol-dependent effect was detected, as decreased mitochondrial calcium loading capacity was only observed in heart mitochondria but solely after a sub-chronic treatment protocol (Fig 6.2 and

6.3). Likewise, this is also the first work where the effects of DOX modulation on mPTP through Complex I are reported and clearly evidential the importance of this alteration on the development of DOX-induced cardiotoxicity but now with experimental support for physiological-like substrates. Moreover, data is in agreement with mitochondrial bioenergetics parameters (see Chapter 5) where effects were only detected in the sub-chronic protocol. This further strengths the idea of normal organ physiology but impaired mitochondrial function.

We concluded in the previous chapter that mitochondrial impairment became noticeable when individuals were subjected to stressful protocols by mimicking an *in vitro* condition of higher energy demand through the addition of ADP to isolated mitochondrial fractions. In this case, since cardiac mitochondrial fractions from both control and DOX-treated groups had identical ultra-structure morphology after isolation (Fig. 6.4) and, despite the latter had lower ability to accumulate calcium, one can state that the heart of these individuals may fail to respond upon stressful situations where increased $[Ca^{2+}]_c$ is observed.

Interestingly, hepatic mitochondria from acutely treated animals appear to be more resistant to mPTP events (Fig 6.2 and 6.3), in agreement with the increased mitochondrial bioenergetics fitness evaluated in Chapter 5. Ascensão *et al.* [178] observed a similar trend for hepatic mitochondria in an identical rodent model. The liver tissue is where most DOX is accumulated immediately after drug administration [215] and it is unclear at the moment how such beneficial effect can be attained. Due to the end-point time chosen in this experimental setup, it is also impossible to determine if the effect is transient or if it evolves to an impaired function. Notwithstanding, a term coined *'DOX pre-conditioning'* can be found in the literature [317]. The idea is that pre-administration of the drug triggers a similar cellular response analogous to ischemia pre-condition which protects tissues against future ischemic events. However, the dosages used in those cases are 10 times lower than the ones used in the current work. Nevertheless, one may consider that despite the concentration discrepancy the very early stages may be common in both circumstances. A similar trigger, for example, may be presented as in the case of *pre-conditioning*, where protection is achieved through modulation of certain heat-shock proteins by ROS.

Although in the previous chapter the liver tissue did not show significant levels of oxidative stress, as evaluated through aconitase activity, the levels of maximum H_2O_2 production through the MRC here reported are significantly higher in DOX-treated animals despite basal levels being equivalents in both treatment groups (Fig. 6.1), sug-

gesting that liver mitochondria may modulate ROS production in certain conditions if necessary. The increased ROS production in liver mitochondria from acutely-treated subjects after addition of mitochondrial inhibitors in the reaction medium is due to their higher electron flux through the MRC as seen in the higher oxygen consumption rates of this experimental group (Fig. 5.4, Chapter 5). Once this higher electron flux is blocked, MRC is directed towards a more reduced state which, in the light of Aon *et al.* [101] unifying hypothesis, favors massive ROS production even in the presence of antioxidant defenses. Similarly, the decreased H_2O_2 production by cardiac mitochondria of sub-chronic protocol on respiration sustained by Complex II substrates might be due to lower electron flux through the MRC has seen in state 4 oxygen consumption and $\Delta\psi$ values (Fig. 5.4 and Table 5.4) which reflect a lower Δp and 'less' reduced MRC state upon addition of inhibitors.

The effect of DOX acute treatment on H_2O_2 production in respiration sustained with Complex II substrates without addition of inhibitors, which derives mostly from RET (Fig. 6.1, Panel A), must also be highlighted. In the author's opinion, the effect is more noticeable in cardiac mitochondria, followed by liver mitochondria. RET occurs when electrons enter the MRC through Complex II level at high Δp and are thermodynamically driven towards Complex I instead of Complex III reducing the NAD^+ pool [100]. However, once the pool becomes fully reduced (NADH) Complex I produces massive amounts of ROS although the actual production site, either at the CoQ binding site or at the FMN prosthetic group, remains unclear [100]. ROS derived from RET were not detected in any of the control mitochondrial preparations (Table 6.1) which could be due to lower Δp or high oxidation of NADH/NAD^+ pool. However, Table 5.4 shows high $\Delta\psi$ values similar to control group therefore, the effect is probably related to lower NADH levels due to depletion of endogenous substrates after isolation. Nevertheless, RET is present at least in cardiac mitochondria from acute protocol, which is most likely related to high NADH levels due to inhibition of Complex I activity by DOX [178]. Moreover, addition of antimycin A to this mitochondria respiring solely with endogenous substrates produced higher H_2O_2 levels compared to control (data not shown), an effect also common to hepatic fractions but to a lesser extent. If this event of Complex I inhibition, which as we referred previously contributes to mPTP inhibition, and the concomitant higher NADH pool is the answer for the absence of differences in mPTP sensitivity for cardiac mitochondria of acutely-treated animals is a point which remains to be clarified.

Nonetheless, an important message that should be retained is that mPTP modulation

between treatment groups in the present experimental setup is independent of ROS modulation through the MRC as H_2O_2 levels remain unaltered between both groups. Obviously, there are other modulators of the pore such as matrix alkalinization, lower $\Delta\psi$, high phosphate and low levels of adenine and pyridine nucleotides [70]. However, most of these variables can be minimized experimentally so the effects observed are due only to intrinsic alterations of the mitochondrial preparations. Since in the previous chapter we have shown that mitochondria under resting conditions (state 4 respiration and $\Delta\psi_{max}$) do not differ significantly from control group, one can say that the classical bioenergetic and chemical modulators of the pore have a minor role in this experimental setup.

Previously, Oliveira *et al.* [177] reported a decrease in ANT content in heart tissue after sub-chronic treatment with DOX and used it to justify the increased susceptibility of cardiac mitochondria to mPTP. However, no analysis were made regarding other tissues therefore, the present work has conducted analysis of mRNA and protein content of mPTP related proteins in the three tissues in an attempt to identify differential effects which could be used to explain the different susceptibility to mPTP. It is important to state that, although the role of phosphate carrier in mPTP mechanism has gained increased popularity recently [76, 93–96], the present analysis was restricted to the classical modulators of the pore, VDAC, ANT and CyP-D.

Although it is not surprising that no alterations in the expression of the studied transcripts were observed in the sub-chronic protocol (Fig. 6.5), since at the time of measurement no traces of the drug were present in the animal, it was rather intriguing that the studied protein content was maintained (Table 6.4). A high number of DOX-related effects are often associated with primary effects when the drug is still present in the organism [299, 318]. However, despite the non-altered content of proteins which expression modulate mPTP extent [86, 88] enhanced sensitivity to MPT induction in the hearts of DOX-treated animals may be due to other factors such as oxidative stress. Moreover, the greater sensitivity to mPTP is not related to the experimental setup as the modulation of H_2O_2 production was not dissimilar from controls (Fig. 6.1) and reflected only intrinsic differences due to DOX treatment. In fact, previously reports using the same treatment protocol schedule showed that cardiac tissue from treated animals had higher protein carbonyl content and consequent higher levels of Vitamin E and TBARS. Also, mitochondrial dysfunction in the heart, observed either as depressed oxygen consumption or Ca^{2+} loading capacity, could be restored by addition of the disulfide reducing agent DTT (but not Trolox) [174, 188]. The

fact that ANT possess two cysteine residues which redox status could determinate the extent of mPTP opening clearly shows how intrinsical alterations prior to *in vitro* analysis are responsible for the observed effect. More important, this alterations may be tissue-specific as the other studied tissues do not behave in the same manner.

Another intrinsic alteration could be the content of CoQ in heart. DOX is known to inhibit CoQ synthesis in cardiac tissue [319] and induce alterations in plasma levels [320] and in the heart [321] of DOX-treated patients. Moreover, co-administration of CoQ to patients in chemotherapy has decreased the risk of cardiotoxicity [322]. Similarly, the protective effect of exercise could be attributed to increased synthesis of CoQ. Although the idea behind this protection is usually ascribed to the antioxidant properties of the molecule or its ability to restore Complex I activity [322], it could be also due do direct inhibition of mPTP. Bernardi's group, as well as others, had previously shown that mPTP might possess an inhibitory binding site for ubiquinone [323] which is normally occupied by endogenous ubiquinones. Once the treatment partially depletes CoQ pool, pre-bound ubiquinones would be released from the pore promoting its opening which could be restored to its closed state by adding exogenous CoQ. Although the current work has not measured CoQ levels, the same treatment protocol in a different rat strain did not detect alterations in CoQ_9 CoQ_{10} content [174]. However, as it have been pointed out throughout the present thesis, differences exist between the strain used in the current protocol and the one used previously [174]. Perhaps, as with the absence of alteration in ANT content in this model, there may also be alterations in CoQ levels, an interesting point which could be addressed in the future. An interesting point to focus is the fact that if ANT is indeed unaltered in the current protocol it may suggest that mPTP modulation after DOX treatment does not depend exclusively on ANT defects. If so, the ubiquitously identity for the pore opening upon DOX treatment is yet to be found.

For the sake of characterization, the same analysis was performed in the acute model. As Ascensão *et al.* [178] previously reported, no significant alterations in mPTP related protein content are observed after 24 h of an acute DOX exposure(Table 6.4). However, the analysis of transcript levels demonstrated lower amounts of mRNA for all proteins (ANT, VDAC and CyP-D; Fig. 6.5). Interestingly, if one performs a two-way ANOVA analysis with respect to treatment and tissue effects to address where alterations occur preferentially in the heart tissue, significance is only attained for ANT1 and CyP-D (data not shown), pointing two differential targets for possible development of therapeutic approaches. Although alterations on mRNA levels were

not followed by concomitant alterations in protein content this could be due to the short end-point time of measurement (24 h). In fact, although reports in the literature inform distinct rates of mitochondrial protein turnover, most agree that turnover rate is greater than 24 h in rodent models [324, 325] while increased rates can be observed in cell lines (7 to 24 h) [326]. Alternatively, either mRNA (in)stability or degradation may be increased in this situation which might result in the observed pattern of no alteration in protein content but opens new perspectives of research and clinical application.

6.4 Conclusion

In conclusion, the work described in the current chapter is the first to provide a three organ analysis of DOX effects on mPTP modulation using two different experimental protocols in Wistar rats. Following the idea of the previous chapter, mitochondrial impairment is present in a tissue-specific protocol-dependent fashion before any morphological alterations or cardiomiopathy hallmarks. The results confirm that mitochondrial calcium homeostasis dysfunction is an early marker of DOX toxicity which results from the gather of primary changes during the early stages of drug accumulation but which are not related to changes in content of the classic participants of the mPTP.

Acknowledgments

The present work would not be possible without contribution of the following people, therefore I am thankful to Maria Sancha Santos (Center for Neuroscience and Cell Biology, Coimbra) for help in hydrogen peroxide quantification; James Bjork and Annette Rod (Department of Biochemistry and Molecular Biology, University of Minnesota Medical School, Duluth, MN, US) for help in real-time qPCR; Inês Barbosa and Rita Garcia (Center for Neuroscience and Cell Biology, Coimbra) for help in Western-Blot; and Susana Pereira (Center for Neuroscience and Cell Biology, Coimbra) for general collaboration.

Chapter 7

Mitochondrial Thresholds Analysis in the Context of Doxorubicin Cardiotoxicity

Even though half a century has passed since DOX discovery, it is still unclear why DOX is selectively cardiotoxic. Even so, a similar effect occurs in hereditary mitochondrial diseases where phenotypic expression is tissue-dependent even if a mutation is constitutively present throughout the organism. However, for the latter case a theory capable of explaining such events has been proposed - metabolic thresholds. Therefore, the present chapter aims to investigate DOX-induced cardiotoxicity in the context of the mentioned theory in a sub-chronic model of toxicity. Global flux (state 3 respiration rates) and isolated step (enzymes activity) curves were obtained for Complex I, III, IV and ANT and revealed alterations in global flux Complex III curves for all studied tissues and Complex IV activity curve in cardiac tissue. Additionally, maximal Complex III activity was decreased in liver and increased for Complex IV in heart and kidney. Although these alterations caused a decrease of 16 % in the cardiac threshold for Complex IV, no other respiratory complex or tissue presented significant alterations. Furthermore, analysis of mRNA levels and protein content of certain OXPHOS-complexes subunits did not reveal any alteration between treatment groups and tissues. In conclusion, the work shows that depressed cardiac mitochondrial respiration might be due to a lower threshold with respect to Complex IV.

7.1 Introduction

One of the most important holy grails pursued in DOX-induced toxicity research is related to the drug specificity to the cardiac tissue. As pointed in Section 2.5.1 several theories have emerged but none has provided a truthful answer to the problem. However, a new theory on why DOX is selectively cardiotoxic can be drawn from the definition of metabolic thresholds [219, 266, 327].

In the context of mitochondrial hereditary disorders it is still unclear why a nuclear mutation in a certain OXPHOS respiratory complex subunit has its phenotypic expression only in some tissues although it results in a modulation of that complex activity with homogeneous distribution of the deficiency among all mitochondria in the organism. Mazat's group suggested that the effect may be related to the degree of enzyme inhibition and to tissue-dependent mitochondrial thresholds [327]. A mitochondrial threshold of a certain enzyme is defined as the percent inhibition before which the fluxes are barely affected but after which a rapid decrease in flux occurs together with the activity of the inhibited complex, with higher threshold values meaning that the tissue would be less affected by the defect [219].

Previous works demonstrated that DOX treatment reduces ANT content and its availability for mitochondrial respiration in heart tissue [177] but it lacks comparisons with other tissues. Similarly, Complex I and IV activity in the heart was shown decreased after treatment [173, 178]. Therefore, the type of analysis mentioned above may reveal new insights regarding the mechanism of DOX-induced mitochondrial respiration inhibition and perhaps new clues with respect to drug selectivity.

Hence, the present chapter aims to investigate whether cardiac mitochondria are most affected due to lower enzyme reserves comparing to other tissues or, as an alternative, if DOX treatment changes the threshold curves profile to an incompatible state against high energy demands. Additionally, it was also investigated if the treatment also induces alterations on the transcript levels of OXPHOS complexes subunits or in its correspondent protein content. The hypothesis is that differences between DOX and control group regarding mitochondrial OXPHOS proteins may not be as visible as in the heart.

Since, impaired cardiac mitochondrial respiration was only present in sub-chronic model (Chapter 5) this model was preferred for the current analysis. Moreover this model has greater importance for clinical practice extrapolation.

7.2 Results

7.2.1 Global step - Titration curves of oxygen consumption

The first step in the evaluation of mitochondrial thresholds of a certain OXPHOS enzyme is the measurement of the global flux of the pathway where it is involved. In the present case, the flux evaluated was the oxygen consumption in the presence of ADP, i.e. state 3 respiration rate sustained by Complex I-linked substrates for the analysis of Complex I, III, IV and ANT; and also, state 3 respiration sustained by Complex II-linked substrates for ANT. Previous data has shown similar inhibition of cardiac ANT activity for both Complex I- and II-linked substrates [177]

Table 7.1 shows the maximal state 3 respiration rates for each tissue and treatment group. It is apparent that all tissues present a steady-state equilibrium different from each other but similar between treatment groups. A possible exception exists between the control and DOX-treated group either with Complex I- (12.1±5.5 %, p =0.061) or Complex II-sustained respiration (16.1±7.1 %, p =0.055).

Inter-tissue comparisons

The first column of Fig. 7.1 shows the titration curves of different inhibitors of OXPHOS enzymes in different tissues. For each multimeric protein, all curves have significantly ($p< 0.05$) distinct traces regardless of the tissue of origin. The sigmoidal shape of the curves is typical of these type of experiments [266] and will be explained in the light of the metabolic control analysis (MCA) theory further in the text. One last observation regarding the steepness of the curves is that it is always more pronounced in the liver followed by kidney and heart.

Two characteristic parameters of each mitochondrial fraction were obtained from the curve-fitting - C_j^I and E_j^0 (Table 7.2). The control coefficients (C_j^I) for each complex was variable among tissues but kidney always showed the lowest control coefficients for all complexes (≥ 0.09). Cardiac mitochondria shared its highest control coefficient between Complex I and II (~ 0.18) while in liver, Complex I had the highest control coefficient (0.30). Still in hepatic mitochondria, Complex IV and ANT control coefficients were higher than in other tissues (~ 0.15). In terms of MCA summation theorem, the evaluated complexes contributed to 45.8±13.4 % (heart), 71.3±19.8 % (liver) and 27.1±8.3 % (kidney) of the global flux.

Table 7.1: Effect of sub-chronic DOX treatment on the mitochondrial state 3 respiration rates.

Substrate	Treat.	Heart		Liver		Kidney	
		Mean	*SE*	Mean	*SE*	Mean	*SE*
		$\mathrm{natms_O\,min^{-1}\,mg^{-1}_{protein}}$					
		$n = 8$		$n = 8$		$n = 8$	
Glutamate	Saline	346.0	31.7	111.6	6.0	115.4	7.1
Malate	DOX	304.1	26.3	108.1	7.2	99.9	9.6
		$n = 8$		$n = 7$		$n = 7$	
Succinate	Saline	368.0	32.8	141.3	6.3	271.8	16.7
	DOX	308.0	27.4	129.8	8.6	269.3	15.7

Tabulated values represent absolute values of state 3 respiration rates in the absence of inhibitors. Differences between treatment groups means were evaluated by matched pairs Student's t test to exclude the variability related to mitochondrial isolation (see 4.19, p. 110). Abbreviations: *Treat.* - treatment.

The total apparent/theoretical enzyme content (E_j^0) of each OXPHOS complex was also different between tissues (Table 7.2). Cardiac mitochondria was the one presenting always the highest content of any of the evaluated respiratory complexes while hepatic mitochondria pertained at the opposite range. Among the evaluated enzymatic complexes, ANT was the protein more abundant independently of the tissue of origin while Complex IV content was consistently lower.

Using Complex IV content as normalizing factor, the intra-tissue proportion of each OXPHOS complexes showed two distinct groups. One formed by heart and kidney with a proportion of Complex I, III and IV of $4:3.5:1$ and $4:3.4:1$, respectively; and, the other one by the liver which had a proportion of $2.75:1.625:1$ for the same complexes. Although heart and kidney had similar proportions of respiratory complexes the same was not observed for the ANT since heart had a $1:27$ ratio relative to Complex IV while in kidney the ratio was $1:19.5$.

Treatment-dependent effects

The titration curves of Complex I, IV and ANT in cardiac mitochondria were similar between control and treated group (Fig. 7.1) and, therefore no differences were found in C_j^I and E_j^0 values between both groups (Table 7.2). However, the titration curve for Complex III in control group was distinct from the one in DOX-treated group

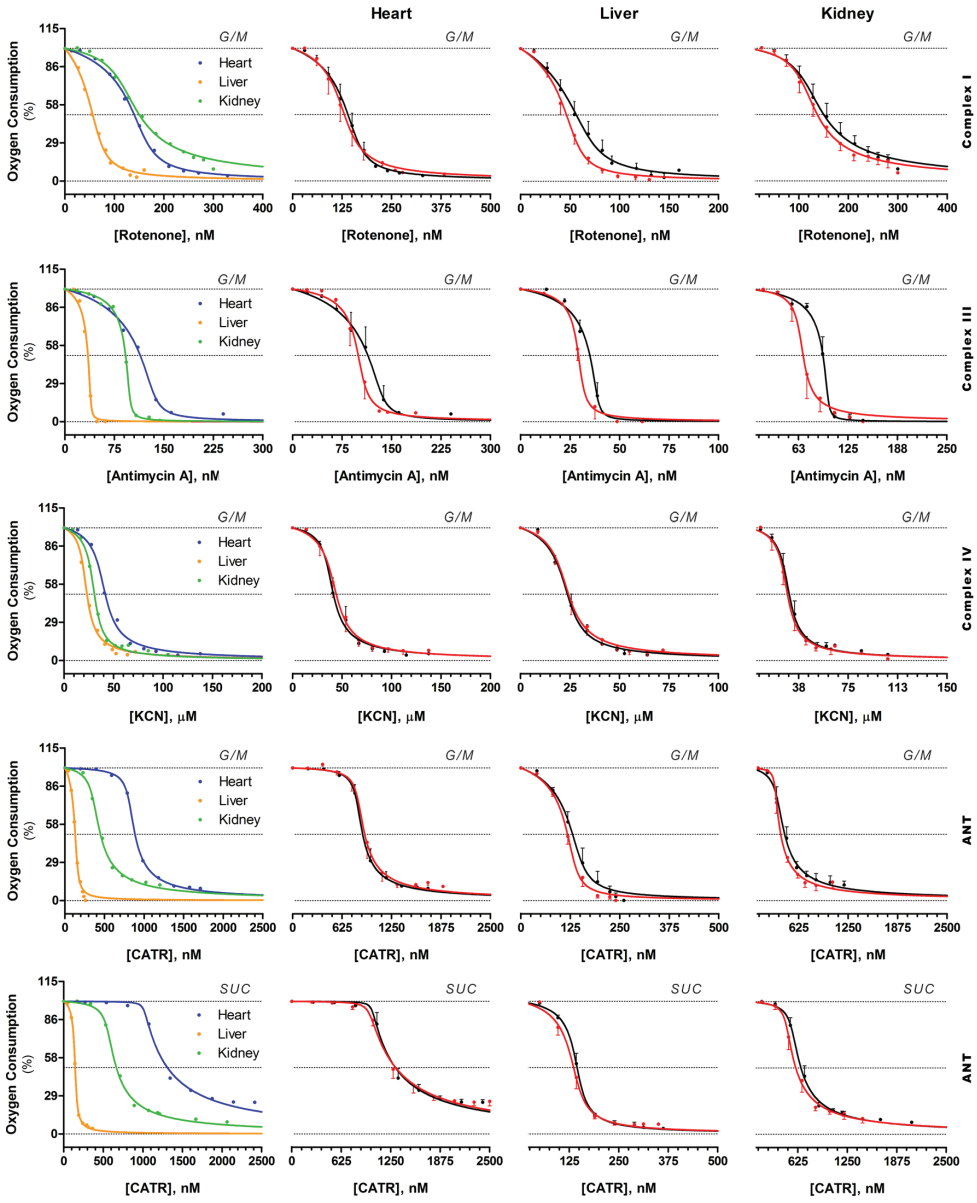

Figure 7.1: Effect of sub-chronic DOX treatment on the profile of dose-response curves of mitochondrial oxygen consumption. Oxygen consumption rates were evaluated as described in Section 4.11.1 (p. 91) and data processed as detailed in Sec. 4.19 (p. 110). Dots represents the mean of each titration points ($n = 4/7$) with SE (black pointing upwards - saline; red pointing down - DOX). Error bars are smaller than symbols when not visible and are absent in the first column (saline group only). Abbreviations: *G/M* - glutamate-malate; *SUC* - succinate; *CATR* - carboxyatractyloside.

Table 7.2: Best-fit parameters from the fitting of global flux curves

	Treat.	**Heart**				**Liver**				**Kidney**			
		C_j^I		E_j^0		C_j^I		E_j^0		C_j^I		E_j^0	
		Mean	*SE*	Mean	*SE*	Mean	*SE*	Mean	*SE*	Mean	*SE*	Mean	*SE*
Complex I	Saline	0.190	0.074	156.6[a]	16.4	0.304	0.161	66.2	13.7	0.086	0.063	126.7	22.0
	DOX	0.142	0.097	132.4	23.8	0.255	0.089	54.4	6.0	0.075	0.046	118.6	14.9
Complex III	Saline	0.191	0.103	133.5[a]	19.2	0.112	0.041	38.6[b]	3.0	0.068	0.025	99.4	3.2
	DOX	0.072	0.038	102.9	9.2	0.056	0.033	30.0[*]	1.5	0.038	0.032	66.3[*]	8.6
Complex IV	Saline	0.060	0.042	37.9[a]	3.6	0.130	0.056	23.8	2.4	0.070	0.048	29.3	3.6
	DOX	0.096	0.076	42.6	6.4	0.110	0.600	23.2	2.9	0.068	0.053	27.8	3.5
ANT	Saline	0.018	0.016	827.7[a]	56.2	0.167	0.093	143.5[b]	20.9	0.046	0.040	379.0[c]	52.3
GM	DOX	0.018	0.012	844.9	49.8	0.154	0.051	130.8	8.5	0.009	0.017	330.6	19.3
$\sum$	Saline	0.458	0.134	n.a.	n.a.	0.713	0.198	n.a.	n.a.	0.272	0.083	n.a.	n.a.
	DOX	0.327	0.130	n.a.	n.a.	0.576	0.123	n.a.	n.a.	0.221	0.080	n.a.	n.a.
ANT	Saline	0.002	0.010	1014.0[a]	53.1	0.067	0.026	145.9[b]	5.8	0.024	0.018	568.3[c]	44.6
Succ	DOX	0.004	0.009	983.2	54.3	0.102	0.038	139.8	8.8	0.017	0.025	490.1	41.0

Data refers to best-fit values obtained from the curve-fitting on Fig. 7.1 where C_j^I is unitless and E_j^0 is in the same units as its correspondent curve abscissa in Fig. 7.1. $\sum$ represents the sum of control coefficients of each respiratory complex except the ANT in the presence of succinate. Inter-tissue comparisons were as follows:
a, $p \geq 0.05$ heart *vs* liver;
b, $p \geq 0.05$ liver *vs* kidney;
c, $p \geq 0.05$ kidney *vs* heart;
within the same respiratory complex group, as evaluated by a one-way ANOVA followed by pair-wise comparisons through Bonferroni pos-hoc analysis (see 4.19, p. 110).
Intra-tissue comparisons were evaluated by an unpaired Student's t test with Wech's correction whenever data was not homoscedastic.
*, $p \geq 0.05$ *vs* saline group of the same treatment protocol.
Abbreviations: *Treat.* - treatment; *SE* - standard error; C_j^I - control coefficient; E_j^0 - enzyme concentration in the absence of inhibitor; *GM* - glutamate/malate; *Succ* - succinate; *n.a.* - not applicable.

(p =0.018), although no alteration was observed in the C_j^I and E_j^0 values of this multimeric protein.

The titration curves of Complex III were also left-shifted in liver and kidney (p =0.012 and $p< 0.001$, respectively) with a concomitant decrease in E_j^0 in both cases but without alteration in C_j^I . The treatment also caused a left shift in the titrations curves of Complex I in liver ($p< 0.001$) and ANT with respiration sustained with Complex II-linked substrates in kidney (p =0.046) but once again without alterations in the values of C_j^I or E_j^0.

The remaining curves as well as the C_j^I and E_j^0 values were similar between treatment groups either in liver or kidney mitochondria. Likewise, despite the general decrease in the sum of control coefficients when compared to control no tissue achieved significancy.

7.2.2 Isolated step - OXPHOS complexes activity dose-response curves

The second step in the evaluation of mitochondrial thresholds of a certain OXPHOS enzyme is the measurement of the isolated step. In the present case, the isolated step represents the maximal enzymatic activity.

Table 7.3 shows the maximal activity of selected OXPHOS enzymes for each tissue and treatment group. It is apparent that all tissues present a V_{max} different from each other but similar between treatment groups with the following exceptions: Complex III activity in DOX-treated livers was significantly lower when compared to control while Complex IV activity in DOX-treated hearts and kidney was significantly increased.

Inter-tissue comparisons

The first column of Fig. 7.2 shows the dose-response curves of different inhibitors of OXPHOS enzymes in different tissues. The reader should note that graphs in the first three rows of Fig. 7.2 have their abscissa axis in *log* form and therefore the activity curves have in fact hyperbolic shapes rather than sigmoidal, which is very important in the context of MCA theory (see Discussion).

Regarding Complex I, the cardiac dose-response curve is distinct ($p< 0.05$) from its liver counterpart but not from kidney. The difference was also observed as a higher

Table 7.3: Effect of sub-chronic DOX treatment on the mitochondrial respiratory complexes maximal activity.

Complex	Treat.	Heart		Liver		Kidney	
		Mean	*SE*	Mean	*SE*	Mean	*SE*
		$n = 5$		$n = 5$		$n = 5$	
Complex I [a]	Saline	260.1	9.8	19.7	2.0	158.5	15.0
	DOX	248.5	16.4	16.8	0.9	161.9	16.2
Complex III [b]	Saline	207.5	2.8	19.8	1.7	60.6	9.0
	DOX	250.1	31.0	16.3*	0.8	63.7	7.5
Complex IV [c]	Saline	1789.0	160.3	534.9	22.8	835.8	59.1
	DOX	2311.0*	138.3	583.9	22.1	964.6*	38.9

Tabulated values represent absolute values of the maximal specific-activity of each respiratory complex which was calculated as the difference between the activity in the absence of inhibitor and the activity in the presence of the highest concentration of inhibitor.
[a] activity expressed as $\mathrm{nmol_{DCPIP}\,min^{-1}\,mg^{-1}_{protein}}$
[b] activity expressed as (increase) $\mathrm{nmol_{cyt-c\,red}\,min^{-1}\,mg^{-1}_{protein}}$
[c] activity expressed as (decrease) $\mathrm{nmol_{cyt-c\,red}\,min^{-1}\,mg^{-1}_{protein}}$
*, $p \geq 0.05$ *vs* saline group within the same tissue and respiratory complex group, as evaluated by a paired Student's t test (see 4.19, p. 110).
Abbreviations: *Treat.* - treatment.

IC_{50} for heart mitochondria when comparing to liver (Table 7.4). However, the opposite occured when analyzing Complex III, heart and liver mitochondria shared the same dose-response curve and had similar IC_{50} but were both different from kidney mitochondria. Only for Complex IV, all preparations were different from each other since none of them shared the same curve ($p < 0.05$) or had similar IC_{50}.

In respect to IC_{50} range, heart mitochondria had the highest values regarding Complex I and Complex IV while liver mitochondria had the lowest ones for the same respiratory complexes. However, for Complex III, liver mitochondria showed the highest IC_{50} among the three analyzed tissues.

Finally, since the activity of ANT cannot be measured separately as it requires Δp to function properly, a simulation of its isolated step was performed by computing and imposing the global flux curve to $C_j^I = 1$ (maximal control coefficient). The last two rows of Fig. 7.2 show those simulations and clearly demonstrate that the activity of ANT is higher in cardiac mitochondria followed by kidney and liver both in Complex I- and Complex II-sustained respiration.

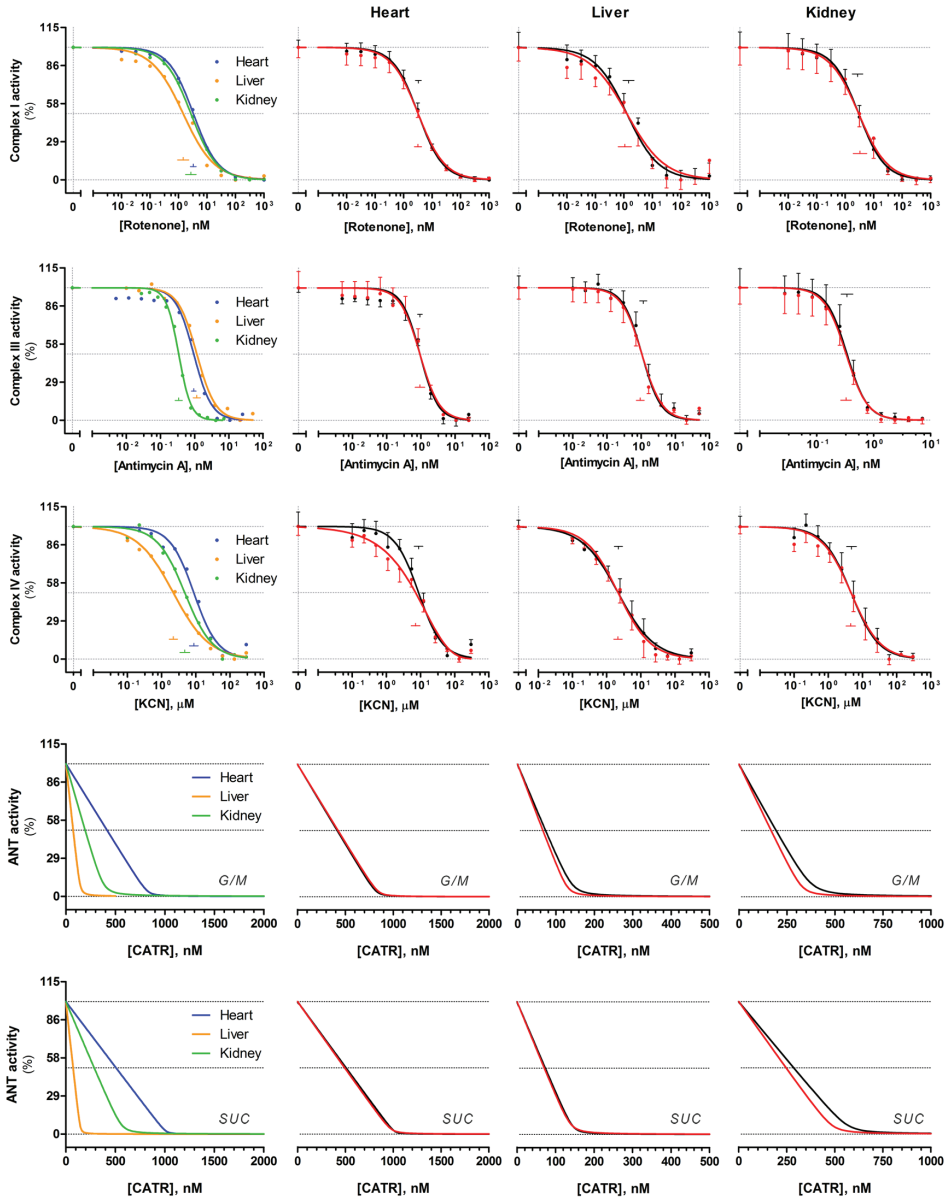

Figure 7.2: Effect of sub-chronic DOX treatment on dose-response curves profile of OXPHOS complexes activity. Dots represents the mean of each titration points ($n = 5$) with SE (black pointing upwards - saline; red pointing down - DOX). Error bars are smaller than symbols when not visible and are absent in the first column (saline group only). Also depicted are IC_{50}: vertical arm of the small T represent mean value and horizontal arm the respective 95% CI. Abbreviations: *G/M* - glutamate-malate; *SUC* - succinate; *CATR* - carboxyatractyloside.

Table 7.4: Inhibitor IC_{50} for the different mitochondrial respiratory complexes.

Complex	Treat.	Heart		Liver		Kidney	
		Mean	95% CI	Mean	95% CI	Mean	95% CI
		$n = 5$		$n = 5$		$n = 5$	
Complex I	Saline	3.32[a]	2.62 to 4.19	1.46	0.93 to 2.28	2.72	1.77 to 4.18
(Rotenone)	DOX	3.15	2.36 to 4.21	1.08	0.63 to 1.86	3.32	1.92 to 5.74
Complex III	Saline	0.94	0.80 to 1.10	1.15[b]	0.90 to 1.48	0.34[c]	0.27 to 0.43
(Antimycin A)	DOX	0.94	0.68 to 1.31	0.94	0.72 to 1.23	0.33	0.26 to 0.41
Complex IV	Saline	8.78[a]	6.55 to 11.7	2.21[b]	1.68 to 2.92	4.78[c]	3.44 to 6.63
(KCN)	DOX	6.20	4.58 to 8.39	2.14	1.61 to 2.84	4.54	3.31 to 6.22

Tabulated values were withdrawn from the non-linear curve-fitting model of Fig. 7.2 and were back-transformed to the linear scale. IC_{50} values for Complex I and III are expressed in nM and in µM for Complex IV. Confidence intervals are in the form of "upper bound" to "lower bound". Inter-tissue comparisons were as follows:
a, $p \geq 0.05$ heart *vs* liver;
b, $p \geq 0.05$ liver *vs* kidney;
c, $p \geq 0.05$ kidney *vs* heart;
within the same respiratory complex group, as evaluated by a one-way ANOVA followed by pair-wise comparisons through Bonferroni pos-hoc analysis (see 4.19, p. 110). Intra-tissue comparisons were evaluated by an unpaired Student's t test.
Abbreviations: *Treat.* - treatment; *CI* - confidence interval.

Treatment-dependent effects

Although DOX-treatment affected the maximal activity of certain OXPHOS enzymes (Table 7.3) most of the curves were similar between treatment groups ($p > 0.05$; Fig. 7.2) with the exception of Complex IV, where a *five parameter logistic* curve-fitting was preferred over the *four parameter logistic* used for the control group. Nevertheless, IC_{50} of all OXPHOS respiratory complexes remained unchanged after the sub-chronic treatment (Table 7.4).

7.2.3 Mitochondrial thresholds

The last step in the evaluation of mitochondrial thresholds of a certain OXPHOS enzyme is the generation of threshold curves emerging from the titration curves of the global flux (Fig. 7.1) and isolated step (Fig. 7.2) and, representing therefore the state 3 respiration rate as a function of OXPHOS enzyme inhibition. To accomplish that, the curve with best-fit values of the isolated step was solved for the inhibitor concentration and then substituted in the global flux curve with its correspondent

best-fit values. The reader should note that no error bars are presented in this type of curves because one is working solely with the best-fit values of each individual curve and no error propagation calculus was performed. Consequently, no quantitative comparison between curves can also be performed.

Fig. 7.3 shows the thresholds curves of the OXPHOS enzymes being evaluated in this chapter. Two type of curves can be distinguished: one with a well defined initial plateau which remains constant until a certain value of inhibition where a sharply decline occurs, and is called Type I curve; and, another where the initial plateau is not evident and therefore no sudden change in flux is observed, being designated as Type II curve [219].

Inter-tissue comparisons

In the first column of Fig. 7.3 are shown the threshold curves of different OXPHOS enzymes in different tissues. Complex I, III and IV present Type I curves although each one has minor details that makes them unique from each other. For example, Complex III plateau extends almost until 100 % inhibition and Complex IV curve presents a sigmoidal shape on the descending arm after the plateau. However, despite this behaviors no differences exist between the studied tissues for each respiratory complex. A possible exception may exist for Complex I in which the liver shows a slight left shift in its threshold curve. The inter-tissue differences are more perceptible in ANT threshold curves with cardiac mitochondria presenting a Type I curve, its liver counterpart a Type II and kidney mitochondria presenting a curve positioned between the two.

Consequently, the threshold values shown in Table 7.5 are consistently higher for Type I curves. However, for this class of curves no apparent difference exists in the thresholds values regardless of the respiratory complex or tissue being analyzed.

Treatment-dependent effects

Subsequent analysis of the remaining curves presented in Fig. 7.3 shows that sub-chronic treatment did not alter significantly the profile of the threshold curves of OXPHOS respiratory complexes. One exception, however, are Complex IV curves in heart mitochondria, where treatment caused a transition curve from Type I to Type II. Concomitantly, the threshold value for this particular complex showed a decrease of

Table 7.5: Threshold values of the different OXPHOS complexes.

Complex	Treat.	Heart	Liver	Kidney
		Mean	Mean	Mean
			%	
Complex I	Saline	96.8	92.5	96.6
	DOX	95.7	89.6	94.6
Complex III	Saline	99.7	99.6	100.0
	DOX	99.6	99.8	100.0
Complex IV	Saline	82.6	83.8	84.5
	DOX	66.9	86.5	83.2
ANT (GM)	Saline	98.2	85.8	95.6
	DOX	98.3	86.7	99.1
ANT (SUC)	Saline	99.8	93.7	97.6
	DOX	99.6	90.8	98.3

The threshold value was defined as the abscissa of the intersection point between the two tangents of Fig. 7.3. Abbreviations: *Treat.* - treatment; *GM* - glutamate-malate; *SUC* - succinate.

$\sim$ 16 units of percentage while the values for all other complexes remained unchanged (Table 7.5).

In ANT curves only minor differences can be detected and in the case of DOX-treated kidney, despite the upper right drag of the curve, the threshold value increased only $\sim$ 4 percentage units.

7.2.4 Expression of OXPHOS complexes subunits

The next step in finding an explanation for the previous reported alterations was the evaluation of the transcript levels of certain OXPHOS respiratory complexes subunits. Due to the small number of transcripts coded by mtDNA, we have decided to quantify all of them. However, since the same decision would not be feasible for transcripts encoded by nuclear DNA, the screening was narrowed to those which coded proteins could be semi-quantified by commercially available antibodies.

Fig. 7.4 summarizes Table 7.7 as a treemap representation of the transcript levels of selected OXPHOS complexes subunits as evaluated by qPCR. Qualitatively, it appears that DOX sub-chronic treatment caused a general decrease in the measured transcripts. Hepatic tissue presented the most dramatic changes both in nuclear-

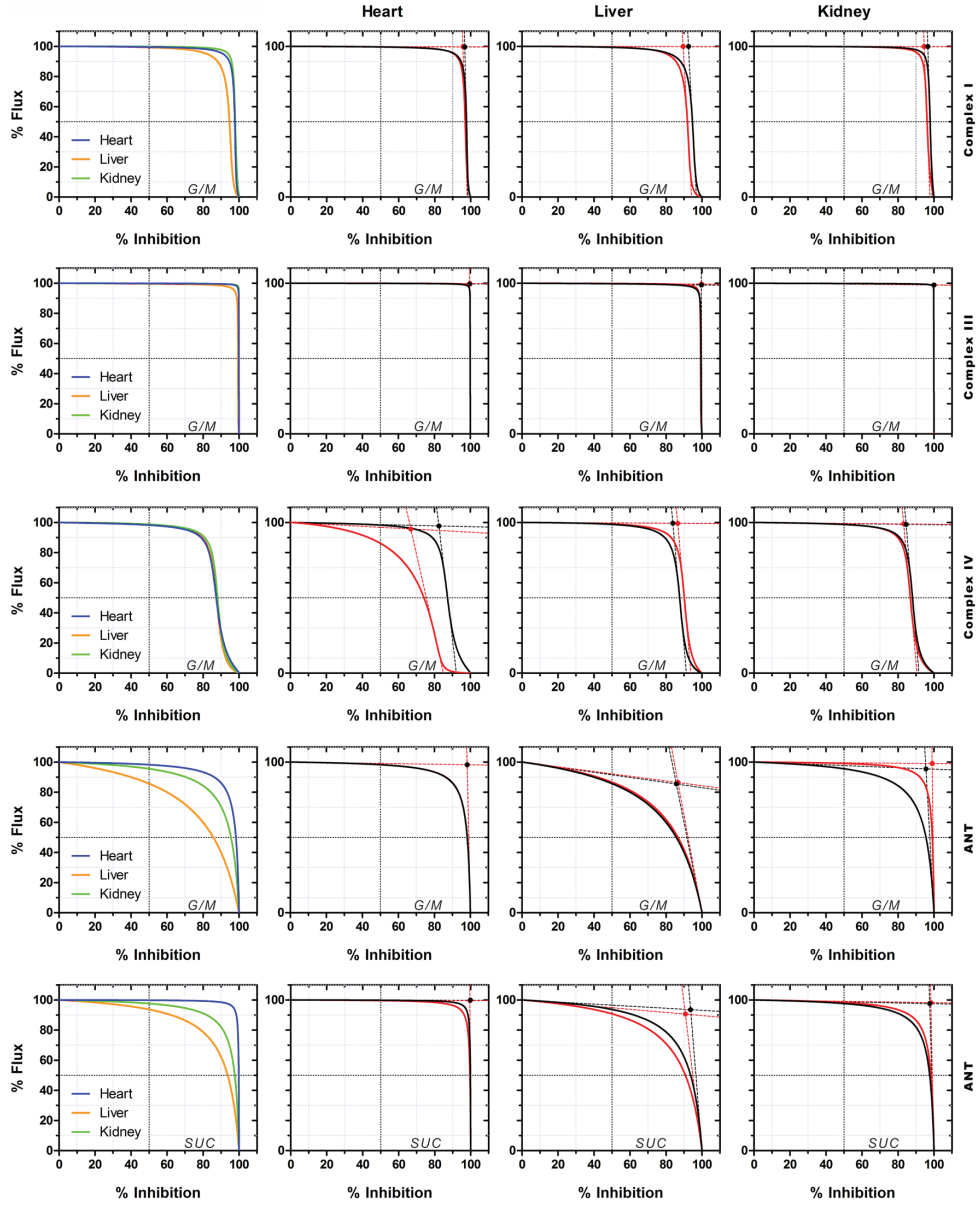

Figure 7.3: Effect of sub-chronic DOX treatment on the profile of mitochondrial thresholds curves for OXPHOS complexes. Curves were simulated as described in Sec. 4.19 (p. 110) using the parameters obtained in Fig. 7.1 and 7.2. Dashed lines represent linear regressions (see 4.19, p. 110) at the beginning (1% inhibition) and at the end (inflection point) of the curve, and were used to determine the *threshold* value which is represent by the full circle. Absolute values of the thresholds are presented in Table 7.5. Abbreviations: *G/M* - glutamate-malate; *SUC* - succinate.

Table 7.6: Effects of DOX treatment on the protein content of selected OXPHOS respiratory complexes subunits.

			Sub-chronic				Acute			
Protein	**DNA**	**Tissue**	**Saline**		**DOX**		**Saline**		**DOX**	
			Mean	*SE*	Mean	*SE*	Mean	*SE*	Mean	*SE*
			protein r.u. of densitometry / actin r.u. of densitometry							
Complex I			$n = 8$		$n = 8$		$n = 6$		$n = 6$	
NDUFS3	Nuc	Heart	1.062	0.019	0.975	0.017	1.082	0.048	1.003	0.037
		Liver	0.963	0.024	1.076	0.029	1.029	0.017	1.010	0.023
		Kidney	0.986	0.032	1.033	0.025	0.956	0.030	1.062	0.023
NDUFB8	Nuc	Heart	1.018	0.031	0.926	0.103	0.946	0.040	1.082	0.048
		Liver	0.967	0.058	1.019	0.053	0.952	0.035	1.109	0.057
		Kidney	0.927	0.027	1.214	0.050	0.906	0.031	1.099	0.020
Complex II			$n = 8$		$n = 8$		$n = 6$		$n = 6$	
SDHA	Nuc	Heart	1.029	0.044	0.948	0.043	1.057	0.054	1.020	0.043
		Liver	0.968	0.017	1.059	0.013	0.984	0.015	1.042	0.027
		Kidney	1.010	0.021	1.021	0.016	0.999	0.027	1.017	0.029
SDHB	Nuc	Heart	1.075	0.025	0.927	0.030	1.059	0.061	1.076	0.047
		Liver	0.886 [a]	0.024	1.194	0.037	1.008	0.015	1.044	0.027
		Kidney	0.996	0.032	1.140	0.034	1.004	0.016	1.002	0.014
Complex III			$n = 8$		$n = 8$		$n = 6$		$n = 6$	
UQCRFS1	Nuc	Heart	1.069	0.034	0.896	0.048	1.006	0.030	1.050	0.032
		Liver	0.996	0.035	1.009	0.036	1.058	0.036	1.015	0.032
		Kidney	0.988	0.480	0.989	0.040	1.001	0.017	0.999	0.015

continues on next page

Table 7.6 – Continued

Complex IV			$n = 8$		$n = 8$		$n = 6$		$n = 6$	
COX I	Mt	Heart	1.136	0.021	0.870	0.040	1.047	0.051	1.080	0.046
		Liver	1.070	0.040	0.928	0.055	1.073	0.048	1.084	0.055
		Kidney	0.992	0.032	0.914	0.032	1.008	0.020	0.989	0.025
COX IV	Nuc	Heart	1.013	0.025	0.974	0.026	1.018	0.050	1.067	0.055
		Liver	0.966	0.028	1.064	0.030	1.152	0.061	1.031	0.048
		Kidney	1.060	0.018	0.968	0.023	0.996	0.027	1.024	0.045
Complex V			$n = 8$		$n = 8$		$n = 6$		$n = 6$	
ATP5A1	Nuc	Heart	1.094	0.057	0.810	0.059	1.083	0.062	1.066	0.049
		Liver	1.030	0.290	0.997	0.045	1.066	0.039	1.048	0.034
		Kidney	1.039	0.029	1.070	0.018	1.022	0.016	0.992	0.014
ATP5O	Nuc	Heart	1.000	0.073	1.120	0.047	1.019	0.072	1.132	0.063
		Liver	1.036	0.060	0.994	0.098	0.980	0.037	1.017	0.036
		Kidney	0.914	0.054	1.047	0.079	0.989	0.060	1.047	0.056
Others			$n = 8$		$n = 8$		$n = 6$		$n = 6$	
CYCS	Nuc	Heart	0.991	0.052	1.064	0.037	1.058	0.052	0.984	0.020
		Liver	0.988	0.044	1.008	0.035	1.036	0.042	1.009	0.012
		Kidney	1.030	0.036	1.001	0.033	1.044	0.044	0.982	0.027
ANT	Nuc	Heart					1.022	0.019	0.970	0.032
		Liver	1.073	0.113	1.040	0.073	0.966	0.030	1.043	0.017
		Kidney	1.054	0.156	0.980	0.070	1.016	0.019	0.988	0.018

For statistical analysis, tabulated values were *log* transformed and differences in fold-change of each tissue were detected by a two-way ANOVA with planned contrasts and adjusted for multiple comparisons through the Sidak test (see 4.19, p. 110):
[a] $p \geq 0.05$ heart *vs* liver.
Sub-chronic and acute model were analyzed independently.
Abbreviations: *SE* - standard error; *Mt* - mitochondrial; *Nuc* - nuclear; *r.u.* - relative units.

and in mitochondrial-encoded mRNAs followed by heart and then kidney tissue. In the latter, most of the nuclear-encoded mRNAs were unchanged except for ANT1. However, the statistical test applied, where the question asked was "*is the treatment effect larger in amplitude in heart than in other tissues?*", did not retrieve a single positive result (Table 7.7).

Although no differences were measured in terms of OXPHOS (Chapter 5), the same approach was applied in the acute model of DOX toxicity. In that case, nuclear-encoded transcripts in heart tissue were down-regulated in comparison to its mitochondrial counterparts. Alterations in hepatic mRNA levels were more heterogeneous, while in kidney it appears that most mRNAs were slightly increased except for cytochrome c.

In general, mitochondria-encoded transcripts showed minimal and heterogeneous increase in their levels. However, this time the statistical test used revealed that acute treatment with DOX caused NDUFS4, NDUFS8, CYCS and ANT (both isoforms) transcripts to be altered in a different proportion in heart compared to the other tissues. Nevertheless, only for NDUFS8 and ANT1 the fold-change was greater in heart than in liver *and* kidney.

7.2.5 Content of OXPHOS complexes subunits

The last step in this analysis of mitochondrial thresholds was the confirmation that alterations at the level of mRNA were translated to the protein level or, alternatively, in those situations where no genetic alterations were found, alterations in protein content would be measured. However, despite our main objective of obtaining mRNA–protein correlation, the number of proteins analyzed by western blot and summarized in Table 7.6 is quite reduced. This is explained by the difficulty in obtaining a specific and reliable signal from the commercially available antibodies. Nevertheless, at least one protein subunit from each complex was analyzed through this methodology (Table 7.6).

As can be observed in Fig. 7.5, all protein levels remain similar to control after subchronic treatment with DOX regardless of the respiratory complex or tissue being analyzed. Likewise, western blot analysis of selected proteins in the acute model did not retrieve detectable differences between treatment groups in the different tissues (Table 7.6). However, alterations in this acute model were more heterogeneous

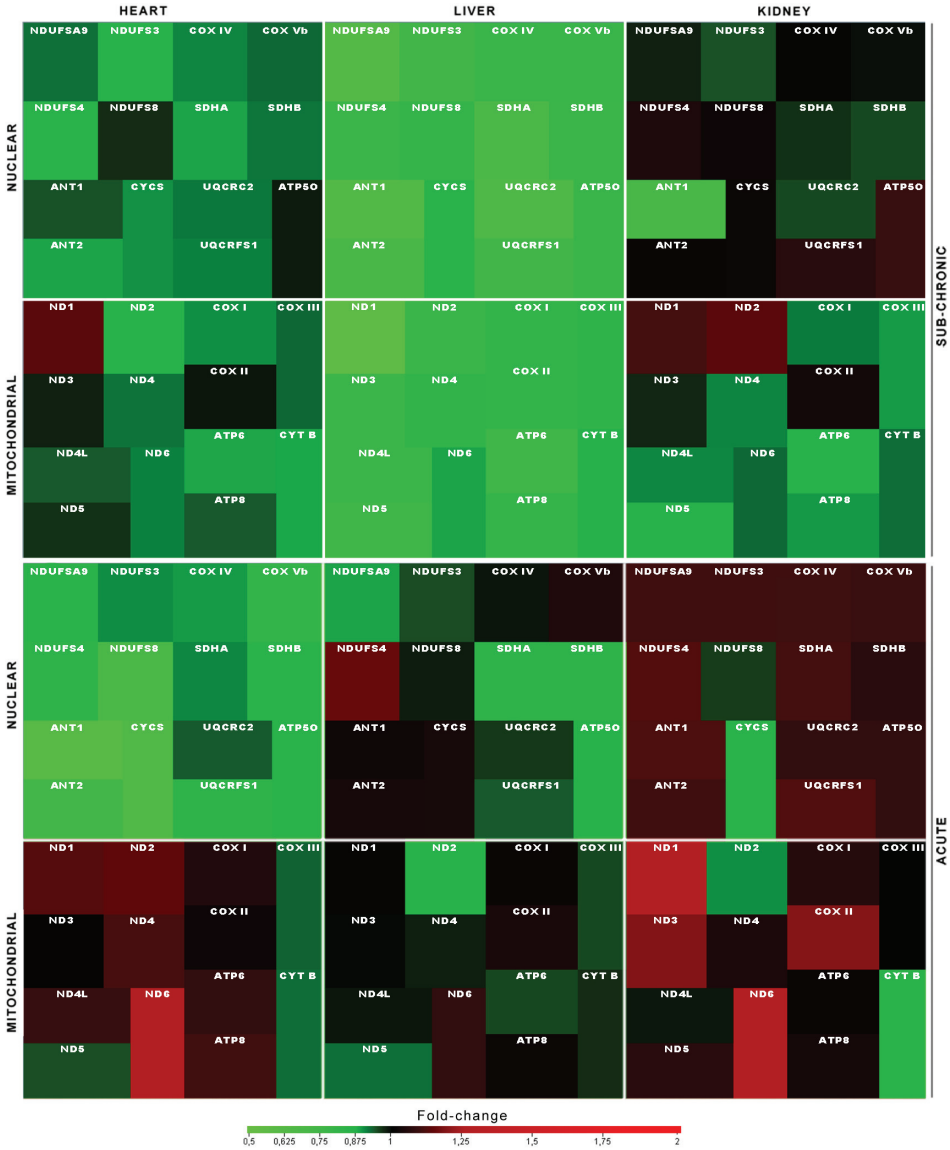

Figure 7.4: Treemap diagram of mRNA fold-change of OXPHOS transcripts after DOX sub-chronic treatment. Data from Table 7.7 was hierarchically organized in tissue, type of DNA-encoding and OXPHOS complex (I, II, III, IV and 'Others') by using the software Treemap© version 4.1.2 (available at www.cs.umd.edu/hcil/treemap/). Data from the sub-chronic and acute model were analyzed independently. Note that the size/area of the square has no significance in this diagram interpretation. Colors represent fold-change in the number of copies of a specific transcript relative to the saline group of same tissue, accordingly to the scale presented below the diagram.

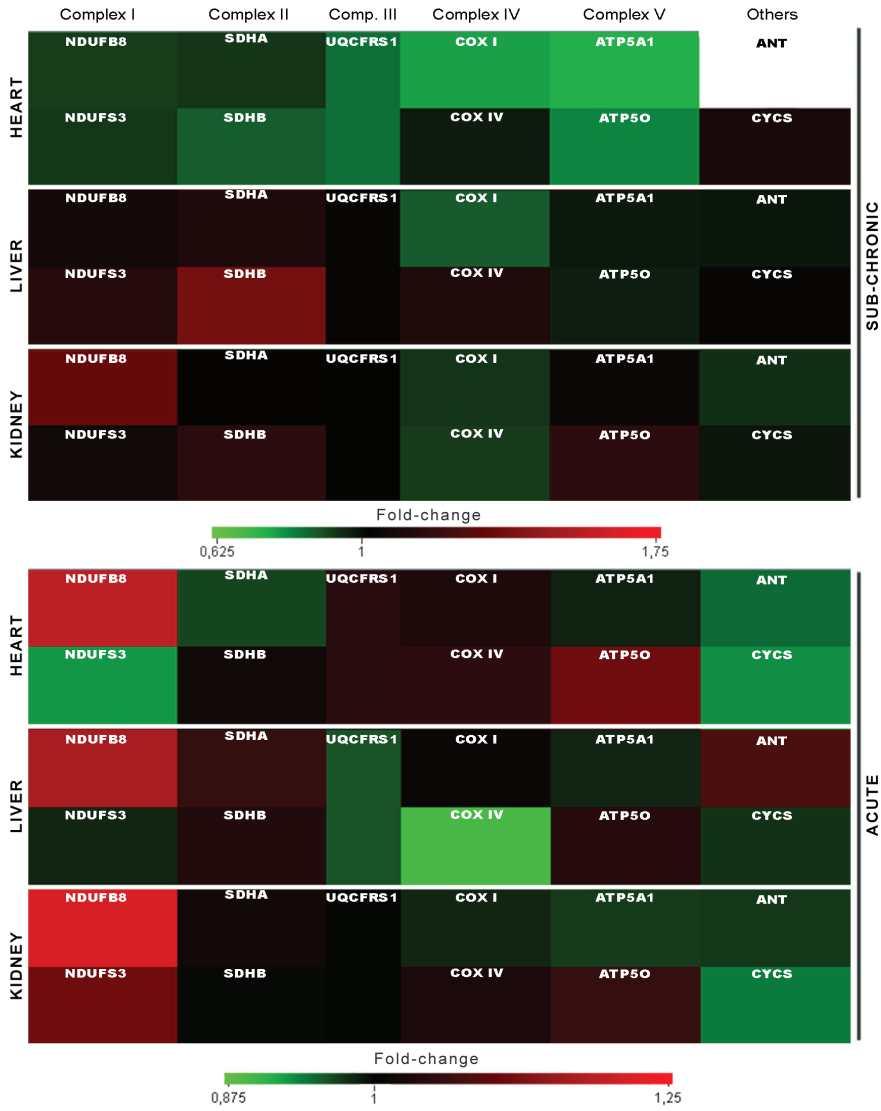

Figure 7.5: Treemap diagram of content fold-change of OXPHOS proteins after DOX sub-chronic treatment. Data from Table 7.6 was hierarchically organized in tissue, type of DNA-encoding and OXPHOS complex (I, II, III, IV and 'Others') by using the software Treemap© version 4.1.2 (available at www.cs.umd.edu/hcil/treemap/). Data from the sub-chronic and acute model were analyzed independently. Note that the size/area of the square has no significance in this diagram intrepertation. Colors represent fold-change in the number of copies of a specific transcript relative to the saline group of same tissue, accordingly to the scale presented below the diagram. Since it was impossible to quantify the ANT content in cardiac tissue of the sub-chronic model (see Chapter 6) the respective square was filled with white.

Table 7.7: Effects of DOX treatment on the mRNA expression levels of certain OXPHOS respiratory complexes subunits.

		Sub-chronic				Acute			
Transcript	**Tissue**	**Saline**		**DOX**		**Saline**		**DOX**	
		Mean	*SE*	Mean	*SE*	Mean	*SE*	Mean	*SE*
		transcript copy number / 18S copy number							
Complex I		$n = 8$		$n = 8$		$n = 6$		$n = 6$	
ND1 ^{Mt}	Heart	4.94×10^{-2}	1.23×10^{-2}	4.26×10^{-2}	4.76×10^{-3}	5.62×10^{-3}	2.57×10^{-4}	6.31×10^{-3}	5.45×10^{-4}
	Liver	1.23×10^{-2}	1.13×10^{-3}	9.68×10^{-3}	1.05×10^{-3}	1.73×10^{-3}	2.46×10^{-4}	1.74×10^{-3}	1.91×10^{-4}
	Kidney	4.39×10^{-2}	5.03×10^{-3}	4.97×10^{-2}	3.86×10^{-2}	7.63×10^{-3}	8.54×10^{-4}	2.11×10^{-2}	8.65×10^{-3}
ND2 ^{Mt}	Heart	1.08×10^{-2}	1.55×10^{-3}	1.06×10^{-2}	9.15×10^{-4}	7.88×10^{-2}	5.52×10^{-3}	8.96×10^{-2}	1.02×10^{-2}
	Liver	2.68×10^{-3}	4.39×10^{-4}	2.08×10^{-3}	2.15×10^{-4}	2.05×10^{-2}	2.10×10^{-3}	1.78×10^{-3}	2.05×10^{-3}
	Kidney	1.06×10^{-2}	1.14×10^{-3}	1.03×10^{-2}	1.19×10^{-3}	8.90×10^{-2}	1.15×10^{-2}	8.02×10^{-2}	8.00×10^{-3}
ND3 ^{Mt}	Heart	2.06×10^{-2}	3.35×10^{-3}	1.89×10^{-2}	1.19×10^{-3}	1.52×10^{-2}	1.07×10^{-3}	1.52×10^{-2}	9.88×10^{-4}
	Liver	8.62×10^{-3}	1.29×10^{-3}	7.04×10^{-3}	9.09×10^{-4}	2.74×10^{-3}	1.90×10^{-4}	$2.7\ \times10^{-3}$	2.84×10^{-4}
	Kidney	3.24×10^{-2}	2.94×10^{-3}	2.94×10^{-2}	2.23×10^{-3}	1.66×10^{-2}	8.36×10^{-4}	7.34×10^{-2}	6.78×10^{-3}
ND4 ^{Mt}	Heart	2.69×10^{-2}	4.82×10^{-3}	2.52×10^{-2}	1.45×10^{-3}	4.07×10^{-2}	2.04×10^{-3}	4.51×10^{-2}	3.77×10^{-3}
	Liver	1.09×10^{-2}	1.08×10^{-3}	8.41×10^{-3}	8.92×10^{-4}	1.02×10^{-2}	1.14×10^{-3}	9.95×10^{-3}	1.17×10^{-3}
	Kidney	4.10×10^{-2}	3.30×10^{-3}	3.71×10^{-2}	2.15×10^{-3}	7.05×10^{-2}	8.00×10^{-3}	7.34×10^{-2}	6.78×10^{-3}
ND4L ^{Mt}	Heart	2.80×10^{-2}	5.02×10^{-3}	2.70×10^{-2}	2.08×10^{-3}	5.55×10^{-2}	2.60×10^{-3}	6.03×10^{-2}	6.00×10^{-3}
	Liver	1.18×10^{-2}	1.49×10^{-3}	9.02×10^{-3}	9.07×10^{-4}	1.99×10^{-2}	1.14×10^{-3}	9.95×10^{-3}	1.17×10^{-3}
	Kidney	4.92×10^{-2}	3.88×10^{-3}	4.27×10^{-2}	3.07×10^{-3}	8.81×10^{-2}	1.21×10^{-2}	8.68×10^{-2}	8.50×10^{-3}
ND5 ^{Mt}	Heart	1.18×10^{-2}	1.84×10^{-3}	1.08×10^{-2}	8.80×10^{-4}	5.02×10^{-2}	2.28×10^{-3}	4.75×10^{-2}	5.05×10^{-3}
	Liver	5.56×10^{-3}	7.12×10^{-4}	4.94×10^{-3}	4.14×10^{-4}	1.89×10^{-2}	1.17×10^{-3}	1.75×10^{-2}	1.60×10^{-3}
	Kidney	1.43×10^{-2}	1.60×10^{-3}	1.32×10^{-2}	1.04×10^{-3}	1.01×10^{-1}	9.74×10^{-3}	1.07×10^{-1}	1.10×10^{-2}
ND6 ^{Mt}	Heart	2.48×10^{-3}	1.90×10^{-4}	2.34×10^{-3}	1.64×10^{-4}	2.24×10^{-2}	1.58×10^{-3}	2.82×10^{-2}	1.46×10^{-3}
	Liver	6.56×10^{-5}	1.60×10^{-5}	4.16×10^{-5}	5.50×10^{-6}	1.00×10^{-2}	8.61×10^{-4}	1.08×10^{-2}	5.96×10^{-4}

continues on next page

Table 7.7 – Continued

	Kidney	9.58×10^{-4}	1.16×10^{-4}	6.76×10^{-4}	8.69×10^{-5}	3.15×10^{-2}	3.48×10^{-3}	4.00×10^{-2}	3.23×10^{-3}
NDUFA9 [Nuc]	Heart	4.70×10^{-4}	4.23×10^{-5}	4.56×10^{-4}	1.84×10^{-5}	6.48×10^{-4}	3.82×10^{-5}	5.46×10^{-4}	2.62×10^{-5}
	Liver	7.46×10^{-5}	9.67×10^{-6}	5.96×10^{-5}	6.66×10^{-6}	2.36×10^{-4}	2.08×10^{-5}	2.09×10^{-4}	2.11×10^{-5}
	Kidney	2.22×10^{-4}	2.88×10^{-5}	2.25×10^{-4}	3.53×10^{-5}	7.19×10^{-4}	7.51×10^{-5}	7.90×10^{-4}	6.50×10^{-5}
NDUFS3 [Nuc]	Heart	1.90×10^{-4}	5.32×10^{-5}	1.61×10^{-4}	8.30×10^{-6}	1.47×10^{-5}	1.13×10^{-6}	1.33×10^{-5}	1.07×10^{-6}
	Liver	6.74×10^{-5}	9.94×10^{-6}	5.18×10^{-5}	3.87×10^{-6}	1.87×10^{-5}	1.49×10^{-6}	1.77×10^{-5}	1.39×10^{-6}
	Kidney	2.12×10^{-4}	1.66×10^{-5}	2.21×10^{-4}	3.43×10^{-5}	5.98×10^{-5}	5.25×10^{-6}	6.57×10^{-5}	5.07×10^{-6}
NDUFS4 [Nuc]	Heart	1.27×10^{-1}	2.16×10^{-2}	1.14×10^{-1}	9.99×10^{-3}	3.16×10^{-4}	1.42×10^{-5}	2.62×10^{-4}	9.92×10^{-6}
	Liver	4.00×10^{-2}	4.66×10^{-3}	3.25×10^{-2}	3.51×10^{-3}	5.84×10^{-5}	4.70×10^{-6}	6.70×10^{-5} [b]	4.74×10^{-6}
	Kidney	1.21×10^{-1}	1.05×10^{-2}	1.11×10^{-1}	7.48×10^{-3}	3.76×10^{-4}	3.05×10^{-5}	4.22×10^{-4}	2.77×10^{-5}
NDUFS8 [Nuc]	Heart	1.36×10^{-3}	2.14×10^{-4}	1.25×10^{-3}	7.05×10^{-5}	2.99×10^{-4}	1.82×10^{-5}	2.06×10^{-4} [a]	9.44×10^{-6}
	Liver	2.64×10^{-4}	5.69×10^{-5}	1.73×10^{-4}	3.62×10^{-5}	1.06×10^{-4}	8.09×10^{-6}	1.04×10^{-4}	5.06×10^{-6}
	Kidney	9.37×10^{-4}	6.58×10^{-5}	8.89×10^{-4}	5.06×10^{-5}	3.31×10^{-4}	3.18×10^{-5}	3.17×10^{-4}	2.02×10^{-5}
Complex II		$n=8$		$n=8$		$n=6$		$n=6$	
SDHA [Nuc]	Heart	1.52×10^{-3}	7.68×10^{-5}	1.40×10^{-3}	1.34×10^{-4}	2.21×10^{-3}	1.25×10^{-4}	2.00×10^{-3}	1.16×10^{-4}
	Liver	2.71×10^{-4}	3.75×10^{-5}	2.09×10^{-4}	1.99×10^{-5}	1.08×10^{-3}	9.17×10^{-5}	8.88×10^{-4}	9.30×10^{-5}
	Kidney	6.93×10^{-4}	4.58×10^{-5}	6.57×10^{-4}	2.59×10^{-5}	5.12×10^{-3}	5.08×10^{-4}	5.66×10^{-3}	5.07×10^{-4}
SDHB [Nuc]	Heart	2.80×10^{-4}	7.66×10^{-6}	2.58×10^{-4}	1.73×10^{-5}	8.76×10^{-4}	4.84×10^{-5}	7.41×10^{-4}	3.18×10^{-5}
	Liver	7.47×10^{-5}	1.91×10^{-5}	4.61×10^{-5}	1.26×10^{-5}	3.71×10^{-4}	3.12×10^{-5}	3.07×10^{-4}	2.74×10^{-5}
	Kidney	2.39×10^{-4}	1.65×10^{-5}	2.34×10^{-4}	1.36×10^{-5}	1.43×10^{-3}	1.04×10^{-4}	1.53×10^{-3}	1.06×10^{-4}
Complex III		$n=8$		$n=8$		$n=6$		$n=6$	
CytB [Mt]	Heart	6.14×10^{-3}	1.42×10^{-3}	6.94×10^{-3}	1.39×10^{-3}	1.72×10^{-2}	6.88×10^{-4}	1.59×10^{-2}	9.20×10^{-4}
	Liver	4.06×10^{-3}	1.37×10^{-3}	2.31×10^{-3}	3.79×10^{-5}	3.38×10^{-3}	2.84×10^{-4}	3.27×10^{-3}	2.71×10^{-4}
	Kidney	9.97×10^{-3}	2.73×10^{-5}	1.10×10^{-2}	6.92×10^{-5}	1.97×10^{-2}	1.45×10^{-3}	1.68×10^{-2}	1.71×10^{-3}
UQCRC2 [Nuc]	Heart	2.11×10^{-4}	$4.8\ \times10^{-6}$	1.92×10^{-4}	1.01×10^{-5}	1.35×10^{-3}	7.28×10^{-5}	1.26×10^{-3}	6.68×10^{-5}
	Liver	7.86×10^{-5}	1.32×10^{-5}	5.86×10^{-5}	7.80×10^{-6}	3.16×10^{-4}	2.57×10^{-5}	3.03×10^{-4}	2.28×10^{-5}

continues on next page

Table 7.7 – Continued

	Kidney	2.39×10^{-4}	1.41×10^{-5}	2.54×10^{-4}	1.26×10^{-5}	1.22×10^{-3}	1.38×10^{-4}	1.31×10^{-3}	1.06×10^{-4}
UQCRFS1 ^{Nuc}	Heart	7.96×10^{-5}	4.23×10^{-6}	7.62×10^{-5}	5.95×10^{-6}	5.29×10^{-4}	3.87×10^{-5}	4.35×10^{-4}	1.48×10^{-5}
	Liver	6.75×10^{-5}	1.48×10^{-5}	8.74×10^{-5}	1.93×10^{-5}	1.87×10^{-4}	1.71×10^{-5}	1.76×10^{-4}	1.77×10^{-5}
	Kidney	2.06×10^{-4}	9.67×10^{-6}	2.26×10^{-4}	1.30×10^{-5}	6.81×10^{-4}	7.07×10^{-5}	7.62×10^{-4}	6.05×10^{-5}
Complex IV		$n=8$		$n=8$		$n=6$		$n=6$	
COX I ^{Mt}	Heart	2.82×10^{-2}	1.59×10^{-3}	2.78×10^{-2}	2.41×10^{-3}	2.23×10^{-1}	8.57×10^{-3}	2.35×10^{-1}	1.83×10^{-2}
	Liver	1.21×10^{-2}	1.69×10^{-3}	9.74×10^{-3}	9.70×10^{-4}	6.57×10^{-2}	5.63×10^{-3}	6.65×10^{-2}	6.61×10^{-3}
	Kidney	3.75×10^{-2}	3.51×10^{-3}	3.85×10^{-2}	3.99×10^{-3}	2.17×10^{-1}	2.41×10^{-2}	2.30×10^{-1}	2.05×10^{-2}
COX II ^{Mt}	Heart	1.20×10^{-1}	7.25×10^{-3}	1.12×10^{-1}	9.38×10^{-3}	6.24×10^{-2}	3.89×10^{-3}	6.36×10^{-2}	4.24×10^{-3}
	Liver	3.28×10^{-2}	4.66×10^{-3}	2.69×10^{-2}	2.53×10^{-3}	1.55×10^{-2}	8.28×10^{-4}	1.60×10^{-2}	1.12×10^{-3}
	Kidney	1.26×10^{-1}	9.69×10^{-3}	1.12×10^{-1}	7.67×10^{-3}	6.96×10^{-2}	4.81×10^{-3}	8.26×10^{-2}	9.70×10^{-3}
COX III ^{Mt}	Heart	1.30×10^{-2}	9.46×10^{-4}	1.14×10^{-2}	1.19×10^{-3}	2.30×10^{-1}	1.11×10^{-2}	2.14×10^{-1}	2.14×10^{-2}
	Liver	4.00×10^{-3}	5.99×10^{-4}	3.49×10^{-3}	2.61×10^{-4}	4.67×10^{-2}	4.03×10^{-3}	4.44×10^{-2}	3.56×10^{-3}
	Kidney	1.49×10^{-2}	1.03×10^{-3}	1.37×10^{-2}	1.30×10^{-3}	2.25×10^{-1}	2.54×10^{-2}	2.25×10^{-1}	1.83×10^{-2}
COX IV ^{Nuc}	Heart	5.88×10^{-4}	2.23×10^{-5}	5.46×10^{-4}	4.04×10^{-5}	1.38×10^{-3}	1.01×10^{-4}	1.23×10^{-3}	6.04×10^{-5}
	Liver	2.02×10^{-4}	2.98×10^{-5}	1.58×10^{-4}	2.21×10^{-5}	5.29×10^{-4}	3.56×10^{-5}	5.22×10^{-4}	4.21×10^{-5}
	Kidney	9.76×10^{-4}	5.53×10^{-5}	9.69×10^{-4}	1.26×10^{-4}	1.59×10^{-3}	1.23×10^{-4}	1.74×10^{-3}	9.97×10^{-5}
COX Vb ^{Nuc}	Heart	1.69×10^{-3}	8.75×10^{-5}	1.52×10^{-3}	1.13×10^{-4}	1.23×10^{-3}	7.71×10^{-5}	9.93×10^{-4}	4.95×10^{-5}
	Liver	6.79×10^{-4}	7.99×10^{-5}	5.74×10^{-4}	2.95×10^{-5}	5.18×10^{-4}	4.30×10^{-5}	5.42×10^{-4}	4.05×10^{-5}
	Kidney	2.29×10^{-3}	1.36×10^{-4}	2.32×10^{-3}	1.17×10^{-4}	2.01×10^{-3}	1.23×10^{-4}	2.19×10^{-3}	1.13×10^{-4}
Complex V		$n=8$		$n=8$		$n=6$		$n=6$	
ATP6 ^{Mt}	Heart	2.10×10^{-4}	2.85×10^{-5}	1.86×10^{-4}	2.02×10^{-5}	2.84×10^{-1}	1.41×10^{-2}	3.07×10^{-1}	2.46×10^{-2}
	Liver	6.71×10^{-4}	1.29×10^{-4}	4.67×10^{-4}	7.90×10^{-5}	8.49×10^{-2}	8.39×10^{-3}	8.05×10^{-2}	7.42×10^{-3}
	Kidney	2.96×10^{-3}	1.56×10^{-4}	2.99×10^{-3}	1.48×10^{-4}	3.67×10^{-1}	3.31×10^{-2}	3.71×10^{-1}	2.77×10^{-2}
ATP8 ^{Mt}	Heart	5.57×10^{-6}	2.94×10^{-7}	4.78×10^{-6}	3.94×10^{-7}	6.94×10^{-1}	3.21×10^{-2}	7.63×10^{-2}	7.26×10^{-2}
	Liver	9.97×10^{-6}	1.50×10^{-6}	7.39×10^{-6}	8.57×10^{-7}	1.70×10^{-1}	1.49×10^{-2}	1.73×10^{-1}	1.45×10^{-2}

continues on next page

Table 7.7 – Continued

	Kidney	1.99×10^{-5}	1.42×10^{-6}	1.87×10^{-5}	9.66×10^{-7}	8.05×10^{-1}	8.37×10^{-2}	8.28×10^{-1}	6.81×10^{-2}
ATP5O ^{Nuc}	Heart	9.11×10^{-4}	2.58×10^{-5}	8.27×10^{-4}	4.03×10^{-5}	3.72×10^{-4}	2.57×10^{-5}	3.14×10^{-4}	1.89×10^{-5}
	Liver	4.41×10^{-4}	5.02×10^{-5}	3.50×10^{-4}	3.61×10^{-5}	1.39×10^{-4}	1.29×10^{-5}	1.21×10^{-4}	8.65×10^{-6}
	Kidney	9.77×10^{-4}	3.77×10^{-5}	9.82×10^{-4}	6.92×10^{-5}	6.88×10^{-4}	2.44×10^{-5}	7.41×10^{-4}	2.79×10^{-5}
Others		$n=8$		$n=8$		$n=6$		$n=6$	
CYCS ^{Nuc}	Heart	3.15×10^{-4}	1.00×10^{-5}	2.79×10^{-4}	2.27×10^{-5}	1.75×10^{-3}	1.29×10^{-4}	1.13×10^{-3}	3.87×10^{-5}
	Liver	1.15×10^{-4}	2.57×10^{-5}	7.83×10^{-5}	1.72×10^{-5}	4.51×10^{-4}	3.12×10^{-5}	4.66×10^{-4} [b]	4.68×10^{-5}
	Kidney	5.05×10^{-4}	2.84×10^{-5}	4.87×10^{-4}	3.40×10^{-5}	3.98×10^{-3}	4.27×10^{-4}	0.39×10^{-3}	3.44×10^{-4}
ANT1 ^{Nuc}	Heart	1.91×10^{-4}	8.82×10^{-6}	1.88×10^{-4}	1.07×10^{-5}	8.04×10^{-3}	5.35×10^{-4}	4.82×10^{-3} [a]	1.94×10^{-4}
	Liver	9.72×10^{-5}	1.30×10^{-5}	7.66×10^{-5}	7.63×10^{-6}	1.96×10^{-4}	1.54×10^{-5}	2.00×10^{-4}	1.03×10^{-5}
	Kidney	3.07×10^{-4}	1.68×10^{-5}	3.34×10^{-4}	4.87×10^{-5}	2.36×10^{-3}	2.01×10^{-4}	2.63×10^{-3}	2.45×10^{-4}
ANT2 ^{Nuc}	Heart	2.60×10^{-1}	1.55×10^{-2}	2.43×10^{-1}	2.01×10^{-2}	2.55×10^{-4}	1.51×10^{-5}	1.87×10^{-4}	1.29×10^{-5}
	Liver	8.11×10^{-2}	1.17×10^{-2}	6.51×10^{-2}	6.68×10^{-3}	1.08×10^{-3}	6.41×10^{-5}	1.12×10^{-3}	8.38×10^{-5}
	Kidney	3.35×10^{-1}	2.12×10^{-2}	2.99×10^{-1}	1.62×10^{-2}	5.18×10^{-3}	4.70×10^{-4}	5.9×10^{-3} [c]	4.53×10^{-4}

Transcripts upperscript denotes if it is *Mt* (mitochondrial) or *Nuc* (nuclear) -encoded. For statistical analysis, tabulated values were *log* transformed and differences in fold-change of each tissue were detected by a two-way ANOVA with planned contrasts and adjusted for multiple comparisons through the Sidak test (see 4.19, p. 110):
[a] $p\geq 0.05$ heart *vs* liver and heart *vs* kidney;
[b] $p\geq 0.05$ heart *vs* liver;
[c] $p\geq 0.05$ heart *vs* kidney;
Sub-chronic and acute model were analyzed independently.
Abbreviations: *SE* - standard error; *Mt* - mitochondrial; *Nuc* - nuclear.

comparing to the sub-chronic (Fig. 7.5).

7.3 Discussion

In the context of MCA, control coefficient is defined by the extent to which an enzyme in a specific pathway controls the flux. Moreover, if more than one enzyme is present in the network, the sum of all control coefficient must equal 1 (summation theorem)[328]. Therefore, if one enzyme completely controls the flux ($C_j^I \sim 1$) the global flux and isolated step curves would be superimposable. However, most of biological pathways do not present a true rate-limiting step enzyme hence, their C_j^I would fall between 0.1 to 0.8 [328]. In this case, the global and isolated step curves would be distinct with the former adapting a sigmoidal shape rather than the typical hyperbolic function of the isolated step because the flux is shared between several enzymes or there are enzyme reserves that become available once the pre-active ones are inhibited.

In our experimental conditions, the global flux curves were distinct between tissues for all the respiratory complexes studied (Fig. 7.1), probably reflecting intrinsic differences between each tissue. In fact, not only the maximal state 3 respiration rate (Table 7.1) was different between tissues as the fitted parameter E_j^0, which reflects the amount of non-inhibited enzyme, also followed the same pattern of contrast. Nonetheless, the determined control coefficients, in our experimental conditions, were low and largely distributed, demonstrating that OXPHOS is not controlled by a single enzyme or limiting step (Table 7.5), as previously reported ([266] and references therein).

Despite what occurred in liver tissue, ANT had low control (C_j^I) in our experimental setup indicating that ADP supply was not a limiting step. A possible explanation for the discrepancy may be due to the different levels of available enzyme (E_j^0) which is 2-3 times lower in liver mitochondria in comparison to other tissues (Table 7.2). Nevertheless, analysis of control coefficient distribution has shown that heart and liver are primarily controlled by the MRC while kidney is not. One must not forget that the network of oxygen consumption in the presence of ADP includes the contribution of at least two others important enzymes that would also contribute to the flux control, and which we have not measured: Complex V and the phosphate carrier [266]. Hence, with this fact in mind, it may be acceptable to infer that kidney may be primarily controlled at the phosphorylation level as previously reported [266]. Moreover, the control coefficients determined and presented in this chapter are close to the ones

already reported ([266] and references therein). The few exceptions may be related to differences in buffer composition, temperature, pH as well as the respiratory substrates used, all of which have been reported to be critical variables in the determination of these coefficients [219].

DOX treatment caused a left-shift in the flux curve for Complex III in all tissues indicating that the amount of enzyme activity may be decreased in this situation. However, maximal enzyme (theoretical) content Complex III was found decreased solely in the liver. Furthermore, IC_{50} values for this complex remained the same after the treatment for all the analyzed tissues. Therefore, curve shift may be better explained through the framework of MCA [328], i.e. in a given metabolic network, individual step perturbations are *buffered* through kinetic properties of the enzymes, structure of the system or the intermediary pools of intermediates. However, it was surprising and still unclear at this time that these alterations did not cause any modification in the threshold curve profiles for Complex III.

In the present chapter the threshold curves were simulated by using fitting parameters of the experimental data from the global flux and isolated step. This is however not the standard procedure where normally the threshold curves are plotted graphically from the raw titration data, i.e. one point of the threshold curve represents the mean of several observation on both global and isolated curves for the same inhibitor concentration [329]. However, in our experimental setup the range and the inhibitor concentrations used were not shared between both experiments. Nevertheless, this approach allowed us to calculate with more certainty the threshold values for Type II by using the tangent of line at the inflection point rather than simple regression lines on the last points of the threshold curve [219].

The threshold curves as well as their respective threshold values were very similar between tissues regardless of the respiratory complex in study (Fig. 7.3 and Table 7.5), indicating that at least in our *in vitro* conditions there must be other variables to condition the observed effects on mitochondrial respiration. However, we must not forget that other cellular events may control *in vivo* the pathway, such as cellular steady state, energy demand and energy supply [219, 329]. Moreover, since all threshold values are high, this may signify that a large excess of enzyme activity exists in all tissues.

Nonetheless, DOX treatment caused a change from Type I to Type II curve for Complex IV in cardiac tissue. The change could be in part explained by one of the following

events:

a) a decrease in enzyme activity, which does not seem to be the case since maximal Complex IV activity was in fact increased in DOX-treated hearts;
b) modulation of the enzyme kinetic properties such as its K_m which could be related to alterations in the lipid environment as, for example, due to DOX interaction with cardiolipin [161];
c) buffering effect by the metabolic network.

Previous *in vitro* studies regarding drug interaction with respiratory complexes [330] demonstrated that DOX targeted preferentially Complex III and IV activity with minor effects on Complex I. It was suggested that DOX competes for cytochrome c binding sites, including cardiolipin, which is a previously described target of the drug [161]. Additionally, CYCS mRNA levels are here reported to be decreased in heart although these were not followed by lower protein content which in part could be due to the low sensitivity associated with western blot analysis which may not detect small differences between treatment groups.

Nevertheless, the increase in Complex IV activity found in heart and kidney may be related to cellular adaptation to this decrease in cytochrome c. In fact, CYCS was lower in heart when compared to liver but not in kidney. Similarly, Complex IV activity was increased in heart and kidney but not in liver. The observed increase in maximal activity *in vitro* may be related to the fact that cytochrome c content was not limiting or by an intrinsic modulation of the enzyme existed that could increase its inherent activity. In conclusion, perhaps Complex IV activity is regulated in cardiac mitochondria to compensate a possible alteration in cytochrome c. The same event could also explain the differences due to DOX treatment in the global flux curves of Complex III.

Although the mechanism for some of these alterations is unknown, cardiac tissue may not be able to respond or adapt to higher energy demands [329]. In other words, it may denote that the lower state3 respiration observed in cardiac mitochondria after DOX treatment might be due to different buffering capacities between treatment groups.

As it was pointed out before in Section 2.4.3, reports regarding OXPHOS complexes activity are not coherent among the literature [178, 193]. Although this could be a

case of treatment effects, it could also be a technical problem in the determination of enzymes activities. In the current work, we have used *state of the art* protocols optimized for the detection of mitochondrial diseases [273].

Although genetic and proteomic analysis evaluated only a small fraction of the bulk of OXPHOS complexes subunits, it is known that respiratory complexes assembly is an intricate process and even finite alterations in certain subunits levels can target the multimeric protein for degradation [331]. Nevertheless, from the selected transcripts our data does not show any particular alteration meaning that enzyme content may not alter during treatment. Additionally, as it was already pointed out [299], the use of whole heart extract may mask minor differences due to the fact that expression profile is different among each organ chamber. Interestingly, after the acute treatment the genetic profile of cardiac tissue, namely transcripts encoded by nuclear DNA, presents several alterations demonstrating the preferential affinity of DOX for DNA. These alterations could produce a transient response in cell which could be responsible for the modulation and buffering of the previous described aspects related to Complex IV.

Alternatively, the present data could also be analyzed in the light of aging theory and through comparison to a recent report which has demonstrated that the falling heart in age is proportional to loss of respiratory supercomplexes [332]. The idea that DOX decreases the reserve capacity of cardiac mitochondria is not new and the same mechanism is believed to be responsible for the decline in mitochondrial function during aging. However, Gómez et al. suggests that destabilization of inter-fibrillary mitochondrial string supercomplexes is the responsible for the decline. Moreover, the authors pointed the possible role of Complex IV in the underlying mechanism as it is the only respiratory complex present in all supercomplexes. Additionally, loss or mutation in certain subunits of Complex IV are associated with destabilization of supercomplexes [332].

Since DOX targets cardiolipin, a crucial component in the biogenesis and stabilization of supercomplexes, and its effects on Complex IV it may be rationale to consider that another possible mechanism is alteration of mitochondrial supercomplexes. However, so far no report has been found in the literature regarding this topic.

Finally, the absence of protein content alteration despite variation in mRNA levels following acute treatment could be due to higher turnover times for mitochondrial proteins in rodents [324, 325], as also explained in Discussion of Chapter 6. Nev-

ertheless, mRNA (in)stability may be increased which may explain the absence of alteration in protein content.

7.4 Conclusion

In conclusion, the present chapter demonstrates that in the experimental model used, although state 3 respiration differs between mitochondrial preparations, all are controlled through similar processes. However, it was clear that DOX treatment induced a larger alteration in the threshold of Complex IV in cardiac tissue. This may well be a reasonable explanation for the decrease in oxygen consumption during state 3 despite no alterations in the expression and content of OXPHOS proteins and even higher maximal enzyme activities. Nevertheless, current data supports once again the idea that cardiac mitochondria from DOX-treated rats might not have the fitness and elasticity to adapt themselves to higher energy demands or simply that their reserve capacity has decreased.

Acknowledgments

The present work would not be possible without contribution of the following people, therefore I am thankful to James Bjork and Annette Rod (Department of Biochemistry and Molecular Biology, University of Minnesota Medical School, Duluth, MN, US) for help in real-time qPCR; Ron Regal (Department of Mathematics and Statistics, University of Minnesota, Duluth, MN, US) for help in statistical analysis; Susana Pereira, Ludgero Tavares, Filipa Carvalho and Maria Sancha Santos (Center for Neuroscience and Cell Biology, Coimbra) for general collaboration.

Part III

Conclusion

Chapter 8

Final Discussion

8.1 Conclusion

In 1st of July, US National Institute of Health[1] reported 416 clinical trials (open studies) regarding the use of DOX in clinical practice (Fig 8.1). Fig. 8.1 shows the growing number of DOX publications indexed in MEDLINE over the past four decades. The numbers demonstrate the on-going research on DOX regarding antineoplastic and cardiotoxic activity. If the reader takes a carefully observation to those results, one may easily identify that most of the reports concern the co-administration of DOX with other chemical compound or in its lipossomal form, common attempts to counteract the well known DOX-induced cardiotoxicity.

However, a problem received great attention in the past months as a recent report submitted to the American Society of Clinical Oncology suggests that physicians need more education about following up cancer survivors [333]. Researchers found that only 6 % of primary doctors were capable of identifying the long-term side effects of four widely used chemotherapy drugs, including DOX, compared to 65 % of oncologists. Notwithstanding, with respect to DOX, almost all (95 %) oncologists identified cardiac dysfunction as its long-term side effects but only half (55 %) of the primary care physicians were able to do the same association. The conclusion of this report is clear: although oncologists scored better, as prescribing persons of chemo-drugs they often do not follow of the long-term side effects of those drugs which remain then unknown to their family medicine physician.

[1] public available at http://clinicaltrials.gov

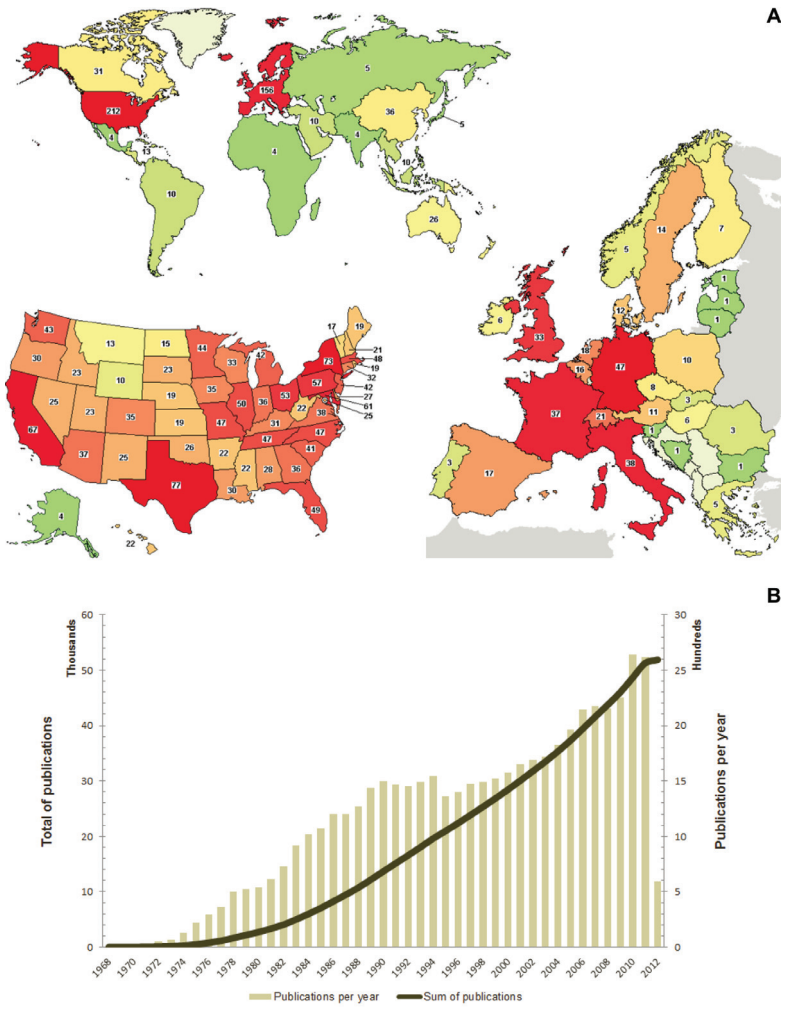

Figure 8.1: Worldwide distribution of clinical trials regarding the use of DOX (**Panel A**) and publications indexed in MEDLINE regarding the same drug over the past four decades (**Panel B**). In **A** a magnification of the US and European Union is also depicted. Data and maps were obtained from the public website http://clinicaltrials.gov (access date 1st of July). Data in **B** was collected from PubMed (http://www.ncbi.nlm.nih.gov/pubmed/; access date March).

Since the best technique nowadays to detect DOX cardiotoxicity is to continuously monitor cardiac function and since no effective counteractive strategies exist (Chapter 2), scientists still have to investigate the progress of DOX-induced cardiomyopathy and identify possible cardiac-specific and rate-limiting steps in pathways that are likely DOX targets, not only for early detection or identification of susceptible patients but

also for the developing of more advantageous preventive strategies.

The present dissertations provides results that show that mitochondrial dysfunction is a primary event during DOX-induced cardiotoxicity. Although it is not the first time that the idea disseminates throughout the scientific community, it may well be the first time that a complete mitochondrial impairment is characterized concomitantly with heart function and cardiac morphology. Moreover, alongside with the drug main target, the study was also performed in other non-target organs to better address possible key factors in DOX-induced cardiotoxicity. However, despite the recognized DOX-induced mitochondrial dysfunction, it is not the author's objective to imply that mitochondrial function should be the ultimate tool for DOX cardiotoxicity identification. In fact, it may be difficult as endomyocardial biopsy are invasive and not widely available to physicians [144].

The author suggests that therapies aimed at preserving cardiac mitochondrial function during and after the treatment should be used. In Chapter 6, it was shown that loss of mitochondrial ability to handle Ca^{2+} is involved in DOX cardiotoxicity. Therefore, targeting chemicals to cardiac mitochondria which are capable to inhibit mPTP opening are probably one of the best choices. However, the correct choice of compounds and their co-treatment schedule are crucial since data from Chapter 6 showed that decreased calcium-loading capacity is a late-onset occurrence. Therefore, it may be convenient for the physician to prescribe the preventive measure sometime after the end of treatment.

However, despite several attempts already described in the literature (see Chapter 2) none has achieved great success. Perhaps, those protective approaches simply targeted one effect that was common in the toxic response but not specific to the heart or the preventive compound used has several cellular targets (e.g. CsA). Alternatively, animal data was obtained in a model or they have tested their hypothesis in a model that was not close enough to a regular cancer patient. In fact, a tremendous number of treatment protocols exist in the literature (see Discussion of Chapter 5), most in rodents and applying high dosages of DOX and measuring the outcome sometime (not long) after the treatment. Nevertheless, in most of those cases, the researcher is administrating higher doses than those used in chemotherapy and due to the short resting period, the study dealt with acute effects rather than the most important chronic ones.

However, data collected for this dissertation may provide a new *in vivo* model of

DOX-induced cardiotoxocity closest to what is actually observed in clinical practice. Not only our sub-chronic treated animals received low sub-clinical doses of DOX as the duration of the treatment, the schedule and the method of application is, in the author's view, similar to human practice. Moreover, the subcutaneous administration may provide a resemblance to the continuous-bolus administration given in humans. However, the drug application plan is not the interesting part but the effects that it has caused in this rat strain. The same protocol has been previously applied by others in Sprague-Dawley rats which suffered from severe enlarged cardiomyopathy associated with mitochondrial dysfunction [77, 172, 185, 187, 188]. In Wistar rats (this work), mitochondrial dysfunction appeared before any alteration in ultrastructure and morphology of cardiac tissue, heart function or even before any evidence of congestive heart failure.

Since both protocols measured the outcome after the same resting time, it may mean not only that mitochondrial impairment is the cause for the progression of DOX cardiotoxicity as Wistar rats are slightly more resistant to the drug or that they express late-onset cardiomyopathy at a different time frame. However, to be certain, more work is needed or, in other words, one has to investigate if the outcome (heart function) is altered in longer time points. If positive, this model may become a powerful tool in DOX research as it will allow a wider time window where researchers could evaluate important steps during heart function decline.

Besides, the fraction of treated patients that develop chronic cardiotoxicity is small although, once diagnosed, the risk to succumbing to heart failure is quite high [147]. This demonstrates the possible host factors in the response of DOX treatment, a behavior that is somehow mimicked with this $8 + 1$ protocol where two rat strains with distinctly backgrounds responded differently. However, in the author's point of view, the conclusions should be made carefully as even though the genetic background is distinct, both strains are outbred and therefore the variability in this case become more a random/noise factor than actually a true independent variable. In the author's opinion, the discrepancy between both strains demonstrates the demand for treatments *à la carte* and in terms research approach, a true factorial design with different inbred strains to pinpoint sensitive genetic backgrounds deserves further investigation.

For those familiar with DOX studies on Sprague-Dawley and Wistar, one interesting result regarded differences in the ANT [177]. Decreased calcium-loading capacity and depressed mitochondrial respiration (state 3) were common observation in both models. However, Oliveira *et al.* suggested decreased ANT content as the main

responsible for both events. In our model, it appears that ANT may not be the key behind DOX response since its levels remained constant (titration with CATR) despite western blot quantification is still missing. Since our understanding of ANT role in the mPTP pore changed from structural to modulator (see Chapter 1), it is possible that other modulators may be responsible for DOX mitochondrial cardiotoxic response (e.g. GSK3β).

The present thesis is also novel as it introduced the mitochondrial threshold analysis in the context of DOX toxicity. No apparent distinction regarding OXPHOS respiratory threshold values between tissues was present and therefore one cannot imply that heart is more affected due to higher dependence on one in particular. Nonetheless, the reader should remember that assays were performed during state 3 respiration which reflects quite high energy demand so, *in situ* mitochondria may control differently their respiration. However, a noticeable effect was detect in Complex IV threshold after sub-chronic treatment. In the light of "binary mitochondrial heteroplasmy" [327] this could be result of:

i) low number of total mitochondria - DOX was already reported to decrease mtDNA-copy number (e.g. [318]) although interpretation should be rationale taking into account a recent report regarding the determination of mtDNA-copy number [334] which states that commonly used mtDNA primers co-amplify homologous pseudogenes found in the nuclear genome and the size difference of mitochondrial and nuclear genomes can cause a "dilution bias" in certain circumstances.
ii) co-existence of fully-active and fully-inactive mitochondria - it would mean that the targeted Complex IV would have to resideor be concentrated in some of the mitochondria which, in other words, is the same has having less *total* mitochondria. Although the other respiratory complexes are active, the full-inhibited enzyme completely blocks the flux in that precise mitochondria.
iii) partial inhibition of all Complex IV across all mitochondria - this is perchance the most plausible explanation although the same level of enzyme inhibition can have a significantly greater effect in the previous model than in an homogenous distribution [327]

Nevertheless, due to this alteration in electron transfer, cardiac mitochondria will probably fail to respond or adapt in situations of higher energy demand. As GSK3β

has also its role in supercomplexes stabilization/maintenance [335] in addition to its function in mPTP regulation [76], it may be an attractive target in DOX toxicity prevention as DOX treatment already reported low levels of the phosphorylated form of the kinase [336].

In conclusion, the present dissertation present new findings in the development of DOX cardiotoxicity by showing the *bridge* point between drug administration and (possible) late-onset cardiomyopathy. However it remains to be elucidate the factors upstream the observed mitochondrial dysfunction, i.e. enhanced sensitivity to mPTP opening and decreased threshold of Complex IV.

8.2 Future work

Although this dissertation has clarified some questions regarding DOX-induced cardiotoxicity and has provided new clues with respect to its mechanism of action, it has also opened several *doors* for DOX-induced toxicity to move forward. For example, and not in any particular order:

To the author knowledge the $8 + 1$ protocol was never tested as able to "treat" cancer in either Sprague-Dawley or Wistar rats. This would be a ultimate factor to strengthen its use as a chemotherapy protocol capable of inducing late-onset cardiotoxoxicity. The idea would be simply tested by either treating rats with spontaneous tumors due to x-ray irradiation or rats with tumor implantation. The results should show decreased tumor growth without diminished incidence of cardiotoxicity.

It would be interesting to access if the mitochondrial dysfunction here described is accompanied by the metabolic shift previously reported [195]. Although both works used the same treatment protocol, none evaluated cell metabolism and mitochondrial function simultaneously. Additionally, the outcomes were slightly different with the latter work reporting minor cellular ultrastructure alterations. Therefore, the aim of this *task* would be to address if mitochondrial dysfunction is a cause for the metabolic shift observed during the progression of heart function decline of DOX toxicity or, alternatively, a consequence of that shift which could diminish reducing equivalents for the MRC.

Huang *et al.* demonstrated that young mice treated with DOX only developed heart failure in adults when subjected to a stressful protocol [183]. Although the treatment protocol, age and strain are different as compared to our current model, it would be interesting to address if the absence of cardiomyopathy-specific end-points in our study could become detectable when animals were subjected to that type of protocol. There are several methodologies to accomplish this objective, for example, animals could be put through an exhaustive swimming or a treadmill running protocol. Alternatively, one can mimic the hemodynamic situation of congestive heart failure by inducing an acute volume overload with isotonic fluids or colloids [337]. The author hypothesizes that DOX-treated group would had a decreased adaptive response and would present noticeable hypertrophy. If confirmed, the work would corroborate the hypothesis that mitochondrial dysfunction play an important role in the decline of heart function of DOX-treated patients.

Zhou *et al.* demonstrated that DOX cardiotoxicity is cumulative and irreversible [77]. The 8+1 treatment protocol was the minimum time necessary to observe mitochondrial dysfunction and altered ultrastructure. Perhaps in the current protocol the minimum time needed to observe altered ultrastructure is larger since one is using a different rat strain. Therefore, it would be interesting to follow the evolution of DOX toxicity in these animals and access if any signs of cardiomyopathy become noticeable. If true, one may have *accidentally* created a model of cumulative and irreversible DOX toxicity closest to what is observed in humans, where most cases emerge several years after the treatment has ceased [142]

Regarding the differences between strains it would be interesting to access how the genetic background influence the phenotypic expression of the well known DOX cardiotoxicity. Currently, two strains were used under the same treatment protocol but since they are both outbred strains (heterozygous) the conclusions are ambiguous. Therefore, the author suggests a strategy to use several inbred strains in a factorial experimental design [338]. This would allow to test whether toxicity is the same across all species with the major advantage being that genetic variation is under the control of the researcher and does not contribute to *noise* which can obscure treatment effects. Moreover, several strains with few animals in

each group (e.g. 3 to 4) could be an alternative experimental design.

One aspect that remains obscure in the field is the reason for the late occurrence of DOX cardiomyopathy. This effect is sometimes referred as *toxicity memory*. The answer to this problem would be more easily addressed by means of cardiac cell lines but apart from their intrinsic limitations for extrapolations, the design for a *controlled time-lapse* experiment would be challenging.

In Chapter 7 data may suggest a possible interference in mitochondrial supercomplexes. Besides, DOX is known to interact with cardiolipin and displace its normal protein-lipid complexes [161]. Therefore, it would be interesting to access if alterations in mitochondrial bioenergetics following DOX treatment are due to destabilization of supercomplexes despite no alteration in protein content or OXPHOS enzymes activity.

Usually, when a mitochondrion is damaged, the cell attempts to remove it by means of an autophagic process. However, it might not be the case in DOX-treated hearts. The reason remains unclear and therefore it would be of interest to approach the topic of autophagy in DOX cardiotoxicity in a different perspective. This approach would aim the better understanding of why cardiomyocytes cannot remove DOX-damaged mitochondria, rather then simply evaluate if autophagic process is increase/decreased or if the process is another mechanism of cell death.

Appendix A

PubMead Search

The Venn diagram presented in Fig. 5.6, page 132, was elaborated after collecting data from the PubMed website (www.ncbi.nlm.nih.gov/pubmed) using specific *#keywords* to obtain the desired output.

Briefly, one wanted to retrieve papers in the database that included works related to the *#drug* and *#mitochondria*, restricting the output for ones performed in the defined *#tissue*, excluding *#reviews* publications and works performed in *#humans* as long as they are not indexed with other animals.

Therefore, the base of the search string was as follow:

$$(((\#mitochondria \text{ AND } \#drug) \text{ AND } \#tissue) \text{ NOT } \#reviews) \text{ NOT } \#humans \quad \text{(A.1)}$$

Further explanation about each of the keywords is given in Table I. The author recognizes that the present search string is not flawless; however, the idea is to give the reader an overview of report rankings across the selected tissues.

In fact, he acknowledges the fact that, for example, the keyword *#humans* will not include recent reports since they are yet to be indexed to MEDLINE[1].

Moreover, using search terms as *heart* or *liver* may be ambiguous as abstracts containing any possible expression resulted from automatic explosion of MeSH terms[2] will be retrieved.

[1] standing for Medical Literature Analysis and Retrieval System Online, is a bibliographic database of life sciences and biomedical information

[2] is a comprehensive controlled vocabulary thesaurus in a hierarchical structure created by the (US) National Library of Medicine for the purpose of indexing journal articles and books for MEDLINE

Table A.1: Description of keywords used in PubMed search for construction of Venn diagram of Fig. 5.6, p. 132, as well as the number of results retrieved with for each corresponding keyword.

No.	Keyword	Search term	Objective	No. results
1	*#mitochondria*	mitochondri*	truncation is used to retrieve all possible terms related to mitochondria, e.g. mitochondrion, mitochondrial, mitochondriac, mitochondrionopathy, etc.	–
2	*#drug*	(doxorubicin OR adriamycin)	sometimes reports use the term *adriamycin* rather than *doxorubicin*; allow inclusion of non-MeSH indexed reports	–
3	*#reviews*	(review[tiab] OR review[pt])	exclude review publication even if they are not yet indexed by searching the word review in title or abstract of the report	–
4	*#humans*	(humans[mh] NOT animals[mh:noexp])	exclude indexed reports performed in humans as long as they are not indexed with other animals	–
5	*#tissue*	(heart OR liver OR kidney)	reports which include any of the tissues	534
6		heart	reports which include the selected tissue but might also include any of the other non-mentioned tissues or both	447
7		liver		138
8		kidney		35
9		(heart AND liver NOT kidney)	reports which include the both selected tissues but exclude the last one	52
10		(heart AND kidney NOT liver)		1
11		(liver AND kidney NOT heart)		0
12		(heart AND liver AND kidney)	reports which include all tissues together	16

continues on next page

Table A.1 – Continued

No.	Keyword	Search term	Objective	No. results
13		(heart NOT liver NOT kidney)	reports which include only the selected tissue	378
14		(liver NOT heart NOT kidney)		69
15		(kidney NOT heart NOT liver)		17

The search strings were as follow:
(((1 AND 2) AND 5) NOT 3) NOT 4
(((1 AND 2) AND 6) NOT 3) NOT 4
(((1 AND 2) AND 7) NOT 3) NOT 4
(((1 AND 2) AND 8) NOT 3) NOT 4
(((1 AND 2) AND 9) NOT 3) NOT 4
(((1 AND 2) AND 10) NOT 3) NOT 4
(((1 AND 2) AND 11) NOT 3) NOT 4
(((1 AND 2) AND 12) NOT 3) NOT 4
(((1 AND 2) AND 13) NOT 3) NOT 4
(((1 AND 2) AND 15) NOT 3) NOT 4

Bibliography

[1] L'Engle, M. (1973) *A wind in the door*, Time Quintet. (Farrar, Straus and Giroux, New York), p. 211.

[2] Scatena, R, Bottoni, P, Botta, G, Martorana, G. E, & Giardina, B. (2007) The role of mitochondria in pharmacotoxicology: a reevaluation of an old, newly emerging topic. *Am. J. Physiol. Cell Phys.* **293**(1), C12–21.

[3] Montero, J, Mari, M, Colell, A, et al. (2010) Cholesterol and peroxidized cardiolipin in mitochondrial membrane properties, permeabilization and cell death. *Biochim. Biophys. Acta* **1797**(6-7), 1217–24.

[4] Schatz, G. (1996) The protein import system of mitochondria. *J. Biol. Chem.* **271**(50), 31763–6.

[5] Nicholls, D. G & Ferguson, S. J. (2001) *Bioenergetics 3*. (Academic Press, London, UK), 3 edition, p. 297.

[6] Hom, J & Sheu, S.-S. (2009) Morphological dynamics of mitochondria–a special emphasis on cardiac muscle cells. *J. Mol. Cell. Cardiol.* **46**(6), 811–20.

[7] Mohrman, D. E & Heller, L. J. (2010) *Cardiovascular physiology*, LANGE Physiology Series. (McGraw-Hill Medical, New York), 6 edition, p. 256.

[8] Kane, L. A & Youle, R. J. (2010) Mitochondrial fission and fusion and their roles in the heart. *J. Mol. Med.* **88**(10), 971–9.

[9] Beraud, N, Pelloux, S, Usson, Y, et al. (2009) Mitochondrial dynamics in heart cells: very low amplitude high frequency fluctuations in adult cardiomyocytes and flow motion in non beating Hl-1 cells. *J. Bioenerg. Biomembr.* **41**(2), 195–214.

[10] Michaelis, L. (1899) Die vitale Färbung, eine Darstellungsmethode der Zellgranula. *Archiv fur Mikroskopische Anatomie* **55**(1), 558–575.

[11] Ernster, L & Schatz, G. (1981) Mitochondria: a historical review. *J. Cell Biol.* **91**(3 Pt 2), 227s–255s.

[12] Slater, E. C. (1953) Mechanism of phosphorylation in the respiratory chain. *Nature* **172**(4387), 975–8.

[13] Nelson, D. L & Cox, M. M. (2008) *Lehninger Principles of Biochemistry*. (W. H. Freeman, New York), 5 edition, p. 1100.

[14] Boyer, P. D. (1965) *Oxidases and related redox systems*, eds. King, T. E, HS, M, & M, M. (A.R. Liss), pp. 994–1008.

[15] Mitchell, P. (1961) Coupling of phosphorylation to electron and hydrogen transfer by a chemi-osmotic type of mechanism. *Nature* **191**, 144–8.

[16] Mitchell, P. (2011) Chemiosmotic coupling in oxidative and photosynthetic phosphorylation. 1966. *Biochim. Biophys. Acta* **1807**(12), 1507–38.

[17] Nicholls, D. G. (2010) Mitochondrial ion circuits. *Essays Biochem.* **47**, 25–35.

[18] Arechederra, R & Minteer, S. (2008) Organelle-based biofuel cells: Immobilized mitochondria on carbon paper electrodes. *Electrochim. Acta* **53**(23), 6698–6703.

[19] de Bari, L, Atlante, A, Guaragnella, N, Principato, G, & Passarella, S. (2002) D-Lactate transport and metabolism in rat liver mitochondria. *Biochem. J.* **365**(Pt 2), 391–403.

[20] Wikström, M, Krab, K, & Saraste, M. (1981) Proton-translocating cytochrome complexes. *Annu. Rev. Biochem.* **50**, 623–55.

[21] Wikström, M & Krab, K. (1979) Proton-pumping cytochrome c oxidase. *Biochim. Biophys. Acta* **549**(2), 177–22.

[22] Gnaiger, E. (2007) *Mitochondrial Pathways and Respiratory Control.* ed. Gnaiger, E. (OROBOROS MiPNet Publications, Innsbruck), 1st edition, p. 96.

[23] Rich, P. R & Maréchal, A. (2010) The mitochondrial respiratory chain. *Essays Biochem.* **47**, 1–23.

[24] De Giorgi, F, Brini, M, Bastianutto, C, et al. (1996) Targeting aequorin and green fluorescent protein to intracellular organelles. *Gene* **173**(1 Spec No), 113–7.

[25] D'Souza, G. G. M, Rammohan, R, Cheng, S.-M, Torchilin, V. P, & Weissig, V. (2003) DQAsome-mediated delivery of plasmid DNA toward mitochondria in living cells. *J. Controlled Release* **92**(1-2), 189–97.

[26] Murphy, M. P & Smith, R. A. (2007) Targeting antioxidants to mitochondria by conjugation to lipophilic cations. *Annu. Rev. Pharmacol. Toxicol.* **47**, 629–56.

[27] Anderson, S, Bankier, A. T, Barrell, B. G, et al. (1981) Sequence and organization of the human mitochondrial genome. *Nature* **290**(5806), 457–65.

[28] Gibson, D. G, Smith, H. O, Hutchison, C. A, Venter, J. C, & Merryman, C. (2010) Chemical synthesis of the mouse mitochondrial genome. *Nat. Methods* **7**(11), 901–3.

[29] Keeney, P. M, Quigley, C. K, Dunham, L. D, et al. (2009) Mitochondrial gene therapy augments mitochondrial physiology in a Parkinson's disease cell model. *Hum. Gene Ther.* **20**(8), 897–907.

[30] Rossignol, R, Faustin, B, Rocher, C, et al. (2003) Mitochondrial threshold effects. *Biochem. J.* **370**(Pt 3), 751–62.

[31] Duchen, M. R & Szabadkai, G. (2010) Roles of mitochondria in human disease. *Essays Biochem.* **47**, 115–37.

[32] Picard, M, Taivassalo, T, Ritchie, D, et al. (2011) Mitochondrial structure and function are disrupted by standard isolation methods. *PLoS One* **6**(3), e18317.

[33] Brandt, U. (2006) Energy converting NADH:quinone oxidoreductase (complex I). *Annu. Rev. Biochem.* **75**, 69–92.

[34] Tran, Q. M, Rothery, R. A, Maklashina, E, Cecchini, G, & Weiner, J. H. (2006) The quinone binding site in Escherichia coli succinate dehydrogenase is required for

electron transfer to the heme b. *J. Biol. Chem.* **281**(43), 32310–7.

[35] Covian, R & Trumpower, B. L. (2008) The dimeric structure of the cytochrome bc(1) complex prevents center P inhibition by reverse reactions at center N. *Biochim. Biophys. Acta* **1777**(7-8), 1044–52.

[36] Brzezinski, P & Gennis, R. B. (2008) Cytochrome c oxidase: exciting progress and remaining mysteries. *J. Bioenerg. Biomembr.* **40**(5), 521–31.

[37] Dickson, V. K, Silvester, J. A, Fearnley, I. M, Leslie, A. G. W, & Walker, J. E. (2006) On the structure of the stator of the mitochondrial ATP synthase. *EMBO J.* **25**(12), 2911–8.

[38] Yoshida, M, Muneyuki, E, & Hisabori, T. (2001) ATP synthase–a marvellous rotary engine of the cell. *Nat. Rev. Mol. Cell Biol.* **2**(9), 669–77.

[39] Sambongi, Y, Iko, Y, Tanabe, M, et al. (1999) Mechanical rotation of the c subunit oligomer in ATP synthase (F0F1): direct observation. *Science* **286**(5445), 1722–1724.

[40] Boyer, P. D. (2002) Catalytic site occupancy during ATP synthase catalysis. *FEBS Lett.* **512**(1-3), 29–32.

[41] Okuno, D, Iino, R, & Noji, H. (2011) Rotation and structure of FoF1-ATP synthase. *J. Biochem.* **149**(6), 655–64.

[42] Dudkina, N. V, Kouril, R, Peters, K, Braun, H.-P, & Boekema, E. J. (2010) Structure and function of mitochondrial supercomplexes. *Biochim. Biophys. Acta* **1797**(6-7), 664–70.

[43] Schägger, H & Pfeiffer, K. (2000) Supercomplexes in the respiratory chains of yeast and mammalian mitochondria. *EMBO J.* **19**(8), 1777–83.

[44] Claypool, S. M. (2009) Cardiolipin, a critical determinant of mitochondrial carrier protein assembly and function. *Biochim. Biophys. Acta* **1788**(10), 2059–68.

[45] Chen, C, Ko, Y, Delannoy, M, et al. (2004) Mitochondrial ATP synthasome: three-dimensional structure by electron microscopy of the ATP synthase in complex formation with carriers for Pi and ADP/ATP. *J. Biol. Chem.* **279**(30), 31761–8.

[46] Carafoli, E. (2010) The fateful encounter of mitochondria with calcium: how did it happen? *Biochim. Biophys. Acta* **1797**(6-7), 595–606.

[47] De Stefani, D, Raffaello, A, Teardo, E, Szabò, I, & Rizzuto, R. (2011) A forty-kilodalton protein of the inner membrane is the mitochondrial calcium uniporter. *Nature* **476**(7360), 336–40.

[48] Contreras, L, Drago, I, Zampese, E, & Pozzan, T. (2010) Mitochondria: the calcium connection. *Biochim. Biophys. Acta* **1797**(6-7), 607–18.

[49] Santo-Domingo, J & Demaurex, N. (2010) Calcium uptake mechanisms of mitochondria. *Biochim. Biophys. Acta* **1797**(6-7), 907–12.

[50] Rizzuto, R, Pinton, P, Carrington, W, et al. (1998) Close contacts with the endoplasmic reticulum as determinants of mitochondrial Ca2+ responses. *Science* **280**(5370), 1763–1766.

[51] Pacher, P, Csordás, P, Schneider, T, & Hajnóczky, G. (2000) Quantification of calcium signal transmission from sarco-endoplasmic reticulum to the mitochondria. *J. Phys.* **529 Pt 3**, 553–64.

[52] Gunter, T. E & Gunter, K. K. (2001) Uptake of calcium by mitochondria: transport and possible function. *IUBMB Life* **52**(3-5), 197–204.

[53] Szabadkai, G & Duchen, M. R. (2008) Mitochondria: the hub of cellular Ca2+ signaling. *Physiology* **23**, 84–94.

[54] Feissner, R. F, Skalska, J, Gaum, W. E, & Sheu, S.-S. (2009) Crosstalk signaling between mitochondrial Ca2+ and ROS. *Front. Biosci.* **14**, 1197–218.

[55] Gellerich, F. N, Gizatullina, Z, Trumbeckaite, S, et al. (2010) The regulation of OXPHOS by extramitochondrial calcium. *Biochim. Biophys. Acta* **1797**(6-7), 1018–27.

[56] Gunter, T. E, Yule, D. I, Gunter, K. K, Eliseev, R. A, & Salter, J. D. (2004) Calcium and mitochondria. *FEBS Lett.* **567**(1), 96–102.

[57] Gincel, D, Zaid, H, & Shoshan-Barmatz, V. (2001) Calcium binding and translocation by the voltage-dependent anion channel: a possible regulatory mechanism in mitochondrial function. *Biochem. J.* **358**(Pt 1), 147–55.

[58] Lemasters, J. J & Holmuhamedov, E. (2006) Voltage-dependent anion channel (VDAC) as mitochondrial governator–thinking outside the box. *Biochim. Biophys. Acta* **1762**(2), 181–90.

[59] Shoshan-Barmatz, V & Ben-Hail, D. (2012) VDAC, a multi-functional mitochondrial protein as a pharmacological target. *Mitochondrion* **12**(1), 24–34.

[60] Hajnóczky, G, Csordás, G, & Yi, M. (2002) Old players in a new role: mitochondria-associated membranes, VDAC, and ryanodine receptors as contributors to calcium signal propagation from endoplasmic reticulum to the mitochondria. *Cell Calcium* **32**(5-6), 363–77.

[61] O'Rourke, B. (2007) Mitochondrial ion channels. *Annu. Rev. Physiol.* **69**, 19–49.

[62] Pagliarini, D. J, Calvo, S. E, Chang, B, et al. (2008) A mitochondrial protein compendium elucidates complex I disease biology. *Cell* **134**(1), 112–23.

[63] Baughman, J. M, Perocchi, F, Girgis, H. S, et al. (2011) Integrative genomics identifies MCU as an essential component of the mitochondrial calcium uniporter. *Nature* **476**(7360), 341–5.

[64] Perocchi, F, Gohil, V. M, Girgis, H. S, et al. (2010) MICU1 encodes a mitochondrial EF hand protein required for Ca(2+) uptake. *Nature* **467**(7313), 291–6.

[65] Buntinas, L, Gunter, K. K, Sparagna, G. C, & Gunter, T. E. (2001) The rapid mode of calcium uptake into heart mitochondria (RaM): comparison to RaM in liver mitochondria. *Biochim. Biophys. Acta* **1504**(2-3), 248–61.

[66] Drago, I, Pizzo, P, & Pozzan, T. (2011) After half a century mitochondrial calcium in- and efflux machineries reveal themselves. *EMBO J.* **30**(20), 4119–25.

[67] Jiang, D, Zhao, L, & Clapham, D. E. (2009) Genome-wide RNAi screen identifies Letm1 as a mitochondrial Ca2+/H+ antiporter. *Science* **326**(5949), 144–7.

[68] Halestrap, A. P, Clarke, S. J, & Javadov, S. A. (2004) Mitochondrial permeability transition pore opening during myocardial reperfusion–a target for cardioprotection. *Cardiovasc. Res.* **61**(3), 372–85.

[69] Zoratti, M, De Marchi, U, Gulbins, E, & Szabò, I. (2009) Novel channels of the inner mitochondrial membrane. *Biochim. Biophys. Acta* **1787**(5), 351–63.

[70] Halestrap, A. P. (2009) Mitochondria and reperfusion injury of the heart–a holey death but not beyond salvation. *J. Bioenerg. Biomembr.* **41**(2), 113–21.

[71] Crompton, M. (1999) The mitochondrial permeability transition pore and its role in cell death. *Biochem. J.* **341 Pt 2**, 233–49.

[72] Singh, B. K, Tripathi, M, Pandey, P. K, & Kakkar, P. (2011) Alteration in mitochondrial thiol enhances calcium ion dependent membrane permeability transition and dysfunction in vitro: a cross-talk between mtThiol, Ca(2+), and ROS. *Mol. Cell. Biochem.* **357**(1-2), 373–85.

[73] Baines, C. P. (2009) The mitochondrial permeability transition pore and ischemia-reperfusion injury. *Basic Res. Cardiol.* **104**(2), 181–8.

[74] Kass, G. E. N. (2006) Mitochondrial involvement in drug-induced hepatic injury. *Chem. Biol. Interact.* **163**(1-2), 145–59.

[75] Gogvadze, V, Orrenius, S, & Zhivotovsky, B. (2009) Mitochondria as targets for cancer chemotherapy. *Semin. Cancer Biol.* **19**(1), 57–66.

[76] Rasola, A, Sciacovelli, M, Pantic, B, & Bernardi, P. (2010) Signal transduction to the permeability transition pore. *FEBS Lett.* **584**(10), 1989–96.

[77] Zhou, S, Starkov, A, Froberg, M. K, Leino, R. L, & Wallace, K. B. (2001) Cumulative and irreversible cardiac mitochondrial dysfunction induced by doxorubicin. *Cancer Res.* **61**(2), 771–7.

[78] Solem, L. E & Wallace, K. B. (1993) Selective activation of the sodium-independent, cyclosporin A-sensitive calcium pore of cardiac mitochondria by doxorubicin. *Toxicol. Appl. Pharmacol.* **121**(1), 50–7.

[79] Sokolove, P. M. (1990) Inhibition by cyclosporin A and butylated hydroxytoluene of the inner mitochondrial membrane permeability transition induced by adriamycin aglycones. *Biochem. Pharmacol.* **40**(12), 2733–6.

[80] Machado, N. G, Alves, M. G, Carvalho, R. A, & Oliveira, P. J. (2009) Mitochondrial involvement in cardiac apoptosis during ischemia and reperfusion: can we close the box? *Cardiovasc. Toxicol.* **9**(4), 211–27.

[81] Javadov, S, Karmazyn, M, & Escobales, N. (2009) Mitochondrial permeability transition pore opening as a promising therapeutic target in cardiac diseases. *J. Pharmacol. Exp. Ther.* **330**(3), 670–8.

[82] Juhaszova, M, Wang, S, Zorov, D. B, et al. (2008) The identity and regulation of the mitochondrial permeability transition pore: where the known meets the unknown. *Ann. N. Y. Acad. Sci.* **1123**, 197–212.

[83] Leung, A. W. C & Halestrap, A. P. (2008) Recent progress in elucidating the molecular mechanism of the mitochondrial permeability transition pore. *Biochim. Biophys. Acta* **1777**(7-8), 946–52.

[84] Woodfield, K, Rück, A, Brdiczka, D, & Halestrap, A. P. (1998) Direct demonstration of a specific interaction between cyclophilin-D and the adenine nucleotide translocase confirms their role in the mitochondrial permeability transition. *Biochem. J.* **336 (Pt 2**, 287–90.

[85] Crompton, M, Ellinger, H, & Costi, A. (1988) Inhibition by cyclosporin A of a Ca2+-dependent pore in heart mitochondria activated by inorganic phosphate and oxidative

stress. *Biochem. J.* **255**(1), 357–60.

[86] Baines, C. P, Kaiser, R. A, Purcell, N. H, et al. (2005) Loss of cyclophilin D reveals a critical role for mitochondrial permeability transition in cell death. *Nature* **434**(7033), 658–62.

[87] He, L & Lemasters, J. J. (2002) Regulated and unregulated mitochondrial permeability transition pores: a new paradigm of pore structure and function? *FEBS Lett.* **512**(1-3), 1–7.

[88] Kokoszka, J. E, Waymire, K. G, Levy, S. E, et al. (2004) The ADP/ATP translocator is not essential for the mitochondrial permeability transition pore. *Nature* **427**(6973), 461–5.

[89] Nakagawa, T, Shimizu, S, Watanabe, T, et al. (2005) Cyclophilin D-dependent mitochondrial permeability transition regulates some necrotic but not apoptotic cell death. *Nature* **434**(7033), 652–8.

[90] Schinzel, A. C, Takeuchi, O, Huang, Z, et al. (2005) Cyclophilin D is a component of mitochondrial permeability transition and mediates neuronal cell death after focal cerebral ischemia. *Proc. Natl. Acad. Sci. U. S. A.* **102**(34), 12005–10.

[91] Basso, E, Fante, L, Fowlkes, J, et al. (2005) Properties of the permeability transition pore in mitochondria devoid of Cyclophilin D. *J. Biol. Chem.* **280**(19), 18558–61.

[92] Baines, C. P. (2011) The mitochondrial permeability transition pore and the cardiac necrotic program. *Pediatr. Cardiol.* **32**(3), 258–62.

[93] Leung, A. W. C, Varanyuwatana, P, & Halestrap, A. P. (2008) The mitochondrial phosphate carrier interacts with cyclophilin D and may play a key role in the permeability transition. *J. Biol. Chem.* **283**(39), 26312–23.

[94] Basso, E, Petronilli, V, Forte, M. A, & Bernardi, P. (2008) Phosphate is essential for inhibition of the mitochondrial permeability transition pore by cyclosporin A and by cyclophilin D ablation. *J. Biol. Chem.* **283**(39), 26307–11.

[95] Giorgio, V, Soriano, M. E, Basso, E, et al. (2010) Cyclophilin D in mitochondrial pathophysiology. *Biochim. Biophys. Acta* **1797**(6-7), 1113–8.

[96] Varanyuwatana, P & Halestrap, A. P. (2012) The roles of phosphate and the phosphate carrier in the mitochondrial permeability transition pore. *Mitochondrion* **12**(1), 120–5.

[97] Traba, J, Del Arco, A, Duchen, M. R, Szabadkai, G, & Satrústegui, J. (2012) SCaMC-1 promotes cancer cell survival by desensitizing mitochondrial permeability transition via ATP/ADP-mediated matrix Ca(2+) buffering. *Cell Death Differ.* **19**(4), 650–60.

[98] Chinopoulos, C & Adam-Vizi, V. (2012) Modulation of the mitochondrial permeability transition by cyclophilin D: moving closer to F(0)-F(1) ATP synthase? *Mitochondrion* **12**(1), 41–5.

[99] Boveris, A, Oshino, N, & Chance, B. (1972) The cellular production of hydrogen peroxide. *Biochem. J.* **128**(3), 617–30.

[100] Murphy, M. P. (2009) How mitochondria produce reactive oxygen species. *Biochem. J.* **417**(1), 1–13.

[101] Aon, M. A, Cortassa, S, & O'Rourke, B. (2010) Redox-optimized ROS balance: a unifying hypothesis. *Biochim. Biophys. Acta* **1797**(6-7), 865–77.

[102] Brown, G. C & Borutaite, V. (2012) There is no evidence that mitochondria are the

main source of reactive oxygen species in mammalian cells. *Mitochondrion* **12**(1), 1–4.

[103] Chance, B, Sies, H, & Boveris, A. (1979) Hydroperoxide metabolism in mammalian organs. *Physiol. Rev.* **59**(3), 527–605.

[104] Forman, H. J, Maiorino, M, & Ursini, F. (2010) Signaling functions of reactive oxygen species. *Biochemistry* **49**(5), 835–42.

[105] Jones, D. P. (2006) Disruption of mitochondrial redox circuitry in oxidative stress. *Chem. Biol. Interact.* **163**(1-2), 38–53.

[106] Forkink, M, Smeitink, J. A. M, Brock, R, Willems, P. H. G. M, & Koopman, W. J. H. (2010) Detection and manipulation of mitochondrial reactive oxygen species in mammalian cells. *Biochim. Biophys. Acta* **1797**(6-7), 1034–44.

[107] Jastroch, M, Divakaruni, A. S, Mookerjee, S, Treberg, J. R, & Brand, M. D. (2010) Mitochondrial proton and electron leaks. *Essays Biochem.* **47**, 53–67.

[108] Marcus, R & Sutin, N. (1985) Electron transfers in chemistry and biology. *BBA. Reviews on Bioenergetics* **811**(3), 265–322.

[109] Moser, C. C, Farid, T. A, Chobot, S. E, & Dutton, P. L. (2006) Electron tunneling chains of mitochondria. *Biochim. Biophys. Acta* **1757**(9-10), 1096–109.

[110] Andreyev, A. Y, Kushnareva, Y. E, & Starkov, A. A. (2005) Mitochondrial metabolism of reactive oxygen species. *Biochemistry (Moscow)* **70**(2), 200–14.

[111] Lambert, A. J & Brand, M. D. (2009) Reactive oxygen species production by mitochondria. *Methods Mol. Biol.* **554**, 165–81.

[112] Starkov, A. A. (1997) "Mild" uncoupling of mitochondria. *Biosci. Rep.* **17**(3), 273–279.

[113] Go, Y.-M & Jones, D. P. (2008) Redox compartmentalization in eukaryotic cells. *Biochim. Biophys. Acta* **1780**(11), 1273–90.

[114] Meredith, M. J & Reed, D. J. (1982) Status of the mitochondrial pool of glutathione in the isolated hepatocyte. *J. Biol. Chem.* **257**(7), 3747–53.

[115] Cocco, T, Cutecchia, G, Montedoro, G, & Lorusso, M. (2002) The antihypertensive drug carvedilol inhibits the activity of mitochondrial NADH-ubiquinone oxidoreductase. *J. Bioenerg. Biomembr.* **34**(4), 251–8.

[116] Sedelnikova, O. A, Redon, C. E, Dickey, J. S, et al. (2010) Role of oxidatively induced DNA lesions in human pathogenesis. *Mutat. Res.* **704**(1-3), 152–9.

[117] Tsutsui, H, Kinugawa, S, & Matsushima, S. (2009) Mitochondrial oxidative stress and dysfunction in myocardial remodelling. *Cardiovasc. Res.* **81**(3), 449–56.

[118] Hori, M & Nishida, K. (2009) Oxidative stress and left ventricular remodelling after myocardial infarction. *Cardiovasc. Res.* **81**(3), 457–64.

[119] Youle, R. J & Narendra, D. P. (2011) Mechanisms of mitophagy. *Nat. Rev. Mol. Cell Biol.* **12**(1), 9–14.

[120] Ott, M, Gogvadze, V, Orrenius, S, & Zhivotovsky, B. (2007) Mitochondria, oxidative stress and cell death. *Apoptosis* **12**(5), 913–22.

[121] Dykens, J. A & Will, Y. (2007) The significance of mitochondrial toxicity testing in drug development. *Drug Discov. Today* **12**(17-18), 777–85.

[122] Szigeti, A, Hocsak, E, Rapolti, E, et al. (2010) Facilitation of mitochondrial outer and

inner membrane permeabilization and cell death in oxidative stress by a novel Bcl-2 homology 3 domain protein. *J. Biol. Chem.* **285**(3), 2140–51.

[123] Kim, R, Emi, M, Tanabe, K, et al. (2006) Regulation and interplay of apoptotic and non-apoptotic cell death. *J. Pathol.* **208**(3), 319–26.

[124] Petrosillo, G, Ruggiero, F. M, & Paradies, G. (2003) Role of reactive oxygen species and cardiolipin in the release of cytochrome c from mitochondria. *FASEB J.* **17**(15), 2202–8.

[125] Kagan, V. E, Bayir, H. A, Belikova, N. A, et al. (2009) Cytochrome c/cardiolipin relations in mitochondria: a kiss of death. *Free Radic. Biol. Med.* **46**(11), 1439–53.

[126] Pereira, S. P, Fernandes, M. A. S, Martins, J. a. D, et al. (2009) Toxicity assessment of the herbicide metolachlor comparative effects on bacterial and mitochondrial model systems. *Toxicol. in Vitro* **23**(8), 1585–90.

[127] Nadanaciva, S, Dillman, K, Gebhard, D. F, Shrikhande, A, & Will, Y. (2010) High-Content Screening for Compounds That Affect mtDNA-Encoded Protein Levels in Eukaryotic Cells. *J. Biomol. Screen.* **15**(8), 937–948.

[128] Witte, M. E, Geurts, J. J. G, de Vries, H. E, van der Valk, P, & van Horssen, J. (2010) Mitochondrial dysfunction: a potential link between neuroinflammation and neurodegeneration? *Mitochondrion* **10**(5), 411–8.

[129] Sivitz, W. I & Yorek, M. A. (2010) Mitochondrial dysfunction in diabetes: from molecular mechanisms to functional significance and therapeutic opportunities. *Antioxid. Redox Signaling* **12**(4), 537–77.

[130] Rosca, M. G, Vazquez, E. J, Kerner, J, et al. (2008) Cardiac mitochondria in heart failure: decrease in respirasomes and oxidative phosphorylation. *Cardiovasc. Res.* **80**(1), 30–9.

[131] Szewczyk, A & Wojtczak, L. (2002) Mitochondria as a pharmacological target. *Pharmacol. Rev.* **54**(1), 101–27.

[132] Pereira, C. V, Moreira, A. C, Pereira, S. P, et al. (2009) Investigating drug-induced mitochondrial toxicity: a biosensor to increase drug safety? *Curr. Drug. Saf.* **4**(1), 34–54.

[133] Nadanaciva, S & Will, Y. (2009) The role of mitochondrial dysfunction and drug safety. *IDrugs* **12**(11), 706–10.

[134] Sardão, V. A, Pereira, S. L, & Oliveira, P. J. (2008) Drug-induced mitochondrial dysfunction in cardiac and skeletal muscle injury. *Expert Opin. Drug Saf.* **7**(2), 129–46.

[135] Dykens, J. A & Will, Y. (2008) *Preface*, eds. Dykens, J. A & Will, Y. (John Wiley & Sons, Inc.), pp. i–xvii.

[136] Arcamone, F, Cassinelli, G, Di Marco, A, & Gaetani, M. (1971) Adriamycin derivatives.

[137] Arcamone, F, Cassinelli, G, Fantini, G, et al. (1969) Adriamycin, 14-hydroxydaunomycin, a new antitumor antibiotic from S. peucetius var. caesius. *Biotechnol. Bioeng.* **11**(6), 1101–10.

[138] Arcamone, F, Franceschi, G, Penco, S, & Selva, A. (1969) Adriamycin (14-hydroxydaunomycin), a novel antitumor antibiotic. *Tetrahedron Lett.* **13**(13), 1007.

[139] Di Marco, A, Gaetani, M, & Scarpinato, B. (1969) Adriamycin (NSC-123,127): a new antibiotic with antitumor activity. *Cancer Chemother. Rep.* **53**(1), 33–7.

[140] Bonadonna, G, Monfardini, S, De Lena, M, & Fossati-Bellani, F. (1969) Clinical evaluation of adriamycin, a new antitumour antibiotic. *Br. Med. J.* **3**(5669), 503.

[141] Bonadonna, G, Monfardini, S, De Lena, M, Fossati-Bellani, F, & Beretta, G. (1970) Phase I and preliminary phase II evaluation of adriamycin (NSC 123127). *Cancer Res.* **30**(10), 2572–82.

[142] Steinherz, L. J, Steinherz, P. G, Tan, C. T, Heller, G, & Murphy, M. L. (1991) Cardiac toxicity 4 to 20 years after completing anthracycline therapy. *JAMA : the journal of the American Medical Association* **266**(12), 1672–7.

[143] Weiss, R. B. (1992) The anthracyclines: will we ever find a better doxorubicin? *Semin. Oncol.* **19**(6), 670–86.

[144] Singal, P. K & Iliskovic, N. (1998) Doxorubicin-induced cardiomyopathy. *N. Engl. J. Med.* **339**(13), 900–5.

[145] Carvalho, C, Santos, R. X, Cardoso, S, et al. (2009) Doxorubicin: the good, the bad and the ugly effect. *Curr. Med. Chem.* **16**(25), 3267–85.

[146] Takemura, G & Fujiwara, H. (2007) Doxorubicin-induced cardiomyopathy from the cardiotoxic mechanisms to management. *Prog. Cardiovasc. Dis.* **49**(5), 330–52.

[147] Von Hoff, D. D, Layard, M. W, Basa, P, et al. (1979) Risk factors for doxorubicin-induced congestive heart failure. *Ann. Intern. Med.* **91**(5), 710–7.

[148] Minotti, G, Menna, P, Salvatorelli, E, Cairo, G, & Gianni, L. (2004) Anthracyclines: molecular advances and pharmacologic developments in antitumor activity and cardiotoxicity. *Pharmacol. Rev.* **56**(2), 185–229.

[149] Ludke, A. R, Al-Shudiefat, A. A, Dhingra, S, Jassal, D. S, & Singal, P. K. (2009) A concise description of cardioprotective strategies in doxorubicin-induced cardiotoxicity. *Can. J. Physiol. Pharmacol.* **87**(10), 756–63.

[150] Robert, J, Morvan, V. L, Smith, D, Pourquier, P, & Bonnet, J. (2005) Predicting drug response and toxicity based on gene polymorphisms. *Crit. Rev. Oncol. Hematol.* **54**(3), 171–96.

[151] Deng, S & Wojnowski, L. (2007) Genotyping the risk of anthracycline-induced cardiotoxicity. *Cardiovasc. Toxicol.* **7**(2), 129–34.

[152] Smibert, E, Carlin, J. B, Vidmar, S, et al. (2004) Exercise echocardiography reflects cumulative anthracycline exposure during childhood. *Pediatr. Blood Cancer* **42**(7), 556–62.

[153] Neilan, T. G, Jassal, D. S, Perez-Sanz, T. M, et al. (2006) Tissue Doppler imaging predicts left ventricular dysfunction and mortality in a murine model of cardiac injury. *Eur. Heart J.* **27**(15), 1868–75.

[154] Germanakis, I, Anagnostatou, N, & Kalmanti, M. (2008) Troponins and natriuretic peptides in the monitoring of anthracycline cardiotoxicity. *Pediatr Blood Cancer* **51**(3), 327–33.

[155] Christiansen, S. (2010) Surgical treatment of doxorubicin-induced heart failure. *Thorac. Cardiovasc. Surg.* **58**(1), 8–10.

[156] Bodley, A, Liu, L. F, Israel, M, et al. (1989) DNA topoisomerase II-mediated inter-

action of doxorubicin and daunorubicin congeners with DNA. *Cancer Res.* **49**(21), 5969–78.

[157] Canobbio, L, Fassio, T, Gasparini, G, et al. (1986) Cardiac arrhythmia: possible complication from treatment with cisplatin. *Tumori* **72**(2), 201–4.

[158] Wallace, K. B. (2007) Adriamycin-induced interference with cardiac mitochondrial calcium homeostasis. *Cardiovasc. Toxicol.* **7**(2), 101–7.

[159] Berthiaume, J. M & Wallace, K. B. (2007) Adriamycin-induced oxidative mitochondrial cardiotoxicity. *Cell Biol. Toxicol.* **23**(1), 15–25.

[160] Anderson, A. B, Xiong, G, & Arriaga, E. A. (2004) Doxorubicin accumulation in individually electrophoresed organelles. *J. Am. Chem. Soc.* **126**(30), 9168–9.

[161] Jung, K & Reszka, R. (2001) Mitochondria as subcellular targets for clinically useful anthracyclines. *Adv. Drug Deliv. Rev.* **49**(1-2), 87–105.

[162] Doroshow, J. H. (1983) Effect of anthracycline antibiotics on oxygen radical formation in rat heart. *Cancer Res.* **43**(2), 460–72.

[163] Nohl, H, Gille, L, & Staniek, K. (1998) The exogenous NADH dehydrogenase of heart mitochondria is the key enzyme responsible for selective cardiotoxicity of anthracyclines. *Z. Naturforsch., C, J. Biosci.* **53**(3-4), 279–85.

[164] Simnek, T, Stérba, M, Popelová, O, et al. (2009) Anthracycline-induced cardiotoxicity: overview of studies examining the roles of oxidative stress and free cellular iron. *Pharmacol. Rep.* **61**(1), 154–71.

[165] Cairo, G, Recalcati, S, Pietrangelo, A, & Minotti, G. (2002) The iron regulatory proteins: targets and modulators of free radical reactions and oxidative damage. *Free Radic. Biol. Med.* **32**(12), 1237–43.

[166] Hrdina, R, Gersl, V, Klimtová, I, et al. (2000) Anthracycline-induced cardiotoxicity. *Acta medica* **43**(3), 75–82.

[167] Cole, M. P, Chaiswing, L, Oberley, T. D, et al. (2006) The protective roles of nitric oxide and superoxide dismutase in adriamycin-induced cardiotoxicity. *Cardiovasc. Res.* **69**(1), 186–97.

[168] Fogli, S, Nieri, P, & Breschi, M. C. (2004) The role of nitric oxide in anthracycline toxicity and prospects for pharmacologic prevention of cardiac damage. *FASEB J.* **18**(6), 664–75.

[169] Cotton, J. M, Kearney, M. T, & Shah, A. M. (2002) Nitric oxide and myocardial function in heart failure: friend or foe? *Heart* **88**(6), 564–6.

[170] Mukhopadhyay, P, Rajesh, M, Bátkai, S, et al. (2009) Role of superoxide, nitric oxide, and peroxynitrite in doxorubicin-induced cell death in vivo and in vitro. *Am. J. Physiol. Heart Circ. Physiol* **296**(5), H1466–83.

[171] Evig, C. B, Kelley, E. E, Weydert, C. J, et al. (2004) Endogenous production and exogenous exposure to nitric oxide augment doxorubicin cytotoxicity for breast cancer cells but not cardiac myoblasts. *Nitric oxide* **10**(3), 119–29.

[172] Zhou, S, Palmeira, C. M, & Wallace, K. B. (2001) Doxorubicin-induced persistent oxidative stress to cardiac myocytes. *Toxicol. Lett.* **121**(3), 151–7.

[173] Chandran, K, Aggarwal, D, Migrino, R. Q, et al. (2009) Doxorubicin inactivates myocardial cytochrome c oxidase in rats: cardioprotection by Mito-Q. *Biophys. J.*

96(4), 1388–98.

[174] Oliveira, P. J, Santos, M. S, & Wallace, K. B. (2006) Doxorubicin-induced thiol-dependent alteration of cardiac mitochondrial permeability transition and respiration. *Biochemistry (Moscow)* **71**(2), 194–199.

[175] Costantini, P, Chernyak, B. V, Petronilli, V, & Bernardi, P. (1996) Modulation of the mitochondrial permeability transition pore by pyridine nucleotides and dithiol oxidation at two separate sites. *J. Biol. Chem.* **271**(12), 6746–51.

[176] Pereira, G. C & Oliveira, P. J. (2008) Pharmacological strategies to counteract doxorubicin-induced cardiotoxicity: the role of mitochondria. *J Theor Exp Pharm* **1**(2), 39–53.

[177] Oliveira, P. J & Wallace, K. B. (2006) Depletion of adenine nucleotide translocator protein in heart mitochondria from doxorubicin-treated rats–relevance for mitochondrial dysfunction. *Toxicology* **220**(2-3), 160–8.

[178] Ascensão, A, Lumini-Oliveira, J, Machado, N. G, et al. (2011) Acute exercise protects against calcium-induced cardiac mitochondrial permeability transition pore opening in doxorubicin-treated rats. *Clin. Sci.* **120**(1), 37–49.

[179] Al-Nasser, I. A. (1998) In vivo prevention of adriamycin cardiotoxicity by cyclosporin A or FK506. *Toxicology* **131**(2-3), 175–81.

[180] Chacon, E & Acosta, D. (1991) Mitochondrial regulation of superoxide by Ca2+: an alternate mechanism for the cardiotoxicity of doxorubicin. *Toxicol. Appl. Pharmacol.* **107**(1), 117–28.

[181] Guo, H.-x, Wang, F, Yu, K.-q, et al. (2005) Novel cyclophilin D inhibitors derived from quinoxaline exhibit highly inhibitory activity against rat mitochondrial swelling and Ca2+ uptake/ release. *Acta Pharmacol. Sin.* **26**(10), 1201–11.

[182] Waldmeier, P. C, Feldtrauer, J.-J, Qian, T, & Lemasters, J. J. (2002) Inhibition of the mitochondrial permeability transition by the nonimmunosuppressive cyclosporin derivative NIM811. *Mol. Pharmacol.* **62**(1), 22–9.

[183] Huang, C, Zhang, X, Ramil, J. M, et al. (2010) Juvenile exposure to anthracyclines impairs cardiac progenitor cell function and vascularization resulting in greater susceptibility to stress-induced myocardial injury in adult mice. *Circulation* **121**(5), 675–83.

[184] Ascensão, A, Magalhães, J, Soares, J. M. C, et al. (2005) Moderate endurance training prevents doxorubicin-induced in vivo mitochondriopathy and reduces the development of cardiac apoptosis. *Am. J. Physiol. Heart Circ. Physiol.* **289**(2), H722–31.

[185] Santos, D. J, Moreno, A. J, Leino, R. L, Froberg, M. K, & Wallace, K. B. (2002) Carvedilol protects against doxorubicin-induced mitochondrial cardiomyopathy. *Toxicol. Appl. Pharmacol.* **185**(3), 218–27.

[186] Sardão, V. A, Santos, D. L, & Oliveira, P. J. (2006) *Cardiac mitochondrial dysfunction induced by doxorubicin; tole of calcium and oxidative stress*, ed. Moreno, A. J. (Transworld Research Network, Kerala, India), p. 270.

[187] Oliveira, P. J, Bjork, J. A, Santos, M. S, et al. (2004) Carvedilol-mediated antioxidant protection against doxorubicin-induced cardiac mitochondrial toxicity. *Toxicol. Appl. Pharmacol.* **200**(2), 159–68.

[188] Berthiaume, J. M, Oliveira, P. J, Fariss, M. W, & Wallace, K. B. (2005) Dietary vitamin E decreases doxorubicin-induced oxidative stress without preventing mitochondrial dysfunction. *Cardiovasc. Toxicol.* **5**(3), 257–67.

[189] Oliveira, P. J, Coxito, P. M, Rolo, A. P, et al. (2001) Inhibitory effect of carvedilol in the high-conductance state of the mitochondrial permeability transition pore. *Eur. J. Pharmacol.* **412**(3), 231–7.

[190] Stěrba, M, Popelová, O, Lenčo, J, et al. (2011) Proteomic insights into chronic anthracycline cardiotoxicity. *J. Mol. Cell. Cardiol.* **50**(5), 849–62.

[191] Robert, J. (2007) Long-term and short-term models for studying anthracycline cardiotoxicity and protectors. *Cardiovasc. Toxicol.* **7**(2), 135–9.

[192] Le Bot, M. A, Bégué, J. M, Kernaleguen, D, et al. (1988) Different cytotoxicity and metabolism of doxorubicin, daunorubicin, epirubicin, esorubicin and idarubicin in cultured human and rat hepatocytes. *Biochem. Pharmacol.* **37**(20), 3877–3887.

[193] Pointon, A. V, Walker, T. M, Phillips, K. M, et al. (2010) Doxorubicin in vivo rapidly alters expression and translation of myocardial electron transport chain genes, leads to ATP loss and caspase 3 activation. *PloS one* **5**(9), e12733.

[194] Wakasugi, S, Fischman, a. J, Babich, J. W, et al. (1993) Myocardial substrate utilization and left ventricular function in adriamycin cardiomyopathy. *J. Nucl. Med.* **34**(9), 1529–35.

[195] Carvalho, R. A, Sousa, R. P. B, Cadete, V. J. J, et al. (2010) Metabolic remodeling associated with subchronic doxorubicin cardiomyopathy. *Toxicology* **270**(2-3), 92–8.

[196] Tokarska-Schlattner, M, Zaugg, M, Zuppinger, C, Wallimann, T, & Schlattner, U. (2006) New insights into doxorubicin-induced cardiotoxicity: the critical role of cellular energetics. *J. Mol. Cell. Cardiol.* **41**(3), 389–405.

[197] Saks, V, Dzeja, P, Schlattner, U, et al. (2006) Cardiac system bioenergetics: metabolic basis of the Frank-Starling law. *J. Phys.* **571**(Pt 2), 253–73.

[198] Younes, A, Schneider, J. M, Bercovici, J, & Swynghedauw, B. (1985) Redistribution of creatine kinase isoenzymes in chronically overloaded myocardium. *Cardiovasc. Res.* **19**(1), 15–9.

[199] Bittner, V, Reeves, R. C, Digerness, S. B, Caulfield, J. B, & Pohost, G. M. (1991) 31P NMR spectroscopy in chronic adriamycin cardiotoxicity. *Magn. Reson. Med.* **17**(1), 69–81.

[200] Zhang, Y. W, Shi, J, Li, Y. J, & Wei, L. (2009) Cardiomyocyte death in doxorubicin-induced cardiotoxicity. *Arch. Immunol. Ther. Exp. (Warsz.)* **57**(6), 435–45.

[201] Shizukuda, Y, Matoba, S, Mian, O. Y, Nguyen, T, & Hwang, P. M. (2005) Targeted disruption of p53 attenuates doxorubicin-induced cardiac toxicity in mice. *Mol. Cell. Biochem.* **273**(1-2), 25–32.

[202] Sardão, V. A, Oliveira, P. J, Holy, J, Oliveira, C. R, & Wallace, K. B. (2009) Doxorubicin-induced mitochondrial dysfunction is secondary to nuclear p53 activation in H9c2 cardiomyoblasts. *Cancer Chemother. Pharmacol.* **64**(4), 811–27.

[203] L'Ecuyer, T, Sanjeev, S, Thomas, R, et al. (2006) DNA damage is an early event in doxorubicin-induced cardiac myocyte death. *Am. J. Physiol. Heart Circ. Physiol.* **291**(3), H1273–80.

[204] Nithipongvanitch, R, Ittarat, W, Velez, J. M, et al. (2007) Evidence for p53 as guardian of the cardiomyocyte mitochondrial genome following acute adriamycin treatment. *J. Histochem. Cytochem.* **55**(6), 629–39.

[205] De Angelis, A, Piegari, E, Cappetta, D, et al. (2010) Anthracycline cardiomyopathy is mediated by depletion of the cardiac stem cell pool and is rescued by restoration of progenitor cell function. *Circulation* **121**(2), 276–92.

[206] Gustafsson, A. B & Gottlieb, R. A. (2008) Recycle or die: the role of autophagy in cardioprotection. *J. Mol. Cell. Cardiol.* **44**(4), 654–61.

[207] Iglewski, M, Hill, J. A, Lavandero, S, & Rothermel, B. A. (2010) Mitochondrial Fission and Autophagy in the Normal and Diseased Heart. *Curr. Hypertens. Rep.* **12**(6), 418–25.

[208] Carreira, R. S, Lee, Y, Ghochani, M, Gustafsson, A. B, & Gottlieb, R. A. (2010) Cyclophilin D is required for mitochondrial removal by autophagy in cardiac cells. *Autophagy* **6**(4), 462–472.

[209] Gottlieb, R. A & Carreira, R. S. (2010) Autophagy in Health and Disease: V. Mitophagy as a Way of Life. *Am. J. Physiol. Cell Phys.* **299**(2), C203–10.

[210] Elmore, S. P, Qian, T, Grissom, S. F, & Lemasters, J. J. (2001) The mitochondrial permeability transition initiates autophagy in rat hepatocytes. *FASEB J.* **15**(12), 2286–7.

[211] Scherz-Shouval, R & Elazar, Z. (2011) Regulation of autophagy by ROS: physiology and pathology. *Trends Biochem. Sci.* **36**(1), 30–8.

[212] Gottlieb, R. A & Gustafsson, A. B. (2011) Mitochondrial turnover in the heart. *Biochim. Biophys. Acta* **1813**(7), 1295–301.

[213] Kobayashi, S, Volden, P, Timm, D, et al. (2010) Transcription factor GATA4 inhibits doxorubicin-induced autophagy and cardiomyocyte death. *J. Biol. Chem.* **285**(1), 793–804.

[214] Lu, L, Wu, W, Yan, J, et al. (2009) Adriamycin-induced autophagic cardiomyocyte death plays a pathogenic role in a rat model of heart failure. *Int. J. Cardiol.* **134**(1), 82–90.

[215] Peters, J. H, Gordon, G. R, Kashiwase, D, & Acton, E. M. (1981) Tissue distribution of doxorubicin and doxorubicinol in rats receiving multiple doses of doxorubicin. *Cancer Chemother. Pharmacol.* **7**(1), 65–9.

[216] Lal, S, Mahajan, A, Chen, W. N, & Chowbay, B. (2010) Pharmacogenetics of target genes across doxorubicin disposition pathway: a review. *Curr. Drug Metab.* **11**(1), 115–28.

[217] Odom, A. L, Hatwig, C. A, Stanley, J. S, & Benson, A. M. (1992) Biochemical determinants of Adriamycin toxicity in mouse liver, heart and intestine. *Biochem. Pharmacol.* **43**(4), 831–6.

[218] Rumsey, W. L & Wilson, D. F. (2010) *Tissue Capacity for Mitochondrial Oxidative Phosphorylation and its Adaptation to Stress.* (John Wiley & Sons, Inc.), pp. 1095–1113.

[219] Rossignol, R, Malgat, M, Mazat, J. P, & Letellier, T. (1999) Threshold effect and tissue specificity. Implication for mitochondrial cytopathies. *J. Biol. Chem.* **274**(47),

33426–32.

[220] Palmeira, C. M, Serrano, J, Kuehl, D. W, & Wallace, K. B. (1997) Preferential oxidation of cardiac mitochondrial DNA following acute intoxication with doxorubicin. *Biochim. Biophys. Acta* **1321**(2), 101–6.

[221] Cardoso, S, Santos, R. X, Carvalho, C, et al. (2008) Doxorubicin increases the susceptibility of brain mitochondria to Ca(2+)-induced permeability transition and oxidative damage. *Free Radic. Biol. Med.* **45**(10), 1395–402.

[222] Machado, N. G, Baldeiras, I, Pereira, G. C, Pereira, S. P, & Oliveira, P. J. (2010) Sub-chronic administration of doxorubicin to Wistar rats results in oxidative stress and unaltered apoptotic signaling in the lung. *Chem. Biol. Interact.* **188**(3), 478–86.

[223] Legha, S. S, Benjamin, R. S, Mackay, B, et al. (1982) Reduction of doxorubicin cardiotoxicity by prolonged continuous intravenous infusion. *Ann. Intern. Med.* **96**(2), 133–139.

[224] Casper, E. S, Gaynor, J. J, Hajdu, S. I, et al. (1991) A prospective randomized trial of adjuvant chemotherapy with bolus versus continuous infusion of doxorubicin in patients with high-grade extremity soft tissue sarcoma and an analysis of prognostic factors. *Cancer* **68**(6), 1221–9.

[225] Iarussi, D, Indolfi, P, Casale, F, et al. (2001) Recent advances in the prevention of anthracycline cardiotoxicity in childhood. *Curr. Med. Chem.* **8**(13), 1649–60.

[226] Patil, R. R, Guhagarkar, S. A, & Devarajan, P. V. (2008) Engineered nanocarriers of doxorubicin: a current update. *Crit. Rev. Ther. Drug Carrier Syst.* **25**(1), 1–61.

[227] Drummond, D. C, Meyer, O, Hong, K, Kirpotin, D. B, & Papahadjopoulos, D. (1999) Optimizing liposomes for delivery of chemotherapeutic agents to solid tumors. *Pharmacol. Rev.* **51**(4), 691–743.

[228] Hideg, K & Kálai, T. (2007) Novel antioxidants in anthracycline cardiotoxicity. *Cardiovasc. Toxicol.* **7**(2), 160–4.

[229] Wattanapitayakul, S. K, Chularojmontri, L, Herunsalee, A, et al. (2005) Screening of antioxidants from medicinal plants for cardioprotective effect against doxorubicin toxicity. *Basic Clin. Pharmacol. Toxicol.* **96**(1), 80–7.

[230] Glantzounis, G. K, Yang, W, Koti, R. S, et al. (2006) The role of thiols in liver ischemia-reperfusion injury. *Curr. Pharm. Des.* **12**(23), 2891–2901.

[231] Ferrari, R, Ceconi, C, Curello, S, et al. (1991) Oxygen free radicals and myocardial damage: protective role of thiol-containing agents. *Am. J. Med.* **91**(3C), 95S–105S.

[232] Horenstein, M. S, Vander Heide, R. S, & L'Ecuyer, T. J. (2000) Molecular basis of anthracycline-induced cardiotoxicity and its prevention. *Mol. Genet. Metab.* **71**(1-2), 436–44.

[233] Fox, J. H, Barber, D. S, Singh, B, et al. (2004) Cystamine increases L-cysteine levels in Huntington's disease transgenic mouse brain and in a PC12 model of polyglutamine aggregation. *J. Neurochem.* **91**(2), 413–22.

[234] Unverferth, D. V, Jagadeesh, J. M, Unverferth, B. J, et al. (1983) Attempt to prevent doxorubicin-induced acute human myocardial morphologic damage with acetylcysteine. *J. Natl. Cancer Inst.* **71**(5), 917–20.

[235] Quiles, J. L, Huertas, J. R, Battino, M, Mataix, J, & Ramírez-Tortosa, M. C. (2002)

Antioxidant nutrients and adriamycin toxicity. *Toxicology* **180**(1), 79–95.

[236] Kang, Y. J, Chen, Y, Yu, A, Voss-McCowan, M, & Epstein, P. N. (1997) Overexpression of metallothionein in the heart of transgenic mice suppresses doxorubicin cardiotoxicity. *J. Clin. Invest.* **100**(6), 1501–6.

[237] Skulachev, V. P, Anisimov, V. N, Antonenko, Y. N, et al. (2009) An attempt to prevent senescence: a mitochondrial approach. *Biochim. Biophys. Acta* **1787**(5), 437–61.

[238] Hasinoff, B. B & Kala, S. V. (1993) The removal of metal ions from transferrin, ferritin and ceruloplasmin by the cardioprotective agent ICRF-187 [(+)-1,2-bis(3,5-dioxopiperazinyl-1-yl)propane] and its hydrolysis product ADR-925. *Agents Actions* **39**(1-2), 72–81.

[239] Hofland, K. F, Thougaard, A. V, Sehested, M, & Jensen, P. B. (2005) Dexrazoxane protects against myelosuppression from the DNA cleavage-enhancing drugs etoposide and daunorubicin but not doxorubicin. *Clin. Cancer Res.* **11**(10), 3915–24.

[240] Hampton, J. R. (1996) Beta-blockers in heart failure–the evidence from clinical trials. *Eur. Heart J.* **17 Suppl B**, 17–20.

[241] Fazio, S, Palmieri, E. A, Ferravante, B, et al. (1998) Doxorubicin-induced cardiomyopathy treated with carvedilol. *Clin. Cardiol.* **21**(10), 777–9.

[242] Matsui, H, Morishima, I, Numaguchi, Y, et al. (1999) Protective effects of carvedilol against doxorubicin-induced cardiomyopathy in rats. *Life Sci.* **65**(12), 1265–74.

[243] Oliveira, P. J & Moreno, A. J. (2006) *Carvedilol, an hypertensive drug, protects heart mitochondria from oxidative damage*, ed. Moreno, A. J. (Transworld Research Network, Kerala, India), p. 270.

[244] Facundo, H. T. F, Fornazari, M, & Kowaltowski, A. J. (2006) Tissue protection mediated by mitochondrial K+ channels. *Biochim. Biophys. Acta* **1762**(2), 202–12.

[245] Garlid, K. D & Halestrap, A. P. (2012) The mitochondrial K(ATP) channel-Fact or fiction? *J. Mol. Cell. Cardiol.* **52**(3), 578–83.

[246] Carreira, R. S, Facundo, H. T. F, & Kowaltowski, A. J. (2005) Mitochondrial K+ transport and cardiac protection during ischemia/reperfusion. *Braz. J. Med. Biol. Res.* **38**(3), 345–52.

[247] Bednarczyk, P, Doowy, K, & Szewczyk, A. (2005) Matrix Mg2+ regulates mitochondrial ATP-dependent potassium channel from heart. *FEBS Lett.* **579**(7), 1625–32.

[248] Fisher, P. W, Salloum, F, Das, A, Hyder, H, & Kukreja, R. C. (2005) Phosphodiesterase-5 inhibition with sildenafil attenuates cardiomyocyte apoptosis and left ventricular dysfunction in a chronic model of doxorubicin cardiotoxicity. *Circulation* **111**(13), 1601–10.

[249] Emanuelov, A. K, Shainberg, A, Chepurko, Y, et al. (2010) Adenosine A3 receptor-mediated cardioprotection against doxorubicin-induced mitochondrial damage. *Biochem. Pharmacol.* **79**(2), 180–7.

[250] Hydock, D. S, Lien, C.-Y, Schneider, C. M, & Hayward, R. (2008) Exercise preconditioning protects against doxorubicin-induced cardiac dysfunction. *Med. Sci. Sports Exerc.* **40**(5), 808–17.

[251] Wonders, K. Y, Hydock, D. S, Schneider, C. M, & Hayward, R. (2008) Acute exercise protects against doxorubicin cardiotoxicity. *Integr. Cancer Ther.* **7**(3), 147–54.

[252] Hydock, D. S, Wonders, K. Y, Schneider, C. M, & Hayward, R. (2009) Voluntary wheel running in rats receiving doxorubicin: effects on running activity and cardiac myosin heavy chain. *Anticancer Res.* **29**(11), 4401–7.

[253] Ascensão, A, Ferreira, R, & Magalhães, J. (2007) Exercise-induced cardioprotection–biochemical, morphological and functional evidence in whole tissue and isolated mitochondria. *Int. J. Cardiol.* **117**(1), 16–30.

[254] Kavazis, A. N, Smuder, A. J, Min, K, Tumer, N, & Powers, S. K. (2010) Short-term exercise training protects against doxorubicin induced cardiac mitochondrial damage independent of HSP72. *Am. J. Physiol. Heart Circ. Physiol.* **299**(5), H1515–24.

[255] Ragan, C. I, Wilson, M. T, Darley-Usmar, V. M, , & Lowe, P. N. (1987) *Subfractionation of mitochondria and isolation of the proteins of oxidative phosphorylation.*, Practical approach series, eds. Darley-Usmar, V. M, Rickwood, D, & Wilson, M. T. (IRL Press, Oxford, England), pp. 79–111.

[256] Birch-Machin, M. A & Turnbull, D. M. (2001) Assaying mitochondrial respiratory complex activity in mitochondria isolated from human cells and tissues. *Methods Cell Biol.* **65**, 97–117.

[257] Brás, C, Roque, H, & de Souza, I. A. (2007) Echocardiographic Evaluation in Experimental Pathology. *Exp. Path. Health Sci.* **1**(1), 17–20.

[258] Toth, P. P, Ferguson-Miller, S. M, & Suelter, C. H. (1986) Isolation of highly coupled heart mitochondria in high yield using a bacterial collagenase. *Methods Enzymol.* **125**, 16–27.

[259] Gazzotti, P, Malmstron, K, & Crompton, M. (1979) *Preparation and assay of animal mitochondria and submitochondrial vesicles.*, eds. Carafoli, E, Semenza, G, & Affolter, H. (Springer-Verlag, Berlin), pp. 62–69.

[260] Gornall, A. G, Bardawill, C. J, & David, M. M. (1949) Determination of serum proteins by means of the biuret reaction. *J. Biol. Chem.* **177**(2), 751–66.

[261] Smith, P. K, Krohn, R. I, Hermanson, G. T, et al. (1985) Measurement of protein using bicinchoninic acid. *Anal. Biochem.* **150**(1), 76–85.

[262] Estabrook, R. W. (1967) in *Oxidation and Phosphorylation*, eds. Estabrook, R. W & Pullman, M. E. (Academic Press) Vol. Volume 10, pp. 41–47.

[263] Rickwood, D & Darley-Usmar, V. M. (1987) *Isolation and characteristics of intact mitochondria*, Practical approach series, eds. Darley-Usmar, V. M, Rickwood, D, & Wilson, M. T. (IRL Press, Oxford, England), pp. 1–16.

[264] Chance, B & Williams, G. R. (1956) Respiratory enzymes in oxidative phosphorylation. VI. The effects of adenosine diphosphate on azide-treated mitochondria. *J. Biol. Chem.* **221**(1), 477–89.

[265] Villani, G & Attardi, G. (1997) In vivo control of respiration by cytochrome c oxidase in wild-type and mitochondrial DNA mutation-carrying human cells. *Proc. Natl. Acad. Sci. U. S. A.* **94**(4), 1166–71.

[266] Rossignol, R, Letellier, T, Malgat, M, Rocher, C, & Mazat, J. P. (2000) Tissue variation in the control of oxidative phosphorylation: implication for mitochondrial diseases. *Biochem. J.* **347 Pt 1**, 45–53.

[267] Kamo, N, Muratsugu, M, Hongoh, R, & Kobatake, Y. (1979) Membrane potential of

mitochondria measured with an electrode sensitive to tetraphenyl phosphonium and relationship between proton electrochemical potential and phosphorylation potential in steady state. *J. Membr. Biol.* **49**(2), 105–21.

[268] Moreno, A. J. (1992) Ph.D. thesis (School of Science and Technology, University of Coimbra).

[269] Madeira, V. M. (1975) A rapid and ultrasensitive method to measure Ca++ movements across biological membranes. *Biochem. Biophys. Res. Commun.* **64**(3), 870–6.

[270] Masini, A, Ceccarelli-Stanzani, D, & Muscatello, U. (1984) An investigation on the effect of oligomycin on state-4 respiration in isolated rat-liver mitochondria. *Biochim. Biophys. Acta* **767**(1), 130–7.

[271] Rajdev, S & Reynolds, I. J. (1993) Calcium green-5N, a novel fluorescent probe for monitoring high intracellular free Ca2+ concentrations associated with glutamate excitotoxicity in cultured rat brain neurons. *Neurosci. Lett.* **162**(1-2), 149–52.

[272] Barja, G. (2002) The quantitative measurement of H2O2 generation in isolated mitochondria. *J. Bioenerg. Biomembr.* **34**(3), 227–33.

[273] Spinazzi, M, Casarin, A, Pertegato, V, et al. (2011) Optimization of respiratory chain enzymatic assays in muscle for the diagnosis of mitochondrial disorders. *Mitochondrion* **11**(6), 893–904.

[274] Janssen, A. J. M, Trijbels, F. J. M, Sengers, R. C. A, et al. (2007) Spectrophotometric assay for complex I of the respiratory chain in tissue samples and cultured fibroblasts. *Clin. Chem.* **53**(4), 729–34.

[275] Barrientos, A. (2002) In vivo and in organello assessment of OXPHOS activities. *Methods* **26**(4), 307–16.

[276] Krähenbühl, S, Talos, C, Wiesmann, U, & Hoppel, C. L. (1994) Development and evaluation of a spectrophotometric assay for complex III in isolated mitochondria, tissues and fibroblasts from rats and humans. *Clin. Chim. Acta* **230**(2), 177–87.

[277] Luo, C, Long, J, & Liu, J. (2008) An improved spectrophotometric method for a more specific and accurate assay of mitochondrial complex III activity. *Clin. Chim. Acta* **395**(1-2), 38–41.

[278] Nadanaciva, S, Bernal, A, Aggeler, R, Capaldi, R, & Will, Y. (2007) Target identification of drug induced mitochondrial toxicity using immunocapture based OXPHOS activity assays. *Toxicol. in Vitro* **21**(5), 902–11.

[279] Minchenko, J, Williams, A. J, & Christodoulou, J. (2003) Adaptation of a mitochondrial complex III assay for automation: examination of reproducibility and precision. *Clin. Chem.* **49**(2), 330–2.

[280] Jewess, P. J & Devonshire, A. L. (1999) Kinetic microplate-based assays for inhibitors of mitochondrial NADH:ubiquinone oxidoreductase (complex I) and succinate:cytochrome c oxidoreductase. *Anal. Biochem.* **272**(1), 56–63.

[281] Long, J, Ma, J, Luo, C, et al. (2009) Comparison of two methods for assaying complex I activity in mitochondria isolated from rat liver, brain and heart. *Life Sci.* **85**(7-8), 276–80.

[282] Bénit, P, Slama, A, & Rustin, P. (2008) Decylubiquinol impedes mitochondrial respiratory chain complex I activity. *Mol. Cell. Biochem.* **314**(1-2), 45–50.

[283] Rodenburg, R. J, Stoltenborg-Hogenkamp, B. J, Wintjes, L. T, et al. (2008) In Reply. *Clin. Chem.* **54**(11), 1922–1924.

[284] de Wit, L. E. A, Scholte, H. R, & Sluiter, W. (2008) Correct assay of complex I activity in human skin fibroblasts by timely addition of rotenone. *Clin. Chem.* **54**(11), 1921–2; author reply 1922–4.

[285] Hausladen, A & Fridovich, I. (1996) Measuring nitric oxide and superoxide: rate constants for aconitase reactivity. *Methods Enzymol.* **269**, 37–41.

[286] Laemmli, U. K. (1970) Cleavage of structural proteins during the assembly of the head of bacteriophage T4. *Nature* **227**(5259), 680–5.

[287] Gallagher, S. R. (2006) One-dimensional SDS gel electrophoresis of proteins. *Curr Protoc Mol Biol* **Chapter 10**, Unit 10.2A.

[288] Burnette, W. N. (1981) "Western blotting": electrophoretic transfer of proteins from sodium dodecyl sulfate–polyacrylamide gels to unmodified nitrocellulose and radiographic detection with antibody and radioiodinated protein A. *Anal. Biochem.* **112**(2), 195–203.

[289] Gallagher, S, Winston, S. E, Fuller, S. A, & Hurrell, J. G. R. (2008) Immunoblotting and immunodetection. *Curr Protoc Mol Biol* **Chapter 10**, Unit 10.8.

[290] Feinberg, A. P & Vogelstein, B. (1983) A technique for radiolabeling DNA restriction endonuclease fragments to high specific activity. *Anal. Biochem.* **132**(1), 6–13.

[291] VanGuilder, H. D, Vrana, K. E, & Freeman, W. M. (2008) Twenty-five years of quantitative PCR for gene expression analysis. *Biotechniques* **44**(5), 619–26.

[292] Zar, J. H. (1999) *Biostatistical analysis*. (Prentice Hall, Englewood Cliffs, NJ), 4 edition, p. 929.

[293] Gellerich, F. N, Kunz, W. S, & Bohnensack, R. (1990) Estimation of flux control coefficients from inhibitor titrations by non-linear regression. *FEBS Lett.* **274**(1-2), 167–70.

[294] Small, J. R. (1993) Flux control coefficients determined by inhibitor titration: the design and analysis of experiments to minimize errors. *Biochem. J.* **296 (Pt 2)**, 423–433.

[295] Wallace, K. B. (2003) Doxorubicin-induced cardiac mitochondrionopathy. *Pharmacol. Toxicol.* **93**(3), 105–15.

[296] Sacco, G, Bigioni, M, Evangelista, S, et al. (2001) Cardioprotective effects of zofenopril, a new angiotensin-converting enzyme inhibitor, on doxorubicin-induced cardiotoxicity in the rat. *Eur. J. Pharmacol.* **414**(1), 71–8.

[297] Ahmed, H. H, Mannaa, F, Elmegeed, G. A, & Doss, S. H. (2005) Cardioprotective activity of melatonin and its novel synthesized derivatives on doxorubicin-induced cardiotoxicity. *Bioorg. Med. Chem.* **13**(5), 1847–57.

[298] van Leeuwen, B. L, Kamps, W. A, Hartel, R. M, et al. (2000) Effect of single chemotherapeutic agents on the growing skeleton of the rat. *Ann. Oncol.* **11**(9), 1121–6.

[299] Berthiaume, J. M & Wallace, K. B. (2007) Persistent alterations to the gene expression profile of the heart subsequent to chronic Doxorubicin treatment. *Cardiovasc. Toxicol.* **7**(3), 178–91.

[300] Okuda, S, Oh, Y, Tsuruda, H, et al. (1986) Adriamycin-induced nephropathy as a model of chronic progressive glomerular disease. *Kidney Int.* **29**(2), 502–10.

[301] Baba, H, Stephens, L. C, Strebel, F. R, et al. (1991) Protective effect of ICRF-187 against normal tissue injury induced by adriamycin in combination with whole body hyperthermia. *Cancer Res.* **51**(13), 3568–77.

[302] Lushnikova, E. L, Klinnikova, M. G, Molodykh, O. P, & Nepomnyashchikh, L. M. (2004) Morphological manifestations of heart remodeling in anthracycline-induced dilated cardiomyopathy. *Bull. Exp. Biol. Med.* **138**(6), 607–12.

[303] Solem, L. E, Heller, L. J, & Wallace, K. B. (1996) Dose-dependent increase in sensitivity to calcium-induced mitochondrial dysfunction and cardiomyocyte cell injury by doxorubicin. *J. Mol. Cell. Cardiol.* **28**(5), 1023–32.

[304] Riad, A, Bien, S, Westermann, D, et al. (2009) Pretreatment with statin attenuates the cardiotoxicity of Doxorubicin in mice. *Cancer Res.* **69**(2), 695–9.

[305] Migrino, R. Q, Aggarwal, D, Konorev, E. A, et al. (2008) Early detection of doxorubicin cardiomyopathy using two-dimensional strain echocardiography. *Ultrasound. Med. Biol.* **34**(2), 208–14.

[306] Shakir, D. K & Rasul, K. I. (2009) Chemotherapy induced cardiomyopathy: pathogenesis, monitoring and management. *J. Clin. Med. Res.* **1**(1), 8–12.

[307] Verdun, C, Brasseur, F, Vranckx, H, Couvreur, P, & Roland, M. (1990) Tissue distribution of doxorubicin associated with polyisohexylcyanoacrylate nanoparticles. *Cancer Chemother. Pharmacol.* **26**(1), 13–8.

[308] Bai, P, Mabley, J. G, Liaudet, L, et al. (2004) Matrix metalloproteinase activation is an early event in doxorubicin-induced cardiotoxicity. *Oncol. Rep.* **11**(2), 505–8.

[309] Todorova, V. K, Kaufmann, Y, Hennings, L, & Klimberg, V. S. (2010) Oral glutamine protects against acute doxorubicin-induced cardiotoxicity of tumor-bearing rats. *J. Nutr.* **140**(1), 44–8.

[310] Mas, M, Sabater, E, Olaso, M. J, Horga, J. F, & Faura, C. C. (2000) Genetic variability in morphine sensitivity and tolerance between different strains of rats. *Brain Res.* **866**(1-2), 109–15.

[311] Kacew, S & Festing, M. F. (1996) Role of rat strain in the differential sensitivity to pharmaceutical agents and naturally occurring substances. *J. Toxicol. Environ. Health* **47**(1), 1–30.

[312] Schwartz, C. L. (1999) Long-term survivors of childhood cancer: the late effects of therapy. *Oncologist* **4**(1), 45–54.

[313] Halestrap, A. P. (2009) What is the mitochondrial permeability transition pore? *J. Mol. Cell. Cardiol.* **46**(6), 821–31.

[314] Broekemeier, K. M, Dempsey, M. E, & Pfeiffer, D. R. (1989) Cyclosporin A is a potent inhibitor of the inner membrane permeability transition in liver mitochondria. *J. Biol. Chem.* **264**(14), 7826–30.

[315] Bernardi, P, Krauskopf, A, Basso, E, et al. (2006) The mitochondrial permeability transition from in vitro artifact to disease target. *FEBS J.* **273**(10), 2077–99.

[316] Fontaine, E, Eriksson, O, Ichas, F, & Bernardi, P. (1998) Regulation of the permeability transition pore in skeletal muscle mitochondria. Modulation By electron flow

through the respiratory chain complex i. *J. Biol. Chem.* **273**(20), 12662–8.

[317] Ito, K, Ozasa, H, Sanada, K, & Horikawa, S. (2000) Doxorubicin preconditioning: a protection against rat hepatic ischemia-reperfusion injury. *Hepatology* **31**(2), 416–9.

[318] Lebrecht, D, Geist, A, Ketelsen, U.-P, et al. (2007) Dexrazoxane prevents doxorubicin-induced long-term cardiotoxicity and protects myocardial mitochondria from genetic and functional lesions in rats. *Br. J. Pharmacol.* **151**(6), 771–8.

[319] Folkers, K, Liu, M, Watanabe, T, & Porter, T. H. (1977) Inhibition by adriamycin of the mitochondrial biosynthesis of coenzyme Q10 and implication for the cardiotoxicity of adriamycin in cancer patients. *Biochem. Biophys. Res. Commun.* **77**(4), 1536–42.

[320] Eaton, S, Skinner, R, Hale, J. P, et al. (2000) Plasma coenzyme Q(10) in children and adolescents undergoing doxorubicin therapy. *Clin. Chim. Acta* **302**(1-2), 1–9.

[321] Cortes, E. P, Gupta, M, Chou, C, Amin, V. C, & Folkers, K. (1978) Adriamycin cardiotoxicity: early detection by systolic time interval and possible prevention by coenzyme Q10. *Cancer Treat. Rep.* **62**(6), 887–91.

[322] Conklin, K. A. (2005) Coenzyme q10 for prevention of anthracycline-induced cardiotoxicity. *Integr. Cancer Ther.* **4**(2), 110–30.

[323] Fontaine, E, Ichas, F, & Bernardi, P. (1998) A ubiquinone-binding site regulates the mitochondrial permeability transition pore. *J. Biol. Chem.* **273**(40), 25734–40.

[324] Brunner, G & Neupert, W. (1968) Turnover of outer and inner membrane proteins of rat liver mitochondria. *FEBS Lett.* **1**(3), 153–155.

[325] Miwa, S, Lawless, C, & von Zglinicki, T. (2008) Mitochondrial turnover in liver is fast in vivo and is accelerated by dietary restriction: application of a simple dynamic model. *Aging Cell* **7**(6), 920–3.

[326] Basoah, A, Matthews, P. M, & Morten, K. J. (2005) Rapid rates of newly synthesized mitochondrial protein degradation are significantly affected by the generation of mitochondrial free radicals. *FEBS Lett.* **579**(28), 6511–7.

[327] Korzeniewski, B, Malgat, M, Letellier, T, & Mazat, J. P. (2001) Effect of 'binary mitochondrial heteroplasmy' on respiration and ATP synthesis: implications for mitochondrial diseases. *Biochem. J.* **357**(Pt 3), 835–42.

[328] Moreno-Sánchez, R, Saavedra, E, Rodríguez-Enríquez, S, et al. (2010) Metabolic control analysis indicates a change of strategy in the treatment of cancer. *Mitochondrion* **10**(6), 626–39.

[329] Mazat, J. P, Letellier, T, Bédes, F, et al. (1997) Metabolic control analysis and threshold effect in oxidative phosphorylation: implications for mitochondrial pathologies. *Mol. Cell. Biochem.* **174**(1-2), 143–8.

[330] Nicolay, K & de Kruijff, B. (1987) Effects of adriamycin on respiratory chain activities in mitochondria from rat liver, rat heart and bovine heart. Evidence for a preferential inhibition of complex III and IV. *Biochim. Biophys. Acta* **892**(3), 320–330.

[331] Rep, M & Grivell, L. A. (1996) The role of protein degradation in mitochondrial function and biogenesis. *Curr. Genet.* **30**(5), 367–80.

[332] Gómez, L. A, Monette, J. S, Chavez, J. D, Maier, C. S, & Hagen, T. M. (2009) Supercomplexes of the mitochondrial electron transport chain decline in the aging rat heart. *Arch. Biochem. Biophys.* **490**(1), 30–5.

[333] Nekhlyudov, L, Aziz, N, Lerro, C. C, & Virgo, K. S. (2012) *Oncologists' and primary care providers' awareness of late effects of cancer treatment: Implications for survivorship care.*

[334] Malik, A. N, Shahni, R, Rodriguez-de Ledesma, A, Laftah, A, & Cunningham, P. (2011) Mitochondrial DNA as a non-invasive biomarker: accurate quantification using real time quantitative PCR without co-amplification of pseudogenes and dilution bias. *Biochem. Biophys. Res. Commun.* **412**(1), 1–7.

[335] Wong, R, Aponte, A. M, Steenbergen, C, & Murphy, E. (2010) Cardioprotection leads to novel changes in the mitochondrial proteome. *Am. J. Physiol. Heart Circ. Physiol.* **298**(1), H75–91.

[336] Zhu, W, Shou, W, Payne, R. M, Caldwell, R, & Field, L. J. (2008) A mouse model for juvenile doxorubicin-induced cardiac dysfunction. *Pediatr. Res.* **64**(5), 488–94.

[337] Monnet, E & Chachques, J. C. (2005) Animal models of heart failure: what is new? *Ann. Thorac. Surg.* **79**(4), 1445–53.

[338] Festing, M. F. W, Ltd, L. A, & of Medicine (Great Britain), R. S. (2002) *The Design of Animal Experiments: Reducing the Use of Animals in Research Through Better Experimental Design*, Laboratory Animal Handbooks. (Royal Society of Medicine).